# Characterisation of the cellular responses to CDC7 inhibition in breast-derived human cells

A thesis submitted to the National University of Ireland, Galway in fulfilment of the requirement for the degree of

Doctor of Philosophy

By

**Huong Quach Thi Thu**

Centre for Chromosome Biology

Discipline of Biochemistry, School of Natural Sciences,

National University of Ireland, Galway

Supervisor: Prof. Corrado Santocanale

- October 2017 -

# Table of Contents

# List of figures

# List of tables

# Abbreviations

| | |
|---|---|
| 4KO | DBF4 knockout cell line |
| Ab | Antibody |
| APC/C | Anaphase-promoting complex/cyclosome |
| mAb | Monoclonal antibody |
| pAb | Polyclonal antibody |
| BrdU | 5-Bromo-2-deoxyuridine |
| BSA | Bovine serum albumin |
| CDK | Cyclin-dependent kinase |
| CDC | Cell division cycle |
| Cyc or Cln | Cyclin |
| Clb | B-type cyclin |
| CldU | 5-Chloro-2′-deoxyuridine |
| DAPI | 4',6-Diamidino-2-phenylindole |
| kDa | kilo Dalton |
| DMEM | Dulbecco's Modified Eagle's medium |
| DMSO | Dimethyl sulfoxide |
| DMC | Delta-MC |
| DN | Delta-N |
| dsDNA | Double-stranded DNA |
| EDTA | Ethylenediamine tetra-acetic acid |
| EdU | 5-Ethynyl-2'-deoxyuridine |
| ER | Estrogen receptor |
| EV | Empty vector |
| FBS | Foetal bovine serum |
| FCS | Foetal calf serum |
| FL | Full-length (DBF4) |
| H or h | Hour(s) |
| HER2 | Human epidermal growth factor receptor 2 |
| HTS | High throughput screening |
| HU | Hydroxyurea |
| IdU | 5-Iodo-2′-deoxyuridine |

| | |
|---|---|
| IMDM | Iscove's Modified Dulbecco's Medium |
| M | Molar |
| mM | Millimolar |
| µM | Micromolar |
| nM | Nanomolar |
| MCMs | Mini-chromosome maintenance proteins |
| PBS | Phosphate buffered saline |
| PBS-T | PBS-Tween 20 |
| PBS-TX | PBS-Triton X-100 |
| PHA | PHA-767491 |
| PI | Propidium iodide |
| PKIS | Published Kinase Inhibitor Set |
| PR | Progesterone receptor |
| Pre-RC | Pre-replication complex |
| Pre-IC | Pre-replicative initiation complex |
| Rb | Retinoblastoma |
| Rpm | Revolutions per minute |
| RT | Room temperature |
| S40/41 | Serine 40/41 |
| siRNA | Small-interfering RNA |
| siSCR | Scrambled siRNA |
| ssDNA | Single-stranded DNA |
| SDS | Sodium dodecyl sulfate |
| STAU, Stau | Staurosporine |
| TC | Tissue culture |
| TetR | Tetracycline repressor |
| v/v | Volume/volume |
| XL | XL413 |
| w/v | Weight/volume |
| WT | DBF4 wild-type cell line |

# Author’s Declaration

I, Huong Quach Thi Thu, hereby declare that I am the sole author of this thesis and that I have not obtained a degree in this University or elsewhere on the basis of any of this work. All published or other sources of materials have been acknowledged within the context or in the References section.

_____

Huong Quach Thi Thu

# Acknowledgements

First of all, I would like to thank my supervisor, Prof. Corrado Santocanale, for all of his great help and his guidance to overcome the difficulties during my PhD, especially his invaluable suggestions to improve my thesis. (Thanks a lot, Corrado).

I would especially want to thank Prof. Afshin Samali, Prof. Kevin Sullivan, Dr. Andrew Flaus and all of my GRC committee for their kindness to help me when I was in trouble (I would never forget all of your help).

I hope to say thank to Dr Michael Rainey, Dr Guan-nan Wang, Kevin, Gemma, Dr Alessandro Natoni, Edel, Aisling, Rachel and other members of Corrado's lab for their help during my PhD. They are important parts of my busy PhD life. (Miss you, guys).

I would like to thank Dr Michael Carty and Prof Marco Muzi Falconi who spent time on carefully reading my thesis and gave me a lot of interesting questions and suggestions during my viva and thesis correction (Best wishes for you).

I would like to send my thanks to my friend Ricky Connolly for his support. Even he was very busy and being far away but still always agreed to help me. I also want to thank Ashla Ward, Chinatsu and other friends in Biochemistry and Biomedical Sciences for their kind support. (Wish you all the best).

A special thanks to my dear boyfriend, Aaron O'Reilly, who is always next to me, listen to and encourages me. (Love you, Aar. And congratulations for your ni-dan, sensei ^^).

I also want to say thank to my friends in Aikido club, specially Declan Clarke. I'm lucky to be his student and also his friend. (Thank you very much, Declan).

Last but not least, I would like to thank my parents, my aunt Huong, my best friend Oanh, Thu, Ngoc and other friends who always believe on me and support me. (Con xin cảm ơn bố mẹ, cô Hương và cả nhà đã luôn ở bên cạnh con, tin tưởng và động viên con những lúc con khó khăn nhất. Cảm ơn em Oanh đã luôn ở cạnh chị và ủng hộ chị. Cảm ơn các bạn đẹp đã luôn ở cạnh tớ và rủ tớ đi mỗi khi tớ bị stress nha).

Finally, I would like to thank Molecular Medicine of Ireland (MMI) who gave me the chance to make my dreams come true. I also want to thank National University of Ireland, Galway that sponsored me during my PhD and my thesis writing.

# Abstract

CDC7 plays a role in DNA replication initiation and cell cycle regulation. Inhibition of CDC7 kinase by siRNA triggers a p53-independent apoptotic cell death in cancer cells but not in human fibroblast suggesting this Ser/Thr kinase as one of potential therapeutic targets for cancer treatment. To investigate the role of CDC7 kinase activity in DNA replication and cell cycle progression, we employed small molecule CDC7 inhibitors XL413 and PHA-767491 in testing the biological effects on human cell lines. We also performed high-throughput screenings with the Public Kinase Inhibitor Set (PKIS) for the purpose of finding a potential kinase inhibitor that is potentiated by XL413 or the knock-out of CDC7 regulatory subunit DBF4. Finally, we generated stably expressing TREx-293 cell lines to characterise the phenotype of overexpressing DBF4 and its fragments in human cells and to detect novel DBF4 interactors.

We found that XL413 does not affect the cell growth of MCF10A but slightly restrains cell proliferation of MDA-MB-231 during a long-term treatment. XL413 delays S-phase but no effect on replication fork progression was observed. In contrast, PHA-767491 blocks DNA synthesis and prevents cells from going through mitosis to enter the next cell cycle suggesting a potential inhibitory effect of combination of kinase inhibitors. PKIS screening performed in the presence of XL413 and in the absence of DBF4 revealed several potential kinases which are involved in controlling cell proliferation. PLK1 was identified as one of those candidates. Inhibition of PLK1 causes a blockade in G2/M-phase and apoptosis. However, cells lacking DBF4 become less sensitive to PLK1 inhibition suggesting an unknown role of CDC7-DBF4 in humans. The overexpression of DBF4 or its domains does not affect cell cycle progression nor cell proliferation of TREx-293 cells. Two new DBF4 interactors were found.

In summary, XL413 and PHA-767491 have distinct biological effects on human cells. PKIS screenings revealed potential kinase inhibitors that are potentiated by CDC7 inhibition. The lack of DBF4 enhances the drug resistance of human cells to PLK1 inhibitor BI2676. Novel DBF4 interactors were identified.

# Chapter 1: Introduction

## 1.1. Cell cycle

The cell cycle is composed of a series of stages by which a parental cell can grow and divide into two daughter cells. Depending on the cell type, a diploid cell can enter the mitotic cell cycle to produce two identical diploid daughter cells or the meiotic cell cycle to generate four germline haploid cells. During cell proliferation, cells can exit cell cycle at any stage to enter quiescence or senescence.

### 1.1.1. G0-phase

Under specific cell growth condition, cells either exit cell cycle and stay reversibly in quiescence (G0) or irreversibly in senescence. Quiescence or G0-phase is commonly triggered when growth conditions are unfavourable. Cells are able to re-enter the cell cycle at any time once those conditions are bypassed. In metazoans, quiescence is also required to arrest the growth of organism when it reaches its optimal size. In the human body, most cells at any given time are in G0-phase, but this transient state varies because each organism has a different optimal size (reviewed in [1,2]). Similar to quiescence, senescence is a state where cells have arrested the cell cycle. However, this state is permanent and irreversible. Senescence is required to eliminate unnecessary cells during tissue remodelling and embryonic development, or as part of a response to tissue damage (reviewed in [3]).

### 1.1.2. Mitotic cell cycle

In a mitotic cell cycle, cells synthesise DNA in S-phase and divide in M-phase. Between those stages, cells have G1- and G2-phase as preparation gaps (discussed later). The duration of a mitotic cell cycle varies between species. A typical human cell has a doubling time of 24 hours, in which S-phase occurs within 8 hours. Meanwhile, a budding yeast cell only needs 90 minutes [4]. It is critical for cells to reach their optimal size at each stage, i.e. double in size prior to cell division [5].

#### 1.1.2.1.G1-phase

Entering a cell cycle or exiting into quiescence, cells require external factors such as extracellular growth signals and internal signals such as CDKs to decide and pass through the restriction point START in yeast or the R point in metazoan during G1-phase [6]. In yeast, the START checkpoint in late G1-phase is sensitive to nutrient levels [7]. In mammalian cells, the restriction (R) point occurring in early G1-phase is stimulated by growth factor signals. The R point controls the decision to proceed with the cell cycle or to enter a senescent state [8].

However, in a study of Spencer *et al.*, the authors suggested that the decision could occur during the G2-phase of the previous cell cycle and was mainly dependent on mitogen-induced Ras and CDK2 activity [9]. The absence of mitogens, inhibition of mitogen-activated proteins, or CDK2 inhibition could block S-phase progression of the next cell cycle, suggesting that the decision to engage in cell division may be even made before cells enter G1-phase.

#### 1.1.2.2.S-phase

After entering S-phase, DNA replication occurs with many steps including licensing, initiation, elongation and termination. Each step is strictly regulated to assure that there is no DNA re-replication (discussed further).

#### 1.1.2.3.G2-phase

In G2-phase, cells continue to grow and synthesise proteins required for M-phase. One of them is cyclin B (CycB). During this phase, CycB concentration increases and peaks at early mitosis. In human cells, CycB first accumulates in cytoplasm, then is transported to the nucleus, suggesting that mitotic entry is also regulated by the transportation of this B-type cyclin. By binding to CDK1, CycB can activate this kinase and trigger initiation of mitosis. During G2-phase, DNA damage is detected and repaired before cells enter mitosis (reviewed in [10]).

#### 1.1.2.4.M-phase

The M-phase of the mitotic cell cycle is subdivided into 6 stages: prophase, prometaphase, metaphase, anaphase and telophase and cytokinesis. In brief, at prophase, replicated chromosomes condense, and the mitotic spindle is formed and assembled between two centrosomes. The nuclear envelope breaks down at the beginning of prometaphase, leading to the binding of spindle kinetochores to the chromosomes. During metaphase, the microtubule-attached chromosomes are aligned. The sister chromatids separate as two sets of daughter chromosomes and are pulled slowly toward two opposite spindle poles in anaphase, then start to decondense during telophase. The nuclear envelope reassembles around each set and forms two new nuclei. Finally, the cytoplasm is divided into two by a contractile ring and two new daughter cells are formed during cytokinesis (reviewed in [11]).

#### 1.1.2.5. Regulation of mitotic cell cycle by CDKs and CDC7 activity

The cell cycle requires a control system to ensure that each step is performed properly and with the right timing. For example, during G1-phase there is a restriction point by which cells must sense that they have enough materials to commit to cell replication. If not, cells will stay in G0-phase until they are ready. Similarly, cells have S- and M-phase checkpoints which are required to assure that cells can duplicate DNA and all DNA damage is properly repaired prior to mitosis. CDKs and CDC7 play a main role in this control system.

In budding yeast, a single Cdc28/CDK1 human homolog can bind to different classes of cyclins and govern cell cycle events [12,13] (Table 1.1). Cdc28 and Clb5/6 form an S-phase promoting factor (SPF) complex that is maintained in an inactive state by activity of CDK inhibitor Sic1. During G1/S transaction, Sic1 is degraded by the activity of Cdc28-Cln1/2 promoting the activation of S-CDK and the S-phase progression. Lack of S-specific cyclins Clb5/6 does not prevent the occurrence of S-phase as other B-type cyclins such as Clb1-4 can substitute later for this absence [14].

Meanwhile in vertebrates, there is a diversity of CDKs and cyclins, mirroring the complexity of the eukaryotic cell cycle. There are at least four major CDKs including CDK1, 2, 4 and 6 and four types of cyclins A, B, D and E [11,15]. Cyclins are known as regulatory subunits of CDKs, but their interactions are not strictly specific. A CDK can be activated by different cyclins, e.g. CDK2 with CycA and CycE, and *vice versa*, a cyclin can form a complex with multiple CDKs, e.g. CycD with CDK4/6 (Table 1.1).

**Table 1.1 Roles of cyclins and their CDK partners in a cell cycle**

Table adapted from [11,16].

| | Vertebrate | | Budding yeast | |
|---|---|---|---|---|
| Cyclin-CDK role | Cyclin | CDK partner | Cyclin | CDK partner |
| G1-CDK | CycD (D1, D2, D3) | CDK4, CDK6 | Cln3 | CDK1* |
| G1/S-CDK | CycE | CDK2 | Cln1, 2 | |
| S-CDK | CycA | CDK2, CDK1* | Clb5, 6 | |
| M-CDK | CycB (B1, B2) | CDK1* | Clb 1, 2, 3, 4 | |

*(*) CDK1 has different names in different species: CDC2 in vertebrate and fission yeast and Cdc28 in budding yeast.*

To regulate CDK activity, in addition to cyclins, the role of CDK-activating kinase (CAK) was identified. The binding of cyclins triggers the release of a protein loop at active site of CDK, hence partially activating CDKs. CAK is a kinase that can phosphorylate CDK to induce a conformational change in CDK structure, increasing CDK kinase activity [11]. During the cell cycle, CDK levels are mostly constant, but cyclin expression varies. The induction of cyclins through gene expression and their degradation by proteolysis are main mechanisms of cell cycle regulation [17].

In G1-phase, upon receiving mitogenic signals, transcription regulatory factor Myc is activated leading to the upregulation of G1-phase cyclin CycD. Subsequently, CDK4/6 is activated and phosphorylates retinoblastoma (Rb), a tumour suppressor that is critical in G1/S transition. The hyperphosphorylation of Rb occurring later in G1-phase inactivates this protein and allows the release of transcription factor E2F triggering the expression of E2F-targted genes, including G1/S-phase cyclin CycE. Rb also stabilises CDK inhibitor (CKI) $p27^{Kip1}$ and protects this CKI from

ubiquitination by binding the S-phase kinase-associated protein 2 (Skp2). The inactivation of Rb and the increase of CycD level mediates the sequestration of $p27^{Kip1}$ aiding in the activation of CDK2. In a positive feedback loop, CDK2-CycE phosphorylates Rb and fully liberates E2F resulting in the expression of genes required for S-phase, i.e. S-phase cyclin CycA and the activation of S-CDK. The CDK2-mediated phosphorylation Rb enables cells to pass through the restriction point R and to enter S-phase in a growth factor-independent manner [6,18–21] (Figure 1.1).

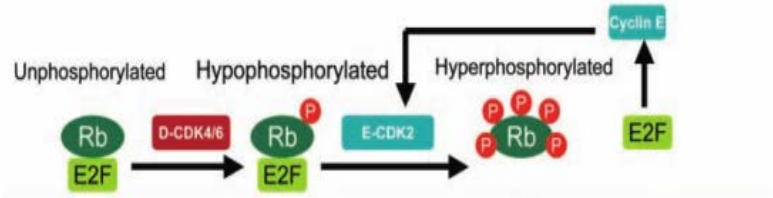


**Figure 1.1 Regulation of G1/S transition by CDK activities**
Details were described in the text. Figure adapted from [6].

During S-phase, CDKs are required to promote DNA replication by phosphorylating MCM complexes and to prevent DNA re-replication by regulating licensing proteins. This CDK-mediated phosphorylation of MCMs is involved in activating the pre-replication complex (pre-RC) to initiate DNA replication. At the G1/S transition, S-CDKs trigger the ubiquitin-mediated degradation of cell division cycle 6 (CDC6) and nuclear export of Chromatin licensing and DNA replication factor 1 (CDT1) in budding yeast. In contrast, the CDK-mediated phosphorylation is required for the proteolysis of CDT1 and the transport of CDC6 into cytoplasm in higher eukaryotes [16].

To enter mitosis, CDKs and PLK1 activities are required. During G2, M-phase cyclin is induced and binds to CDK1, forming a Maturation-Promoting Factor (MPF) complex that can stimulate the M-phase entry of the mitotic cell cycle. MPF is kept inactive by the inhibitory phosphorylation of Wee1 until the activation of CDC25A phosphatase, triggered by PLK1 activity. CDC25A removes the inhibitory phosphorylation of CDK1 leading to an increase in G2/M-CDK activity. Subsequently, CDK1 activates CDC25A and inactivates Wee1, promoting mitotic entry (reviewed in [10,22,23]).

CDK1-cycB is one of the main regulators of M-phase. During early M-phase, M-CDK mediates the phosphorylation of APC/C subunits and facilitates the binding of CDC20 to activate anaphase promoting complex/cyclosome-CDC20 ($APC/C^{CDC20}$). In parallel, M-CDK phosphorylation prevents CDH1 from APC/C binding maintaining the major part of $APC/C^{CDC20}$. At late M-phase, $APC/C^{CDC20}$ triggers the degradation of CycA and B through ubiquitination leading the release of CDC20-homologue 1 (CDH1) from CDK1 regulation and the binding of CDH1 to APC/C. By targeting CDC20, $APC/C^{CDH1}$ promotes mitotic exit and keeps its major role until G1-phase of the next cell cycle. During this, CDK inhibitors (CKIs) are stabilised to maintain a low kinase activity of CDKs in G1-phase (reviewed in [16]). Once G1/S-phase cyclins are induced due to the activation of growth signals, G1/S-CDK activity inactivates $APC/C^{CDH1}$. S- and M-phase cyclins then accumulate and CKIs are inhibited, leading an increase in S-CDK activity and the initiation of DNA replication. $APC/C^{CDH1}$ activity is blocked by Emi1 in S- and G2-phase (reviewed in [24]).

In addition to CDKs, CDC7 also plays a role in regulating the cell cycle, mainly by activating the pre-RC complex during S-phase (discussed later).

### 1.1.3. Meiotic cell cycle progression and regulation

Meiosis begins with a diploid cell that undergoes DNA replication (meiotic S-phase) but then undergoes two separate cycles (meiosis I and II) of nuclear division to produce four haploid daughter cells [11] (Figure 1.2).

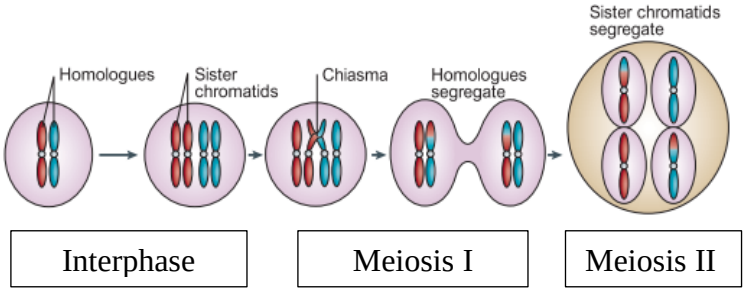


**Figure 1.2 Meiotic cell cycle progression.**
The cell duplicates its chromosomes in meiotic S-phase, sister chromatids are produced and tightly linked to each other by cohesion activity. During meiosis I, the crossover of duplicated homologues (chiasma) is required to hold two non-sister chromatids leading to DNA recombination. Afterwards, each pair of homologues lines up on the spindle and segregates to opposite poles during the first meiotic anaphase, forming two diploid daughter nuclei. In the meiosis II, sister chromatids line up and are pulled apart to produce two haploid daughter nuclei, resulting four haploid nuclei after one complete meiotic cycle. Figure adapted from [25].

To enter the meiotic cell cycle, cells require some regulators that are different from the mitotic cell cycle. In budding yeast, two critical meiotic inducers, inducer of meiosis 1 (IME1) and inducer of meiosis 2 (IME2), were identified. During the G1/S-phase transition, IME1 is a transcription factor that is involved in regulating the transcription of meiotic regulators, including IME2, a serine threonine kinase with a sequence homology related to CDC28. IME2 is able to trigger the degradation of CDK inhibitor Sic1 that blocks meiotic S-phase entry [14]. IME2 also inhibits the ubiquitin-mediated proteolysis of APC/$C^{CDH1}$ leading to the stabilisation of B-type cyclins Clb5 and Clb6 to facilitate chromosome segregation [26].

In fission yeast, entry into the meiotic cell cycle requires activation of the RNA-binding protein involved in meiosis 2 (Mei2) that is blocked by the activity of Pat 1 kinase. The expression of Pat1-inhibitor Mei3 in response to meiotic-induced conditions releases the repression and triggers the initiation of meiotic cell cycle (reviewed in [25]).

In pre-meiotic S-phase, S-CDKs and CDC7 play a critical role in regulating the progression similarly in pre-mitotic S-phase. In budding yeast, the same replicative

machinery is used, and replication forks progress at similar rates; CDC7-DBF4 and S-phase CDKs Cdc28 in complex with B-type cyclins Clb5 and Clb6 are required to initiate DNA replication. However, pre-meiotic S-phase is longer than pre-mitotic S-phase presumably due to the preparation for DNA recombination in meiosis [27]. Additional factors such as muddled meiosis 2 (MUM2) is essential for pre-meiotic but not for pre-mitotic S-phase because it is required for the interaction between homologue pairs before their segregation during meiosis I [28].

In meiosis I, homologue pairs are formed as a four-chromatid structure (called bivalent). Cells establish meiotic recombination by producing chiasmata or cross-over between non-sister chromatids of the bivalent [11]. This process is essential to hold homologue pairs together and it initiates after the occurrence of double-stranded breaks (DSBs) triggered by Spo11 [29]. S-CDKs and CDC7 are involved in controlling DSBs by phosphorylating Mer2, one of critical proteins that regulate Spo11 activity and recruit other essential components of the Spo11-complex to chromatin, e.g. Rec114 (reviewed in [30]). However, DSB formation may cause severe DNA damage, hence, a surveillance system i.e. pachytene checkpoint is activated to ensure that DNA damage is repaired properly prior to the chromosome segregation [31].

To transit to meiosis II, the inhibition of $APC/C^{CDC20}$ and the retention of intermediate to modest level of CDK1 activity at the end of meiosis I are required to suppress DNA replication in *Xenopus*. After meiotic I exit, CDK1 is reactivated with the synthesis of B-type cyclins to promote the meiosis II entry [32,33]. However, a low level of CDK activity is critical in promoting chromosome segregation during anaphase I and spindle disassembly in budding yeast [34].

Finally, in meiosis II, chromosome segregation resembles mitosis with the activity of separase in cleaving cohesion Rec8 and triggering the separation of sister chromatids (reviewed in [25]). To exit mitosis, the inactivation of CDKs is critical to allow cells resetting in G1-phase. In budding yeast, phosphatase Cdc14 regulates CDKs inactivation by mediating the dephosphorylation of $APC^{CDH1}$ leading to the degradation of M-phase cyclins Clb. In addition, Cdc14 mediates the dephosphorylation of Sic1 leading to the stabilisation of this Clb-CDK inhibitor.

Cdc14 also dephosphorylates the transcription factor Swi5 allowing the activation of Swi5-dependent transcription of *sic1* gene. Noticeably, Cdc14 activity is controlled by Mitotic Exit Network (MEN) and by Cdc Fourteen Early Anaphase Release (FEAR) network, suggesting the key roles of Cdc14 and other components of those networks in promoting mitotic exit [35].

## 1.2. Origins, timing and progression of replication

### 1.2.1. Origins and timing of replication

#### 1.2.1.1. Identification of replication origins

##### 1.2.1.1.1. In yeast

In budding yeast, origins are autonomously replicating sequences (ARSs) that initiator proteins bind to, promoting the establishment of replication forks. ARSs contains one essential element, named as domain A, that has an AT-rich content with an ARS consensus consequence (ACS) of 11 or 17 bps and that is recognised by origin recognition complex (ORC) [36–38]. Being adjacent to domain A, domain B with subdivided units B1, B2 and B3 contributes to the origin function. Domain B1 promotes ORC binding, while domain B2 is proposed to be a binding site of MCM2-7 helicase and domain B3 can be bound by ARS-binding factor 1 (ABF1) that is involved in transcription process and nucleosome assembly [37,39,40] (Figure 1.3).

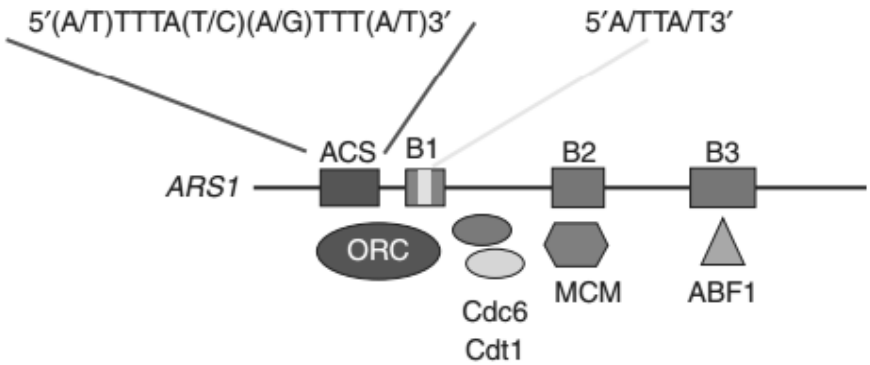


**Figure 1.3 Structure of a replication origin in budding yeast**

ARS1 origins contains an A domain (ACS) and three B domains B1, B2 and B3. Each domain is specifically bound by proteins involved in initiating DNA replication as indicated. Figure take from [40].

In fission yeast, origins are AT-rich regions, except *S.japonicus* cells that have GC-rich content origins. Lacking of core consensus sequence, origins of fission yeast still harbour several functional DNA elements that are essential for their activities and maintains two conserved characteristics: being bound by ORC and located at nucleosome depleted regions [41,42].

#### 1.2.1.1.2. In *Xenopus* and Drosophila

At the early development of *Xenopus* and Drosophila embryo, DNA replication initiates at many sites at the same time to adapt to the requirement of the fast pace of cell division. Origins are formed and fired randomly (reviewed in [43]). In higher differentiated cells of Drosophila, replicative initiation generally occurs at specific sites, one of which is within the promoter region adjacent to *dE2F* gene suggesting a potential correlation between transcriptional activity and origin formation [44,45]. Drosophila ORC also binds to AT-rich and negatively supercoiled sequences with a higher affinity suggesting DNA topology affects the binding of ORC to DNA [46,47].

#### 1.2.1.1.3. In vertebrates

In metazoans, some features of replication origins have been identified. There are more origins than needed that are assembled in each cell cycle. Hence, cells have a flexible choice of origins for firing [48]. Replication origins have three levels of organisation. At the first level, the potential replication origin is identified by the assembly of pre-RC complex. Next, a cluster of origins forms replicon as a replication unit. Finally, an association of replicon clusters establishes a stable chromatin structure named replication domain or replication foci [49]. Nonetheless, no common consensus sequence has been reported except specific sequences identified in β-globin or lamin B2 origins (reviewed in [50]). Recently, some studies found that unmethylated CpG islands are strongly associated with replication origins. Interestingly, a specific G-rich sequence named Origin G-rich Repeated Elements (OGRE) was found at the upstream of DNA replication initiation sites. OGRE is present in 90% of origins in mouse and human cells suggesting this element is a good predictor of origins in mammalian cells [48,51].

Furthermore, the association between transcription and replication is also considered as an important feature of replication origins. In human erythroleukemic cells, an upstream region of β-globin gene named the locus activation region (LAR) containing binding sites for transcription factors is critical for regulating DNA replication initiation from the β-globin origin by establishing an early replicating chromatin structure [52]. Similarly, c-myc is involved in firing replication origins through remodelling of chromatin [53,54]. The overexpression of c-myc triggers excessive origin firing leading to DNA damage or accelerated S-phase while the deficiency of this transcriptional factor results in a prolonged S-phase [55].

Finally, nucleosome positioning is critical to define origins in different species [56,57]. In budding yeast, a nucleosome depleted region (NDR) is found to be adjacent to domain A and flanked on both sides by arrays of nucleosomes which are required for stabilisation of ORC binding to NDR. However, in fission yeast, the existence of NDR in replication origins is still in discussion [58]. The NDR is also observed in human and Chinese hamster origins suggesting its role in predicting replication origins of metazoan, but not for stabilising ORC binding or nucleosome repositioning [58–60].

#### 1.2.1.2. Timing of replication

##### 1.2.1.2.1. Replication timing domain

At each cell cycle, not all origins are activated at the same time. Cells have a temporal replication programme by which DNA replication initiation occurs at specific time in different regions of genome. Replication timing domain is a replicating region in chromosomes where origins are fired at similar times, e.g. early or late replicating domains [61] (Figure 1.4). Interestingly, analyses of replication timing revealed a strong conservation of replication timing domain between close species, even though the regulation of replication timing has not been well understood [62].

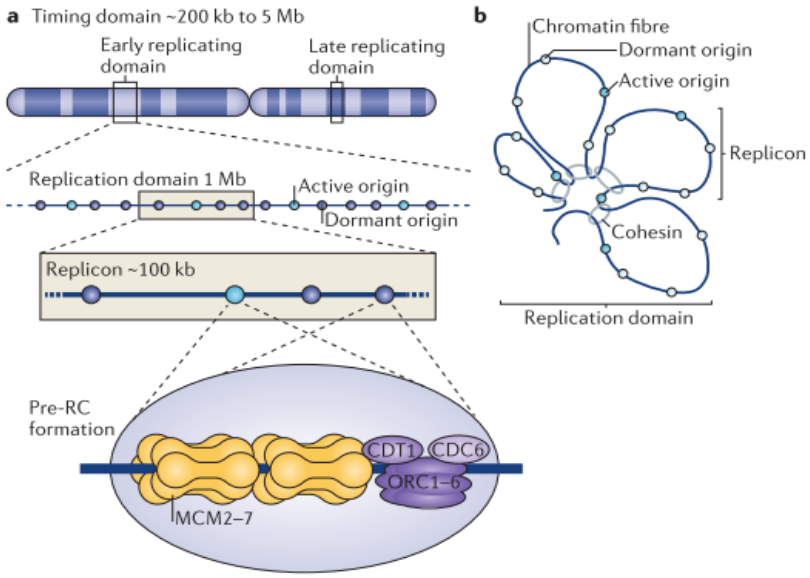


**Figure 1.4 Organisation of origins in replication timing domain**

A timing domain identifies a chromosomal region that have a similar time of replication, either early (early replication domain) or late (late replicating domain). In each timing domain, there are replication domains composed of replicons. At both active and dormant origins, pre-RC complex is still formed with the assembly of ORC1-6 complex, MCM2-7 double hexamer, CDT1 and CDC6. (a) Replication origins are organised at different levels (b) Structure of a replication domain. Figure taken from [63].

#### 1.2.1.2.2. Regulation of replication timing

In budding yeast, the replication timing is determined prior to S-phase [64]. A timing decision point (TDP) identified in early G1 prior to the restriction point confirms this observation in mammalian cells. Notably, this decision point is made prior to the origin decision point (ODP) by which specific origins are selected, indicating that the replication timing is regulated independently and timing patterns are more strongly conserved across species than the origins location [65]. A correlation between replication timing, chromatin reorganisation and the transcriptional potential was also revealed [61,66] (Figure 1.5). .

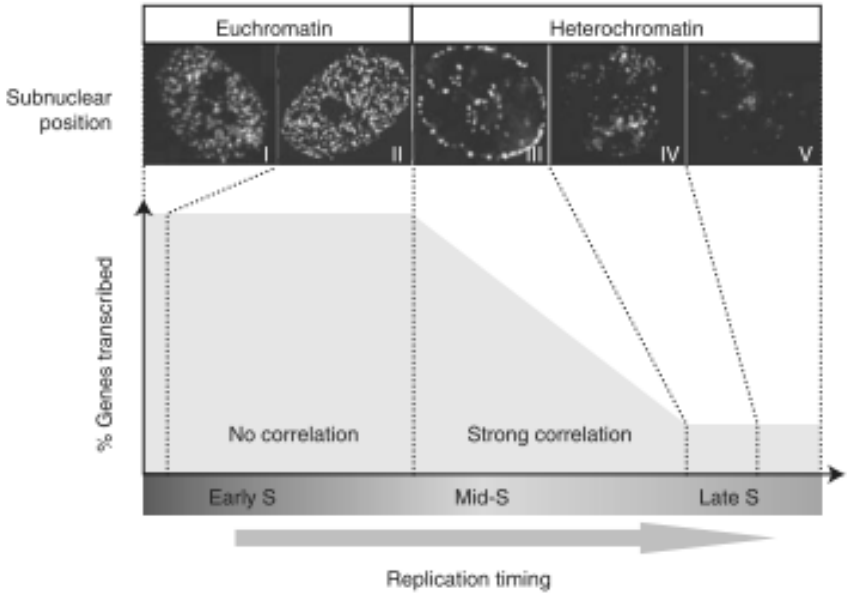


**Figure 1.5 Correlation between gene density and replication timing**

The replication of early S-phase occurs within euchromatin (subnuclear position pattern I, II), meanwhile later replication of mid and late S-phase occurs within heterochromatin (subnuclear position pattern III, IV and V), indicating that the change of replication timing strongly correlates with the reorganisation of chromatin structure. In addition, the change of replication timing only accompanies with transcription in the mid S-phase but not in early S-phase suggesting a correlation between the percentage of transcribed genes and the replication timing. Figure taken from [67].

To explain, heterochromatin enforces late replication by preventing the recruitment of initiation factors to origins. In fission yeast, centromeric chromatin which is frequently transcribed replicates early while most heterochromatin which is more condensed and rarely transcribed usually replicates in the late S-phase [68]. The interaction between Swi6 and Hsk1/CDC7 through the HP1-binding motif in Dfp1 / DBF4 recruits CDC7-DBF4 to the heterochromatic pericentromeric region, stimulates replication factor Sld3 and triggers the early replication of centromere [69].

In addition, the timing of ORC binding to replication origin during M and G1-phase contributes to the timing of origin firing in S-phase. In Drosophila, ORC location was found in specific regions that are coincide with early replication areas [47]. In fission yeast, origins with earlier ORC binding will fire earlier in S-phase. The delay of ORC

binding may affect the chromatin loading of CDC45 leading to the limitation of CDC45-MCMs-GINS complex formation and the inefficient origin firing [70].

#### 1.2.1.2.3. Dormant origins

In eukaryotic cells, only 10% of licensed origins are fired, whereas 90% remain as dormant origins. In unperturbed condition, dormant origins are not selected as primary origins for replication initiation. They only serve as a back-up to ensure the completion of genome duplication under replication stress (reviewed in [71]). Noticeably, a study found that the change of nucleotide pool size affects the selection of replication origin site for initiation. When cells were grown in A+U-enriched medium, the fork progression rate increased and replication initiation mainly occurred in primary replication sites. Meanwhile, the decrease of nucleotide pool due to HU treatment resulted to a decrease of replication fork progression rate and an increase of initiation events in secondary replication sites, i.e. dormant origins [72]. The establishment of replication machinery at new replication origins is restricted to ensure that DNA synthesis at activated origins completes before the replication of new regions occurs (reviewed in [73]). At the same time, DNA damage checkpoint kinases may be activated to facilitate DNA repair at stalled fork sites (Figure 1.6).

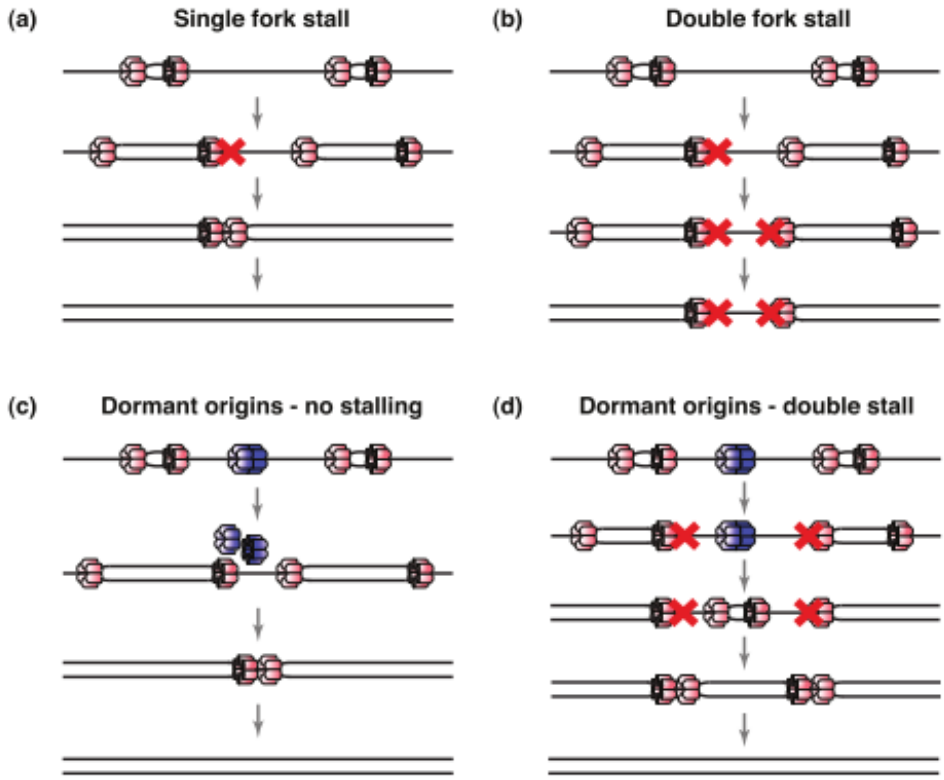


**Figure 1.6 Dormant replication origins**

(a) When a single fork stalls, DNA is replicated from the forks fired from adjacent origin. (b) Without dormant origins, double fork stalls and DNA replication temporarily ceases at stalled site. (c) In the presence of dormant origins, where MCMs complex is inactive (in blue colour), the double replication fork progresses as normal and inactivated MCMs of dormant origins are released. (d) If double fork stall occurs, dormant origins start to be fired with a replication fork progresses in bi-directional way and completed DNA replication. Figure taken from [73].

### 1.2.2. DNA replication progression

#### 1.2.2.1.Initiation

DNA replication initiation is divided into three steps: the recognition of replication origins by ORC, the recruitment of MCMs to ORC-binding site by CDC6 and CDT1 and the formation of bi-directional replication fork [74].

To prevent DNA re-replication, CDKs activities are strictly regulated along two states of cell cycle. In the first state, cells have low CDK activity. The pre-RC assembled but inactivated. In the second state, CDK activity raises up which allows the activation of pre-RC complex and replication initiation but also prevents the assembly of new pre-RC. Those two states exist to ensure that no replication origin can be initiated more than once per cell cycle (reviewed in [24].

#### 1.2.2.1.1. Origin recognition

ORC binds to replication origins in a ATP-dependent manner [75]. To recognise replication origins, ORC has some features to adapt the origin structure of different species, such as ORC containing AT-hook domains at N-terminal end in fission yeast [76]. In yeast, ORC is maintained on chromatin throughout the cell cycle, and recruits CDC6 to the origin during G1-phase. In humans, ORC1 binds to chromosomes during mitosis, promotes the assembly of ORC during the next G1-phase and is degraded in the S-phase entry [77,78].

#### 1.2.2.1.2. Pre-replication complex (pre-RC) assembly

At the end of mitosis, after the binding of ORC to replication origins, MCMs complex is loaded onto chromatin with the aid of ORC, CDC6 and CDT1 to form an ORCs-CDT1-CDC6-MCMs (OCCM) or pre-RC complex (Figure 1.7). The destruction of cyclin B are required for the loading of MCMs suggesting that mitotic kinase activity is critical in preventing the formation of pre-RC complex until late mitosis [79]. After the pre-RC establishment, CDC6 is rapidly released from chromatin, and may be degraded by an ubiquitin-dependent proteolytic pathway, which is activated by CDK2 in *Xenopus* [80]. In humans, MCM2 and MCM4 have a transient interaction with chromatin in telophase. This binding quickly becomes stable in early G1-phase of the next cell cycle and a majority of MCMs are recruited to chromatin prior to G1/S-transition [81].

In yeast, MCMs are proposed to have open-coil structures in which six subunits of MCM complex are composed in a left-handed helical manner with an open gap between MCM2 and MCM5. CDT1 promotes the stability of this hexamer by wrapping around the N-terminal domains (NTDs) of MCM2, MCM4 and MCM6 before the complex is recruited to the replication origin by ORC-CDC6 to form OCCM or pre-RC complex. After the loading of the first MCMs, CDT1 is released from the complex. The second hexamer is recruited and forms a tight junction with the first complex. During the formation of double hexamer, two coiled springs are compressed to store energy that is required for origin melting and the extrusion of single-stranded DNA (ssDNA) through the MCM2-MCM5 gate (Figure 1.7).

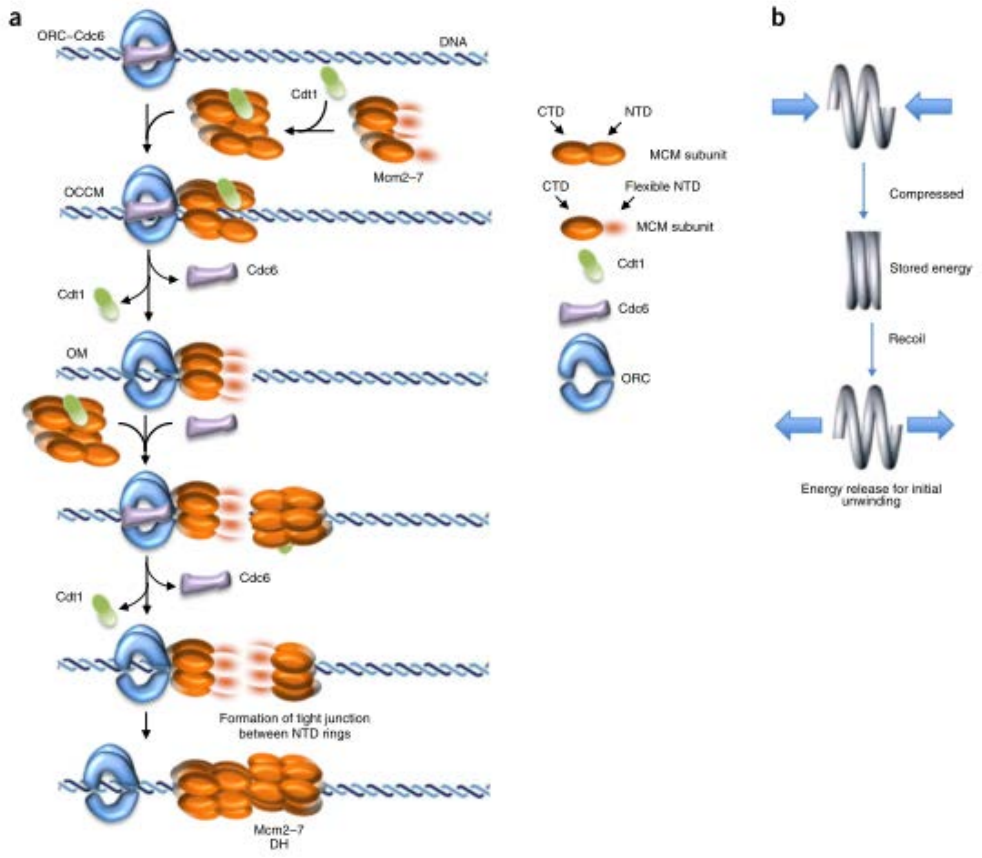


**Figure 1.7 A proposed model of the pre-RC assembly in eukaryotes**

(a) CDT1 binds to NTDs of MCMs complex and induces a conformational change that promotes the recruitment of MCMs to origins and the formation of ORC-CDC6-CDT1-MCMs (OCCM) complex or pre-RC complex. Afterwards, CDC6 and CDT1 are released leaving MCMs complex bound to origins with a flexible NTD. This supports the recruitment of the second CDT1-MCMs complex to the first MCMs. By releasing CDT1, the second MCMs hexamer can tightly bind to the first one with a junction between NTD rings and form a compressed MCM double hexamer coil (b) This compression requires energy and stored energy will be used to melt dsDNA at origin during initiation DNA replication. Figure taken from [82].

#### 1.2.2.1.3. Pre-initiation complex (pre-IC) assembly

After the formation of pre-RC complex, CDKs and CDC7 phosphorylate MCMs complex to activate the helicase activity leading to the unwinding of dsDNA at replication origin and the recruitment of additional factors such as CDC45 and GINS to establish the CDC45-MCMs-GINS (CMG) or pre-IC complex (Figure 1.8).

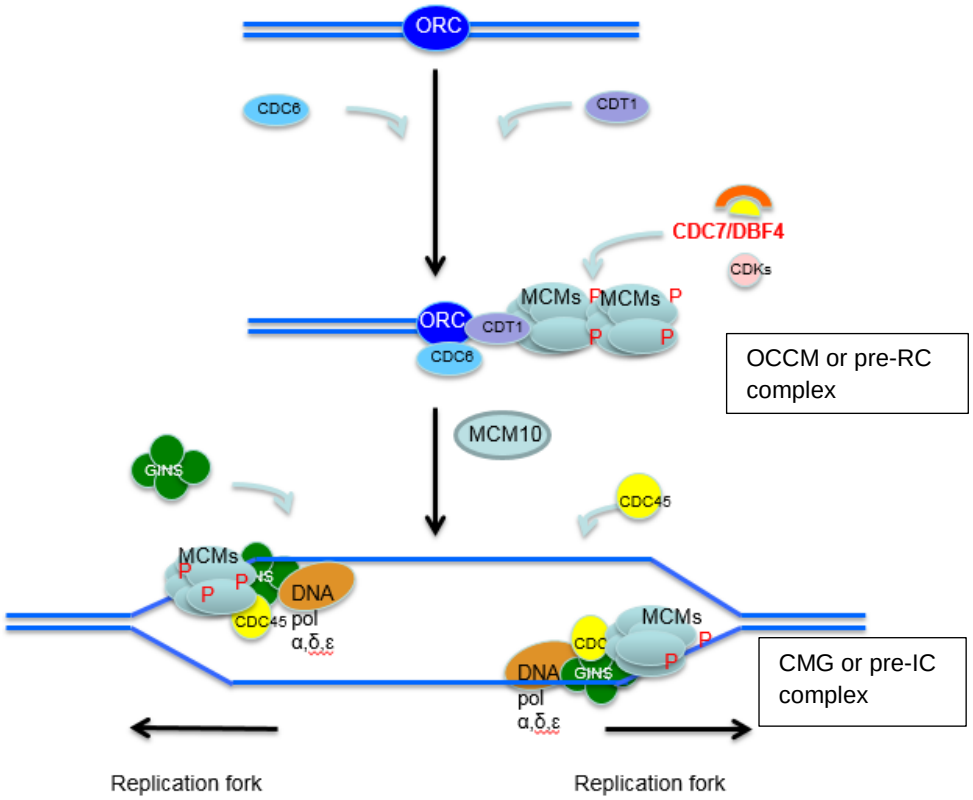


**Figure 1.8 Initiation DNA replication in eukaryotes**

Upon the recruitment of MCMs double hexamer to origins, S-CDK and CDC7-dependent phosphorylation are required to activate this complex and to recruit additional factors including GINS and CDC45 to form CMG complex. Afterwards, MCM10 activity facilitates the separation of double hexamer MCMs to promote origin unwinding mediated by CMG. Finally, replication forks are formed and DNA elongation occurs in bi-directional way. Figure adapted from [83–85].

*In vitro* and *in vivo*, CDC7 phosphorylates MCM2 in at least three different sites, S40, S53 and S108 in which S108 is also phosphorylated by ATR, S40/41 phosphorylation peaked in late S-phase and G2, S53 phosphorylation was observed throughout S- and G2/M-phase, and levels of S108 phosphorylation appeared to be maximal in middle S-phase. CDKs also phosphorylate MCM2 at three different sites, S13, S21 and S41 but they have a constant level throughout cell cycle [86]. The phosphorylation of MCMs mediated by CDC7 is required for origin firing but not for elongation [87].

In eukaryotes, CDC7-DBF4 is required for the recruitment of CDC45 to early origins prior to the activation of S-CDK after which, the second helicase-activating protein GINS complex and other factors of the replisome are loaded [88]. Nonetheless, in a

study of Yeeles *et al.* [89], the authors found that CDC7-DBF4 can either act before or after S-CDK. If CDC7-DBF4 acts after S-CDK, the CDK-mediated re-phosphorylation of Sld2 or Sld3 after CDC7-DBF4 addition, is required to obtain a stable association between GINS and CDC45 and an efficient DNA replication.

S-CDK plays an essential role in replication initiation by phosphorylating Sld2/RecQ4 vertebrate homolog and Sld3/TICRR human homolog. In yeast, the CDK-mediated phosphorylation promotes the interaction between Sld2 and Sld3 with Dbp11/TopBP1 human homolog to initiate DNA replication (reviewed in [90]). However, in *Xenopus*, the RecQ4-TopBP1 interaction is formed in a CDK phosphorylation-independent manner [91]. Meanwhile, in human cells, CDK2-phosphorylation of TICRR is required for its interaction with BRCT-domain of TopBP1 and this phosphorylation is essential for replication initiation [92].

In humans, the formation of TICRR-TOPBP1-MTBP complex is required for integrating signals from cell cycle and DNA damage response pathway to regulate replication initiation in a p53-independent manner. MTBP depletion prevents the assembly of CMG complex during origin firing leading to the inhibition of DNA replication [93]. MTBP regulates the ubiquitin ligase activity of MDM2 which contributes to p53 levels and activity [94]. This origin firing model was proved by using purified recombinant proteins [89].

#### 1.2.2.2.Elongation

After the unwinding of dsDNA by CMG complex, nucleotide polymerisation starts in the leading and lagging strands of the parental DNA. DNA polymerase α - primase complex (Pol α) is involved in DNA replication by synthesising RNA primers, then generating RNA-DNA hybrid molecules that are elongated by the activity of DNA polymerases Pol δ and Pol Ɛ on both strands (reviewed in [95]). Pol α requires RPA to retain its stability while attaching to its primed site; then, RFC disrupts the Pol α – RPA interaction leading to the detachment of Pol α from ssDNA and the loading of PCNA to DNA through the contact with RPA [96]. Pol Ɛ is recruited to replication fork for a major role in replicating the leading strand template (5’ to 3’ end) continuously, while Pol δ mainly acts on the lagging strand (3’ to 5’ end) to synthesise short fragments of 100 - 200 nucleotides (Okazaki fragments)

discontinuously, then those fragments are joined by DNA ligase to form a single uninterrupted strand of DNA (reviewed in [97,98]).

PCNA plays the role of a moving platform for factors that act concomitantly during replication. Those factors mainly interact with PCNA through conserved PCNA interacting peptide (PIP) motif [99]. To promote elongation, PCNA is loaded onto primed DNA in the presence of RFC and by this loading DNA polymerases are oriented toward the end of the elongating DNA (reviewed in [99,100]). The switch from Pol α to replicative polymerases either on leading or lagging strands requires the binding of PCNA onto the primer terminus of the RNA-DNA hybrid [101] (Figure 1.9).

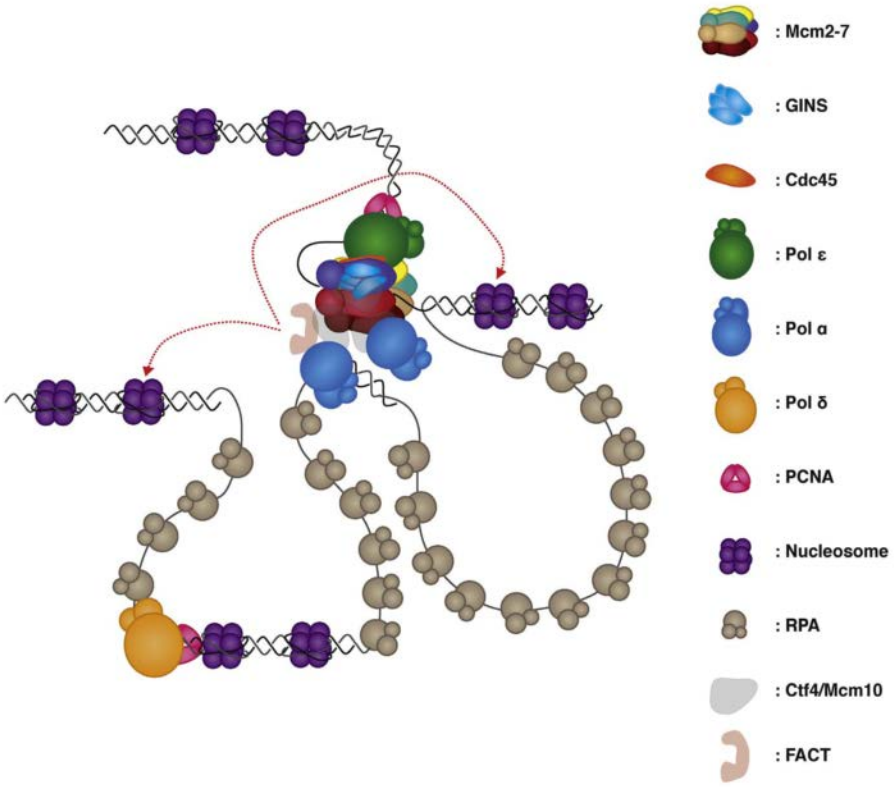


**Figure 1.9 Elongation of eukaryotic DNA**

At the replication fork, DNA polymerases Pol α, δ and Ɛ cooperate to synthesise new DNA in both leading and lagging strand template. Pol α is required to synthesise primers by which, PCNA molecules are loaded. PCNA plays a role as a sliding clamp for Pol δ and Ɛ synthesising DNA with the activity of a histone chaperone Facilitates Chromatin Transactions (FACT) in regulating the assembly of nucleosome at replication fork. Figure taken from [102].

For translesion DNA synthesis (TLS), budding yeast utilises three specific DNA polymerases including Pol η and Rev1 from the Y-family and Pol ζ from the B-family. Mammalian cells have many more polymerases which belong to A, B, X and Y-family (Table 1.2).

**Table 1.2 List of DNA polymerases and their main functions**

| DNA polymerase | Family | Main functions | Reference |
|---|---|---|---|
| α (alpha) | B | DNA replication | [101] |
| β (beta) | X | BER (bypass cdA lesion) | [103] |
| γ (gamma) | A | Mitochondrial replication and repair | [104] |
| δ (delta) | B | DNA replication and TLS (bypass APs) | [105,106] |
| Ɛ (epsilon) | B | DNA replication and repair | [101] |
| ζ (zeta) | B | TLS (discussed later) | - |
| η (eta) | Y | TLS (discussed later) | - |
| Θ (theta) | A | TLS (incorporating A opposite the AP site) and BER | [107] |
| ι (iota) | Y | TLS (bypass CPDs) | [108] |
| κ (kappa) | Y | TLS (incorporate dC opposite the adducted G) and nucleotide-excision repair (NER) | [109,110] |
| λ (lambda) | X | TLS (bypass APs) | [111] |
| μ (mu) | X | DNA repair | |
| ν (nu) | A | TLS (bypass thymine glycol) | [112] |
| Rev1 | Y | TLS (discussed later) | - |
| TdT | X | V(D) J recombination | [113] |

AP: abasic lesion; BER: Base-excision repair; CPD: Cyclobutane pyrimidine dimer; cdA: 5',8-cyclo-dA; DSB: double-stranded break; ICL: interstrand DNA crosslink NER: nucleotide-excision repair; TLS: translesion synthesis

In eukaryotic and mammalian cells, cyclobutane pyrimidine dimers (CPDs) are principal forms of UV-induced DNA lesion. Only Pol η can synthesise DNA using CPDs-containing template. This translesion polymerase has a low fidelity with a large and flexible active site that allows the accommodation of both bases of the dimer during replication [114,115]. Furthermore, Pol η also plays a role in the replication of single-base lesion DNA caused by oxidative stress in budding yeast [116].

Rev1 is a TLS polymerase that is highly specific to incorporate incoming dCTP to an apurinic/apyrimidinic (AP) site or G adducts [117,118]. However, Rev1 does not directly pair the DNA template to the incoming dCTP. This polymerase moves the template G out of the DNA helix, and coordinates it within a specialized loop. In the meantime, $Arg^{324}$ of the polymerase occupies the position of the template G and a hydrogen bond is formed between $Arg^{324}$ and incoming dCTP. By this mechanism, Rev1 bypasses the bulky G adduct and acts as a template-independent dCTP transferase [118,119].

Pol ζ lacks exonuclease activity and generally is inefficient at base insertion to opposite of DNA lesion site. However, this DNA lesion polymerase is critical at extending from mismatched primer termini and the lesions containing abnormal structures *in vivo* (reviewed in [120]). Some polymerases are good at the insertion step, including Pol ι and Rev1, and others are more efficient at extension, especially Pol ζ (reviewed in [121]).

Lesion bypass can occur in a single step by a single DNA polymerase, such as Pol η, but also in two steps when two DNA polymerases act sequentially in incorporating deoxynucleotides opposite DNA lesions with mispaired primer extension [122]. In yeast, the lesion bypass is directly regulated by PCNA through ubiquitylation: monoubiquitylated PCNA triggers the error-prone pathway and the polyubiquitylation of PCNA is required for the error free-mode of TLS (reviewed in [100]).

### 1.2.2.3.Termination.

In budding yeast, the ubiquitin ligase SCF-Dia2 promotes the disassembly of CMG helicase at the end of DNA replication. The segregase Cdc48/p97 mammalian homolog associates with ubiquitylated CMG complex mediated by SCF-Dia2 leading to the disassembly of the helicase complex [123].

In mammalian cells, termination process of vertebrates was determined and described [124] (Figure 1.10) .

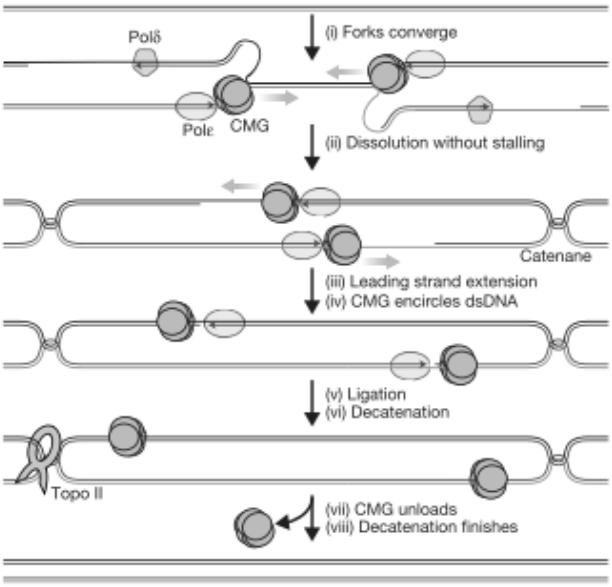


**Figure 1.10 A proposed model of termination in vertebrates**

According to this model, there is not any stalling or pausing when two forks converge and dissolute (i and ii). Leading strand extends and passes over the lagging strand of the opposing fork. The pre-IC or CMG complex continues to move along dsDNA-ssDNA junction (iii and iv). The ligation occurs in parallel with decatenation mediated by Top II activity (v and vi). Finally, pre-IC complex leaves chromatin and cells finish the decatenation (vii and viii). Figure taken from [124].

## 1.3. CDC7

### 1.3.1. Structure of CDC7

CDC7 is a Ser/Thr kinase and a member of the CK1 group in kinase family. There are 11 common kinase domains that are highly conserved in budding yeast homolog Cdc7p and fission yeast homolog Hsk1, and unique features with three kinase inserts

that are divergent between human homolog CDC7, budding yeast Cdc7 and fission yeast Hsk1 [125]. In humans, the kinase insert II and III domains of CDC7 are proposed to play a role in the nuclear import, export and retention of this protein [126]. Crystal structure study revealed that CDC7 contains an active region between its N and C lobes. This region is bound by a nucleotide and $Mg^{2+}$ and has a similar structure to other kinase-nucleotide complex [127]. In addition, authors confirmed that the C lobe harbouring the RD signature, DFG and APE motifs is critical for CDC7 activity [127].

### 1.3.2. Roles of CDC7

#### 1.3.2.1.In DNA replication

CDC7 phosphorylation of MCMs complex is critical in DNA replication initiation. In budding yeast and humans, Cdc7 phosphorylation of Mcm4 promotes the binding of Cdc45 to Mcms complex for a stable establishment of the pre-IC complex (Cdc45-Mcms-GINS). This phosphorylation also alleviates the inhibitory activity residing within the N-terminal NSD of MCM4 (called as proximal NSD) that serves as an inhibitor of origin activation. Cells lacking of this inhibitory region can grow without CDC7-DBF4, but slowly and the stability of pre-IC complex is defective [128–130]. In fission yeast, Hsk1, a homolog of CDC7, and Dfp1, a homolog of DBF4, is also able to phosphorylate Cdc19/MCM2 human homolog, Cdc21/MCM4 human homolog and Mis5/MCM6 human homolog [130–132]. Similarly, in humans, CDC7 phosphorylates MCM2 and MCM4 suggesting that MCMs are conserved substrates of CDC7 between species [86,133].

Cdc7 phosphorylates Mcm2 at S164 and S170 in yeast and the expression of Mcm2-S170A mutant is lethal in cells that lack endogenous Mcm2 [134] suggesting Cdc7-mediated Mcm2 phosphorylation is essential for cell viability of budding yeast. However, lethal effect of *cdc7* deletion can be rescued either by mutated Bob1/MCM5 human homolog at P83L or deletion of N-terminal serine/threonine rich domain (NSD) of Mcm4 in unperturbed cell cycle (discussed later).

Noticeably, a cooperation between CDC7 and CDK2 activities in phosphorylating MCM2 was observed. In a study of Montagnoli *et al.*, the authors found that CDC7-mediated phosphorylation of MCM2 at S40 requires the CDK2-mediated

phosphorylation of MCM2 at S41 [86]. Importantly, this study revealed an overlap between the kinetics of phosphorylation of MCM2 at S40/41, S53 and S108 with the fluctuation of CDC7 kinase activity, suggesting those phosphorylated sites are potential biomarkers of CDC7 kinase activity in cells. Nonetheless, it is noticed that phosphorylated MCM2 at S108 was identified as a phosphorylation site mediated by Ataxia telangiectasia and Rad3 related protein (ATR) [135] indicating an overlap function of both kinases.

In G1-phase, the activation of CDC7 kinase is limited due to the degradation of DBF4 in an APC/C-dependent manner to prevent a premature phosphorylation of MCM2-7. However, some DBF4 might escape from the degradation and activate CDC7. In budding yeast, Rap1-interacting factor (Rif1) is known as a factor that reverses Cdc7-mediated phosphorylation of Mcm2-7 by targeting the protein phosphatase glycogen Glc7/PP1 human homolog to origins and promoting the dephosphorylation of Mcm2 and Mcm4. During S-phase, when CDC7-DBF4 kinase activity increases, this kinase attenuates the activity of Rif1 through phosphorylation [136,137].

In *Xenopus* and humans, the roles of RIF1 complex in recruiting PP1 to origins and reversing the CDC7-mediated phosphorylation MCM2-7 were confirmed. The depletion of RIF1 induces a substantial increase of phosphorylation of MCM4 and MCM2, i.e. MCM2 S40, S53 and S108 and the combination of ectopic expression of RIF1 with CDC7 inhibitor XL413 decreases EdU incorporation more than XL413 treatment alone. In addition, the co-expression of RIF1 and PP1 rescues the slow DNA replication of XL413-treated cells suggesting RIF1 requires PP1 to efficiently oppose CDC7-DBF4 activity [87,138,139]. It is likely that the regulation of DNA replication by RIF1-PP1 through opposing CDC7-DBF4 activity is conserved through species.

#### 1.3.2.2.In DNA replication checkpoint

In DNA replication checkpoint pathway, Rad3/ATR mammalian homolog plays the role of a sensor kinase that is initially activated when replication stress occurs in fission yeast. Afterwards, signals are transduced by the activity of an adaptor or transducer Mrc1/CLASPIN mammalian homolog. Finally, effectors of checkpoint

pathway, i.e. Cds1/CHK2 mammalian homolog are activated and regulate the progression of S-phase or M-phase (reviewed in [140]).

The role of CDC7 in the DNA replication checkpoint response is suggested through the activation of Rad53/Cds1/CHK2 human homolog, a downstream mediator of replication checkpoint control of Rad3/ATR human homolog. In the CDC7 bypass mutant *bob1/MCM5* of budding yeast, phosphorylation level of Rad53 clearly decreases when Cdc7 is depleted during S-phase suggesting Cdc7 is involved in maintaining the hyper-phosphorylation of Rad53 to response to replication checkpoint activation [141,142].

In human cells, depletion of CDC7 impairs the activation of DNA checkpoint response due to the failure of phosphorylating CHK1 [143]. Meanwhile, inhibition of CDC7 kinase by ATP-competitive inhibitor PHA-767491 delays HU-induced phosphorylation of CHK1, and attenuates the phosphorylation of Claspin, but does not affect the maintenance of checkpoint once it is established [144]. Noticeably, in the study of Kim *et al.*, the depletion of CDC7 enhanced CHK2 phosphorylation at T68 and increased γH2AX-positive cells, suggesting CDC7 absence may trigger spontaneous DNA damage [143]. However, in another study of Montagnoli *et al.*, the authors did not observe any increased level of γH2AX nor pCHK2 T68, suggesting no DNA damage nor enhancement of CHK2-mediated checkpoint response upon CDC7 depletion [145]. The discrepancy of results may require further studies to solve.

CDC7 also phosphorylates Mrc1/CLASPIN human homolog, a checkpoint mediator that promotes the activation of CHK1 in an ATR-dependent manner. In *Xenopus* cells and human cells, CDC7-DRF1 directly interacts with CLASPIN and phosphorylates it at conserved binding sites [143,146]. Eliminating the interaction between CDC7 and CLASPIN does not affect the binding of CLASPIN to CHK1 or chromatin, and *vice versa*, but does decrease the DNA replication rate suggesting CDC7-CLASPIN interaction is required for maintaining DNA replication progression [146].

#### 1.3.2.3.In meiosis

In yeast, Cdc7-Dbf4 provides a link between premeiotic S-phase, recombination and monopolar attachment in the first division of meiosis. Cdc7 facilitates DNA replication in pre-meiotic S-phase during which meiotic cohesion complex generates sister chromatid cohesion [147,148]. Cdc7 also promotes double-strand break formation to initiate recombination through Mer2 phosphorylation [149,150]. Cdc7 is required for the recruitment of monopolin complex to kinetochores that are essential for monopolar attachment and mono-orientation of sister chromatids by regulating the localisation of monopolin together with Cdc5/PLK1 human homolog and the cleavage of meiotic cohesion complexes at meiosis I [149,151]. Cdc7 also promotes the transcription of global transcription factor *NDT80* by phosphorylating Sum1 to relieve the repression mediated by Sum1-Rfm1-Hsf1 complex at meiosis 1 [152]

#### 1.3.2.4.In mitosis

In budding yeast, Cdc7-Ddf4 prevents mitotic exit by inhibiting Cdc5/PLK1 function in spindle checkpoint. DBF4 targets CDC7 to Cdc5 mediating an interaction with the Cdc5-substrate binding domain and regulating Cdc5-mediated activation of the mitotic exit network (MEN). This presumably occurs by altering Polo-targeting substrates rather than inhibiting Cdc5 kinase activity. Preventing the interaction between Cdc5 and phosphorylated substrates does not affect cell growth, but does inhibit the MEN activation and affect the spindle elongation rate [153,154].

#### 1.3.2.5.Other roles

In humans, by phosphorylating and stabilising TOB1, CDC7 prevents unnecessary cell death in DNA-damaged cells [155]. TOB1 is a tumour suppressor protein belonging to Tob/B-cell translocation gene (Tob/BTG) family [156]. However, in response to DNA damage induced by low doses of UV, the upregulation of TOB1 is required to prevent cells from activating pro-apoptotic signalling. The stability of TOB1 is regulated by Cul4-DDB1$^{Cdt2}$, a E3 ubiquitin ligase multiprotein complex and by CDC7. Inhibition of CDC7 kinase activity triggers TOB1 degradation in a Cul4-DDB1$^{Cdt2}$ -dependent manner leading to apoptosis.

In addition, CDC7-DBF4 role in DNA repair and recombination was also reported [157]. CDC7 promotes the interaction between Rad18 and TLS polymerase Polη through phosphorylating the S-Box of Rad18 that is necessary for Polη binding. Subsequently, Polη is recruited to stalled fork sites and facilitates TLS.

### 1.3.3. Regulation of CDC7 kinase activity

#### 1.3.3.1.By regulatory subunits

CDC7 levels are abundant during cell cycle but it is only functional in the presence of DBF4 or DRF1 [13,158]. In yeast and human cells, CDC7 interacts with DBF4 *in vitro* and *in vivo*. DBF4 is required for CDC7 kinase activity and both act at a common point in cell cycle [13]. When DNA damage or depletion of cellular dNTP pools occur, Rad53/CHK2 binds to DBF4 through its FHA1 domain resulting in the removal of CDC7-DBF4 from chromatin and the inhibition of further origin firing [159].

In humans, DRF1 is an alternative regulatory subunit required for CDC7 kinase activity [158,160]. Inhibition of CDC7 kinase by depleting the second regulatory subunit DRF1 results an attenuation of cell growth and an increase of late S and G2/M population. A delay of S and M-phases was observed with an increase of γH2AX and the activated form of CHK2 [160]. In *Xenopus*, at early development stage, CDC7-DRF1 is the predominant form that is required for DNA replication initiation, but not CDC7-DBF4. However, after gastrulation, CDC7-DBF4 becomes more abundant suggesting that DRF1 and DBF4 may have distinct roles at different stages of development [161].

#### 1.3.3.2.By CDKs and itself

CDC7 kinase activity is regulated by CDK phosphorylation *in vitro* and *in vivo.* CDC7 contains several CDK-dependent phosphorylation sites. CDC7 can be phosphorylated by Cdc28/CDK1 human homolog in yeast and by CDK2 in mammalian cells (reviewed in [162]). *In vitro,* CDK2 phosphorylates CDC7 at T376 and mutant CDC7 (T376A) has a lower kinase activity possibly due to the effects of this phosphorylation on CDC7 localisation [133]. Alternatively, CDC7 can auto-phosphorylate, and this is critical in regulating its kinase activity [163].

#### 1.3.3.3.By p53/p21

In humans, upon genotoxic stress, CDC7 stability is regulated by the activity of transcription factor p53 via miR-192/215 and Fbxw7β E3 ubiquitin ligase. The expression of miR-192 or miR-215 induces the cell cycle arrest at G1 and G2-phase upon genotoxic stress. Noticeably, the expression of those miRNAs also reduces CDC7 transcription levels [164]. However, the miRNA regulatory loop only induces 30% transcriptional reduction of CDC7 indicating other regulatory factors are involved. These are Fbxw7β E3 ubiquitin ligase and p21. CDC7 forms a complex with Fbxw7β and GSK3β *in vitro.* Silencing of Fbxw7β can partially recover CDC7 protein level in response to the downregulation of CDC7 induced by p53 upregulation [165], suggesting that CDC7 stability is controlled by the activity of Fbxw7β in a p53-dependent manner. Interestingly, p21 contributes to this regulation through CDK2-mediated phosphorylation of CDC7. CDK2 phosphorylates CDC7 at T376 and the upregulation of p21 abrogates this phosphorylation leading to the degradation of CDC7 via Fbxw7β-dependent pathway [165] (Figure 1.11).

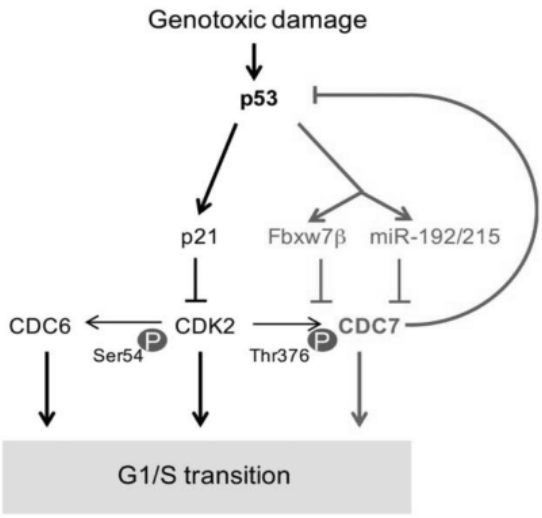


**Figure 1.11 Regulation of stability of CDC7 in a p53-dependent manner**

Upon to genotoxic damage, the upregulation of p53 promotes the inhibition of CDK2 through p21 leading to the abrogation of CDK2-mediated phosphorylation of CDC7. The activity of p53 also triggers the degradation of CDC7 through Fbxw7β- and miR-192/215-dependent pathways. Figure taken from [165].

### 1.3.4. Effects of CDC7 inhibition

#### 1.3.4.1.In yeast

In budding yeast, null mutants of CDC7 and DBF4 are non-viable but mutant Bob1/MCM5 human homolog P83L or a partial deletion of N domain of MCM4 allows the bypass of CDC7-DBF4 requirement and rescue of DNA replication [166]. Mutation of *BOB1/MCM5* triggers a conformational change in the molecular structure of MCM5 that mimics the effects of CDC7 phosphorylation of MCM5. As a result, domain A of MCM5 is pushed away from domain C of MCM5, and this allows the loading of CDC45 into pre-IC complex MCMs-CDC45-GINS and activates replication forks [167]. However, the CDC45-MCMs complex is formed less efficiently or less stably suggesting CDC7 still plays an essential role in facilitating a proper association between CDC45 and MCM2-7 complex. CDC7 null mutant also has a defective intra-S-phase checkpoint with impaired Rad53 kinase activation in the presence of HU [142].

In fission yeast, absence of Hsk1/CDC7 is lethal [168]. Disruption of *hsk1* gene leads to cell death. However, after 8 hours of germination of Δ*hsk1* cells, authors found an

increase of G2-phase population which may be due to the existence of Hsk1 residual protein. This suggests that a low level of Hsk1 is sufficient to maintain cell viability and growth [168]. Hsk1 temperature-sensitive mutants suffer from an abnormal S-phase and exhibit an abnormal nuclear morphology at the non-permissive temperature [169].

#### 1.3.4.2.In *Xenopus*

Depletion of CDC7/DRF1 in *Xenopus* egg extracts results in inhibition of chromatin loading of CDC45 that is important for pre-IC formation. This depletion also reduces activity of Scc2/NIPBL human homolog and Scc4/MAU-2 metazoan homolog that play a role in facilitating the deposition of cohesion into DNA. Those data suggests CDC7 role in DNA replication and sister chromatid cohesion of vertebrates [161,170,171].

#### 1.3.4.3.In mouse

CDC7-knockout mice display early embryonic lethality but can be partially rescued by CDC7 -/- p53-/- double knockout [172] with a development of inner cell mass that is lacking in CDC7-/- only. Conditional knock-out of both CDC7 alleles (CDC7 -/- mutant) induces a cessation of DNA synthesis and S-phase arrest, an increase of p53 level, a generation of RAD51 foci followed by cell death. This indicates that the absence of CDC7 in ES cells arrests DNA replication, triggers checkpoint responses and DNA repair leading to p53-dependent cell death (reviewed in [173]).

Expression of a CDC7 transgene (tg) could rescue the CDC7 knock-out phenotypes, but at different levels. It rescued cell lethality in embryonic stem (ES) *cdc7-/-* cells, but surviving *cdc7-/- tg* mice had a retarded growth, and were infertile. Meanwhile, by expressing an additional copy of CDC7 tg, a normal development and fertility were restored [173]. In *cdc7-/-* transgene ES cells, the expression levels of CDC7 were three to five times higher than in wild-type ES cells. Mouse embryonic fibroblasts (MEFs) derived from *cdc7-/-tg* mutant mice have a delay in S-phase, a decrease of proliferation with a 5-times lower of CDC7 levels in comparison with wild-type MEFs (reviewed in [174]).

#### 1.3.4.4.In humans

CDC7 depletion induces severe effects on the viability and cell cycle progression of human cells. Immuno-neutralisation of CDC7-DBF4 blocks DNA synthesis in HeLa cells [175]. Downregulation of CDC7 by siRNA induces an S-phase defect without triggering any checkpoint response and activates a p53-independent apoptotic cell death in various cancer cell lines. Cells that escaped from apoptosis are unable to divide due to entering an aberrant mitosis [145]. The mechanism of apoptotic cell death induced by CDC7 depletion was considered due to the activation of p38-MAPK kinase in an ATR-dependent manner leading to the activation of pro-apoptotic Cas8 and Cas9 [176].

In normal fibroblast cells, lack of CDC7 leads to a p53-dependent cell cycle arrest [145]. In a study of Tudzarova *et al.* [177], authors found that depletion of CDC7 in diploid human fibroblast cells leads to the origin activation impairment and the activation of proteins involved three axes: FoxO3a -> $p15^{INK4B}$, FoxO3a -> $p14^{ARF}$-| Hdm2 -| p53 ->$p21^{WAF1}$ and p53 -> Dkk3 in driving the origin activation checkpoint. Upregulation of FoxO3a allows the $p15^{INK4B}$-mediated inactivation of CDK4/6. Upregulation of FoxO3a also triggers the $p14^{ARF}$-mediated downregulation of Hdm2 that stabilises p53 and induces an increase of p53 activity. Subsequently, $p21^{WAF1}$ upregulates and inactivates CDK2. P53 activity also upregulates Dkk3 leading to the downregulation of β-catenin that results to the downregulation of CycD1 and Myc. As a result, CDC7-depleted cells have cell cycle arrest at G1-phase [177] (Figure 1.12).

Downregulation of either FoxO3a, Dkk3 or $p15^{INK4B}$ in CDC7-depleted fibroblast cells allows cells to bypass G1-phase arrest and proceed through S to G2-phase. However, no pH3 S10 cells were detected indicating cells are unable to complete mitosis, then die in apoptosis pathway. Noticeably, in cancer cells, tumour suppressor proteins, i.e. p53, are usually inactivated suggesting they could be killed specifically by CDC7 inhibitors [177].

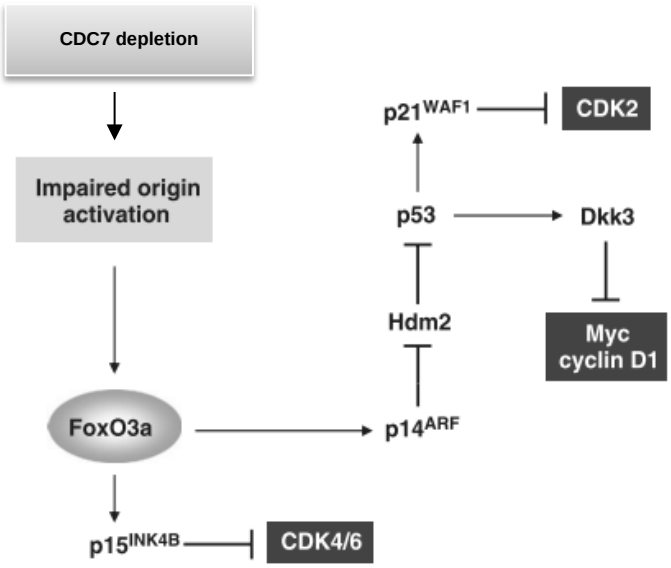


**Figure 1.12 A proposed model of three axes of origin activation checkpoints in human cells**

Details were described in the text. Figure adapted from [177].

## 1.4. CDC7 regulatory subunit DBF4

### 1.4.1. Structure of DBF4

DBF4 harbours motif N, M and C. Motif N is known as the binding site of RAD53 and ORC, while motif M and C are able to bind to the C and N-termini regions of CDC7 contributing to the hydrophobic bipartite interface of this kinase. In humans, DBF4 motif C is composed of three α-helices (α1, α2 and α3) and a pair of β-strands (β3 and β4) forming a compact $Zn^{2+}$ binding domain that is essential for CDC7 functions [127].

### 1.4.2. DBF4 regulation and stability

In yeast, DBF4p is targeted for degradation by ubiquitin-mediated proteolysis [178]. In humans, the CDC7-DBF4 complex is stabilised in an ATR-CHK1 dependent manner. Stalled replication fork-mediated CHK1 activation results the inactivation of $APC/C^{CDH1}$ through degradation of CDH1, leading to the stabilisation of $APC/C^{CDH1}$ substrates including CDC7-DBF4 [179] (Figure 1.13).

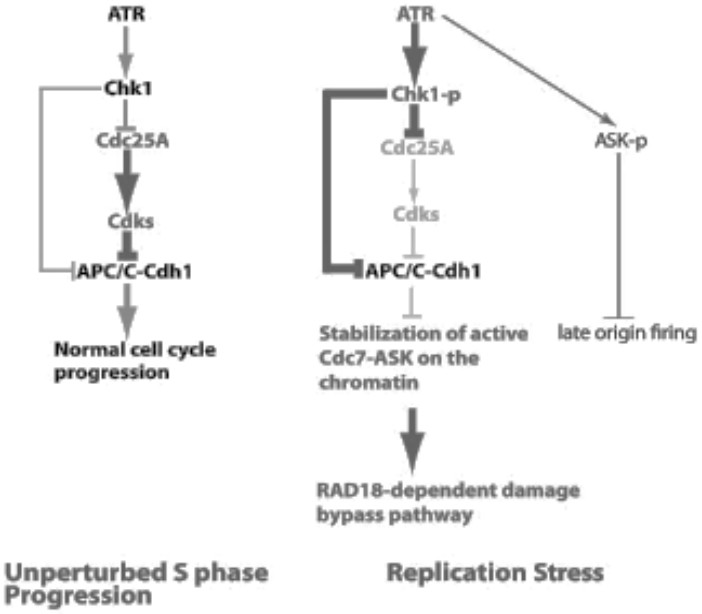


**Figure 1.13 Stabilisation of CDC7-DBF4 in unperturbed and DNA replication stress condition**

Under unperturbed condition, APC/C$^{CDH1}$ is inactivated by the phosphorylation of CDH1 induced by activity of CDKs. When DNA replication fork is stalled due to stress condition, the DNA checkpoint CHK1 is activated promoting the CDC25A-mediated inhibition of CDK activity and the degradation of CDH1. This allows the stabilisation of APC/C$^{CDH1}$ targets including CDC7-DBF4 on the chromatin and the RAD18-dependent lesion bypass. Figure taken from [179].

APC/C inhibition contributes to DBF4 stabilisation but it is unable to solely account for it. A study of Nougarede *et al*. showed that DBF4 levels still decreased in G2/M-arrested cells in which APC/C is inactive [180]. Author also suggested that SCF$^{CDC4}$ is not involved in this instability, then it still remains as an unanswered question.

### 1.4.3. DBF4 interactors and roles

The recruitment of CDC7 to pre-RC complex requires the N-terminal domain of DBF4 [134,181]. Motif N is required for ORC2 and Rad53 interaction. In yeast, Orc2 interacts with Dbf4 motif N which is also a specific binding domain with FHA domains of Rad53 [159]. Removal of motif N disrupts the interaction between Dbf4 and Orc2 resulting in cell growth defect but cells still maintain viability [182].

Motif M plays a role in DBF4 interaction with ARS1 and MCM2 in unperturbed cells [183]. In budding yeast, the ARS1-binding activity of Dbf4 is independent from

Cdc7-activation activity. A truncated Dbf4 protein that lacking ARS1-binding ability by deleting a portion of motif M in *dbf4* gene is still able to bind to and activate Cdc7 [184]. Removal of Dbf4 motif M abrogates the interaction with Mcm2, prevents initiation of DNA replication and induces cell death [182].

Motif C of Dbf4 is involved in maintaining the interaction between Dbf4 with Cdc7 and other known interactors of budding yeast [185]. Deletion of motif C disrupts the association of Dbf4 with Cdc7 and other replication components, i.e. ARS1, Mcm2, Orc2 and ceases cell growth, indicating the crucial role of this motif in Dbf4 function. Dbf4ΔC mutants have a disruption of interaction with ARS1 and Mcm2 but not with Orc2. Mutants also have a defect of S-phase entry and progression even if they have an enhanced association with Orc2, suggesting the interaction with Mcm2 and ARS1 might be more crucial than with Orc2 in regulating S-phase progression [185]. In humans, the role of DBF4 motif C in activating CDC7 was confirmed in a study of Hughes *et al.* [127].

Furthermore, motif C is involved in DNA lesion bypass in yeast and mammalian cells. Cdc7-mediated phosphorylation is required for the interaction Rad18-Polη and also the recruitment of Polη to stalled fork sites [186]. Furthermore, Cdc7 and Dbf4 interacts with Rad18 simultaneously to form a trimeric complex and the association between motif C of Dbf4 and Rad18 is required for the chromatin binding of Rad18, to some extent, for the recruitment of Rad18-Polη to stalling site [179].

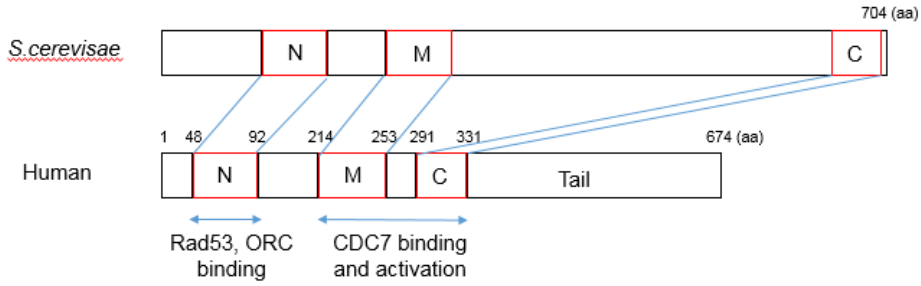


**Figure 1.14 DBF4 structures in yeast and human cells**

(A) Distribution of DBF4 domains in yeasts and the location of its corresponding domains in humans; (B) Structure of human DBF4 with binding domains. Figure adapted from [127,187,188].

## 1.5. CDC7 inhibitors PHA-767491 and XL413

Depletion of CDC7 has distinct effects in primary fibroblast or cancer cells indicating the inhibition of CDC7 kinase activity may be a potential therapeutic treatment for cancer. Until now, several classes of ATP-competitive CDC7 inhibitors were generated and investigated either *in vitro* or *in vivo* in xenograft models or in clinical trials. In this study, our primary aim is to understand the mechanism of action of CDC7 inhibition on DNA replication by using two compounds, PHA-767491 and XL413. Both are the first generation of CDC7 inhibitors and were characterised either *in vitro* through kinase activity assay or *in vivo* through xenograft mouse models (discussed further). However, the knowledge about the inhibitory effects of these compounds and, to lesser extent, of CDC7 kinase inhibition on human cells, especially breast cancer cells are limited.

### 1.5.1. PHA-767491

#### 1.5.1.1.Identification and biochemical potency

PHA-767491 was first identified and characterised in a study of [189]. This compound is a pure ATP-competitive inhibitor with a half-maximal inhibitory concentration ($IC_{50}$) of 10 nM against CDC7 and 34 nM against CDK9, suggesting this compound is a potential dual inhibitor CDC7 and CDK9 kinase.

#### 1.5.1.2.Antitumour activity

PHA-767491 inhibits CDC7 and other kinases, i.e. CDK9 *in vitro* and *in vivo* [127,189]. This compound has an anti-proliferative activity on multiple cancer cell lines in a p53-independent manner with low $IC_{50}$ values of less than 10 μM, suggesting its high potency in inhibiting cancer growth [189]. In this study, authors also found that PHA-767491 abolishes DNA synthesis of human cells by preventing origin firing and triggers apoptotic cell death [189].

In quiescent chronic lymphocytic leukaemia (CLL) cells, PHA-767491 promotes the downregulation of an anti-apoptotic protein Myeloid cell leukaemia 1 (Mcl-1) resulting apoptotic cell death. This primarily results from the inhibition of CDK9 kinase activity. However, in proliferating CLL cells, this compound does not induce any apoptosis even though the blockade of DNA synthesis and the down-regulation

of Mcl-1 still occurred. Indeed, an elevated level of B-cell lymphoma-extra-large (Bcl-xL) was observed, suggesting the survival of proliferating CLL cells may be promoted by this anti-apoptotic protein [190]. A similar phenomenon was observed in PHA-767491 treated multiple myeloma cells. This CDC7 inhibitor kills both cell lines but the apoptosis of multiple myeloma 1 S (MM1S) cells occurred with slower kinetics than of KMS-18 cells. Constant levels of Bcl-xL in MM1S cells in response to PHA-767491 was found suggesting the role of this anti-apoptotic protein in the drug resistance ability of this myeloma cell line [191].

Noticeably, PHA-767491 is cytotoxic in glioblastoma and pancreatic cells [192,193]. This compound kills tumorigenic glioblastoma cell lines, suppresses cell growth and invasiveness. However, it does not remarkably reduce cell viability as well as not increase DNA fragmentation, a marker of apoptosis, in non-tumorigenic cell line 3T3, even if DNA replication is inhibited efficiently [192]. Similarly, PHA-767491 kills pancreatic adenocarcinoma cell lines but does not activate apoptotic machinery of human foetal lung fibroblast cell line IMR-90, even DNA synthesis is abolished in treated cells. This reflects the effects of depletion of CDC7 by siRNA observed in this study and others [193].

Noticeably, inhibition of CDC7 by PHA-767491 affects the efficiency of activating replication checkpoint response [144,189]. A study of Rainey *et al.* [144] found that HU-induced CHK1 phosphorylation was delayed by 3 hours in PHA-767491 treated cells compared to mock-treated cells. PHA-767491 does not affect the checkpoint response once it is established.

However, it is unclear if the effects of PHA-767491 on human cells results from the inhibition of CDC7 kinase activity only or by the inhibition of both CDC7 and CDK9 kinase activity.

### 1.5.2. XL413

#### 1.5.2.1.Identification and biochemical potency

In a study of [194], XL413 was first described and characterised as a potent ATP-competitive CDC7 inhibitor with $IC_{50}$ value of 3.4 nM. This compound has a pyrrolidine side chain that can make an extensive van der Waals contact with the P

loop of CDC7 by which a partial closure of the pocket can be created around this compound. This characteristic may contribute to the more selective effect and higher potency of this compound in comparison with PHA-767491 against a panel of 77 human kinases [127].

#### 1.5.2.2.Antitumour activity

In addition to CDC7, XL413 also targets to other kinases, including casein kinase 2 (CK2) and Proviral integration site for Moloney murine leukaemia virus-1 (PIM-1) but with lower potencies *in vitro*. $IC_{50}$ values of XL413 are 215 nM and 42 nM respectively [194]. This CDC7 kinase inhibitor efficiently prevents MCM2 phosphorylated at S40/41 of Colo-205 cells suggesting it is a potent inhibitor of CDC7 *in vivo.* XL413 suppresses tumour growth with an arrest of tumour cells in late S/G2-phase and was used as an oral compound for patients with haematological malignancies in clinical trials. Phase I trial of this compound was completed in 2010 by Bristol Meyer Squibb (https://clinicaltrials.gov/ct2/show/NCT00838890). However, the mechanism of action of this compound in human cells has not been elucidated yet.

Noticeably, a recent study showed that XL413 specifically inhibited cell growth of Colo-205 but exerts limited effects on other cancer cell lines, i.e. breast cancer [195]. It is unclear if this phenomenon is due to the limitation of the compound in inhibiting CDC7 activity in different cell lines, or unknown drug resistance may exist.

## 1.6. Potential roles of CDC7 inhibition in triple-negative breast cancer treatment

Triple negative breast cancer (TNBC) is a subtype of breast cancer identified by the negative status of hormonal receptors including estrogen receptor (ER-), progesterone receptor (PR-) and the lack of overexpressed human epidermal growth factor receptor 2 (HER2-) (reviewed in [196]). The treatment for TNBC patients are limited in comparison with other subtypes, as TNBC patients are unable to use hormonal therapy targeting ER, PR or chemotherapy targeting HER2, such as Trastuzumab [197]. Hence, finding a potential target for chemotherapy is critically important in TNBC treatment.

In addition to targeting DNA repair complex, i.e. PARP1 inhibitor or p53, i.e. taxanes (reviewed in [198]), DNA replication regulators are also potential targets of chemotherapy. In human, inhibition of CDC7 by siRNA triggers apoptotic cell death in many cancer cell lines, but only induces cell cycle arrest in normal fibroblast cells [145,199] suggesting this kinase is a therapeutic target of chemotherapy, and also a relevant candidate for target therapy. However, to the best of our knowledge, the effects CDC7 inhibitors on TNBC cells have been limitedly reported in a study of Sasi *et al.* [195]. Therefore, we chose two breast-derived human cell lines, MCF10A and MDA-MB-231 in this study for the purpose of expanding knowledge about CDC7 inhibition in human cancer cells, especially in TNBC.

MCF10A is a non-malignant, immortalised breast cell line and MDA-MB-231 is a metastatic breast cancer cell line. Both are triple-negative (ER-/PR-/HER2-) but MCF10A expresses wild-type p53, while MDA-MB-231 expresses a mutant form of p53. In addition, they are CDC7-overexpressing cell lines, in which mRNA expression and protein levels are higher than primary human mammary epithelial cells [199] suggesting they are ideal candidates for testing effects of CDC7 inhibition in humans.

## 1.7. Questions and Aims

In this study, we aim to investigate the molecular effects of CDC7 inhibitors on DNA replication. From then, we want to reveal the mechanism by which CDC7-DBF4 inhibition affects the cell viability and proliferation of human cell lines.

**Questions**

- What is the role of CDC7 kinase activity in human DNA replication?
- Is there any kinase that cooperates with CDC7 in promoting cell proliferation and DNA replication?
- What are the unknown roles of human DBF4?

**Aims**

- To characterise the effects of XL413 and PHA-767491 on cell proliferation, on the progression of DNA replication and mitosis of breast-derived human cell lines MCF10A and MDA-MB-231.
- To detect kinases of which the inhibition potentiates the effects of XL413 or DBF4 knock-out in human cell proliferation.
- To identify DBF4 interactors that had been detected by immune-precipitation (IP) and mass spectrometry (MS-MS).

# Chapter 2: Materials and Methods

## 2.1. Materials

### 2.1.1. Cell culture

#### 2.1.1.1. Cell lines

MCF10A, MDA-MB-231 are breast-derived human cell lines that were obtained from American Type Culture Collection (ATCC), HAP1 wild-type (WT) and DBF4 knock-out (4KO) were from Horizon Discovery and Flp-In T-REx 293 (TREx-293) was from Invitrogen.

#### 2.1.1.2. Cell culture media and reagents

MCF10A cells were maintained in high glucose DMEM supplemented with 5% (v/v) heat-inactivated horse serum, 10 μg/ml insulin, 0.5 μg/ml hydrocortisone, 1 ng/ml cholera toxin, 10 ng/ml epidermal growth factor (EGF) and 1% (v/v) Penicillin-Streptomycin solution. MDA-MB-231 and TREx-293 cells were maintained in high glucose DMEM supplemented with 10% (v/v) heat-inactivated fetal bovine serum (FBS) and 1% (v/v) Penicillin-Streptomycin solution. HAP1 WT and 4KO cells were maintained in IMDM supplemented with 10% (v/v) heat-inactivated FBS and 1% (v/v) penicillin-streptomycin solution.

All reagents were purchased from Sigma, except EGF which was from Peprotech, in a sterile condition. Disposable sterile plastic-ware were mainly purchased from Sarstedt. Cell lines were generally incubated at 37$^{o}$C, 5% $CO_2$ in a humidified Steri-Cycle $CO_2$, HEPA Class 100 incubator (Thermo Fisher Scientific), unless otherwise stated.

### 2.1.2. Reagents and buffers

#### 2.1.2.1. Common reagents and buffers

General chemical reagents were purchased from Sigma-Aldrich and Thermo Fisher Scientific. 5-ethynyl-2-deoxyuridine (EdU) and 6-carboxyfluorescein TEG-azide were purchased from Berry & Associates. Details of other specific reagents were stated in context. All of common reagents and buffers were listed in Table 2.1.

**Table 2.1 Common reagents and buffers**

| Buffer/Reagent | Composition | Application |
|---|---|---|
| CSK lysis buffer | 10 mM PIPES pH 6.8, 100 mM NaCl, 300 mM sucrose, 1 mM $MgCl_2$, 1 mM EGTA pH 8.0, 0.5% (v/v) Triton X-100, 1 mM DTT in sodium acetate pH 5.2 | Protein extraction buffer for Immunoblotting |
| Click reaction I solution | 0.01 mM 6-carboxyfluorescein TEG-azide, 10 mM Sodium L-ascorbate, 2 mM Copper-II sulphate | Click reaction of EdU/DAPI staining for flow cytrometry and immunofluorescence |
| Click reaction II solution | 0.02 mM IRDye 800CW azide, 10 mM Sodium L-ascorbate, 2 mM Copper-II sulphate | Click reaction of InCell Click assay |
| Click reaction III solution | (described in section 2.2.6.2, Table 2.11) | Click reaction of Click-iT EdU microplate assay |
| Laemmli buffer (5X) | 300 mM Tris-HCl pH 6.8, 20% (v/v) Glycerol, 10% (w/v) SDS, 20% (v/v) β-mercaptoethanol, 0.1% (w/v) Bromophenol blue | Sample preparation for SDS-PAGE |
| PBT | PBS-T, 0.5% (w/v) BSA | Immunofluorescence |
| PBS-TX | PBS, 0.1% (v/v) Triton X-100 | Wash buffer |
| PBS-TX 0.2% | PBS, 0.2% (v/v) Triton X-100 | Wash buffer |
| Ponceau S stain | 0.1% (w/v) Ponceau S, 5% (v/v) acetic acid | Immunoblotting |
| SDS-PAGE running buffer | 25 mM Tris, 0.1% SDS, 190 mM Glycine | Gel running buffer for SDS-PAGE |
| SDS-PAGE protein transfer buffer | 25 mM Tris, 190 mM Glycine, 20% Methanol | Transferring protein from gel onto |

| | | |
|---|---|---|
| | | nitrocellulose membrane |
| TGN lysis buffer | 50 mM Tris-HCl pH 7.5, 200 mM NaCl, 50 mM β-glycerophosphate, 50 mM NaF, 1% (v/v) Tween-20, 0.2% (v/v) NP40 | Protein extraction buffer for immunoblotting |

### 2.1.2.2. Chemical compounds

Compounds used in this study were listed in Table 2.2 and mainly purchased from Sigma-Aldrich. XL413 is a home-made compound of Dr Guan-nan Wang (National University of Ireland, Galway). PKIS library was a gift from Dr Bill Zuercher (University of North Carolina).

**Table 2.2 List of chemical compounds**

| Name | Abbreviations | Working concentration | Application |
|---|---|---|---|
| BI6727 | BI | 20 nM | PLK1 inhibitor |
| Cycloheximide | CHX | 10 µM | Protein synthesis inhibitor |
| Doxycycline | Dox | 1 µg/ml | Regulating DBF4 fragment overexpression |
| Etoposide | ETO | 10 µM | Activating DNA damage checkpoint signalling |
| GW84362X | GW | 0.1-1 µM | PLK1 inhibitor |
| Hydroxyurea | HU | 2 mM | Activating DNA damage checkpoint signalling |
| MG132 | | 10 µM | Proteasome inhibitor |
| L-Mimosine | Mim | 0.5 mM | Synchronising cells at G1/S-phase |
| Nocodazole | Noc | 25-50 ng/ml | Arresting cells at G2/M-phase |
| PHA-767491 | PHA | 10 µM | CDC7 inhibitor |

| | | | |
|---|---|---|---|
| Public Kinase Inhibitor Set | PKIS | 0.5 µM | Library of human kinase inhibitors |
| Staurosporine | STAU | 0.5 µM | Inducing apoptotic cell death |
| Thymidine | Thy | 4 mM | Synchronising cells at S-phase |
| XL413 | XL | 10 µM | CDC7 inhibitor |

### 2.1.2.3. Antibodies

For immunoblotting, all primary antibodies were diluted in 5% (w/v) skimmed milk/PBS-T, except primary phospho-antibodies which were diluted in 1% (w/v) BSA/PBS-T, and DBF4 6F4/6 mAb which was diluted in 5% (w/v) skimmed milk/PBS-T 287 mM NaCl (Table 2.3). All secondary antibodies were purchased from LiCOR Biosciences (Lincoln, NE, USA) and diluted in 5% (w/v) skimmed milk/PBS-T (Table 2.4).

**Table 2.3 Primary antibodies for Immunoblotting**

R: rabbit; M: murine; mAb: monoclonal antibody; pAb: polyclonal antibody; Cat. No.: catalogue number.

| **Antibody** | **Mouse/ Rabbit** | **Dilution** | **Company (Cat. No.)** |
|---|---|---|---|
| APE1, mAb | R | 1:1,000 | GeneTex (GTX110558) |
| Caspase 3, mAb | M | 1:1,000 | Cell Signalling (9668S) |
| Cleaved Caspase 3 (Asp175), mAb | R | 1:1,000 | Cell Signalling (9664S) |
| CDC7, mAb | M | 1:1,000 | MBL (K0070-3, DCS 342) |
| CDC2 p34 (C-19) or CDK1, pAb | R | 1:1,000 | Santa Cruz (sc-954) |
| CDK2 (M2), pAb | R | 1:1,000 | Santa Cruz (sc-163) |
| CDK9 (C-20), pAb | R | 1:1,000 | Santa Cruz (sc-484) |
| CHK1 (G-4), mAb | M | 1:1,000 | Santa Cruz (sc-8408) |
| Phospho-CHK1 (S317), pAb | R | 1:1,000 | Cell Signalling (2344L) |

| | | | |
|---|---|---|---|
| CHK2 (A-11), mAb | M | 1:1,000 | Santa Cruz (sc-17747) |
| Phospho-CHK2 (T68), pAb | R | 1:1,000 | Cell Signalling (2661L) |
| DBF4 6F4/6, mAb | M | 1:1,000 | Santocanale's laboratory |
| H2AX, pAb | R | 1:2,000 | Upstate (07-146) |
| Phospho-H2AX (S139), pAb | R | 1:1,000 | Upstate (07-164) |
| MCM2, mAb | M | 1:2,000 | AbD Serotec (Clone CTCt2.1) |
| Phospho-MCM2 (S40/41) | R | 1:5,000 | [86] |
| MCM4, pAb | R | 1:2,000 | Abcam (ab4459) |
| NAP1L1, pAb | R | 1:1,000 | Bethyl Lab (38841) |
| p21 (C-19), pAb | R | 1:1,000 | Santa Cruz (sc-397) |
| p53 (DO-1), mAb | M | 1:1,000 | Santa Cruz (sc-126) |
| Cleaved PARP, mAb | M | 1:1,000 | Cell Signalling (9546S) |
| PARP-1 (F2), mAb | M | 1:1,000 | Santa Cruz (sc-8007) |
| Phospho-RPA32 (S4/8), pAb | R | 1:1,000 | Bethyl Laboratories |
| Strep (NWSHPQFEK), pAb | R | 1:1,000 | GenScript (A00626-100) |
| β Actin, mAb | M | 1:20,000 | Sigma (A1978, clone AC-15) |
| β Tubulin, pAb | R | 1:1,000 | Abcam (ab6046-200) |
| GAPDH (14C10), mAb | R | 1:4000 | Cell Signalling (2118L) |
| Histone H4, pAb | R | 1:1,000 | Abcam (ab10158) |

**Table 2.4 Secondary antibodies for immunoblotting**

| Antibody | Cat. No. | Dilution |
|---|---|---|
| IRDye 680LT Goat α-Mouse IgG | 926-68020 | 1:20,000 |
| IRDye 680LT Goat α-Rabbit IgG | 926-68021 | 1:20,000 |
| IRDye 800CW Goat α-Mouse IgG | 926-32210 | 1:10,000 |
| IRDye 800CW Goat α-Rabbit IgG | 926-32211 | 1:10,000 |

**Table 2.5 Primary and secondary antibodies for flow cytometry**

| Antibody / Reagents | Supplier (Cat. No.) | Dilution | Application |
|---|---|---|---|
| Rabbit α-phospho H3 mitosis marker (IgG) | Upstate (06-570) | 1:33 | Primary antibody |
| Donkey α-Rabbit IgG Alexa Fluor 647 | ThermoFisher (A-31573) | 1:33 | Secondary antibody |

**Table 2.6 Primary and secondary antibodies for DNA fiber labelling**

| Antibody | Supplier (Cat. No.) | Dilution | Application |
|---|---|---|---|
| Rat α-BrdU | Thermo Fisher (MA1-82088) | 1:50 | CldU detection (1st Ab) |
| Chicken α-Rat IgG Alexa Fluor 488 | Invitrogen (A21470) | 1:300 | CldU detection (2nd Ab) |
| Mouse α-BrdU | BD (347580) | 1:50 | IdU detection (1st Ab) |
| Goat α-Mouse IgG1 Alexa Fluor 546 | Invitrogen (A21123) | 1:300 | IdU detection (2nd Ab) |

#### 2.1.2.4. Plasmids

Plasmids listed in Table 2.7 were generated in Santocanale's laboratory.

**Table 2.7 Plasmids for generating stable-transfected cell lines**

| Plasmid | Protein expressed | Epitope tag |
|---|---|---|
| pAB1-DBF4 FL | DBF4 | FLAG-Strep |
| pAB1-DBF4 N | N fragment of DBF4 | FLAG-Strep |
| pAB1-DBF4 N+MC | N+MC fragment of DBF4 | FLAG-Strep |
| pAB1-DBF4 ΔN | MC+Tail fragment of DBF4 | FLAG-Strep |
| pAB1-DBF4 Tail | Tail fragment of DBF4 | FLAG-Strep |
| pAB1-DBF4 ΔMC | N+Tail fragment of DBF4 | FLAG-Strep |

## 2.2. Methods

### 2.2.1. Cell culture

#### 2.2.1.1. Resuscitation and maintenance of cells

Frozen cells were fully thawed in a water bath at 37ºC for 2-3 minutes, then transferred to a tube containing warmed culture medium. Cells were mixed gently by inverting tube 1-2 times, and spun down for 5 minutes at 1,000 -1,200 rpm. Cell pellet was resuspended gently in 1 ml culture medium, then transferred to a culture flask in general or a tissue culture (TC) dish as HAP1 cell lines and incubated at 37ºC, 5% $CO_2$ for 24-48 hours. Fresh medium was replaced and cells were incubated until it reached 70% confluency. Cells were split in an appropriate dilution after every 2-3 days for maintenance.

#### 2.2.1.2. Cell trypsinisation for harvest

Cells were washed once by warm PBS, incubated with 1X or 2X Trypsin-EDTA for 2-10 minutes or until they rounded up. Warm culture medium containing FBS was added to neutralise trypsin. Cells were detached by gently tapping on the wall of the culture flask or dish and resuspended briefly. Cell suspension was transferred to 15-ml conical tube and pelleted by a centrifugation at 450 xg or 2,000 rpm for 5-10

minutes at 4$^{o}$C. Cell pellet was washed once by PBS, resuspended thoroughly in PBS to obtain a single cell suspension and kept on ice until usage.

#### 2.2.1.3. Cell counting

Cell counting was performed with a Countess Automated Cell Counter system (Thermo Fisher Scientific). To count, 10 µl of cell suspension was added into an Eppendorf tube contained 10 µl of Trypan blue solution and mixed by pipetting several times. 10 µl of this mixture was transferred onto a chamber slide, then cell number and viability were determined according to the manufacturer's instruction. Each cell counting was performed at least twice to assure the accuracy.

#### 2.2.1.4. Cell harvest

Cell culture medium was transferred to 15 or 50-ml conical tube for harvested floated or dead cells. Remaining cells were washed once by cold PBS which was also collected, trypsinised, counted and pelleted by a centrifugation at 450 xg for 5-10 minutes for harvesting. For the affinity pull-down (AP) assay, T-Rex 293 cells were plated in TC dishes and harvested by using a sterile scraper.

#### 2.2.1.5. Cell washing

In general, cells were resuspended in PBS or washing buffer, then pelleted by a centrifugation at 450 xg or 2,000 rpm for 5-10 minutes. Supernatant was aspirated carefully and cell pellet was used for experiments.

#### 2.2.1.6. Cell cryopreservation

Cells were trypsinised, counted and resuspended into a supplemented medium at a density of 2-3x10$^{6}$ cells/ml. Supplemented medium contained 20% DMSO was added into cell suspension for a final cell density of 1-1.5x10$^{6}$ cells/ml and 10% DMSO. Cell mixture was rapidly aliquoted into cryogenic tubes with 1-1.5 ml per vials, then gradually frozen at -80$^{o}$C in freezer, then below -150$^{o}$C in liquid nitrogen for a long-term cryopreservation. At each batch of cell cryopreservation, frozen cells of a vial were revived for the quality control.

#### 2.2.1.7. Cell synchronisation

Cells were synchronised at G1/S by double block Thymidine-Mimosine. Cell were plated for 24 hours, treated with 4 mM Thymidine for 15 hours, washed twice with PBS and released in a fresh medium for 9 hours. Cells were treated with 0.5 mM Mimosine for another 15 hours, washed twice by PBS, then incubated with a fresh medium contained either DMSO as a vehicle control or drugs.

#### 2.2.1.8. Clonogenic assay

Cell were plated for 24 hours, treated with drugs or DMSO as a vehicle control for 24 hours, trypsinised and reseeded at concentration of 150 cells per ϕ10cm TC dish in triplicate. Colonies formed after 10-12 days were fixed by 100% methanol, stained by staining reagent (2% (w/v) crystal violet in 25% (v/v) methanol) and counted manually. Only colonies that contained more than 25 cells, assessed briefly by light microscopy, were counted. Plate efficacy (PE) and survival fraction (SF) were calculated as the protocol of Franken [200].

$$PE = \frac{number\ of\ colonies\ formed}{number\ of\ cells\ seeded} \times 100\%$$

$$SF = \frac{number\ of\ colonies\ formed\ after\ treatment}{number\ of\ cells\ seeded \times PE}$$

#### 2.2.1.9. Generation of stable transfected cell lines

##### 2.2.1.9.1. Cell reseeding and colony picking up

TREx-293 cells were harvested 48 hours post-transfection and diluted in selective medium (DMEM, 1:500 (v/v) hygromycin, 1: 2,000 (v/v) blasticidin, 10% (v/v) FBS) at ratio 1:4. Diluted cells were reseeded in a ϕ10cm TC dish for generating monoclonal cell lines or in a T-25 flask for polyclonal cell lines. Cells were incubated with selective medium until colonies appeared with an adequate size for picking up. Fresh selective medium was changed every 3-4 days of incubation.

##### 2.2.1.9.2. Cell growth expansion

Grown-up colonies were picked-up by Corning Cloning Cylinders (Sigma). In brief, sterilised cloning cylinders dipped in a sterile Down Corning silicone grease (Sigma)

were pressed onto the bottom of TC dishes to make an isolated well for each marked colony. 50 µl of 1X Trypsin-EDTA was added into each well and mixed by pipetting several times. Cell suspension of each colony was transferred to each well containing selective medium (DMEM, 1:500 (v/v) hygromycin, 1: 2,000 (v/v) blasticidin, 10% (v/v) FBS) of a TC 96-well plate. Cell colonies were left to grow until they reach 80% confluency, then transferred to 24-, 12-, 6-well plates to expand the growth. Finally, cells were transferred to T-25 and T-75 flasks and left to grow until cryopreservation.

### 2.2.2. Flow cytometry

#### 2.2.2.1. Ethanol fixation and post-fixation recover

Harvested cells were washed once by PBS then resuspended in a 15 ml conical tube containing 300 µl PBS, then 100% ethanol (700 µl/tube) was dropped into the tube while vortexing for a fixation with 70% ethanol. Fixed cells were stored at -20$^{o}$C overnight or at least 2 hours prior to staining and flow cytometry. Fixed cells were recovered by one wash with PBS (3 ml/tube) and another wash with blocking buffer (PBS, 1% (w/v) BSA) (1.5 ml/tube) prior to next steps.

#### 2.2.2.2. EdU/DAPI staining

Cells were incubated with 10 µM EdU for 30 minutes at 37$^{o}$C, 5% $CO_2$. After EdU labelling, cells were harvested and fixed by ethanol overnight. Fixed cells were recovered and resuspended in Click solution I (Table 2.1) (1 ml/sample) and incubated at RT for 30 minutes in dark. After reaction, cells were washed once by washing buffer (PBS-T, 1% (w/v) BSA) to remove excess Copper and azide, then washed again by PBS. Finally, cells were incubated with DAPI/RNAse solution (PBS, 1 µg/ml of DAPI, 100 µg/ml of RNAse) for 15-30 minutes prior to flow cytometry and data analysis.

#### 2.2.2.3. BrdU/PI staining

Cells were incubated with 25 µM BrdU (Sigma, Cat No B5002) for 30 minutes at 37$^{o}$C, 5% $CO_2$. Afterwards, cells were harvested and fixed by ethanol overnight. Fixed cells were recovered and DNA was denatured by an incubation with 4 N HCl

for 15 minutes at RT. Cells were washed once with PBS (1 ml/tube), then another wash with PBT (1 ml/tube) as a blocking step. Afterwards, cells were incubated with following antibodies for 30 minutes at RT: 1) Mu α-BrdU (BD, Cat No 347580) (1:40) and 2) Goat α-mouse Alexa 488 (1:40). Between incubation, cells were washed once with PBS (1 ml/tube), then another wash with PBT (1 ml/tube). Finally, cells were washed once by PBS (1 ml/tube), incubated with 0.5-1 ml PI/RNAse staining buffer (BD, Cat. No. 550825) for 15-30 minutes prior to flow cytometry and data analysis. All the incubations after the blocking step were performed in the dark.

#### 2.2.2.4. PI staining

Fixed cells were recovered, resuspended in 0.5-1 ml PI/RNAse staining buffer (BD, Cat. No. 550825) and incubated at RT for 30 minutes in dark prior to flow cytometry and data analysis.

#### 2.2.2.5. Phospho-H3/EdU/DAPI staining

Fixed cells were recovered and permeabilised by incubating with PBS-TX (1 ml/tube) for 15 minutes on ice, then incubated with blocking solution (PBS, 10% (v/v) FCS, 0.5% (w/v) BSA) (1 ml/tube) at RT for 30 minutes. After blocking step, cells were incubated with Rabbit α-pH3 Ser10 (Millipore) (1:33 dilution) at RT for 2 hours. Cells were washed once with PBS-TX 0.2% (1 ml/tube), resuspended in Click solution I and incubated at RT for 30 minutes. Cells were washed once with PBT (3 ml/tube), once with blocking buffer (1 ml/tube), then incubated with Donkey α-Rabbit Alexa 647 conjugate (Thermo Fisher, Cat. No. A-31573) (1:33 dilution), DAPI (1 μg/ml) and RNAse (100 μg/ml), at RT for 30 minutes. After the final incubation, cells were washed once by PBS-TX 0.2%, once by PBS and resuspended in 0.5-1 ml PBS for flow cytometry and data analysis. All the incubations after the blocking step were performed in the dark.

#### 2.2.2.6. Annexin V/PI staining

Cells were harvested and washed once with PBS. Cell pellet was gently resuspended in AnnexinV buffer (10 mM HEPES, 150 mM NaCl, 5 mM KCl, 1 mM $MgCl_2$, 1.8 mM $CaCl_2$, pH 7.4) (0.5 ml/tube), then incubated with Annexin V reagent (a kind gift of Dr Alessandro Natoni, [190]) (1.5 μl/tube) for 15 minutes, on ice, in dark.

Finally, cells were incubated with PI solution (100 µg/ml) for 5 minutes prior to flow cytometry and data analysis.

#### 2.2.2.7. Flow cytometry and data analysis

Flow cytometry was performed with BD FACS Canto systems, including Canto A and Canto II, according to manufacturer's instruction. After parameters were set up, a FACS tube contained cell suspension was applied to the system. Fluorescence signals of a population of $1x10^4$ live single cells (called "events") were collected by gating different parameters. For gating strategy, forward-scatter light (FSC) and side scatter light (SSC) was used first to exclude debris, then FSC-height/FSC-area (FSC-H/FSC-A) was employed to exclude doublets. Finally, DAPI-area/DAPI-width (DAPI-A/DAPI-W) was used as an alternative and final gate to exclude duplex. Collected fluorescence signals were exported into FCS files and data analysis was performed with FlowJo v.10 software. Based on signals of negative control of fluorescence dyes, background signals were eliminated and fluorescence signals manifested by stained cells were analysed (Table 2.8).

**Table 2.8 Fluorochromes used for flow cytometry**

| Fluorochrome | Filter | To detect fluorescence signals of |
|---|---|---|
| DAPI | 450/50nm | DAPI |
| AF488/FITC/AF545 | 530/30nm | EdU or BrdU |
| PI | 585/42nm | PI |
| AF647 | 660/20nm | pH3 S10 |

### 2.2.3. Immunofluorescence

#### 2.2.3.1. EdU/DAPI staining

Cells were seeded on sterile cover slips in 6-well plates and labelled with 10 µM EdU for 30 minutes. Culture medium was discarded and cells washed gently with cold PBS 3 times, fixed by 4% PFA for 10 minutes, washed with cold PBS another 3 times and incubated with Click reaction I solution (Table 2.1) for 30 minutes at RT in dark. Finally, cells were washed twice with PBT and washed once with cold distilled water. Cover slips were air dried at RT in the dark for a few hours and mounted on glass slides with mountant reagent contained 5 ng/µl DAPI in SlowFade Gold AntiFade

Mountant (Thermo Fisher Scientific, Cat No S36036). Nail polish was applied on the edge of coverslips to secure the position. Slides were stored in slide box at 4ºC until fluorescence microscopy.

#### 2.2.3.2. DNA fiber labelling

To visualise DNA replication intermediates, cells were pulse labelled with 2 different thymidine analogues, IdU and CldU, at the concentration of 25 µM and 200 µM respectively, and in sequence with 30 minutes for each labelling. Between two labellings, cells were washed 3 times either by PBS or a pre-equilibrated medium. After labelling, cells were harvested, diluted to a density of 2.5-5x$10^5$ cells/ml, and mixed with unlabelled cells (1:8). A volume of 2.5 µl of cell mixture was placed on cover slips and lysed with 7.5 µl fresh spreading buffer (0.5% (w/v) SDS, 200 mM Tris-HCl pH 7.4, 50 mM EDTA) for 8-8.5 minutes at RT. DNA from lysed cells were spread by slide tilting, air dried at RT in dark, fixed by a fixative Methanol/Acetic acid (3:1) solution overnight at 4ºC.

The next day, DNA spreads were denatured by incubation with 2.5 M hydrochloric acid for 1 hour at RT, following by blocking for 30 minutes with 1% BSA in PBS-T (0.1% Tween-20). DNA was immunolabelling by an incubation with the following antibodies: 1) Rat anti-BrdU (1:50), 2) Chicken anti-rat Alexa-488 (1:300); 3) Mouse anti-BrdU (1:50) and 4) Goat anti-mouse Alexa-547 (1:300) (Table 2.6). Each antibody was incubated at RT for 30 minutes. Between each incubation, coverslips were washed twice with PBS and once with blocking buffer. After the final antibody incubation, coverslips were washed 3 times either by PBS or by distilled water, air dried at RT in the dark and mounted to glass slides by a Slow-fade Gold AntiFade Mountant (Thermo Fisher Scientific, Cat No S36036). All of incubation steps were performed in the dark. DNA fiber was imaged by fluorescence microscopy using the Olympus IX71 inverted system microscope.

### 2.2.4. Nucleic acid methods

#### 2.2.4.1. Plasmid DNA transfection

Plasmid DNA transfection was performed with Fugene HD transfection reagent (Promega), according to manufacturer's instruction. TREx-293 cells were seeded at 1.5-2x$10^5$ in 6-well plates for 24 hours. In a sterile Eppendorf tube, plasmid pOG44

(Invitrogen) was mixed with plasmid containing DNA fragments at ratio 9:1. Fugene HD transfection reagent (3 µl/well, Promega) and serum-free OptiMEM medium (100 µl/well, Invitrogen) were mixed with DNA components (1 µg/well) by vortexing for 2-3 s and spun down by a brief centrifugation prior to an incubation at RT for 15-30 minutes. After the incubation, the transfection mixture was dropped into appropriate wells and swirled gently. Cells were incubated with transfection reagents at 37ºC, 5 % $CO_2$ for 24 hours, then were left to grow in fresh medium for 24 hours.

#### 2.2.4.2. siRNA transfection

siRNA transfection was performed according to the jetPRIME® in vitro DNA & siRNA transfection reagent protocol (Polyplus Transfection). siRNA duplexes were purchased from Sigma with sequences described in Table 2.9.

Cell was plated 1-2x$10^5$ cells/well in 6-well plates for 24 hours. 5 µl of siRNA were mixed with JetPrime buffer (200 µl) in an Eppendorf tube for a final concentration of 50 nM. For the transfection of siRNA in combination, each duplex was mixed equally (2.5 µl each) and mixed with JetPrime buffer (200 µl) to a total concentration of 50 nM siRNA, Mixture was vortexed and spun down by a brief centrifugation. JetPrime reagent was added afterwards (4 µl), vortexed and spun down again. Transfection mixture was incubated at RT for 20-30 minutes, dropped into an appropriate well and equally distributed in culture medium by gently inverting the plate. A fresh medium was replaced after 6 hours of siRNA incubation and cells were left to grow. After 48 hours of transfection, cells were harvested.

**Table 2.9 Sequences of siRNA duplexed used for siRNA transfection**

| Name | Sequence (5' – 3') | Target | Reference |
|---|---|---|---|
| siSCR_1-2A | GCAUAUCGUCGUAUACUAU | non-target | Self-designed |
| siCDK1-2A | GAUCAACUCUUCAGGAUUU | CDK1 | [201] |
| siCDK1-2B | GGUUAUAUCUCAUCUUUGA | | |
| siCDK2-2A | GUUACUUCUAUGCCUGAUU | CDK2 | [201] |
| siCDK2-2B | GAUCUUAACCAUCCUAAUAUU | | |
| siCDK9-103 | GGUGCUGAUGGAAAACGAG | CDK9 | [202] |
| SiCDC7-A | AAGCUCAGCAGGAAAGGUGUU | CDC7 | [145] |

### 2.2.5. Protein methods

#### 2.2.5.1. Protein purification by Affinity Pull-down (AP) assay

For protein purification by AP, cells were harvested physically by sterile scrapers to avoid unexpected effects of chemical compound on protein-protein interaction. Protein was extracted by an incubation of cell pellets with lysis buffer (50 mM Tris buffer pH 7.4, 300 mM NaCl, 1 mM EDTA, 1% (v/v) TritonX-100, 1% (v/v) Protease Inhibitor Cocktail and 1% (v/v) Phosphatase Inhibitor Cocktail) for 20 minutes at 4$^{o}$C using an end-over-end rotator (Stuart). Lysate was diluted 1:1 in IP buffer (50 mM Tris buffer, pH 7.4, 1 mM EDTA, 1% (v/v) TritonX-100, 1% (v/v) Protease Inhibitor Cocktail and 1% (v/v) Phosphatase Inhibitor Cocktail) then centrifuged at 13,000 rpm for 20 minutes. Supernatant was collected and treated with avidin (10 µg avidin per 1 mg protein) for 30 minutes at 4$^{o}$C with rotation to remove biotinylated proteins (referred as Input sample). Input sample was pre-cleared with equilibrated Sepharose 4B beads by an incubation for 30 minutes at 4$^{o}$C, then supernatant was incubated with equilibrated Streptravidin-Tactin (Strep-Tactin) resin for 3 hours at 4$^{o}$C with rotation. To equilibrate, beads and resin were washed 4 times with wash buffer (50 mM Tris buffer, pH 7.4, 150 mM NaCl) and stored on ice until usage. After incubation, samples were spun down for 1 min at 450 xg. Supernatant was transferred to new tubes (referred as Flow Through sample) and Streptravidin (Strep) resin was washed for 6 times with wash buffer. At each wash, supernatant was kept (referred as Wash 1-6 sample). Finally, Strep resin was boiled with 1X Laemmli buffer at 95$^{o}$C for 3 minutes and supernatant was transferred to new tubes (referred as Boiled beads).

#### 2.2.5.2. Immunoblotting

##### 2.2.5.2.1. Protein extraction

Prior to the extraction, frozen cell pellets were thawed on ice for 10-15 minutes or until being thawed completely.

###### 2.2.5.2.1.1. Total protein extract preparation

- **By tri-chloroacetic acid (TCA) precipitation extraction**

Thawed pellets of 0.8-1x10$^{6}$ cells were resuspended in 1 volume of 20% TCA and vortexed thoroughly to extract and precipitate the total protein. Afterwards, two

volumes of 5% TCA were added and mixed by pipetting several times. The mixture was centrifuged at 3,000 rpm for 10 minutes, then pellets were resuspended in 1X Laemmli buffer to extract the total protein in solution. Several small drops of 1 M Tris solution pH 10.5-12 was added to neutralise acid. Mixture was boiled for 1 min at 95$^{o}$C and spun at 3,000 rpm for 1 min. Supernatant was used as a sample for SDS-PAGE.

#### 2.2.5.2.1.2. Soluble and insoluble protein extract

Thawed cell pellet of 1.5-3x10$^{6}$ cells was resuspended in 100 µl lysis buffer supplemented with 1% (v/v) Protease inhibitor cocktail and 1% (v/v) Phosphatase inhibitors cocktail and incubated on ice for 20 minutes. After incubation, mixture was centrifuged at 450 xg for 5 minutes at 4$^{o}$C. Supernatant or soluble fraction was transferred to a new Eppendorf tube. Remaining pellets were washed once with PBS (150 µl/tube), then once with lysis buffer (150 µl/tube) prior to be resuspended in 50 - 100 µl lysis buffer. The mixture was sonicated at High speed, 30s ON, 15s OFF for 5 cycles once or twice to fragment chromosomal DNA. Each time of sonication, a fresh ice-freezing water was replaced to assure a stable temperature of environment. Soluble and insoluble extracted proteins were stored at -80$^{o}$C until usage.

### 2.2.5.2.2. Determination of protein concentration by Bradford assay

Coomassie Blue in Bradford reagent proportionally binds to total protein of sample, forms a dye-protein complex and changes the colour of reagent. By measuring protein absorbance at 590 nm and constructing a standard curve A590 versus Protein concentration, the protein concentration of unknown sample, is determined. To construct standard curve, BSA was added into a 96-well plate with a serial increase of concentration from 0 to 5 µg/µl. Lysis buffer was used as blank control (1 µl/well). After adding sample into each well (1 µl/well), Bradford reagent was added (180 µl/well) and a gentle shaking for 10-15 s was applied for a complete reaction. All standards and samples were prepared in triplicate. The absorbance at 590nm was read by a Wallac 1420 Victor Multilabel plate reader (Perkin Elmer). Data was analysed by MS Excel 2016 software. The absorbance of different concentrations of BSA at 590 nm was plotted to construct the standard curve with the equation y=Mx+C. Protein concentration of unknown sample was calculated by this equation.

#### 2.2.5.2.3. Sodium dodecyl sulphate-polyacrylamide gel electrophoresis (SDS-PAGE)

##### 2.2.5.2.3.1. SDS-PAGE gel preparation

Resolving and stacking gels were prepared according to gel recipes (Table 2.10) and stored at 4$^{o}$C until electrophoresis. 10% and 12.5% resolving gels were employed as a standard gel for immunoblotting.

**Table 2.10 Polyacrylamide gel recipes for SDS-PAGE**

| **Resolving gel** | **10%** | **12.5%** | Unit |
|---|---|---|---|
| Water (distilled) | 2.76 | 1.95 | ml |
| 30% Bis-acrylamide, 37.5:1 | 3.34 | 4.15 | ml |
| 1M Tris-HCl pH 8.8 | 3.75 | 3.75 | ml |
| 10% SDS | 100 | 100 | µl |
| 10% APS | 50 | 50 | µl |
| TEMED | 5 | 5 | µl |
| Total | 10 | 10 | ml |

| **Stacking gel** | **4%** | Unit |
|---|---|---|
| Water (distilled) | 3.605 | ml |
| 30% Bis-acrylamide, 37.5:1 | 0.665 | ml |
| 1M Tris-HCl pH 6.8 | 0.625 | ml |
| 10% SDS | 50 | µl |
| 10% APS | 25 | µl |
| TEMED | 5 | µl |
| Total | 5 | ml |

##### 2.2.5.2.3.2. Electrophoresis

**Sample preparation and loading**

After extraction, protein lysate was prepared prior to loading into SDS-PAGE gel. For soluble protein, 5X Laemmli buffer and sample were mixed with a required volume of water for a final concentration of 1X Laemmli and 10-20 µg protein per

sample. For insoluble protein, sample was resuspended in 1X Laemmli buffer (100 µl/sample). The mixture protein-Laemmli was spun by a brief centrifugation at 10,000 rpm, boiled at 95$^{o}$C for 2-3 minutes, spun again by a centrifugation at the maximum speed of 14,000 rpm for 1 min and stored on ice until loading.

**Gel running**

Gel was applied into SDS-PAGE apparatus (Biorad). 1X SDS-PAGE running buffer was filled into gel and chamber as manufacturer's instruction. Samples were loaded with the same amount of protein to each well. Protein marker (PageRuler Plus Prestained Protein Ladder, Thermo Scientific) was loaded in adjacent wells. Electrophoresis was performed at 100V for about 90-120 minutes.

#### 2.2.5.2.3.3. Protein transfer

After electrophoresis, SDS-PAGE gels were stored in a tank containing cold SDS-PAGE protein transfer buffer for 5-10 minutes. Protein samples were transferred from gel to Protran nitrocellulose membrane, 0.2 µm pore size (GE Healthcare), by a Mini-Trans Blot cell (Biorad). Gel sandwich was prepared as manufacturer's instruction (Biorad, Electrophoretic Transfer) and applied to a tank filled of 1X cold SDS-PAGE protein transfer buffer. A Bio-ice cooling unit (Biorad) and a stirrer were also employed to cool down the buffer during protein transfer. Power supply was set up at 250 mA for 120 minutes as a standard condition of protein transfer.

### 2.2.5.2.4. Immunoprobing

#### 2.2.5.2.4.1. Blocking

Efficacy of protein transfer was confirmed by Ponceau S staining. Membrane was washed once by water, incubated in Ponceau S stain solution at RT for 3-5 minutes. Image of stained protein was scanned for record. After staining, Ponceau S was removed by several washes with PBS and the membrane was incubated with blocking solution (PBS, 5 % (w/v) skimmed milk) for 30-60 minutes at RT. This blocking step was required to prevent non-specific protein binding onto the membrane.

#### 2.2.5.2.4.2. Antibody incubation

The membrane was incubated with primary antibodies (Table 2.3) at 4$^{o}$C overnight or for 2 hours at RT (5 ml/tube), and with the secondary antibodies (Table 2.4) for 1 hour at RT. After each antibody incubation, the membrane was washed three times with PBS-T (5-10 minutes each wash) to remove unbound antibodies. After the final wash with PBS-T, the membrane was washed with PBS for 10 minutes, then stored at RT in PBS until visualisation. To protect fluorescence secondary antibodies from light bleaching, the membrane was covered by a piece of Aluminium foil during the incubation and washing steps.

#### 2.2.5.2.4.3. Visualisation

Immunoreactive bands were visualised and quantified by a LI-COR Odyssey Infrared Imaging System 9120 (LI-COR Biosciences), using Image Studio software.

### 2.2.6. Screening

#### 2.2.6.1. InCell Click assay

MCF10A cells were seeded at 2x10$^{4}$ cells/well in 96-well plates for 24 hours, labelled with 10 µM EdU for 30 minutes, then fixed by an incubation with 4% (v/v) para-formaldehyde (PFA) at RT for 10 minutes. Cells were permeabilised by washing 4 times with PBS-TX (5 minutes/wash), then washed once by PBS. Next, cells were blocked by an incubation with blocking buffer (PBS, 1% (w/v) BSA) at RT for 30 minutes, and washed once by PBS. Click reaction II solution was prepared (Table 2.1) and added to each well (50 µl/well). Plate was covered in aluminium foil and incubated at RT for 30 minutes. After reaction, cells were washed for 5 times with PBS-T, 4 times with PBS and once with water. Plate were air-dried in dark for 1-2 hours. Signals were detected and quantified by a LI-COR Odyssey Infrared Imaging System 9120 (LI-COR Biosciences), using Image Studio software.

#### 2.2.6.2. Click-iT EdU microplate assay

Click-iT EdU microplate assay was performed according to the manufacturer's instruction (Thermo Fisher Scientific). Cells were seeded at a density of 4-8x10$^{3}$

cells/well in TC 96-well plates for 20 hours, treated with drugs for 24 hours and labelled with EdU for 30 minutes. Click-iT EdU stock solutions were prepared if required. Cells in each well were incubated with 50 µl of Click-iT EdU fixative (component D) for 10 minutes. 2X Click-iT reaction cocktail was prepared (Table 2.11), then 50 µl of solution was directly added into each well containing 50 µl fixative to make 1X Click-iT solution. Cells were incubated with 1X Click-iT solution for 30 minutes, then washed twice with deionised water (200 µl/well). Cells were incubated with 1X blocking buffer (200 µl/well) for 10 minutes, then with α-Oregon Green HRP conjugate (1:400 diluted in blocking buffer) (50 µl/well) for 30 minutes. After incubation, cells were washed twice with Amplex Ultra Red buffer (200 µl/well), then incubated with Amplex UltraRed reaction mixture (prepared as in Table 2.12) (100 µl/well) for 30 minutes. Fluorescence signals were measured by a CytoFluor plate reader. Data was analysed by MS Excel 2016 software.

**Table 2.11 2X Click reaction cocktail solution recipe**

| **Component** | **1 plate (100 samples)** | **Dilution** | **1 sample** |
|---|---|---|---|
| 2X Click reaction buffer | 4.7 ml | - | 47 µl |
| $CuSO_4$ | 120 µl | 1:50 | 1.2 µl |
| Oregon 488 azide | 30 µl | 1:200 | 0.3 µl |
| Click buffer additive | 1.2 ml | 1:5 | 12 µl |
| Total | 6 ml | | 60.5 µl |

**Table 2.12 Amplex UltraRed reaction mixture recipe**

| **Component** | **1 plate (100 samples)** | **Dilution** | **1 sample** |
|---|---|---|---|
| Amplex UltraRed buffer | 12ml | - | 120 µl |
| Amplex UltraRed reagent | 12 µl | 1:1,000 | 0.12 µl |
| Hydrogen peroxide | 12 µl | 1:1,000 | 0.12 µl |
| Total | 12ml | | 120.24 µl |

#### 2.2.6.3. Screening by Alamar Blue assay

##### 2.2.6.3.1. Reformatting PKIS library in 96-well plates

PKIS library was received from University of North Carolina, North Carolina, United States and originally stored in a 384-wells plate. To adapt to the working condition of an automated liquid handling system ZANUS Automated Workstation (Perkin Elmer) which was used for our screening, PKIS library was reformatted in 96-well plates with required criteria, including position of drugs in 96-well plates (called as "mother plates"), concentration of drug in stock solution, and labelling of drugs and plate. The reformation of PKIS library was performed by Dr Enda O'Connell.

We chose 100 µM as the concentration of stock solutions of PKIS drugs in "mother plates", so 5 µl of 1 mM compounds stored in a 384-well plate was dissolved in 45 µl of DMSO for the stock solution of 100 µM, then transferred to seven 96 Well V Bottom Sterilin Plate (Thermo Fisher Scientific, Cat No 11309163). Each "mother plate" contained 48 compounds which were located in the middle of the plate. Each drug was labelled as "cp1" to "cp317". Each "mother plate" was labelled as "BMSE001_A" to "BMSE001_G" and stored at -80$^{o}$C until usage.

##### 2.2.6.3.2. Optimisation and determination of the robustness of Alamar Blue assay for screening

In order to optimise the Alamar Blue assay for identifying potential "hit" compounds of PKIS screening, we identified several key variables of experiments, i.e. cell seeding density, inhibitor treatment time-course and incubation time of cells in Alamar Blue solution.

Cells were seeded at different cell densities: 1) MCF10A cells at $1x10^3$, $2x10^3$ and $4x10^3$ cells/well; 2) MDA-MB-231 cells at $2x10^3$, $4x10^3$ and $8x10^3$ cells/well; 3) HAP1 WT and 4KO at $0.5x10^3$, $1x10^3$ and $2x10^3$ cells/well, in TC 96-well plates for 24 hours. Culture medium was added into no-cell control wells. Cells were incubated with control drugs for a time-course of 48 and 72 hours, then with 0.56 µM Alamar Blue for 4, 6 and 12 hours. Fluorescence signals were read by the multi-label plate reader Victor X5 (Perkin Elmer). The cell seeding, inhibitor and Alamar Blue reagent

addition were performed with the ZANUS Automated Workstation (Perkin Elmer) under the supervision of Dr Enda O'Connell.

During the optimisation, Z-factor (or Z'), a statistical method developed for determining the robustness of an assay, was used. Z' was calculated as below.

$$Z' = 1 - \frac{3SD\ of\ sample + 3SD\ of\ control}{|Mean\ of\ sample - Mean\ of\ control|}$$

"Sample" was defined as fluorescence measured values of drug-treated cells and "control" was fluorescence measured values of vehicle control DMSO-treated cells. If Z-factor is within a range of 0.5-1.0, the assay is robust and it is adequate for a high-throughput screening (HTS). In opposite, if Z-factor is below 0.5, the assay might be designed in a poor format and it is not reliable for the HTS [203].

#### 2.2.6.3.3. Screening process

Prior to PKIS screening, PKIS drugs were diluted to 10 µM in culture medium of new 96 Well V Bottom Sterilin Plate (Thermo Fisher Scientific, Cat No 11309163), named as "daughter plates".

##### 2.2.6.3.3.1. Screening of PKIS in combination with XL413

For PKIS screening, $4x10^3$ cells of MCF10A and $8x10^3$ cells of MDA-MB-231 cells were seeded in each well of TC 96-well plates (90 µl/well) for 24 hours, except 3 no-cell control wells. Cells were treated with 0.5 µM PKIS drug from "daughter plates" and 10 µM XL413 or DMSO for 48 hours, and incubated with 0.56 µM Alamar Blue in sterile PBS for 6 hours. Each sample was performed in duplicate. All of the screening process was performed with a ZANUS Automated Workstation (Perkin Elmer) and fluorescence signals were read by the multi-label plate reader Victor X5 (Perkin Elmer). Data was analysed by MS Excel 2016 software.

##### 2.2.6.3.3.2. Screening of PKIS with genetically modified HAP1 cell lines

$2x10^3$ cells of HAP1 WT and 4KO cells were seeded in each well of TC 96-well plates (95 µl /well) for 24 hours, except 3 no-cell control wells. Cells were treated 0.5 µM PKIS drugs from "daughter plates" for 72 hours, then incubated with 0.56

µM Alamar Blue in sterile PBS for 6 hours. Each sample was performed in triplicate. All of screening process was performed with the ZANUS Automated Workstation (Perkin Elmer) and fluorescence signals were read by the multi-label plate reader Victor X5 (Perkin Elmer). Data was analysed and graphed by MS Excel 2016 software.

#### 2.2.6.4. Data normalisation and evaluation of screening results

##### 2.2.6.4.1. Data normalisation

PKIS screening was performed with 7 "mother plates" of drugs coded from BMSG001_A to BMSG001_G with replicates. To remove the variability of data across plate-to-plate, we used two methods, Z-score and percent of control.

###### 2.2.6.4.1.1. By Z-score

Z-score is a statistical tool to normalize raw data. Z-score is defined by the equation as below.

$$Z(i) = \frac{x(i) - \mu}{\sigma}$$

where x(i) indicates average fluorescent intensity after background correction, µ indicates mean and σ indicates standard deviation (SD) [204]. By normalizing data to Z-score, we can compare the effects of treatment of each compound in the same plate as well as in the different plates.

To calculate, the raw fluorescence intensity of each sample (read by Victor X5) in each 96-well plate was subtracted to the average of fluorescence intensity of no-cell wells (defined as "background fluorescence") (read by Victor X5) in the same plate to obtain the actual fluorescence intensity of each 96-well sample after background correction. As each sample was performed in replicates, then an average of fluorescent intensity was calculated prior to apply the formula. µ is the mean and σ is the SD of all x(i) within the same "mother plate". Data analysis was performed with MS Excel 2016 software.

#### 2.2.6.4.1.2. By percent of control (POC)

Percent of control is a qualitative measure of compound activity, and defined as formula below

$$POC = \frac{X(i)}{\mathrm{C}} \times 100$$

[204]

X(i) indicates the fluorescent intensity of compound and C indicates the mean of negative control DMSO or XL413 within the same "mother plate". As each sample was performed in replicates, then an average of fluorescent intensity was calculated prior to apply the formula.

#### 2.2.6.4.2. Evaluation of screening results

Based on Z-score of each compound, we plotted a graph of Z-score of 317 compounds of each cell line. To detect potential compounds, we defined a "hit" as a compound which belongs to top 1% of compounds. Those compounds are required to have a Z-score (absolute value) which is equal or higher than 2.33, based on Standard Normal Probabilities table of Erickson [205]. In addition, based on POC, we plotted a graph of Fold difference from DMSO/XL413 of 317 compounds of each cell line. Targeted kinase list of "hit" compounds was determined by searching ChemBL database and the effects of compounds on cells were tested by biochemical assays.

# Chapter 3: Investigating the biological effects of CDC7 kinase inhibitors on human cells and the mechanism of cellular responses

## 3.1 Introduction

Cell division cycle 7 (CDC7) is a serine-threonine kinase which was first characterised in the budding yeast, *Saccharomyces cerevisiae* [7], but has also been widely studied in mammalian cells, i.e. in humans. The depletion of CDC7 by small interfering RNA (siRNA) in cancer cells induces DNA replication arrest leading to nuclear DNA damage and apoptotic cell death in various cancer cell lines. Cells surviving from the previous cell cycle will die in mitosis during the next cycle due to the amplification of abnormal chromosomes in nucleus [143,145,173,206]. In contrast, CDC7 ablation does not induce apoptosis in normal fibroblast cells, but instead activates a p53-dependent cell cycle checkpoint system and arrests cells at the boundary of G1/S-phase [177]. This blockade can be abolished by knock-down of p53 [145]. These studies showed that lack of CDC7 affects cell cycle progression and cell proliferation in both cancer and normal cells. However, it is not clear whether these effects were induced by the attenuation of kinase activity of CDC7, or by the lack of its scaffolding role in the protein network, or both.

To address this question, we employed two ATP-competitive CDC7 inhibitors, PHA-767491 and XL413, to investigate the effects of CDC7 kinase inhibition on cell cycle progression and cell proliferation in human cell lines. XL413 was considered as a selective inhibitor of CDC7 [194]. Another, structurally dissimilar, ATP-competitive CDC7 inhibitor PHA-767491, was also used to offset potential off-target effects of XL413. This compound inhibits CDC7 kinase activity, abolishes DNA replication and has an antitumour activity on various cancer cell lines *in vitro* and *in vivo* [189].

Two human cell lines, MCF10A and MDA-MB-231, were treated with the CDC7 inhibitors. MCF10A is an immortalised, non-malignant breast cell line and MDA-MB-231 is a metastatic breast cancer cell line. Both are triple-negative (ER-/PR-

/HER2-) lines, but MCF10A expresses wild-type p53, while MDA-MB-231 expresses a mutant form of p53 [199].

## 3.2 Titration of CDC7 kinase inhibitors to identify the biological active dose

In the study of Koltun *et al.* [194], a 24-hour treatment of Colo-205 adenocarcinoma cells with XL413 at a concentration of 3.3 µM induced an accumulation of cells at the late S/G2-phase. Based on this, cells were treated with XL413 at a range of concentrations from 2.5-50 µM in order to establish the dose at which phosphorylation of MCM2 at S40/41 is fully inhibited. This phosphorylated site has been shown to be a biomarker of CDC7 kinase activity [86]. Alongside this, the phosphorylation status of MCM4 in the presence of CDC7 kinase inhibitors was also evaluated as CDC7 has a role in phosphorylating this MCM subunit [130,207]. Finally, the progression of DNA synthesis in inhibitor-treated cells was tracked using Click chemistry technology.

### 3.2.1 Effects of CDC7 kinase inhibitors on the phosphorylation of MCM complexes

MCM2 phosphorylation at S40/41 was chosen as the main criteria in evaluating effects of the putative CDC7 inhibitors. Cells were plated for 24 hours, then treated with DMSO (vehicle control) or inhibitors (XL413/PHA-767491) at doses from 2.5-50 µM for 24 hours. Treated cells were trypsinised, pelleted and subjected to immunoblotting. Blots were scanned using the LiCOR infrared system and analysed by the Image Studio software.

In MCF10A cells treated with XL413 at 2.5 µM, the level of phospho-MCM2 at Ser40/41 (pMCM2 S40/41) in the soluble fraction was strongly decreased in comparison to DMSO-treated cells (Figure 3.1A, pMCM2 S40/41, lane 2) and almost undetectable at 10 µM (Figure 3.1A, pMCM2 S40/41, lane 4). MCM2 phosphorylation at Ser40/41 was undetectable in the insoluble fraction (Figure 3.1B, pMCM2 S40/41). CDC7 levels in both soluble and insoluble fractions remained unchanged under XL413 treatment (Figure 3.1A and 3.1B, CDC7, lane 2-6).

In XL413-treated MDA-MB-231 cells, similar effects were observed (Figure 3.1C and 3.1D). In the soluble fraction, phosphorylation of MCM2 at S40/41 of XL413-treated was reduced at concentrations as low as 2.5 µM (Figure 3.1C, pMCM2

S40/41, lane 2) and it was undetectable in the insoluble fraction (data not shown). CDC7 levels did not change either in soluble (Figure 3.1C, CDC7, lane 2-6) or in insoluble fractions of treated cells at any dose (Figure 3.1D, CDC7, lane 2-6).

Noticeably, in MCF10A cells, the level of p53 was consistent under XL413 treatment within the range of concentrations from 2.5 to 10μM, and p21, a biomarker of p53 activity, was not detected within this range (Figure 3.1A, p53 and p21, lane 2-4). Taken together, these data suggest that XL413 treatment can strongly decrease MCM2 S40/41 phosphorylation in both cell lines at 10 μM without affecting the protein level of CDC7 or p53.

In MCF10A cells treated with PHA-767491, no MCM2 S40/41 phosphorylation was detected at any dose between 2.5 - 50 μM, but the protein level of CDC7 was reduced at 2.5 μM (Figure 3.1A and 3.1B, CDC7, lane 7-11). Similarly, in MDA-MB-231 cells, MCM2 S40/41 phosphorylation was depleted by 10 μM of PHA-767491 (Figure 3.1C and 3.1D, pMCM2 S40/41) and CDC7 levels were also clearly reduced under this treatment (Figure 3.1C and 3.1D, CDC7). This suggests that PHA-767491 may suppress the synthesis of CDC7 or the stability of this protein in both cell lines. One explanation could be that this compound has a cross-inhibition with other kinases such as CDK9, a kinase involved in transcription elongation through the phosphorylation of RNA polymerase II [190], leading to the down-regulation of CDC7. In addition, CDC7 stability is regulated by the activity of Fbxw7β in a p53-dependent manner at post-translational level under genotoxic stress condition [165].

In addition to observing the effects of XL413 on the phosphorylation of MCM2, we also evaluated the modification of MCM4. Dephosphorylation of MCM4 was detected in CDC7-depleted HeLa cells [207], suggesting phosphorylation of MCM4 might be dependent on CDC7 kinase activity. In our cell lines, the hypophosphorylation of MCM4 in mock-treated (Figure 3.1A and 3.1C, MCM4, lane 1) and hyperphosphorylation of MCM4 in HU-treated cells (Figure 3.1A and 3.1C, MCM4, lane 13) were observed. MCM4 retained some phosphorylation in XL413-treated MCF10A cells, as shown by a decrease of intensity of the shifted band above the MCM4 main band (Figure 3.1A, MCM4, lane 2-6). In MDA-MB-231 cells, a similar phenomenon occurred (Figure 3.1C, MCM4, lane 2-6). This suggests that the

CDC7 kinase inhibition by XL413 at doses between 2.5-50 μM reduces phosphorylated MCM4 levels but does not fully inhibit MCM4 phosphorylation in either cell line. In a previous study, authors showed that MCM4 is phosphorylated by both kinases CDC7 and Cdc2/CDK1 human homolog [130], so other kinases may be responsible for the remaining phosphorylated residues of MCM4.

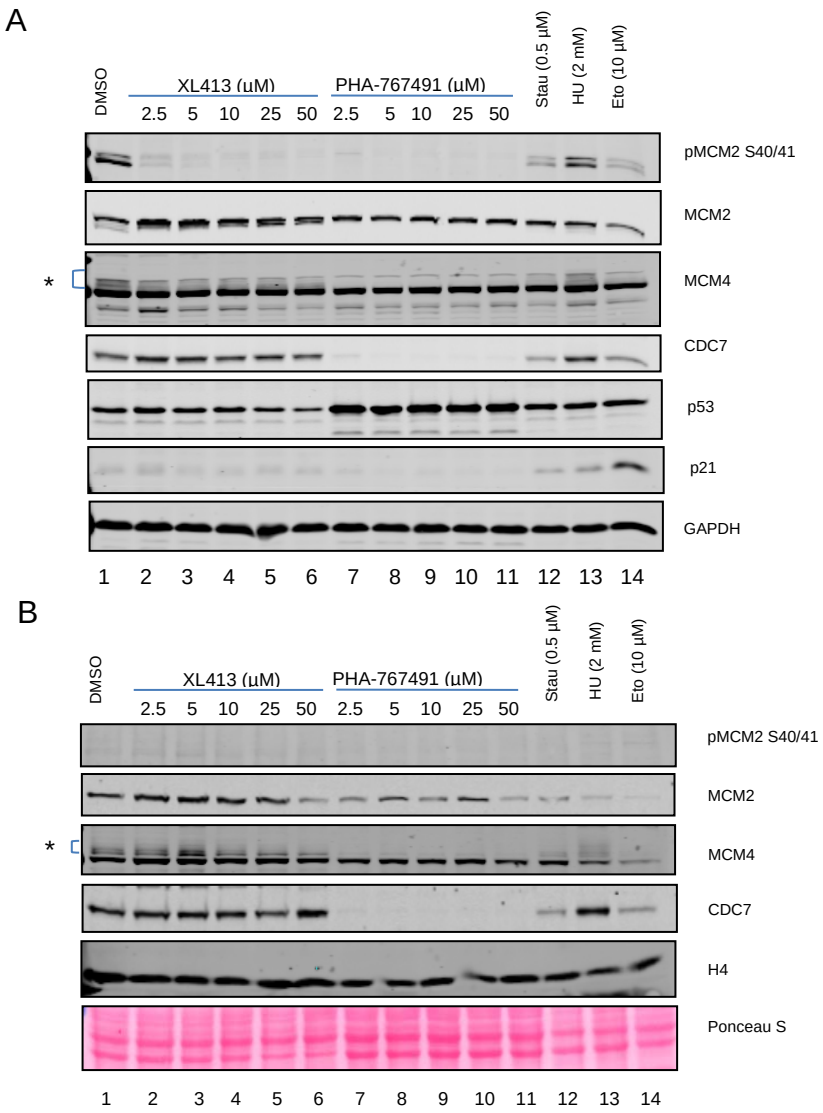


**Figure 3.1 Optimisation of XL413 and PHA-767491 doses in MCF10A and MDA-MB-231 cells.**

Cells were treated with XL413, PHA-767491, DMSO, Staurosporine (Stau), Hydroxyurea (HU) or Etoposide (Eto) at indicated doses for 24 hours, then harvested and subjected to protein extraction with CSK lysis buffer. Both soluble and insoluble fractions were used for immunoblotting. (*) Phosphorylated-MCM4; (A) MCF10A, soluble fraction; (B) MCF10A, insoluble fraction;

(To be continued next page).

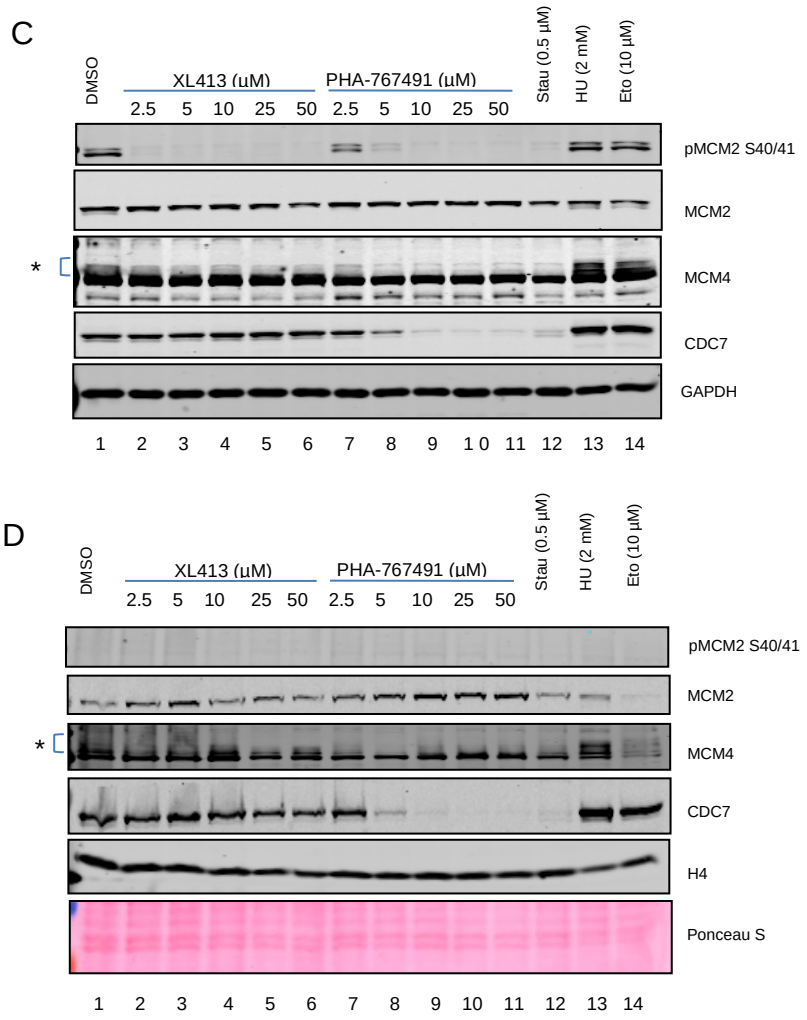


**Figure 3.1 Optimisation of XL413 and PHA-767491 doses in MCF10A and MDA-MB-231 cells (continued).**

(C) MDA-MB-231, soluble fraction; (D) MDA-MB-231, insoluble fraction. Experiments were performed once

### 3.2.2 Dose-dependent effects of CDC7 kinase inhibitors on DNA replication

In this experiment, we employed the Click chemistry to examine DNA replication under CDC7 kinase inhibition. EdU is a thymidine analogue that is incorporated into double-stranded DNA of proliferating cells during DNA synthesis. Subsequently, EdU-labelled DNA can be fluorescently stained using Click chemistry and fluorescence signals can be detected and quantified either by flow cytometry or by fluorescence microscopy [208]. In this study, cells were labelled with EdU at the concentration of 10 µM.

MCF10A and MDA-MB-231 cells were plated for 24 hours, then treated with different doses of XL413 or PHA-767491 for another 24 hours. Cells were incubated with EdU for 30 minutes after each inhibitor treatment, then harvested, fixed and subjected to EdU/DAPI staining for flow cytometry. Signals were detected and analysed with BD FACS/FlowJo software.

In MCF10A cells treated with 2.5 µM XL413, we observed an increase in the percentage of S-phase population from 38.3 to 44.2 and a decrease of G2-phase population from 15.4 to 8.9, without any change of the G1-phase population (Figure 3.2A, DMSO vs XL413 2.5). Over the range of 2.5 to 50 µM of XL413, there was a trend of decreasing cells at G1-phase in a dose-dependent manner (Figure 3.2A, XL413 2.5-50, G1). In cells treated within the range of 2.5-10 µM XL413, an increase of proportion of S-phase population occurred concomitantly with the decrease of G2/M-phase population (Figure 3.2A, XL413 2.5-10, S and G2) without any remarkable increase of subG1-phase population (Figure 3.2A, XL413 2.5-10, subG1) in comparison with mock-treated cells (Figure 3.2A, DMSO). There was also a shift of EdU signal intensity from the area of early S-phase (near G1) in untreated sample (DMSO) to the area of late S-phase (near G2) after XL413 treatment (Figure 3.2A, S-phase of DMSO vs XL413 2.5-10). This suggests that XL413 may trigger a delay of late S- and G2/M-phase, and that inhibition of CDC7 kinase activity is relatively proportional to the induction of cell cycle arrest.

However, the increase of XL413 dose up to 25 and 50 µM of XL413 induces effects that are different from the range of 2.5 to 10 µM. Percentage of S-phase population decreased from 38.3 to 34.3 and 32.1 correspondently (Figure 3.2A, XL413 25-50, S) and percentage of G2/M-phase population increased from 15.4 to 23.3 and 22.7 correspondently (Figure 3.2A, XL413 25-50, G2). Upon this dose, the level of p53 protein also decreases (Figure 3.1A, p53, lane 5-6), suggesting at 25 µM or higher doses, XL413 affects the stability of p53 as an off-target effect.

For MDA-MB-231, an accumulation of cells at S-phase was observed at 2.5 µM of XL413 (Figure 3.2B, S-phase of 2.5). Percentage of S-phase population increased from 37.8 in mock-treated cells to 45.2 in XL413-treated cells and the increase of inhibitor concentration up to 25 µM of XL413 did not noticeably change this

proportion (Figure 3.2B, XL413 2.5-25, S). A trend of decreasing cells at G1-phase in a dose-dependent manner was observed in this cell line (Figure 3.2B, XL413 2.5-50, G1). This indicates that within the range of concentration of 2.5-25 µM of XL413, a delay of late S- and G2/M-phase also occurs in treated MDA-MB-231 cells.

Noticeably, there was no increase in the subG1 population at any dose of XL413, while this population was still observed in PHA-767491- and Staurosporine-treated cells of both cell lines (Figure 3.2, PHA-767491 and Stau). This indicates that 24 hr-treatment of XL413 over the range of concentrations used (2.5-50 µM) does not induce apoptotic cell death in human breast cell lines. Furthermore, DNA replication was not blocked by XL413. At all doses of this compound, EdU-positive cells were still observed (Figure 3.2, XL413 2.5-50, S), while DNA replication was abolished by 10 µM of PHA-767491 (Figure 3.2, PHA-767491, S). Since it is known that both compounds are ATP-competitive CDC7 kinase inhibitors, the different and consistent responses of two cell lines raised a new question of whether there is any additional factor or mechanism involved.

In summary, it was found that 10 µM XL413 is a biologically active dose for CDC7 kinase inhibition in both MCF10A and MDA-MB-231 cell lines. At this dose, the phosphorylation of MCM2 at S40/41, a biomarker of CDC7 activity in cells, is efficiently prevented. However, the phosphorylation of MCM4 and DNA synthesis still occurs at any dose of this compound within the range of 2.5 – 50 µM. Further experiments are required to elucidate this phenomenon.

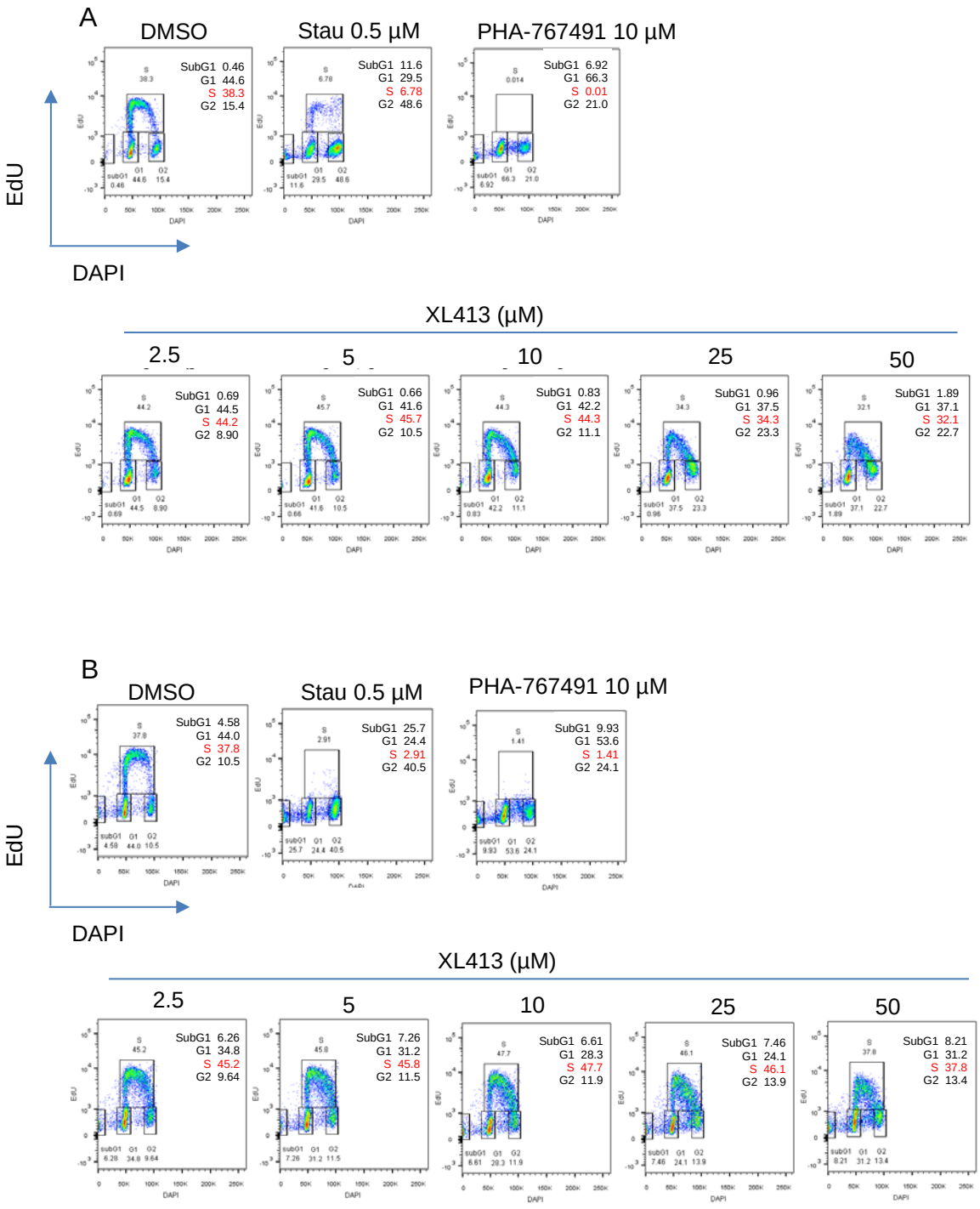


**Figure 3.2 Cell cycle progression of MCF10A and MDA-MB-231 cells following XL413 treatment**

Cells were treated with XL413 at indicated concentrations for 24 hours then incubated with 10 µM EdU for 30 minutes. Fixed cells were subjected to EdU/DAPI staining for flow cytometry. (A) MCF10A; (B) MDA-MB-231. Stau: Staurosporine. Experiment was performed once.

## 3.3 Biological effects of CDC7 kinase inhibitor XL413 on human cells

Previous studies have shown that inhibition of CDC7 by siRNA causes apoptotic cell death and prevents tumour growth in a p53-independent manner [193,209]. The inhibition of CDC7 by PHA-767491 also causes similar events [189,193]. However, these effects may result from the reduction of the protein level of CDC7 due to siRNA transfection, or the combined inhibition of CDC7 with other kinases such as CDK9 [190]. Therefore, in this study, we wanted to confirm whether the inhibition of CDC7 kinase activity specifically by XL413 causes apoptotic cell death or prevents cell proliferation of human cells.

### 3.3.1 XL413 does not trigger apoptotic cell death

First, to examine cell death induced by XL413, an apoptosis assay was performed using fluorescein isothiocyanate (FITC)-conjugated Annexin V staining. Annexin V is a protein that preferably binds to phospholipids of inner leaflet, such as phosphatidylserine, when the phospholipids are translocated to the external surface of membrane during cell death. Hence, binding of Annexin V is considered as a marker of apoptotic/necrotic cells [210].

MCF10A and MDA-MB-231 cells were plated for 24 hours, then treated with XL413 or Staurosporine for 24 hours. At the end of treatment, cells were harvested and subjected to Annexin V/PI staining for flow cytometry without fixation. Annexin V (+) or apoptotic cells were found in Staurosporine-treated samples of both cell lines, providing a positive control for this experiment. In both cell lines, XL413 treatment did not induce any obvious Annexin V (+) population (Figure 3.3), confirming that XL413 does not induce apoptotic cell death in human cell lines after 24 hours of treatment.

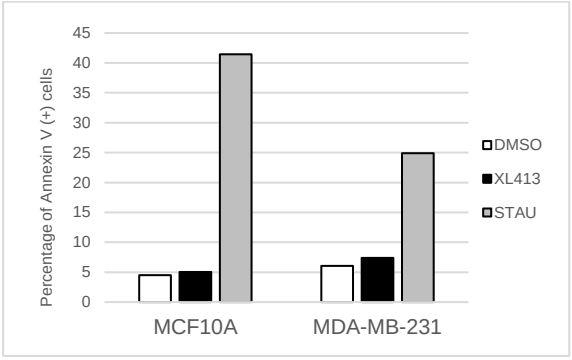


**Figure 3.3 Detection of apoptotic cell death in MCF10A and MDA-MB-231 cells 24 hours post-treatment**

Cells were treated with each compound for 24 hours, then subjected to Annexin V/PI staining for flow cytometry. STAU: Staurosporine. Experiment was performed once

### 3.3.2 XL413 reduces cell proliferation and clonogenicity of MDA-MB-231 cells released from treatment

SubG1-phase or Annexin V-positive population was undetectable in MCF10A and MDA-MB-231 upon 24 hr-treatment with the CDC7 kinase inhibitor XL413, indicating this compound may not trigger apoptosis in both cell lines. This is surprising because different studies emphasised the critical roles of CDC7 in initiating DNA replication and the occurrence of cell death when this kinase is absent [174]. However, we did not exclude the possibility of 24 hours of inhibitor treatment being insufficient to induce apoptotic markers at detectable levels. Instead of repeating experiments with a longer time of treatment, we examined the cell proliferation and clonogenic survival rate of both cell lines released from XL413 treatment. Our hypothesis is that this inhibitor does not prevent cells from proliferating and forming colonies. In theory, if cells cannot survive and proliferate after being released from the inhibitor treatment or, if after the inhibitor treatment for 1 or 2 cycles, cells are unable to proliferate and form colonies from a single cell, then they are still considered to be dead cells [211].

#### 3.3.2.1 MDA-MB-231 cells released from treatment are able to proliferate but at a lower rate

First, the growth curves of MCF10A and MDA-MB-231 cells were assessed upon the release from XL413 treatment. Cells were plated for 24 hours then treated with DMSO (control) or XL413 for 24 hours. After the inhibitor treatment, cells were

released into fresh medium without inhibitor for 24 and 48 hours. Harvested cells at each time point were counted at least twice. Each treatment was performed in triplicate.

It was found that XL413 treatment for 24 hours affects differently the growth rate of both cell lines post-treatment (Figure 3.4, 0h-24h-48h). For MCF10A, the number of XL413-treated cells at 24 hours post-release was triple that at the time of release, in comparison with the number of mock-treated cells that only doubled at the similar time point (Figure 3.4A, 24h vs 0h). This means that although XL413 reduces the growth rate of MCF10A cells during treatment, the surviving cells still can grow and experience an increased number of cells that divided after release. Meanwhile, XL413-treated MDA-MB-231 cells proliferate at a slower pace than mock-treated control (Figure 3.4B, 24h-48h vs 0h). This suggests that XL413 somewhat inhibits the growth rate of MDA-MB-231 cells during and after the release from treatment.

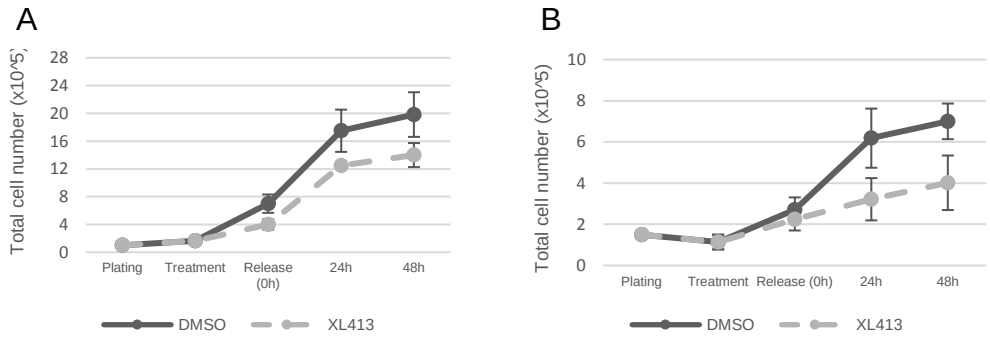


**Figure 3.4 Growth curve of MCF10A and MDA-MB-231 cells released from XL413 treatment**

Cells were treated with XL413 or DMSO for 24 hours, then released into fresh medium, harvested and counted at each time point. Each treatment was performed in triplicate. (A) MCF10A; (B) MDA-MB-231. Error bars represent the Mean ± SD. Experiment was performed once.

#### 3.3.2.2 MDA-MB-231 cells released from treatment are able to form colonies, but at a significantly lower rate

To confirm that XL413 does not prevent cells from forming colony after treatment, we employed a clonogenic assay measuring the survival of cells based on the number

of colonies formed from single clones. Cells were plated for 24 hours, then treated with XL413 for 24 hours, harvested and subjected to the clonogenic assay.

In MCF10A cells, a reduction was observed in the average number of colonies, from 104 in mock-treated to 90 colonies in XL413-treated cells (Table 3.1). The survival fraction of this cell line after inhibitor treatment was 87.1%. For MDA-MB-231 cells, only 45 colonies on average were formed in the XL413-treated sample compared to 71 in the DMSO-treated control (Table 3.1), giving a significant decrease of survival fraction to 63.2% in this cell line. Based on the data analysis of the clonogenic assay, we concluded that XL413 treatment significantly inhibits the survival ability of MDA-MB-231 cells, but not of MCF10A cells. These different responses raised the question of why the two cell lines behave differently in response to the inhibition of CDC7 by XL413, even though both overexpress CDC7.

**Table 3.1 Rates of colony formation after XL413 treatment**

| | DMSO (ave) | XL413 (ave) | Survival fraction | P-value |
|---|---|---|---|---|
| MCF10A | 104 | 90 | 87.1% | NS |
| MDA-MB-231 | 79 | 42 | 53.2% | (*) |

Cells were plated for 24 hours, then treated with XL413 for 24 hours, harvested and subjected to clonogenic assay. Each sample was performed in triplicate. (A) MCF10A; (B) MDA-MB-231. (*): $p<0.01$ (two sample t-test); NS: not significant; ave: average

### 3.3.3 A long-term treatment with XL413 prevents growth of MDA-MB-231 cells but not of MCF10A cells

The previous results showed that CDC7 kinase inhibition by XL413 does not trigger cell death after 24 hours of inhibitor treatment, but MCF10A and MDA-MB-231 cells behaved differently post-release. Therefore, we set out to determine whether long-term treatment with XL413 inhibits the proliferation of both cell lines and if there is a difference in inhibitor response between them. Cells were seeded for 24 hours, then treated with inhibitor (XL413) or vehicle (DMSO) for 24, 48 and 72 hours. At each time point, cells were harvested and counted. Cell viability were also determined by Trypan Blue staining. Each sample was performed in triplicate.

In mock-treated MCF10A cells, the proliferation began after 24 hours plating and the cell number doubled after 48 hours (Figure 3.5A, DMSO, 24 vs 48), suggesting this cell line has a doubling time of 24 hours. At the 72-hour time point, cells continued to proliferate but the cell number was not doubled the number at the 48-hour time point (Figure 3.5A, DMSO, 72 vs 48). An explanation could be that, at the 72-hour time point, either cells reach their stationary phase or they are over-confluent. For XL413-treated samples, the cell number did not increase upon 24 hours, suggesting XL413 may prevent cell growth within 24 hr treatment. However, the number of treated cells doubled 48 hours post-treatment (Figure 3.5A, XL413 24-48). It means XL413 may no longer prevent cell proliferation of this cell line. Cell proliferation continued until 72 hours, but again at a slow rate (Figure 3.5A, XL413 72). Cell viability of treated cells remained at a similar rate as of mock-treated cells suggesting XL413 also does not affect the viability of this cell line during the long-term treatment (Appendix A, Figure S3.1A).

Meanwhile, in MDA-MB-231 untreated cells, the cell number began to double only after 24 hours of cell seeding, suggesting this cell line may need some periods of time to adapt and grow. The cell number doubled after 48 and 72 hours of cell plating, suggesting this cell line has a doubling time of 24 hours that is quite similar to MCF10A cell line (Figure 3.5B, DMSO, 24-48-72). Interestingly, data analysis of growth curve showed that XL413- treated cells did not increase cell number 48- and 72-hour post-treatment, suggesting XL413 inhibits the proliferation of this cancer cell line during the long-term treatment. Data analysis of cell viability also confirmed that XL413 decreased cell viability at the 48 and 72-hour time point (Appendix A, Figure S3.1B)

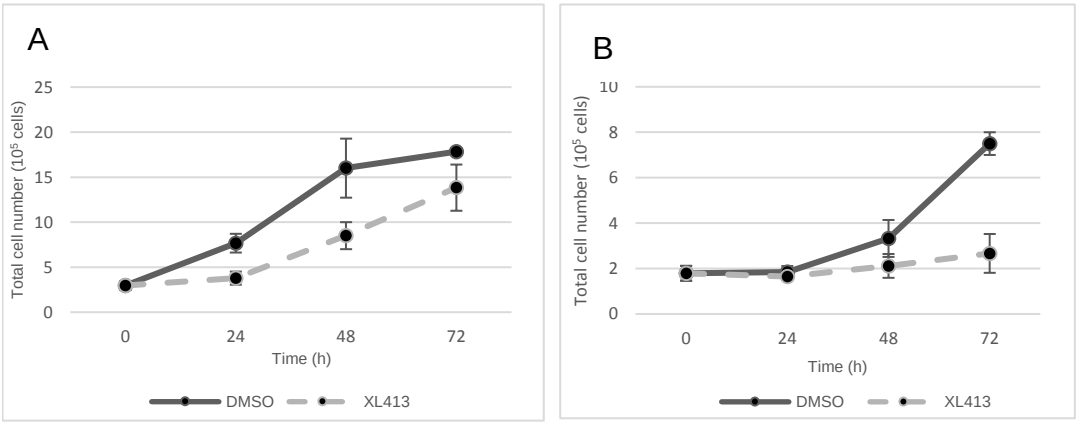


**Figure 3.5 Effects of XL413 on cell growth of MCF10A and MDA-MB-231 cells during a long-term treatment**

Cells were seeded for 24 hours, then treated with inhibitor (XL413) or vehicle (DMSO) for 24, 48 and 72 hours. At each time point, cells were harvested and counted. Cell viability were also determined by Trypan Blue staining. Each sample was performed in triplicate. (A) MCF10A; (B) MDA-MB-231. Error bars represent the Mean ± SD. Experiment was performed once

An explanation for this phenomenon could be that XL413 efficiently inhibits CDC7 kinase activity for 24 hours but not for 48 and 72 hours in MCF10A cells. To test this hypothesis, the protein level of pMCM2 Ser40/41 was examined. Phosphorylation at this site was considered as a biomarker of CDC7 activity *in vivo* [189], and the decrease of protein level was used as an indicator of CDC7 inhibition [194]. Soluble proteins extracted from cell pellets harvested in the previous experiment were subjected to immunoblotting. In MCF10A cells, the protein level of phosphorylated MCM2 at S40/41 was much lower in treated cells than in untreated cells at different time points but some residues still remained (Figure 3.6A, MCM2 S40/41). For MDA-MB-231 cells, inhibitory effects of XL413 on CDC7 kinase activity were also observed with the disappearance of pMCM2 S40/41 bands (Figure 3.6B, MCM2 S40/41). This suggests that the inhibition of CDC7 kinase by XL413 might be less efficient in MCF10A than in MDA-MB-231 cells.

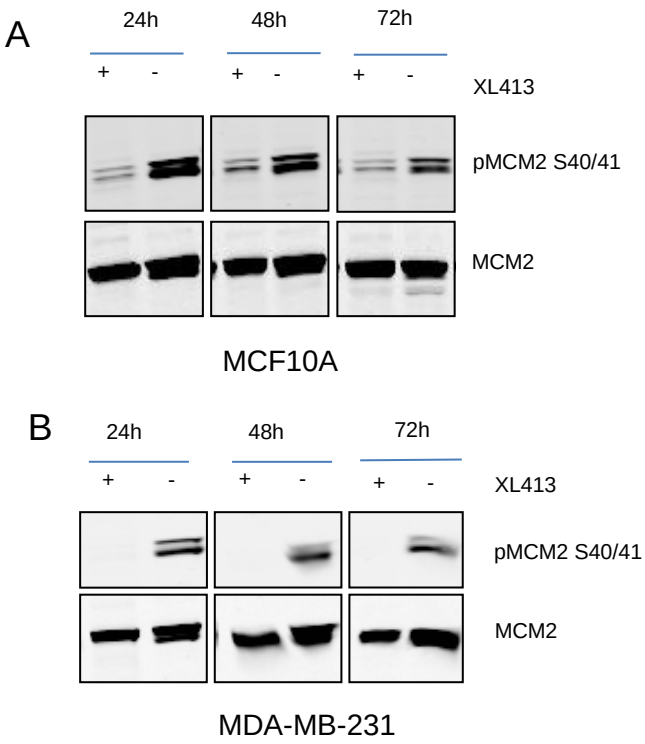


**Figure 3.6 Effects of XL413 on CDC7 kinase activity in MCF10A and MDA-MB-231 cells during a long-term inhibitor treatment.**

Cells harvested from the previous experiment (Figure 3.5, section 3.3.3) were subjected to protein extraction by TGN lysis buffer, and the soluble fraction was used for immunoblotting. (A) MCF10A; (B) MDA-MB-231. Experiment was performed once.

In summary, XL413 inhibits the growth of MDA-MB-231 cells until 72 hours of inhibitor treatment, but not of MCF10A cells. A possibility is that the inhibition of CDC7 by XL413 on MCF10A was not as efficient as on MDA-MB-231 cells. Another possibility could be MCF10A cells may have an alternative mechanism to protect from the effects of CDC7 inhibition by XL413 and continue to grow.

## 3.4 Investigating the mechanism of the cellular responses to CDC7 kinase inhibition

In response to XL413, MCF10A and MDA-MB-231 cells have different phenotypes. MCF10A cells continue to proliferate in the presence of XL413, while MDA-MB-231 cells were unable to grow during the long-term treatment with XL413. No apoptosis was observed after 24 hours of inhibitor treatment in both cell lines. We hypothesised that this compound has different effects upon DNA replication progression of those cell lines, leading to their different growth curves during the

long-term treatment with this compound. Previous studies have shown that CDC7-DBF4 has a critical role in initiating DNA replication and in origin firing during S-phase [175,212]

### 3.4.1 XL413 does not prevent DNA replication under long-term treatment

First, we examined the effects of inhibitor treatment on the EdU incorporation of MCF10A and MDA-MB-231. Cells were plated for 24 hours, then treated with DMSO (control) or XL413 for a period of time from 24 to 48 hours. At each time point, cells were labelled with EdU for 30 minutes prior to harvest, then fixed and subjected to EdU/DAPI staining for flow cytometry.

As seen before, XL413 induces an accumulation of cells in S-phase in both cell lines, either after 24 or 48 hours of inhibitor treatment in comparison with mock-treated cells (Figure 3.7, DMSO vs XL413, S). Noticeably, the EdU-negative S-phase population (red arrow) was detectable at 48-h time point in MDA-MB-231 (Figure 3.7B, XL413, 48h EdU(-) S-phase ) but not in MCF10A cells (Figure 3.7A, XL413, 48h EdU(-) S-phase) or in mock-treated cells of both cell lines (Figure 3.7, DMSO, 48h EdU(-) S-phase). A remarkable increase of percentage of subG1 population was also found in MDA-MB-231 cells, from 1.37 after 24 hours to 8.0 after 48 hours of inhibitor treatment (Figure 3.7, XL413, 24h vs 48h). This indicates that XL413 prevents DNA synthesis during S-phase of MDA-MB-231 cells and induces apoptosis 48 hours post-treatment. However, in MCF10A cells, it seems to be this compound only delays S-phase progression and does not induce any apoptotic cell after the long-term treatment.

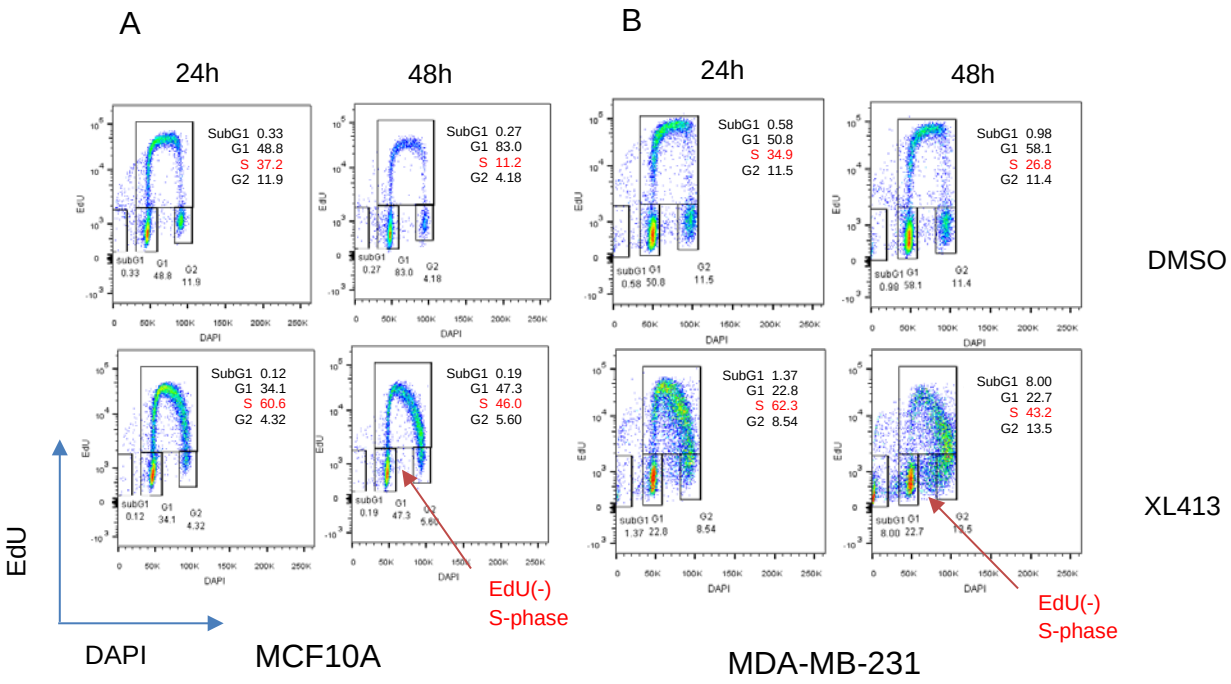


**Figure 3.7 Effects of XL413 on cell cycle progression of breast-derived human cells during long-term inhibitor treatment.**

Cells were treated with XL413 or DMSO for indicated period of time, labelled with EdU for 30 minutes prior to harvest, fixed and subjected to EdU/DAPI staining for flow cytometry. (A) MCF10A; (B) MDA-MB-231 cells. Experiment was performed once

### 3.4.2 XL413 slows the S-phase progression

To confirm that XL413 slows down the progression of DNA replication in MCF10A cell line, we examined the cell cycle progression of a synchronised population of cells in the presence of XL413. In an asynchronous population, cells are at different phases of cell cycle and this distribution within a cell line is constant over time. However, by using chemical compounds such as thymidine or mimosine, cells can be enriched at specific stages, and cell cycle blockade becomes trackable. Flow cytometry analysis showed that cells were successfully synchronised at G1/S by double thymidine-mimosine block. Synchronised cells were harvested and reseeded in fresh media containing XL413 or vehicle control DMSO. At each time point within a range of 1 to 12 hours, cells were harvested, fixed and subjected to PI staining for flow cytometry.

As expected, after being synchronised by double thymidine-mimosine block, almost all MCF10A cells accumulated at G1/S-phase at 0h time point (Figure 3.8B, DMSO,

0). One hour post-release, the G1-phase peaks of control (DMSO) started to decrease until 6 hours (Figure 3.8B, DMSO, 1-6) and increase again until 12 hours (Figure 3.8B, DMSO, 9-12). Meanwhile, in treated (XL413) cells, the G1-phase peaks gradually decreased until 12 hours (Figure 3.8B, XL413, 1-12). We noticed that the G2-phase peaks started to appear in mock-treated cells from 9 hours (Figure 3.8B, DMSO, 9-12) but not in XL413-treated cells even at 12 hours (Figure 3.8B, XL413, 12), suggesting XL413 slows down the S-phase progression of MCF10A cells and this agrees with a study of Bousset and Diffley in budding yeast [212].

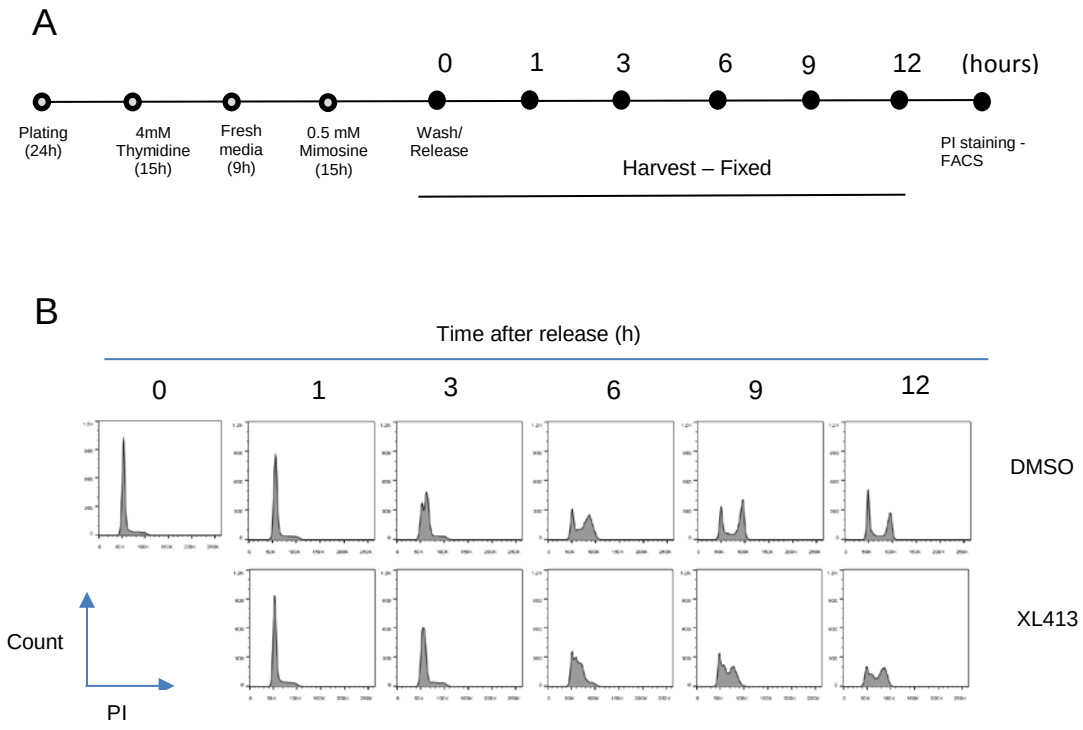


**Figure 3.8 Effects of XL413 on the S-phase progression in synchronised MCF10A cells.**

Cells were synchronised at G1/S-phase by double Thymidine-Mimosine block, then released into a fresh medium with or without 10µM XL413, harvested at indicated time points, and fixed. The DNA of treated cells were stained by PI/RNAse. Fluorescence signals were collected by flow cytometry (FACS Canto A) and data analysis was performed with FlowJo. (A) Schematic illustration of the experiment. (B) Histogram of DNA content. Experiment was performed once

### 3.4.3 XL413 does not cause replication fork stalling, nor does it affect replication fork progression

CDC7 kinase has a role in activating the pre-RC complex in order to fire the replication fork [174]. An alternative hypothesis is that the slow progression of DNA replication recorded in XL413-treated cells results from the inhibitory effects of this compound on replication fork progression. To test this hypothesis, we employed DNA fiber labelling which uses two halogenated nucleotides IdU and CldU to label newly synthesised DNA. As the labelling is performed sequentially with IdU followed by a CldU pulse (Figure 3.9A), the combination of fluorescence signals observed in spread fibers can provide information about the replication fork progression. In unperturbed cells, replication fork patterns are defined as termination (red-only or red-green-red), stalled fork (red-only), ongoing fork (green-red) and newly fired origin (green-only or red-green-red) (Figure 3.9B).

MCF10A and MDA-MB-231 cells were treated with DMSO or XL413 for 24 hours. Prior to the end of treatment, cells were pulse labelled with IdU for 30min, then CldU for another 30 minutes (Figure 3.10A). Harvested cells were subjected to DNA fiber labelling. Stained DNA fibers were detected by fluorescence microscopy. Approximate 250 to 600 fiber tracts were counted manually for each sample. Each individual experiment was performed at least in 3 independent times.

We found that there was no significant change of ratio of stalled fork/termination, new origin firing or ongoing fork progression when either cell line was treated with XL413 (Figure 3.10B and 3.10C). This suggests that XL413 does not induce fork stalling or affect the replication fork progression of human cell lines after 24 hours of inhibitor treatment.

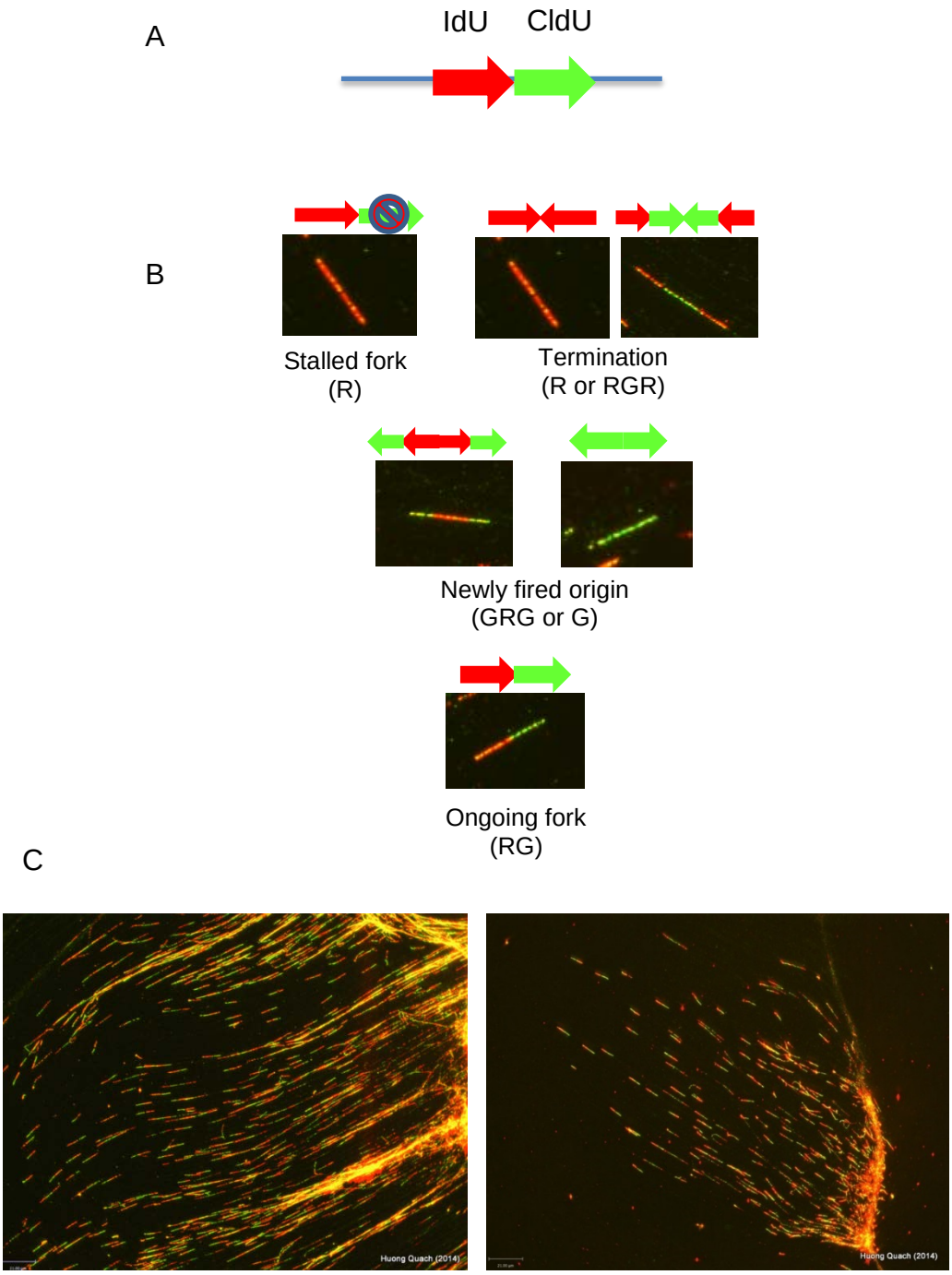


**Figure 3.9 DNA replication fork detected by DNA fiber technique**

(A) Schema of IdU/CldU labelling; (B) Replication fork patterns; (C) Example images of DNA fibers visualised by fluorescence microscopy; R: red-only; G: green-only; RG: red-green; RGR: red-green-red; GRG: green-red-green.

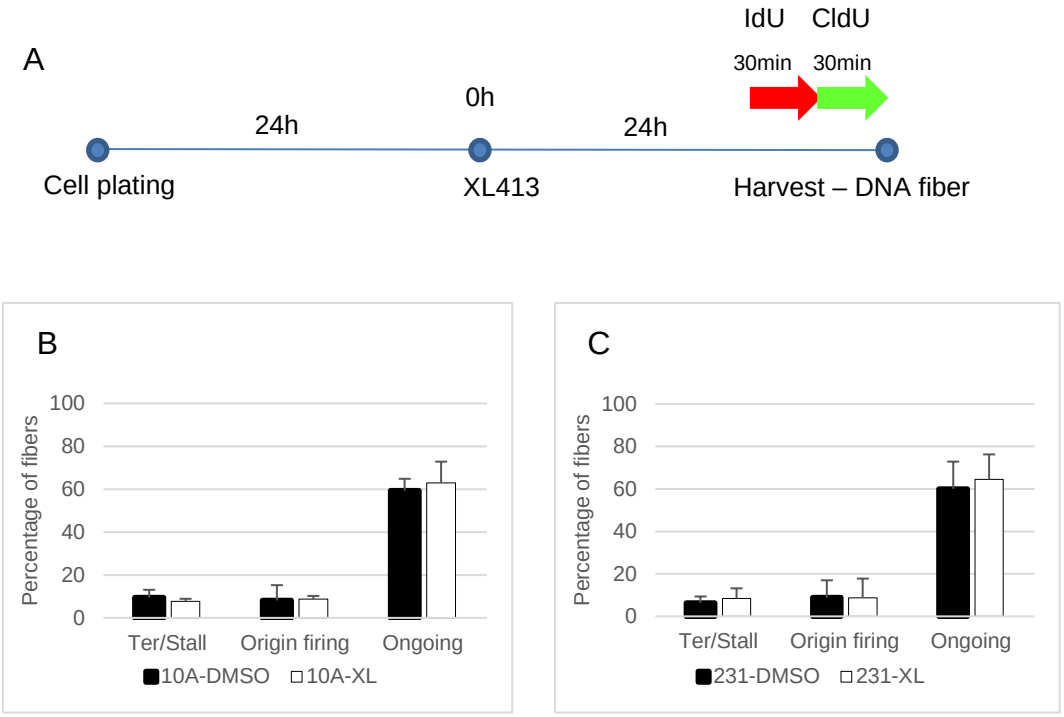


**Figure 3.10 Effects of XL413 on replication fork progression in MCF10A and MDA-MB-231 cells 24 hours post-treatment.**

Cells were treated with DMSO or XL413 for 24 hours, continuously labelled with IdU then pulse CldU prior to the end of treatment. Harvested cells were subjected to DNA fiber labelling. Stained DNA fibers were detected by fluorescence microscopy. Approximate 250 to 600 fiber tracts were counted manually for each sample. (A) Schema of experiment; (B) MCF10A; (C) MDA-MB-231; Ter/Stall: Termination or Stalled fork; Origin firing: Newly origin firing; Ongoing: Ongoing fork. Each individual experiment was performed 3 independent times. Error bars represent the Mean ± SD.

## 3.5 Effects of the CDC7 kinase inhibitor XL413 on mitosis

In the previous experiments (section 3.4.1, Figure 3.7), we found that XL413 inhibits the EdU incorporation during S-phase of MDA-MB-231 and induces apoptosis after 48 and 72 hrs of inhibitor treatment but not in MCF10A cells. However, we did not observe any patterns of fork stalling or any significant change of fork patterns, suggesting the different responses of two cell lines to XL413 might not result from the effects of XL413 on replication fork progression. Previous studies showed that CDC7 regulates mitotic exit network through Cdc5/PLK1 [153,154]. To confirm whether the inhibition of CDC7 by XL413 has effects on the mitotic progression in human cells, we examined the mitotic entry through the change of mitotic population after the inhibitor treatment and the mitotic exit through the percentage of M-phase synchronised cells that can enter S-phase in the presence of this inhibitor.

### 3.5.1 XL413 does not block mitotic entry but decrease mitotic population

First, we investigated the inhibitory effects of XL413 on mitotic entry. MCF10A and MDA-MB-231 cells were plated, then treated with XL413, PHA-767491 as an inhibitor control, or DMSO as a vehicle control for 24 hours. Treated cells were then labelled with EdU for 30 minutes, harvested and subjected to phospho-H3/EdU/DAPI staining for flow cytometry. Cells were stained with EdU/DAPI and the mitotic marker phospho-H3 Ser10 (pH3 S10) in parallel, to ensure a simultaneous staining.

In this experiment, we still observed the EdU incorporation occurring after 24 hrs of XL413 treatment (Figure 3.11A and C, XL413 vs DMSO, S). In XL413-treated cells of MCF10A, the percentage of pH3 S10-positive cells was 2.1, only slightly lower than of mock-treated cells with 2.6 (Figure 3.11B, XL413 vs DMSO, M). Meanwhile, in the PHA-767491-treated cells, only 0.4% of mitotic cells were recorded (Figure 3.11B, PHA-767491, M). Similar observations were made for MDA-MB-231 cells (Figure 3.11D, PHA-767491, M). This means that the inhibition of CDC7 kinase by XL413 does not fully prevent the mitotic entry of either cell line, but may decrease the mitotic population of treated cells.

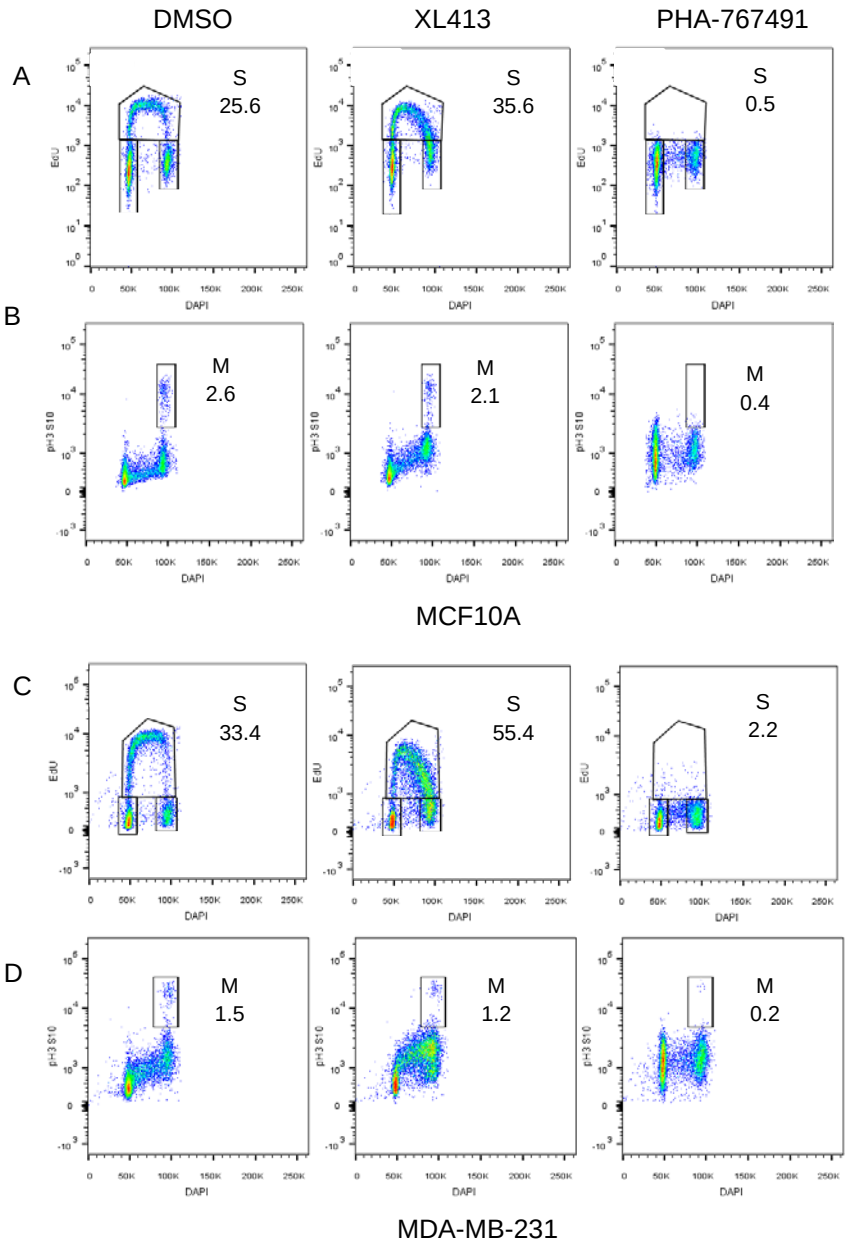


**Figure 3.11 Effects of XL413 on G2/M-phase transition in MCF10A and MDA-MB-231 cells 24 hours post-treatment.**

Cells were treated with XL413, PHA-767491 or DMSO for 24 hours then labelled with EdU for 30 minutes. Harvested cells were fixed and subjected to phospho-H3/EdU/DAPI staining for flow cytometry. (A) Data analysis of EdU/DAPI and (B) pH3 S10/DAPI intensity profile in MCF10A cells; (C) Data analysis of EdU/DAPI and (D) pH3 S10/DAPI intensity profile in MDA-MB-231 cells. Experiment was performed once.

### 3.5.2 XL413 does not prevent mitotic cells from passing through M-phase and re-entering S-phase but decreases S-phase population

We continued to investigate the effects of XL413 on mitotic exit of human cells. In this experiment, cells were synchronised at M-phase, harvested and reseeded into medium containing inhibitor and EdU. By examining the rate of EdU-positive cells after inhibitor treatment, we can confirm whether XL413 prevents cells exiting M-phase and entering G1- and S-phase of the next cell cycle.

MDA-MB-231 cells were plated for 24 hours and treated with nocodazole for 6 hours. Round cells (or mitotic cells) were shaken off, seeded on coverslips and treated with XL413, PHA-767491 or vehicle control DMSO for 15 hours. EdU was added along with the treatment. Finally, cells were fixed by PFA and subjected to EdU/DAPI staining for immunofluorescence. S-phase cells that were EdU-positive were counted from a minimum of 10 randomly selected slides, with 600-800 DAPI-positive cells.

A similar percentage of EdU-positive cells were found in control and XL413-treated samples, 27.4 vs 23 (Figure 3.12C, XL413 vs DMSO), whereas only 3.4% of cells were EdU-positive after 15 hours of PHA-767491 treatment (Figure 3.12C, PHA-767491). This indicates that CDC7 kinase inhibition by XL413 does not prevent MDA-MB-231 cells from passing through M-phase and re-entering S-phase of the next cell cycle, but may decrease the number of S-phase cells.

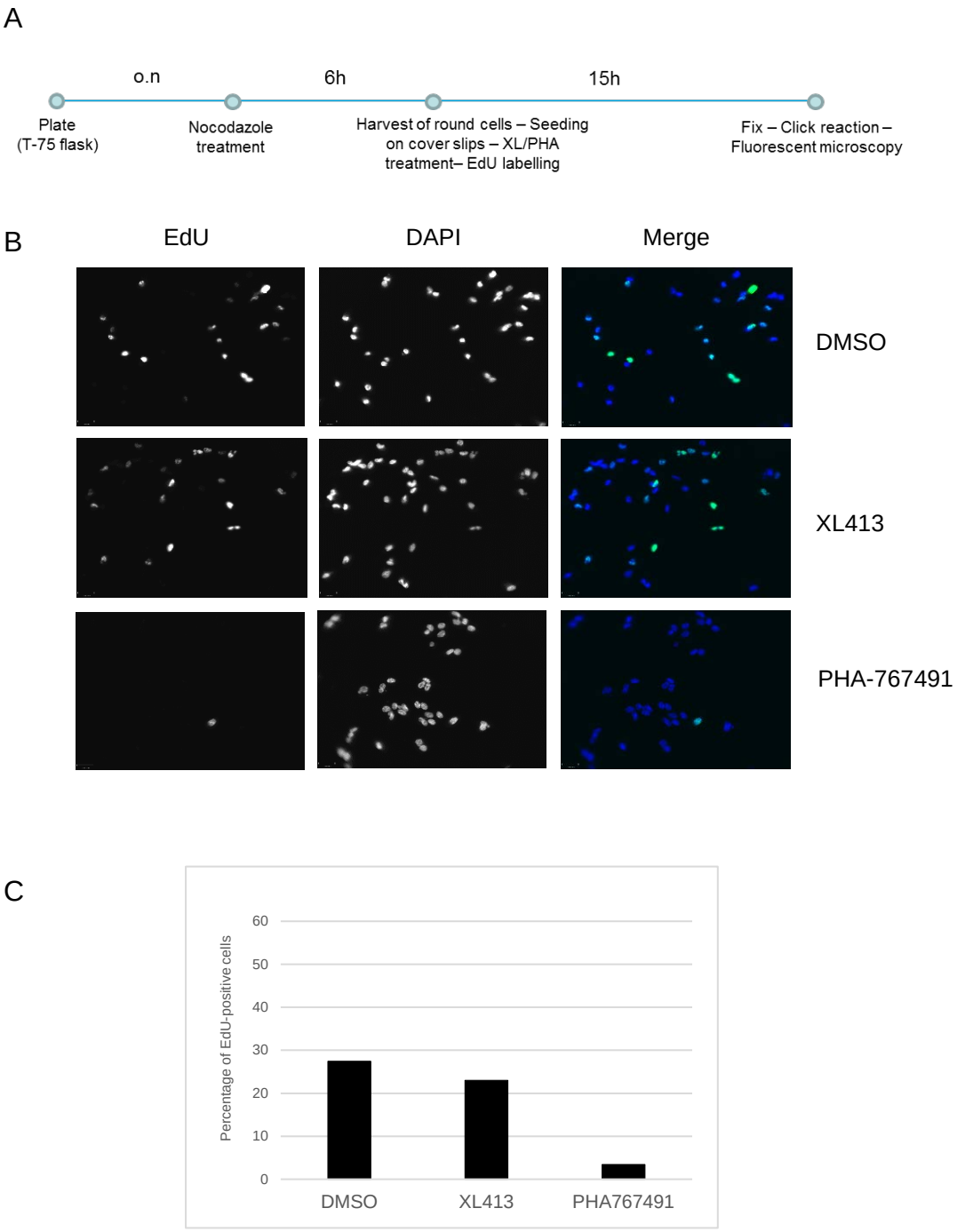


**Figure 3.12 Effects of XL413 on mitotic progression in MDA-MB-231 cells.**

Cells were treated with Nocodazole for 18 hours, harvested by gentle shaking, reseeded on cover slips and treated for 15 hours. (A) Schema of experiment; (B) Representative images of EdU/DAPI-stained cells; (C) Counts of EdU-positive cells. Experiment was performed once

### 3.6 Effects of CDC7 inhibition by XL413 on DNA damage checkpoint

XL413 does not induce any apoptosis nor stalled fork after 24 hours of inhibitor treatment in MCF10A and MDA-MB-231 cells but partially inhibits colony formation after being released from treatments (section 3.3). In some reports, authors suggested CDC7 has a role in regulating DNA damage checkpoint [143,144]. We suspected that inhibition of CDC7 kinase causes DNA damage and but also delays the DNA damage responses (DDRs). Consequently, cells die in the next few cell cycles. To test this hypothesis, we examined the activation of a panel of DDR markers by immunoblotting. MCF10A and MDA-MB-231 cells were treated with XL413, Etoposide, HU or the vehicle control DMSO for 24 hours, then harvested and subjected to a total protein extraction by TCA.

Twenty-four hours post-treatment with XL413, the inhibition of CDC7 kinase activity was confirmed by the decrease of protein level of pMCM2 S40/41 in MCF10A (Figure 3.13, pMCM2 S40/41, lane 4) and MDA-MB-231 cells (Figure 3.13, pMCM2 S40/41, lane 8). Phosphorylation of CHK1 at S317, CHK2 at T68 and RPA32 at S4/8 were undetectable (Appendix A, Figure S3.2), suggesting inhibition of CDC7 by XL413 does not activate the DNA damage checkpoint response. Remarkably, a slight increase of ɣH2AX in XL413-treated MDA-MB-231 cells (Figure 3.13, ɣH2AX, lane 8) but not in MCF10A cells (Figure 3.13, ɣH2AX, lane 4) suggests that double-strand DNA breaks may occur in MDA-MB-231 cells.

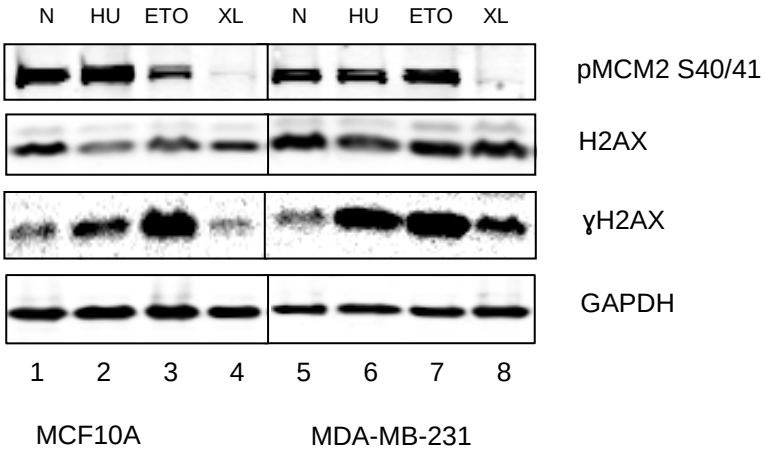


**Figure 3.13 Effects of XL413 on triggering DNA damage response**

Cells were treated with XL413 (XL), Etoposide (ETO), HU or vehicle control DMSO (N) for 24 hours, then harvested and pelleted. Total protein lysate was extracted by TCA extraction and subjected to immunoblotting. Experiment was performed once.

## 3.7 Conclusion

In this chapter, we have shown that CDC7 kinase inhibition by XL413 affects the cell proliferation of two human breast cell lines, MCF10A and MDA-MB-231, differently. The growth of MDA-MB-231 cancer cell line is remarkably inhibited, but only a marginal decrease in growth rate is observed in MCF10A cells derived from normal breast tissue. We also observed that XL413 does not induce apoptotic cell death in both cell lines after 24 hours of inhibitor treatment, but does attenuate the clonogenic ability of MDA-MB-231 cells.

In investigating the mechanism of these differences, we found that XL413 affects the cell cycle progression of both cell lines. This inhibitor triggers a delay at S-phase, but does not prevent cells entering M-phase and passing through G1 to re-enter S-phase of the next cell cycle. XL413 does not affect the origin firing or induce any stalled fork after 24 hours of inhibitor treatment, but a subtle increase of γH2AX protein level was observed in MDA-MB-231 treated cells suggesting a spontaneous DNA damage may occur in this cell line.

# Chapter 4: Identification of human kinases that cooperate with CDC7 in promoting DNA replication

## 4.1 Introduction

CDC7 kinase inhibition by XL413 induces a delay at S-phase in human cells, but does not prevent them from passing through mitosis and re-entering S-phase of the next cell cycle. Meanwhile, PHA-767491, another CDC7 kinase inhibitor, can block DNA synthesis and prevent cells from entering mitosis (Chapter 3). It has been shown that PHA-767491 targets CDC7 and also other kinases such as CDK9 [127,191]. Therefore, we hypothesised that an alternative kinase cooperates with CDC7 to promote DNA replication. To test this hypothesis, we examined the effects of a combined inhibition of CDC7 and several cyclin dependent kinases which are targeted by PHA-767491.

## 4.2 Effects of CDKs and CDC7 inhibition on cell cycle progression in human cell lines

CDK1 and CDK2 are critical kinases involved in cell cycle regulation. CDK9 is Ser/Thr kinase which regulates transcription elongation through phosphorylation of RNA pol II [213]. Cai *et al.* also showed that combined depletion of CDK1-CDK2 along with CDK9 increases apoptotic cell death in a non-small lung cancer cell line, although this effect is limited when cells have a sole depletion of either kinase [214]. However, no study has yet examined the effects of combined depletion of these kinases with the inhibition of CDC7, an important kinase in initiating DNA replication. Therefore, our main aim was to examine the cooperation between CDK1, CDK2 and CDK9 with CDC7 in regulating human DNA replication.

### 4.2.1 In MCF10A cells, XL413 potentiates the effects of CDK1 or CDK9 depletion on treated cells, but not of CDK2

We first examined the effects of CDK1, CDK2 and CDK9 depletion on the human breast cell line MCF10A in the presence of CDC7 inhibitor XL413. Cells were transfected with siRNAs targeted to CDK1, CDK2 and CDK9 at a final concentration of 50 nM for 24 hours, then treated with XL413 or vehicle control DMSO for another 24 hours. Treated cells were EdU labelled for 30 minutes, harvested as cell pellets

and stored at -80$^{o}$C for immunoblotting. A portion of harvested cells were fixed and subjected to EdU/DAPI staining for flow cytometry.

Forty-eight hours post-transfection, CDK1, CDK2 and CDK9 protein levels decreased remarkably in cells transfected with siRNAs targeted either CDK1, CDK2 or CDK9 respectively, indicating the efficacy of down regulating those kinases by siRNAs (Figure 4.1A, lane 3, 4 and 5). The addition of XL413 did not affect the depletion of these kinases (Figure 4.1A, lane 9, 10 and 11).

By flow cytometry data analysis, it was found that siCDK1-transfected cells accumulated at G2/M with an increase of subG1 population to 3.15%, indicating that CDK1 depletion prevents mitotic entry and triggers apoptotic cell death in MCF10A cell line (Figure 4.1B, siCDK1 vs siSCR). In the presence of XL413, the G2/M-phase population increased further (Figure 4.1B, siCDK1 vs siCDK1+XL), suggesting a cooperation between CDK1 and CDC7 kinase activity in promoting mitotic entry.

Interestingly, the S-phase population of CDK1-depleted cells was much lower than the negative control siSCR (Figure 4.1B, siCDK1 vs siSCR), and this population only marginally increased when cells were treated with XL413 (Figure 4.1B, siCDK1 vs siCDK1+XL). It was noticed that in the presence of XL413, cells accumulated in late S- and G2/M-phase with a low intensity of EdU fluorescence emission. This emphasises a role of CDK1 in regulating DNA replication in a CDC7 kinase-independent manner.

The decrease of the S-phase population was also recorded with the CDK9-depleted cells (Figure 4.1B, siCDK9 vs siSCR). In contrast to CDK1, CDK9 down regulation triggered an accumulation of cells at G1 from 63.3% to 72.2% (Figure 4.1B, siCDK9 vs siSCR). This suggests that CDK9 plays a role in the G1/S transition, and inhibition of this kinase prevents cells entering S-phase.

Interestingly, in the presence of XL413, the inhibitory effect of CDK9-depletion was affected. CDK9-depleted cells entered and accumulated in late S and G2/M-phase when cells were treated with XL413 (Figure 4.1B and C, siCDK9 vs siCDK9+XL), suggesting CDK9 depletion has effects on cell cycle progression of human cells in a CDC7 kinase-dependent manner.

No remarkable effects were observed in S-phase population of CDK2-depleted cells when XL413 was present (Figure 4.1B, siCDK2 vs siCDK2+XL).

A

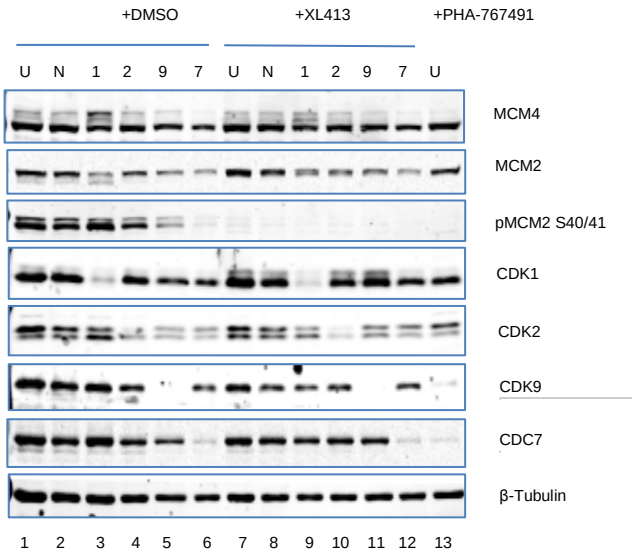


B

| | siSCR | siSCR+XL | siCDK1 | siCDK1+XL | siCDK2 | siCDK2+XL | siCDK9 | siCDK9+XL |
|---|---|---|---|---|---|---|---|---|
| G1 | 63.3 | 50.2 | 33.3 | 22 | 68 | 50.3 | 72.2 | 38.1 |
| S | 23 | 34.4 | 10.5 | 12.2 | 21.5 | 34 | 15.8 | 33.6 |
| G2/M | 12.5 | 13.5 | 51.9 | 60.7 | 9.2 | 14.8 | 10.4 | 26.6 |
| subG1 | 0.87 | 1.39 | 3.15 | 3.11 | 0.9 | 0.45 | 1.2 | 0.74 |

C

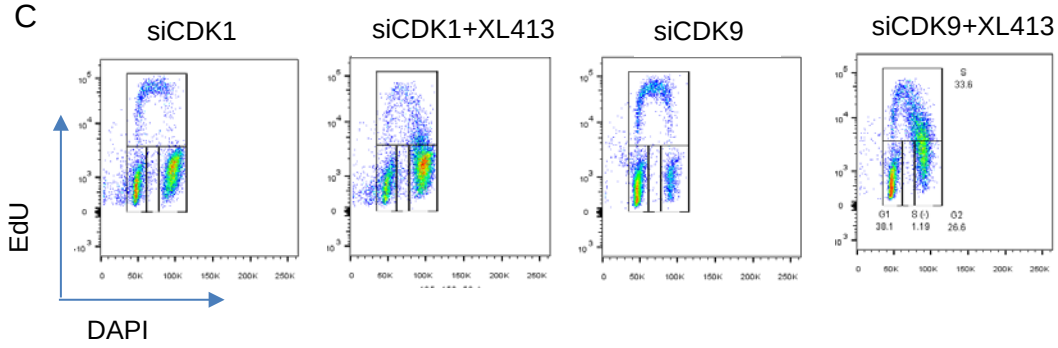


**Figure 4.1 Effects of the depletion of CDK1, CDK2 and CDK9 in combination with XL413 in MCF10A cells.**

Cells were transfected with negative control siSCR or siRNA targeting CDK1, CDK2 and CDK9 for 24 hours, then treated with XL413 for another 24 hours. Transfected cells were labelled with EdU for 30 minutes, harvested and pelleted for immunoblotting. A portion of harvested cells were fixed and subjected to EdU/DAPI staining for flow cytometry. U: Untransfected; N: siSCR; 1: siCDK1; 2: siCDK2; 9: siCDK9; 7: siCDC7; XL: XL413; (A) Immunoblotting data; (B) Flow cytometric data analysis; (C) EdU/DAPI profiles of siCDK1- and siCDK9-transfected cells. Experiment was performed once.

### 4.2.2 In MDA-MB-231 cells, the co-inhibition of CDC7 with CDK1, CDK2 or CDK9 does not have any additional effect on DNA synthesis

In the previous chapter, we showed that MCF10A and MDA-MB-231 cells have different responses to XL413 treatment. In order to further understand the mechanism, we examined the effects of depletion of CDK1, CDK2 or CDK9 on the metastatic breast cancer cells MDA-MB-231 in the presence of XL413. Cells were transfected with siRNAs targeting CDK1, CDK2 and CDK9 or negative control siSCR for 24 hours, then treated with XL413 or vehicle control DMSO for another 24 hours. Treated cells were EdU labelled for 30 minutes, harvested as cell pellets and stored at -80$^{o}$C for immunoblotting. A portion of the harvested cells were fixed and subjected to EdU/DAPI staining for flow cytometry.

In MDA-MB-231 cells, CDK1 down-regulation did not induce any change in the S-phase population but it did cause an accumulation of cells at G2/M and a decrease of cells in G1-phase (Figure 4.2B, siCDK1 vs siSCR), suggesting that CDK1 depletion does not prevent DNA replication of this cancer cell line but only affects the G2/M-phase transition. In the presence of XL413, cells accumulated in late S-phase, and this phenomenon was similarly observed in negative control cells (Figure 4.2B, siCDK1+XL vs siSCR+XL) indicating that the combination of CDK1 depletion with XL413 does not induce any additional effect on DNA replication of MDA-MB-231.

The depletion of CDK2 and CDK9 by siRNAs did not trigger any noticeable change in cell cycle progression either with or without XL413 (Figure 4.2B, siCDK2 vs siCDK2+XL, siCDK9 vs siCDK9+XL). This data suggests that neither CDK1, CDK2 nor CDK9 might play a critical role in regulating DNA replication of MDA-MB-231 and the co-inhibition of these kinases with CDC7 may not have any additional effect on DNA synthesis in this cell line.

A

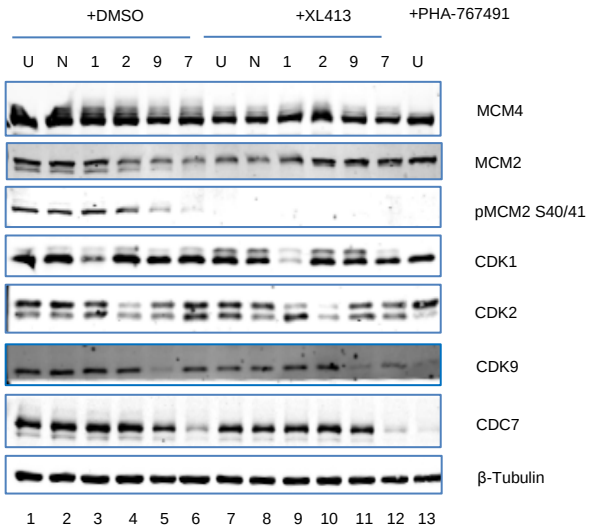


B

| | siSCR | siSCR+XL | siCDK1 | siCDK1+XL | siCDK2 | siCDK2+XL | siCDK9 | siCDK9+XL |
|---|---|---|---|---|---|---|---|---|
| G1 | 54.9 | 24.1 | 41.5 | 16.8 | 52.5 | 21.8 | 51 | 22.4 |
| S | 30.2 | 57.2 | 31.2 | 52.6 | 32 | 62.2 | 32.8 | 57.8 |
| G2 | 12.1 | 12.5 | 23 | 22.9 | 12 | 10.1 | 11.3 | 13.1 |
| subG1 | 1.69 | 2.07 | 1.71 | 2.08 | 1.47 | 2.19 | 2.52 | 1.79 |

**Figure 4.2 Effects of the depletion of CDK1, CDK2 and CDK9 in combination with XL413 in MDA-MB-231 cells.**

Cells were transfected with negative control siSCR or siRNA targeting CDK1, CDK2 and CDK9 for 24 hours, then treated with XL413 for another 24 hours. Transfected cells were labelled with EdU for 30 minutes, harvested and pelleted for immunoblotting. A portion of harvested cells were fixed and subjected to EdU/DAPI staining for flow cytometry. U: Untransfected; N: siSCR; 1: siCDK1; 2: siCDK2; 9: siCDK9; 7: siCDC7 (A) Immunoblotting data; (B) Flow cytometry data analysis. Experiment was performed once.

A previous study showed that CDK1 can compensate for the role of CDK2 in promoting DNA replication of mouse embryonic fibroblast (MEF) cells, and that the ablation of CDK1 (or CDC2) in *Cdk2 -/-* MEF cells greatly decreases S-phase [215]. This could explain the reason why the depletion of CDK1 or CDK2 individually does not block DNA replication of MDA-MB-231. In order to test the hypothesis that CDK2 compensates for CDK1 when CDK1 is knocked down or *vice versa*, we depleted both kinases by siRNA and examined the effects of kinase depletion on cell cycle progression by flow cytometry. We also combined the depletion of CDK1-

CDK2 with the inhibition of CDC7 kinase by XL413 to verify the role of CDC7 in DNA replication when CDK1 and CDK2 are absent.

MDA-MB-231 cells were transfected with siRNAs targeting CDK1 and CDK2 for 24 hours, then treated either with DMSO or XL413 for another 24 hours. PHA-767491 treated cells were used as a positive control. Transfected cells were labelled with EdU for 30 minutes and harvested as cell pellets for immunoblotting. A portion of the harvested cells were fixed and subjected to EdU/DAPI staining for flow cytometry.

The down-regulation of CDK1 and CDK2, either in an individual or a co-depletion was confirmed by immunoblotting (Figure 4.3A, lane 4, 5, 6 and 7). The depletion of both CDK1 and CDK2 caused an accumulation of cells in G2/M-phase from 11% to 36.7% and a decrease of the G1-population from 66% to 32.8% (Figure 4.3B, 1+2 vs N). This suggests that the co-depletion of CDK1 and CDK2 prevents the mitotic exit of MDA-MB-231 cells but does not change the percentage of the S-phase population or to lesser extent, CDK2 does not compensate for the CDK1 role or *vice versa* in regulating DNA replication.

In the presence of XL413, the S-phase population increased to 44.3%, indicating XL413 delays the S-phase progression of CDK1/CDK2 co-depleted cells. A reduction of percentage of G2/M-phase population from 36.7 to 26.8 and a sharp decrease of the G1-phase population from 35.7 to 12.2 were also observed (Figure 4.3B, 1+2+XL413 vs XL413). This indicates that in the absence of CDK1 and CDK2, inhibition of CDC7 kinase by XL413 does prevent the mitotic entry and exit, but does not affect the G1/S-transition nor block DNA replication. This means CDK1 and CDK2 might not be kinases which cooperate with CDC7 in promoting DNA replication of MDA-MB-231 cells.

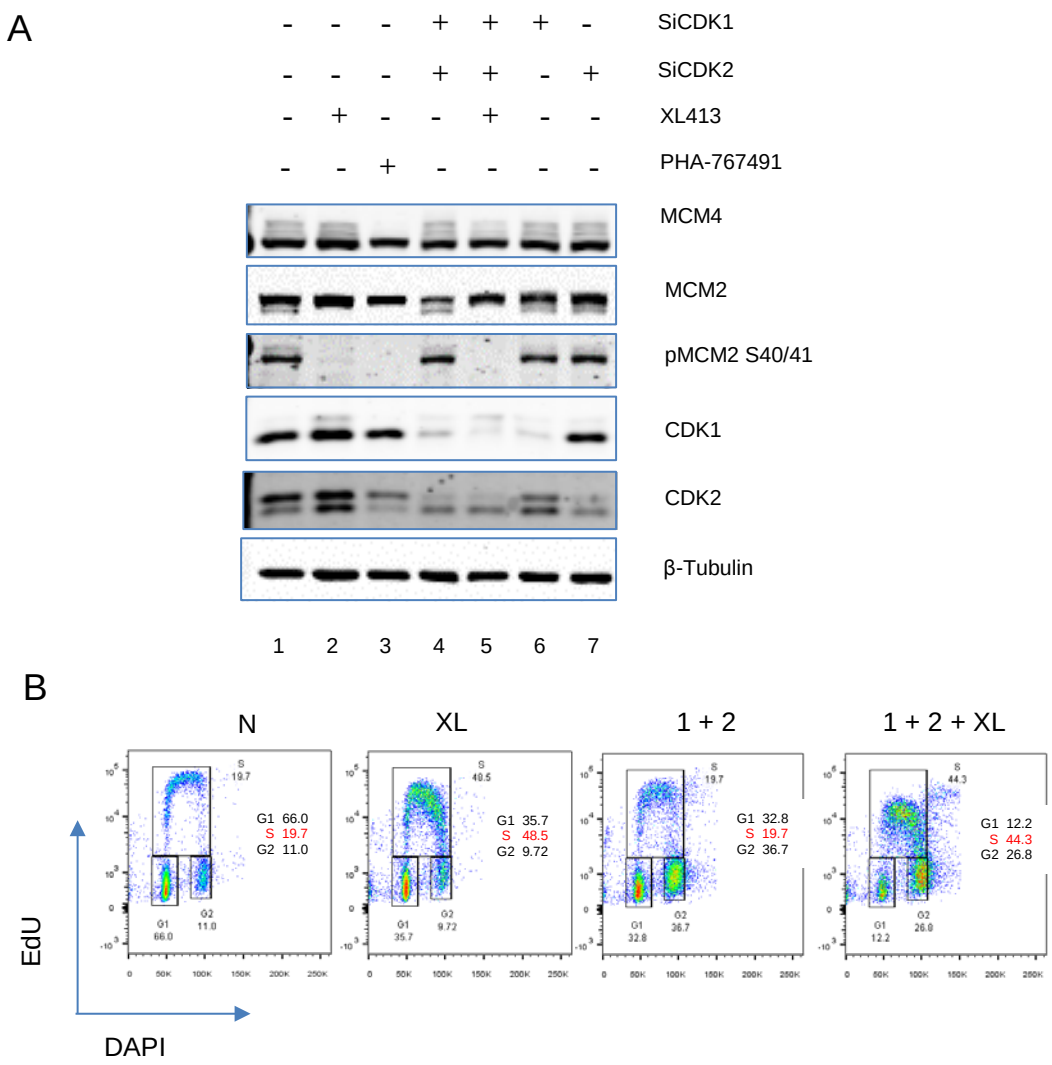


**Figure 4.3 Effects of the co-depletion of CDK1-CDK2 in combination with CDC7 inhibition on cell cycle progression in MDA-MB-231 cells.**

Cells were transfected with siRNA of negative control or siRNA targeting to CDK1 and CDK2 for 24 hours, then treated with DMSO or XL413 (as indicated) for another 24 hours. Transfected cells were EdU labelled for 30 minutes, and harvested as cell pellet for immunoblotting. A portion of harvested cells were fixed and subjected to EdU/DAPI staining for flow cytometry. Flow cytometric data was collected and analysed by FACS/FlowJo v10. N: Negative control; 1: siCDK1; 2: siCDK2; XL: XL413; PHA: PHA-767491. Experiment was performed once.

## 4.3 Assay optimisation for high-throughput screening of a siGENOME siRNA library

### 4.3.1 InCell Click assay

The ablation of CDK1 by siRNA in combination with CDC7 inhibition by XL413 does not affect DNA replication of MDA-MB-231 cells, although it causes a decrease of EdU-incorporated MCF10A cells. Furthermore, the depletion of both CDK1 and CDK2 does not trigger any reduction of the S-phase population in MDA-MB-231 cells either with or without XL413. The depletion of CDK9 kinase affects cell cycle regulation of MCF10A cells in a CDC7 kinase inhibition dependent manner, but does not prevent DNA synthesis. This data suggests that CDK1, CDK2 and CDK9 might not be kinases which can cooperate with CDC7 in regulating DNA replication of human cells, especially cancer cells like MDA-MB-231.

In order to identify kinases which concomitantly regulate DNA replication with CDC7 in human cells, we wished to perform a high-throughput screening of a human siRNA library (siGENOME, GE Healthcare Dharmacon Inc). In this library, genes for more than 400 human kinases are targeted by a set of siRNA pools with a high efficacy of silencing. Prior to the primary screening, a cell-based EdU-incorporation microplate assay assessing the inhibitory effects of siRNA transfection on DNA replication of human cell lines was optimised.

The InCell Click (ICC) assay allows synthesised DNA to be detected through a fluorescent IRDye 800CW Infrared azide (LiCOR) which reacts with DNA-incorporated EdU in cells as described in Figure 4.4A. For optimisation, MCF10A cells were first seeded at $1.5x10^3$ cells/well in 96-well plates for 72 hours, labelled with EdU or vehicle control DMSO for 30 minutes, fixed and subjected to the ICC assay. Each sample was measured in triplicate. It was found that the signal intensity of EdU-labelled cells was nearly 4 times higher than in DMSO-treated cells (Figure 4.4B). This means that using the ICC assay, we can assess the EdU incorporation into human cells. However, this assay required expensive reagents such as IRDye azide and is time-consuming so it may not be appropriate for screening.

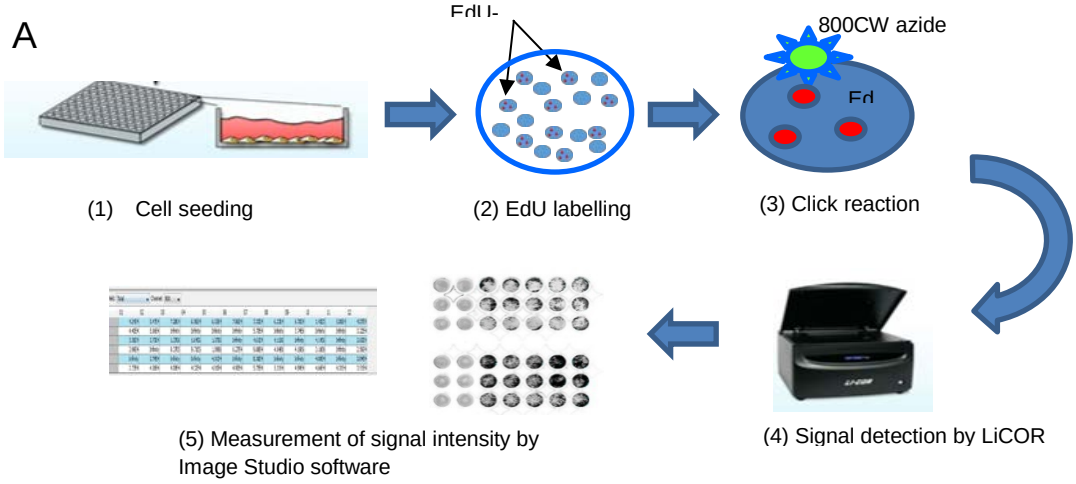


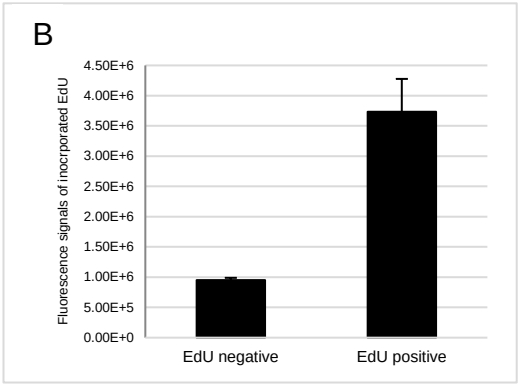


**Figure 4.4 Optimisation of InCell Click assay.**

Cells were seeded in 96-well plate for 72 hours, incubated with 10 μM EdU for 30min prior to harvest. Harvested cells were fixed and subjected to ICC assay. Signals were detected by LiCOR system. Each sample was performed in triplicate. (A) Outline of ICC assay; (B) Quantitation of fluorescence signals measured by LiCOR/Image Studio software. Each assay was performed in triplicate. Error bars represent the Mean ± SD. Experiment was performed twice.

### 4.3.2 Click-iT EdU microplate assay

The Click-iT EdU microplate assay (Thermo Fisher Scientific) was also optimised for screening. This assay is based on the principle that Oregon Green 488 azide (Thermo Fisher Scientific) specifically reacts with the alkyne group of EdU and forms a covalent bond by the Click reaction [208]. The signal of EdU/488 azide is amplified by the binding of an anti-Oregon Rb IgG antibody conjugated to a

horseradish peroxidase (HRP) enzyme. In the presence of HRP, Amplex Ultra red reagent reacts with $H_2O_2$ and is converted into a highly fluorescent Resorufin (Figure 4.5). This compound has a pink/red colour with fluorescence emission that is detectable at 530/580nm (Thermo Fisher Scientific). By measuring the fluorescence emission intensity of Resorufin in medium, we can estimate the amount of DNA-incorporated EdU in cells and assess the inhibitory effect of compounds or RNAi on DNA replication (Figure 4.5). This method has the advantage of high sensitivity through a strong signal, which is important for a robust assay.

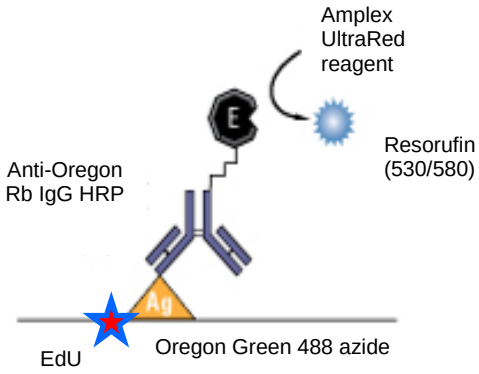


**Figure 4.5 Principle of Click-iT EdU microplate assay.**
Details were described in the text. Figure adapted from Molecular Probe's handbook (Thermo Fisher Scientific).

MCF10A cells were seeded at $1.5x10^3$ cells/well in 96-well plates for 24 hours, treated with XL413, DMSO, PHA-767491 or HU for 24 hours, then labelled with EdU for 30 minutes. Harvested cells were fixed and subjected to the Click-iT EdU microplate assay following the manufacturer's instructions. Each assay was performed in triplicate.

As expected, EdU-positive control cells have the highest intensity of fluorescence signals that are about 2.5 times higher than EdU-negative control cells (Figure 4.6B, DMSO(+) vs DMSO(-)). XL413- and HU-treated cells have a slightly lower signal intensity than EdU-positive control cells (Figure 4.6B, XL(+) vs DMSO(+)). PHA-767491-treated cells had the lowest intensity of fluorescence signals which were nearly equal to EdU-negative control (Figure 4.6B, PHA(+) vs DMSO(-)) indicating that this compound blocks EdU incorporation.

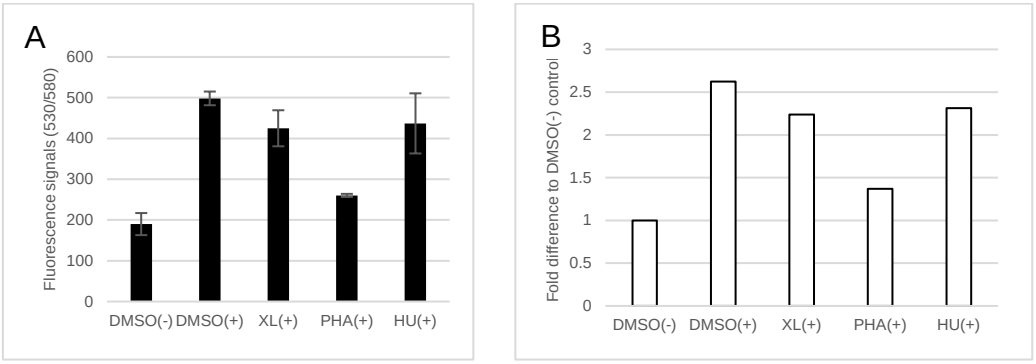


**Figure 4.6 Click-iT EdU microplate assay of MCF10A cells using manufacturer protocols.**

Cells were treated with XL413, PHA-767491, HU or DMSO for 24 hours, labelled with EdU for 30 minutes, fixed and subjected to the assay. (A) Raw data of fluorescence signals; (B) Fold difference of fluorescence signals to DMSO (-). Each sample was performed in triplicate. Error bars represent the Mean ± SD. Experiment was performed once.

Since we had observed an increase of the late S-phase and G2/M populations when cells were treated with XL413 (Section 4.2, Figure 4.1 and 4.2), the reduction of EdU fluorescent intensity in XL413-treated cells was expected. This suggests that the assay recapitulates flow cytometric results and may be reliable in assessing effects of compounds or RNAi on DNA replication.

However, in HU-treated cells we found a similar intensity of EdU fluorescence emission signals in comparison with XL413-treated cells (Section 4.3.2, Figure 4.6, HU vs XL413), even though HU is considered to be a compound which can arrest fibroblast cells at G1/S upon 30 hours of inhibitor treatment [216]. We hypothesised that MCF10A cells are able to restore the ability of incorporating EdU after a 24 hours HU-exposure. To test this possibility, we carried out an experiment in which MCF10A cells were treated with HU for different periods of time. The 24-hours treated cells with DMSO, XL413 and PHA-767491 were used as controls. After treatment, cells were labelled with EdU for 30 minutes, then subjected to EdU/DAPI staining for flow cytometry.

By flow cytometric analysis, it was found that the S-phase population of HU-treated cells starts to increase after 6 hours of HU treatment and this augmentation continues until 24 hours (Figure 4.7, HU 6H-24H), suggesting that this compound might not be a reliable control for primary screening. To avoid data bias, we decided to use PHA-

767491 as the only positive control since it blocks DNA replication as assessed by the Click-iT EdU microplate assay.

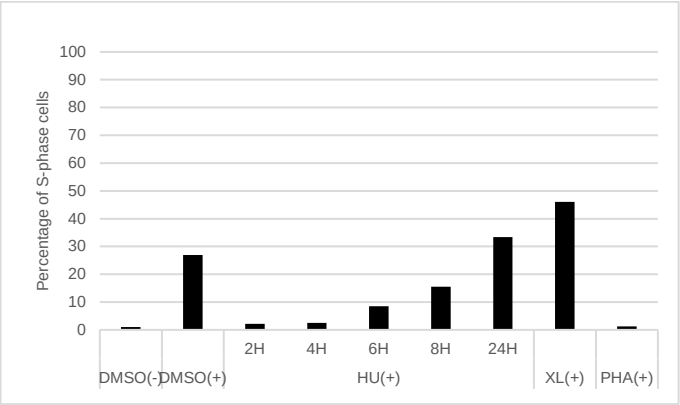


**Figure 4.7 Effects of HU treatment on MCF10A cells during different periods of time.** Cells were treated with DMSO, XL413 and PHA-767491 for 24 hours, with HU for within indicated periods of time, and labelled with EdU for 30 minutes prior to harvest. Harvested cells were fixed and subjected to EdU/DAPI staining for flow cytometry. Experiment was performed once.

For a robust high-throughput screen (HTS), the fold-difference in signal intensity between negative and positive controls must be at least greater than 2-fold, and ideally greater than 4-fold. Therefore, several parameters were considered for optimisation including incubation time of substrate, antibody and Click reaction.

MCF10A cells were seeded at $1.5x10^3$ cells/well in 96-well plates for 24 hours, treated with XL413, DMSO or PHA-767491 for 24 hours, then labelled with EdU for 30 minutes. Harvested cells were fixed and subjected to Click-iT EdU microplate assay, according to the manufacturer's protocol except for an increase of incubation time of Amplex UltraRed substrate from 15 to 90 minutes. Fluorescence emission intensity was measured by CytoFluor.

An increase of signal intensity of EdU-positive control from 2 to 4.5 times above EdU-negative control resulted from increasing the substrate incubation time to 30 minutes (Figure 4.8B, DMSO(-) vs DMSO(+)). Longer incubations did not improve this fold difference, as the intensity of EdU-negative DMSO control increased in parallel (Figure 4.8B, DMSO(-) vs DMSO(+) 45min, 60 min, 90 min). The increase of EdU labelling or Click reaction time did not improve the fold difference of signals

(data not shown). Therefore, 30 minutes is an optimised incubation time of Amplex UltraRed substrate for this Click-iT microplate assay.

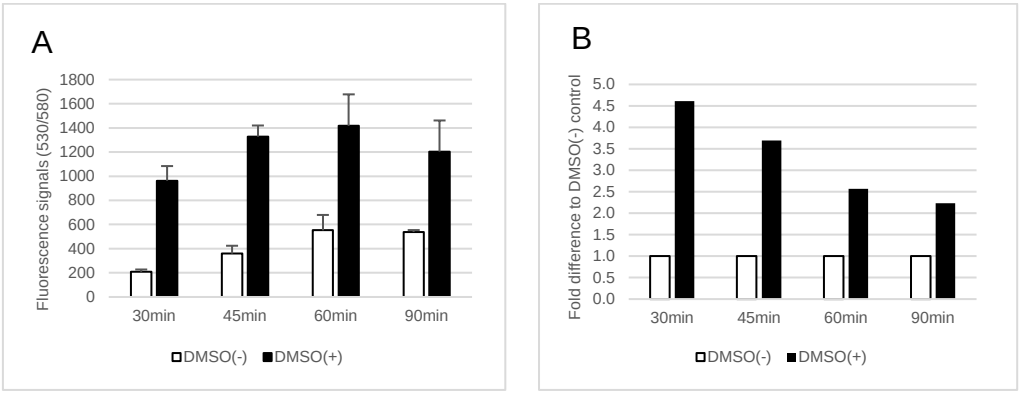


**Figure 4.8 Improvement of Click-iT microplate assay by increasing the incubation time of Amplex UltraRed substrate**

MCF10A cells were treated with DMSO for 24 hours, labelled with EdU for 30 minutes and subjected to Click-iT EdU microplate assay. (A) Raw data of fluorescence signals; (B) Fold difference of fluorescence signals to DMSO (-). Each sample was performed in triplicate. Error bars represent the Mean ± SD. Experiment was performed once.

Another critical factor affecting the robustness of an siRNA-based HTS is the cell density of plating. This density should not be too low otherwise the signal detection by CytoFluor will be limited. It also should not be too high otherwise the over confluency of cells and the serum starvation in each well may occur. A blockade of DNA replication due to serum starvation could lead to a false positive data for screening.

To enable an effective assay, MCF10A cells were plated at different cell densities from $2x10^3$ to $2x10^4$ cells/well in triplicate, then transfected with negative control siSCR for 48 hours. An untransfected sample with cell density of $4x10^3$ cell/well was included as a control. 48 hr-post transfection cells were labelled with EdU for 30 minutes and subjected to the Click-iT EdU microplate assay.

An approximately 6.5-fold difference to the control was observed in cells plated at $8x10^3$ cells/well and $1x10^4$ cells/well and those cell densities also had the highest intensities of fluorescence signals (Figure 4.9B). However, at $2x10^4$ cells/well, the signal intensities decreased. This suggests that MCF10A cells reach over-confluency at cell density of $2x10^4$ cells/well, and that it is unwise to plate cells at $1x10^4$

cells/well (Figure 4.9B, 1x10^4 vs 2x10^4). Hence, $8x10^3$ cells/well was considered as the optimal cell density for this screen.

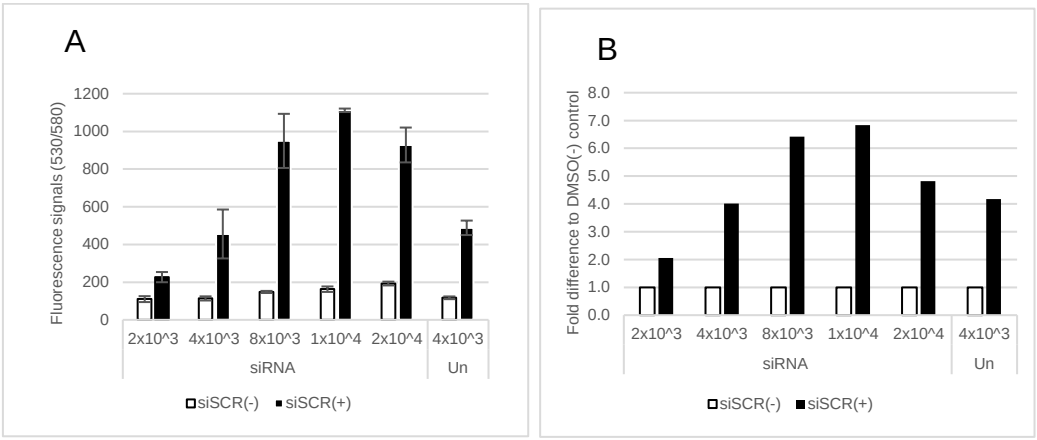


**Figure 4.9 Optimisation of cell density for Click-iT EdU microplate assay**

MCF10A cells were plated at different densities as indicated, transfected with siSCR for 48 hours, then labelled with EdU for 30 minutes and subjected to Click-iT EdU microplate assay. (A) Fluorescence signals measured at 530/580; (B) Fold difference of fluorescence signals to siSCR(-) control. Each experiment was performed in triplicate. Error bars represent the Mean ± SD. Experiment was performed once.

We tested all optimised conditions with transfection reagents to be used for siGENOME library screening. MCF10A cells were seeded at $8x10^3$ cells/well for 24 hours, transfected with siRNA targeted against CDK1 or siSCR as negative control for 24 hours, then treated with XL413 or DMSO for another 24 hours and labelled with EdU for 30 minutes prior to being fixed and subjected to the Click-iT EdU microplate assay.

The signal intensity of positive control siSCR(+) was 4.5 times higher than that of negative control siSCR(-), and this fold difference was lower than our previous experiment (Section 4.3.2, Figure 4.9B, $8x10^3$). An explanation could be the extra step of XL413/DMSO treatment after siRNA transfection alters the sensitivity of assay.

SiCDK1-transfected cells had a lower fluorescence emission intensity (Figure 4.10B, siCDK1 vs siSCR(+), DMSO), suggesting that CDK1 depletion causes a reduction of EdU incorporation. This data was consistent with flow cytometric observations of MCF10A cells transfected with siCDK1 (section 4.2, Figure 4.1B, siCDK1).

However, CDK1-depleted cells had a higher fluorescence emission intensity when subsequently treated with XL413 (Figure 4.10B, siCDK1, DMSO vs XL413), suggesting the amount of EdU-incorporated DNA increased. By flow cytometry, we found that CDK1 depletion in combination with XL413 greatly reduces EdU incorporation (Section 4.2, Figure 4.1C, siCDK1+XL). This disagreement may be explained by the reduction of siRNA transfection efficacy and the resistance to XL413 treatment when cells are plated at a high density, i.e. $8x10^3$ cells/well.

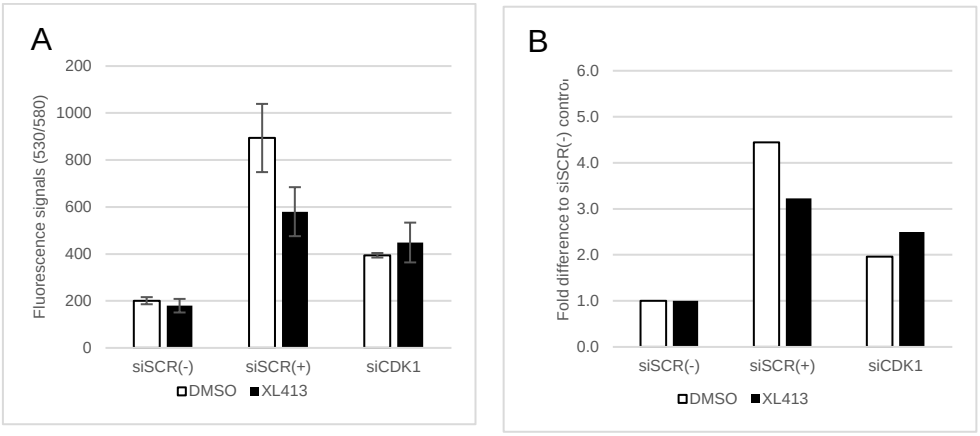


**Figure 4.10 Click-iT microplate assay with cell density of $8x10^3$ cells/well**

MCF10A cells were plated at $8x10^3$ cells/well for 24 hours, transfected with siRNA of negative control siSCR or siRNA targeting CDK1 for 24 hours, then treated with XL413 or DMSO control for another 24 hours. After treatment, cells were labelled with EdU for 30 minutes and subjected to Click-iT EdU microplate assay. (A) Raw data of fluorescent intensity measured by CytoFluor; (B) Fold difference of fluorescence signals to siSCR (-) control. Each assay was performed in triplicate. Error bars represent the Mean ± SD. Experiment was performed once.

To obtain the highest siRNA transfection efficacy and to avoid the off-target effects as seen at the density of $8x10^3$ cells/well (Section 4.3.2, Figure 4.10), the plating density was decreased to $4x10^3$ cells/well. Experiments were performed under the same optimised condition: MCF10A cells were seeded at $4x10^3$ cells/well for 24 hours, transfected with siRNA targeted CDK1 or siSCR as negative control, then treated with XL413 or DMSO for another 24 hours and labelled with EdU for 30 minutes prior to being fixed and subjected to the Click-iT EdU microplate assay.

It was observed that at a density of $4x10^3$ cells/well, cells showed a 4.5 fold difference in fluorescence intensity over negative control siSCR(-) which was similar to cells

plated at $8x10^3$ cells/well (Figure 4.11B, siSCR(+)). Depletion of CDK1 decreased the fluorescence intensity, and had a greater effect in the presence of XL413 (Figure 4.11B, siCDK1 vs siCDK1+XL(+)). This data is in agreement with our flow cytometric data. Hence, the cell density of $4x10^3$ cells/well was chosen for robustness.

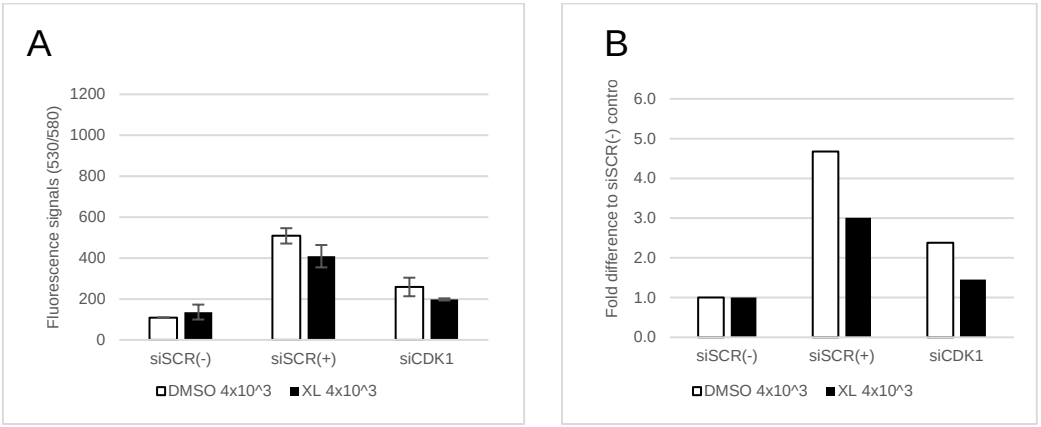


**Figure 4.11 Click-iT microplate assay with cell density of $4x10^3$ cells/well.**
MCF10A cells were plated at $4x10^3$ cells/well for 24 hours, transfected with siRNA of negative control siSCR or siRNA targeting CDK1 for 24 hours, then treated with XL413 or DMSO control for another 24 hours. After treatment, cells were labelled with EdU for 30 minutes and subjected to Click-iT EdU microplate assay. (A) Raw data of fluorescent intensity measured by CytoFluor; (B) Fold difference of fluorescence signals relative to siSCR(-) control. Each sample was performed in triplicate. Error bars represent the Mean ± SD. Experiment was performed once.

Finally, the robustness of the Click-iT EdU microplate assay under optimised condition was examined using the Z-factor calculation. Z-factor was developed as a statistical tool to evaluate the robustness of HTS assays using a large unbiased sample set. By definition, Z-factor is "the ratio of separation band to the signals dynamic range of the assay" [217].

To calculate the Z-factor, we first needed to measure the extent of the separation band, which is equal to the difference between the mean of sample ($\mu_s$) and the mean of control ($\mu_c$) minus the sum of 3 standard deviations of sample (3SDs of sample or 3 $\sigma_s$) added to 3 standard deviations of control (3SDs of control or 3 $\sigma_c$). Secondly, the signal dynamic range was calculated as the difference between two means ($\mu_s$)

and ($\mu_c$). The ratio between these two values reflects the robustness of the assay (Figure 4.12).

A

$$Z' = 1 - \frac{3SD\ of\ sample + 3SD\ of\ control}{|Mean\ of\ sample - Mean\ of\ control|}$$

B

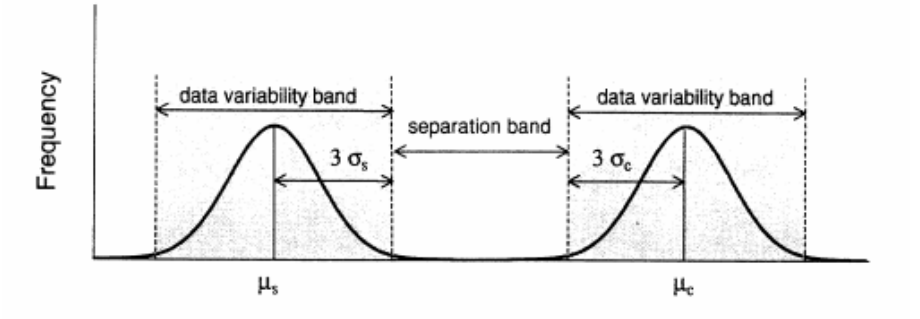


**Figure 4.12 Illustration of variables in Z-factor formula.**
(A): Z-factor formula; (B): Illustration image [217].

If Z-factor is within a range of 0.5-1.0, the assay has a high robustness and it is adequate for a high-throughput screening (HTS). In opposite, if Z-factor is below 0.5, the assay might be designed in a poor format and it is not reliable for the HTS [203].

This statistical tool requires data from a large sample set. According to manufacturer's protocol, it is recommended to calculate Z-factor using data from at least a full 96-well plate assay. Therefore, cells were plated at $4x10^3$ cells/well for 24 hours in all wells of a 96-well plate, (excluding 3 empty wells for background), then transfected with siRNA of negative control siSCR or siRNA targeting CDK1 for 24 hours and treated with XL413 or DMSO vehicle control for another 24 hours. After treatment, cells were EdU labelled for 30 minutes and subjected to the Click-iT EdU microplate assay. Each sample was therefore represented by 24 replicates.

EdU-positive control cells had an intensity of signals which was 3.5 times higher than EdU-negative control cells (Figure 4.13A, siSCR(+) vs siSCR(-)). XL413-treated cells had a reduction of fluorescence emission intensity with a fold difference of 2.5 and CDK1-depleted cells had the lowest intensity (Figure 4.13A, siSCR+XL(+) siCDK1(+) vs siSCR(-)). These observations confirm that this assay

with optimised protocol reflects the effects of CDK1 depletion and XL413 treatment on MCF10A cells with a large number of replicates.

Z-factor values for each sample in comparison with the control siSCR(-) was within a range of -0.2 to 0.2. According to Zhang [217], a Z-factor value of -0.2 suggests that there would be an overlap between signals of positive control siSCR+XL(+) or siCDK1(+) with negative control siSCR(-) (Figure 4.13A) and the Z-factor value of 0.2 suggests that the assay could be marginal for HTS (Figure 4.13A, siSCR(+) vs siSCR(-)). Thus, the assay with optimised condition may not be suitable for HTS.

A

| Treatment | Mean | Fold difference to siSCR(-) | SD | Z-factor |
|---|---|---|---|---|
| siSCR(-) | 260.75 | 1 | 26.76346 | (n/a) |
| siSCR(+) | 907.5833 | 3.5 | 130.0762 | 0.272581 |
| siSCR+XL(+) | 661.9167 | 2.5 | 142.6272 | -0.26674 |
| siCDK1(+) | 584.1667 | 2.24 | 105.0518 | -0.22271 |

B

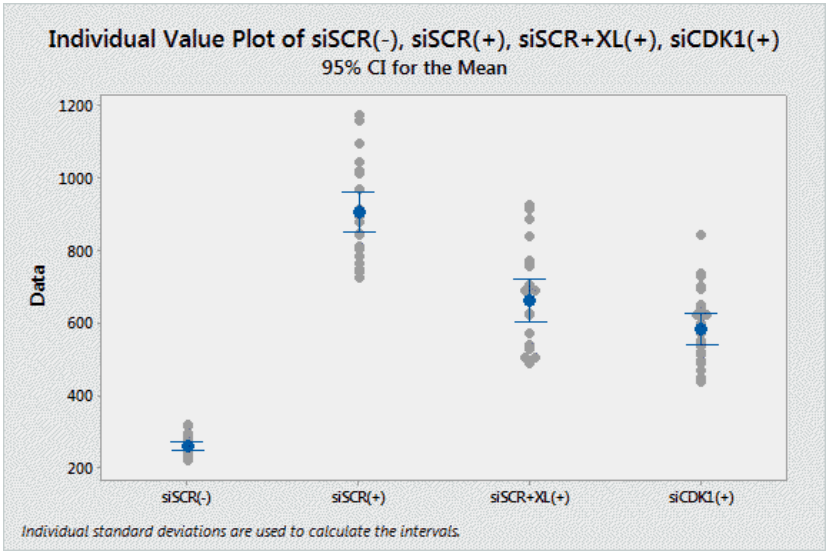


**Figure 4.13 Z-factor values and data distribution of MCF10A cells with optimised condition of Click-iT microplate assay for HTS.**

MCF10A cells were plated for 24 hours, then transfected with siRNAs. 24 hours post-transfection, cells were labelled with EdU for 30 minutes and subjected to Click-iT EdU microplate assay. (A) Table of mean, fold difference, SD signals and Z-factor values of each sample (n=24); (B) Plot graph of data distribution of each sample (n=24); (n/a): not applicable.

The ICC and Click-iT microplate assays were not ideal for a HTS using siRNA transfection because of their limitations. The fold difference between negative and positive controls was around 2.5-3.5 times which is quite a small range. Both assays were performed in multiple steps with different reagents, leading to the risk of technical errors. Finally, their Z-factor values were not within the range expected for a robust assay. Therefore, we changed the approach to optimise a simpler but highly robust assay.

## 4.4 High-throughput screening of Published Kinase Inhibitor Set (PKIS) library in combination with XL413

### 4.4.1 PKIS library

PKIS library was obtained from University of North Carolina. This library is a collection of 317 ATP-competitive kinase inhibitors published by GSK for public screening. Compounds in the library are well-characterised through more than 200 kinase assays and have been tested with the US National Cancer Institute 60 (NCI-60) human tumour cell lines [218,219]. Screening with the PKIS library does not requires any extra reagents for treatment. In contrast, the siGENOME library generated by GE Healthcare Dharmacon requires expensive transfection reagents and it is also expensive to perform screening for multiple trials. Therefore, in addition to changing the screening method, we also changed our library to PKIS for screening.

### 4.4.2 Optimisation of Alamar Blue assay for screening with combined inhibitor treatment

The microplate Alamar Blue assay is a viability assay which has advantages of simplicity, non-toxicity to cells, low cost and high reproducibility which are suitable for HTS. This assay is based on the metabolic conversion of the non-fluorescent chemical dye rezasurin (the active ingredient of Alamar Blue) into resorufin, a chemical product which is red/pink and highly fluorescent. This product is released from the cells, producing a measurable change in colour and fluorescence of the medium. By measuring the fluorescent emission intensity of cells at different time points, we can assess the inhibitory effects of compounds on cell proliferation and select potential hit(s).

Prior to PKIS screening, the assay conditions were optimised in order to have a robust assay with Z-factor value within 0.5 - 1. Cell density for plating, inhibitor treatment time, and Alamar Blue incubation time were considered the principal parameters for optimisation. MCF10A and MDA-MB-231 cells were plated at different cell densities for 24 hours, treated with PHA-767491, HU or DMSO for 48 and 72 hours, incubated with Alamar Blue for 4, 6, or 12 hours, and fluorescence emission intensity was recorded. DMSO-treated samples were performed in 21 replicates (n=21). PHA-767491- and HU-treated samples had 28 replicates each (n=28) and no-cell control

had 7 replicates (n=7). Z-factors were calculated as described (Section 4.3.2, Figure 4.12A).

With a cell density of $4x10^3$ cells/well, 48 hours of PHA-767491 treatment and 6 hours of Alamar Blue incubation, the assay of MCF10A cells gave a Z-factor value of 0.74 which is within the range of a robust assay for HTS (Figure 4.14). Increasing the Alamar Blue incubation period to 12 hours led to an increase of Z-factor values to 0.84-0.9 (Appendix B, Figure S4.1A, Z' factor (PHA), 12H read, 4x10^3 cells). Increasing inhibitor treatment time to 72 hours did not improve the Z-factor values (Appendix B, Figure S4.1B, Z' factor (PHA), 6H read, 4x10^3 cells). Z-factor value increased from 0.1 to 0.74 when the cell density increased from $1x10^3$ to $4x10^3$ cells/well (Figure 4.14).

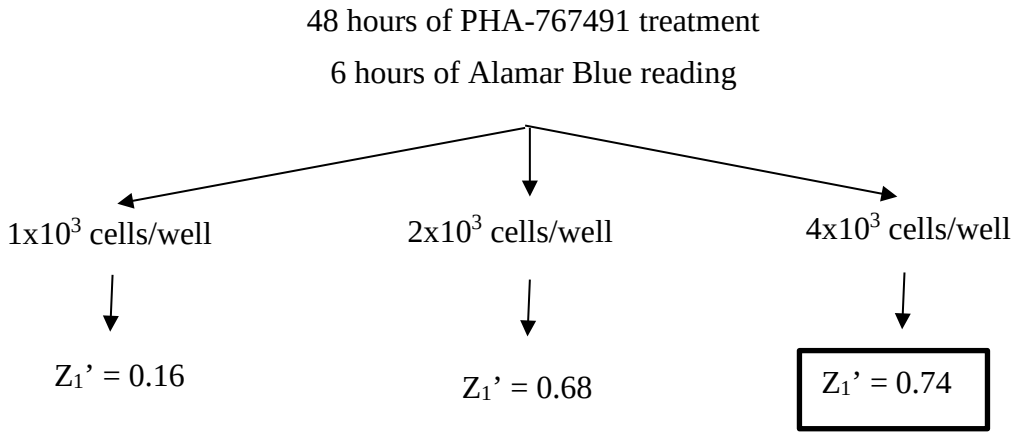


**Figure 4.14 Z-factor values of Alamar Blue assay in MCF10A at different cell density**
Cells were plated at different cell densities for 24 hours and treated with PHA-767491, HU or DMSO for 48 and 72 hours. At the end of treatment, Alamar Blue was added and the fluorescence emission intensity was measured after 4, 6 and 12 hours of incubation. Experiment was performed once.

For MDA-MB-231, cell density of $8x10^3$ cells/well, 48 hours of PHA-767491 treatment and 6 hours of Alamar Blue incubation are the conditions in which the cell proliferation assay gave a Z-factor value of 0.77 (Figure 4.15). This value was in the range of a robust assay suggesting that these conditions are suitable for screening with MDA-MB-231. Similar observations were made for Z-factor value of inhibitor treatment time and Alamar Blue incubation time (Appendix B, Figure S4.2, Z' factor

(PHA)) and cell density also greatly affects the robustness of assay assessed by Z-factor (Figure 4.15).

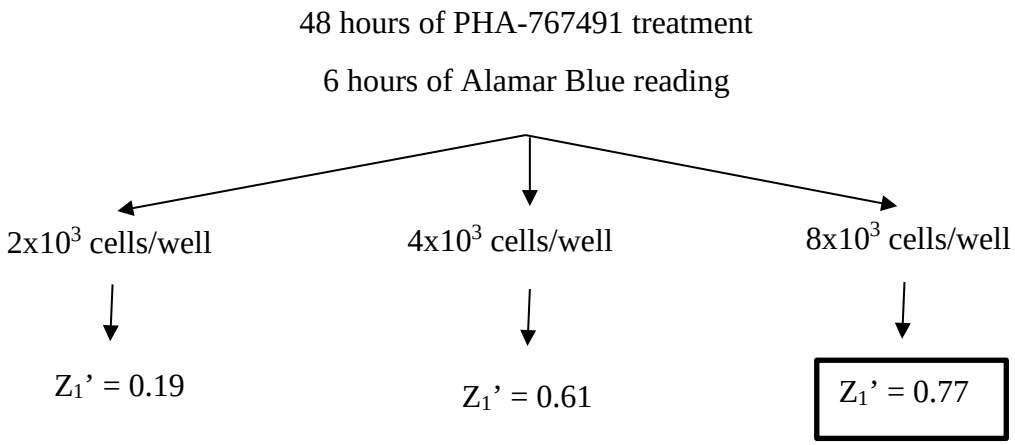


**Figure 4.15 Z-factor values of Alamar Blue assay in MDA-MB-231 at different cell densities.**

Cells were plated at different cell densities for 24 hours and treated with PHA-767491, HU or DMSO for 48 and 72 hours. At the end of treatment, Alamar Blue was added and the fluorescence emission intensity was measured after 4, 6 and 12 hours of incubation. Experiment was performed once.

### 4.4.3 Screening of MCF10A and MDA-MB-231 cells using PKIS library

The PKIS library contains more than 300 compounds which target over 200 human kinases, and has been used widely *in vitro* and *in vivo* [219]. In this study, PKIS screening was performed to identify inhibitor(s) of which the anti-proliferative activity is enhanced by the presence of XL413. Since in a Nanosync heatmap assay, PKIS compounds were tested at concentrations 0.1 and 1 µM, so we chose 0.5 µM as a starting concentration for treatment [220].

MCF10A cells were plated at $4x10^3$ cells/well, while MDA-MB-231 cells were plated at $8x10^3$ cells/well. Cells were allowed to recover for 24 hours, then treated with each PKIS compound at 0.5 µM, together with XL413 or DMSO for 48 hours. Each sample assay was performed in duplicate. Control cells were treated with DMSO and PHA-767491 for 48 hours. Each control was performed in 6 replicates. Treated cells were incubated with Alamar Blue reagent for 6 hours, and fluorescence signals were measured by a Victor X5 system (Perkin Elmer). Data was normalised by Z-score and percent of control (POC) calculated then graphed using MS Excel.

In this study, a "hit" compound was predefined as a compound which statistically belongs to top 1% out of 317 compounds. This means that the "hit" compound has an absolute value of Z-score of XL413 treatment which is larger than 2.33, according to the normal distribution frequency [205]. We found that 13 compounds from PKIS screening with MCF10A cells satisfied this selection criteria (Figure 4.16A and Appendix B, Figure S4.3).

In our criteria, the “hit” compound should have a greatly different effect on cell proliferation in the presence of XL413. To achieve this goal, we used the percent of control (POC) measurement to compare inhibitory effects between compounds. Only GW680191X (cp18), with the highest difference between POC of XL413- and DMSO-treated cells of 9.5% (Figure 4.16B), satisfied the criteria (discussed later). The other compounds with a maximal difference of 4% were excluded from the target list (Appendix B, Figure S4.3).

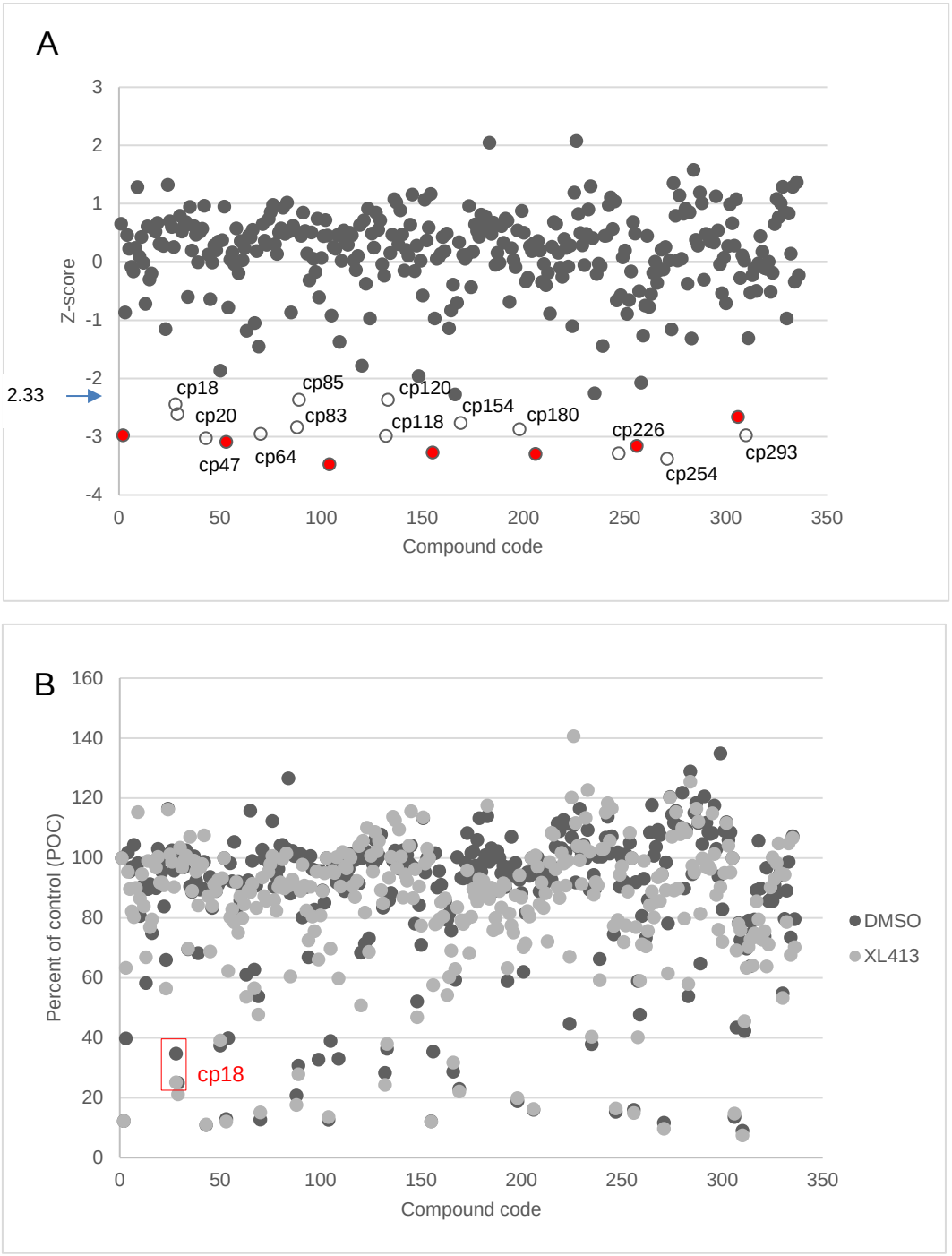


**Figure 4.16 Scatter graphs of PKIS screening with XL413 in MCF10A cells.**

Cells were treated with PKIS compounds in combination with DMSO or XL413 for 48 hours. Control cells were treated with DMSO, PHA-767491 or HU for 48 hours. Treated cells were incubated with Alamar Blue reagent for 6 hours and fluorescence signals were measured by a Victor X5 system (Perkin Elmer). (A): Z-score graph of XL413-treated cells; (B): POC graph of DMSO- and XL413-treated cells. : PHA-767491-treated cells. Each sample was performed in duplicate. Experiment was performed once.

Similarly, in PKIS screening with MDA-MB-231, we observed 6 “hit” compounds that have the absolute values of Z-score higher than 2.33 (Figure 4.17A and Appendix B, Figure S4.4). However, only GW801372X (cp64) had a POC of XL413-treated cells which was 7.5% lower than of DMSO-treated cells, suggesting this compound prevents cell proliferation in the presence of XL413 (Figure 4.17B) (discussed later). The other compounds either had POC of XL413-treated cells which were higher than of DMSO-treated cells, or had a difference of POCs less than 5% (Appendix B, Figure S4.4), so those compounds were all excluded from the target list.

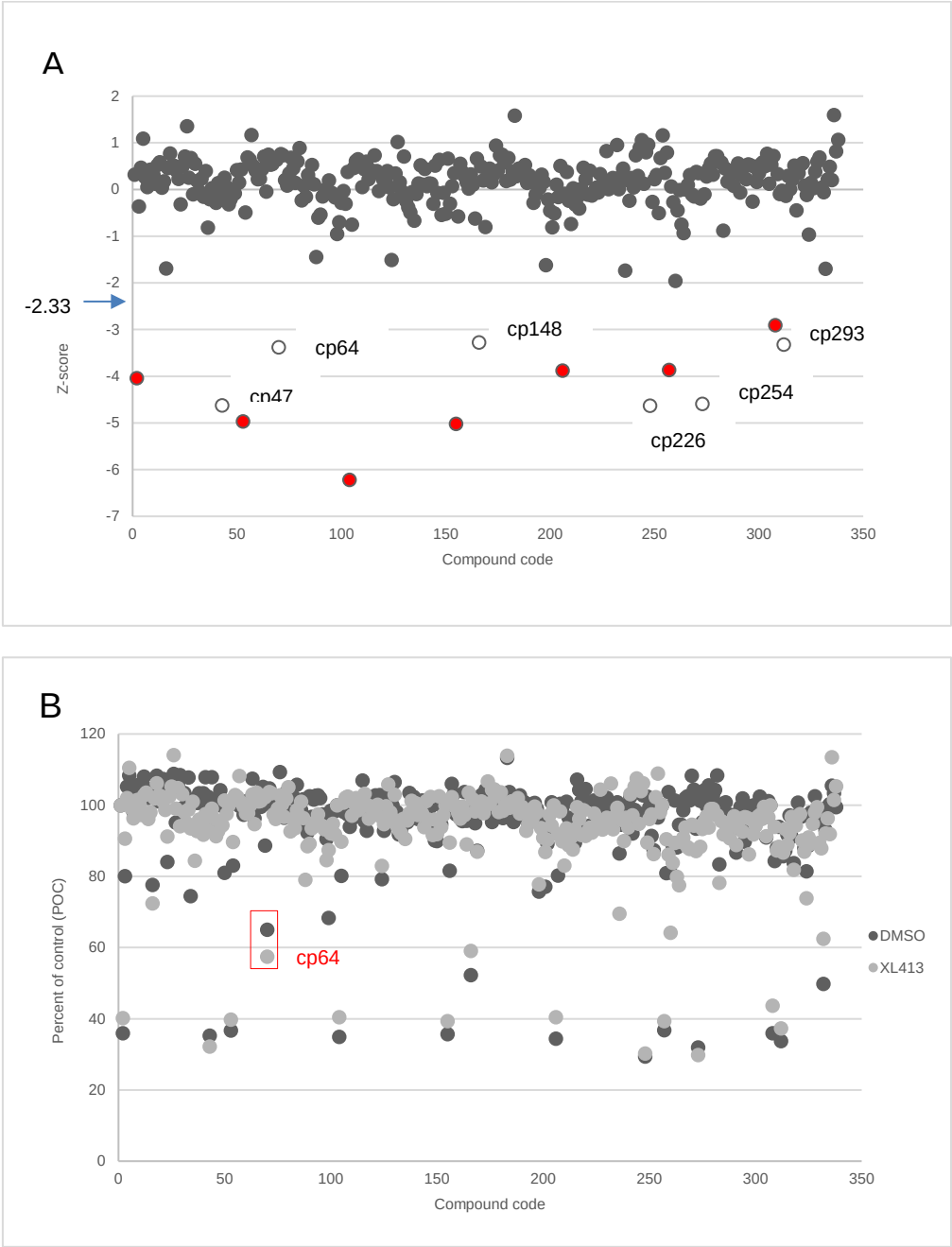


**Figure 4.17 Scatter graphs of PKIS screening with XL413 in MDA-MB-231 cells.**
Cells were treated with PKIS compounds in combination with DMSO or XL413 for 48 hours. Control cells were treated with DMSO, PHA-767491, HU for 48 hours. Treated cells were incubated with Alamar Blue reagent for 6 hours and fluorescence signals were measured by a Victor X5 system (Perkin Elmer). (A): Z-score graph of XL413-treated cells; (B): POC graph of DMSO and XL413-treated cells. : PHA-767491-treated cells; Each sample was performed in duplicate. Experiment was performed once.

A search of kinase targets for identified "hit" compounds was performed in the ChemBL database (https://www.ebi.ac.uk/chembl/). Each compound has a profile listing kinases tested and their percent of inhibition (Figure 4.18). Based on the profile, we found that GW680191X (cp18) mainly targets ErbB1/HER1, ErbB4/HER4 and Lok/STK10 (Appendix B, Figure S4.5) whereas GW801372X (cp64) targets multiple kinases which belongs to CMGC, CAMK and S-T-PK groups (Appendix B, Figure S4.6).

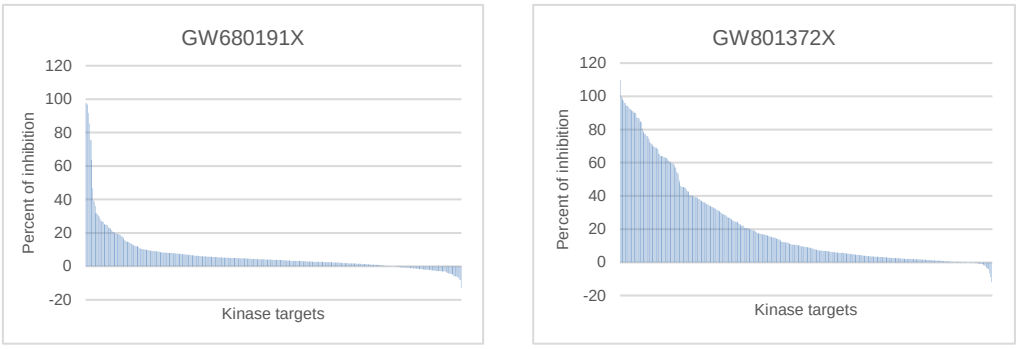


**Figure 4.18 Kinase inhibition profile of GW680191X (cp18) and GW801372X (cp64).** (data collected from the ChemBL database https://www.ebi.ac.uk/chembl/).

Overall, by using PKIS screening with two breast-derived human cell lines, we identified two “hit” compounds GW680191X (cp18) and GW801372X (cp64) that are able to kill more cells in the presence of CDC7 inhibitor XL413.

However, for the secondary screening, we changed our method. This change was based on the idea which is the co-administration of two compounds may induce off-targets effects, e.g. drug-drug interaction effects [221]. Therefore, instead of using XL413, we employed the knock-out of DBF4, a CDC7 regulatory subunit, to inhibit CDC7 kinase activity.

## 4.5 High-throughput screening of PKIS library with a DBF4 knock-out cell line

Data analysis of PKIS screening in combination with XL413 treatment revealed several potential compounds (section 4.4). To confirm these screening results, instead of performing a secondary screening with XL413, we performed PKIS screening with a HAP1-genetically modified cell line in which CDC7 kinase activity is attenuated due to the lack of its regulatory subunit DBF4. A DBF4-WT cell line was used in parallel as a control.

### 4.5.1 Characterisation of genetically modified HAP1 DBF4 knock-out cell line

HAP1 is a fibroblast-like haploid cell line derived from the myelogenous leukaemia cell line KBM-7. The existence of only one copy of each chromosome facilitates the genome modification, i.e. gene inactivation. By using CRISPR-Cas9 technique, the inactivation of *dbf4* gene was achieved by deleting 17bp at exon 3 (Horizon Discovery).

As DBF4 is one of critical CDC7 regulatory subunits, we hypothesised that DBF4 knock-out (4KO) attenuates CDC7 kinase activity, leading to the effects on DNA replication progression and MCM2 phosphorylation of HAP1 cells. To test this hypothesis, HAP1 WT and 4KO cell lines were plated for 24 hours, labelled with EdU for 30 minutes and harvested. Cells pellets were subjected to total protein extraction using CSK lysis buffer and immunoblotting. A portion of harvested cells were fixed and subjected to EdU/DAPI staining for flow cytometry.

By immunoblotting, we confirmed that the 4KO cell line lacks the DBF4 protein main band at 100 kDa (Figure 4.19A). This cell line also had a low level of phosphorylated MCM2 at S40/41 and a noticeable reduction of MCM2 phosphorylation in comparison with the WT cell line (Figure 4.19B). This suggests that in the absence of DBF4, the kinase activity of CDC7 assessed by the biomarker pMCM2 S40/41 decreases. Flow cytometric data analysis confirmed that both cell lines had more than 92% of haploid cells. The percent of S-phase population increased from 41.6 to 58.5% and of G2-phase decreased from 15.0 to 7.1% in HAP1

cells lacking DBF4, suggesting that the knock-down of DBF4 affects the cell cycle distribution in this cell line (Figure 4.19C, WT vs 4KO).

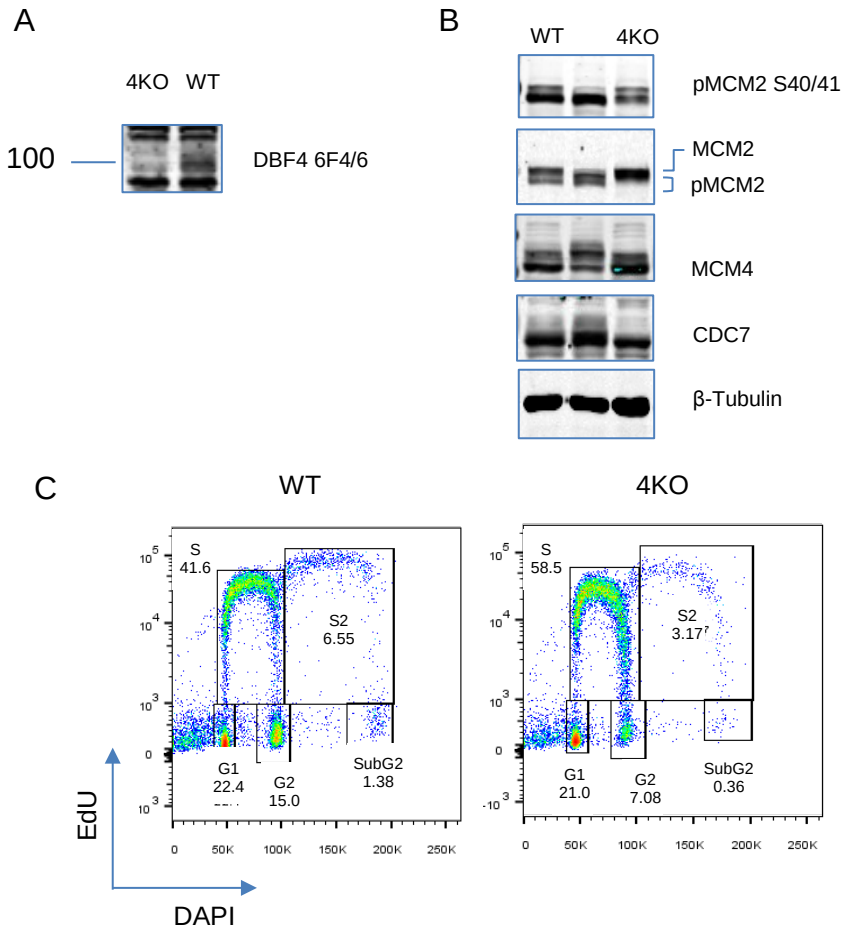


**Figure 4.19 Characterisation of HAP1 WT and 4KO cell lines for PKIS screening.** Cells were plated for 24 hours, harvested as cell pellets and subjected to immunoblotting. A portion of harvested cells were fixed and subjected to EdU/DAPI staining for flow cytometry. (A-B) Immunoblotting data of detecting overexpressed DBF4 by monoclonal antibody (A) and the effects of overexpressed DBF4 on MCM2-4 phosphorylation (B); (C) Flow cytometric data analysis. Experiment A and C were performed twice and experiment B was performed once.

### 4.5.2 Optimisation of Alamar Blue assay for screening with HAP1 cell lines

In order to have a robust assay for HTS, conditions for the Alamar Blue assay were optimized with HAP1 WT and 4KO cell lines. Cells were plated at cell densities of $0.5x10^3$, $1x10^3$ and $2x10^3$ cells/well for 24 hours, treated with PHA-767491, HU or DMSO for 48 and 72 hours, incubated with Alamar Blue and fluorescence emission intensities were measured after 4 and 6 hours of reagent incubation. The DMSO-

treated sample was performed in 21 replicates (n=21). PHA-767491- and HU-treated samples had 28 replicates each (n=28) and no-cell control had 7 replicates (n=7). All the steps were performed using a ZANUS automated liquid handling station (Perkin Elmer) and fluorescence signals were read by a Victor X5 plate reader. The Z-factor was calculated by MS Excel.

The highest Z-factor value for the assay was 0.9 in both cell lines when the Alamar Blue assays were conducted with $2x10^3$ cells/well for cell density of plating, 72 hours of inhibitor treatment and 6 hours of Alamar Blue incubation. Z-factor values decreased when cells were plated at $0.5x10^3$ and $1x10^3$ cells/well suggesting that the cell density for plating is also a critical factor to have a robust assay in HAP1 cell lines. The change of inhibitor treatment duration to 48 hours or Alamar Blue incubation time to 4 hours only slightly decreased this Z-factor to 0.8 (Appendix B, Figure S4.7 and S4.8).

### 4.5.3 Screening of DBF4 knock-out cell line using PKIS library

Prior to screening, HAP1 WT and 4KO cell lines were recovered from frozen stocks and split for 1 or 2 passages. Cells were plated for 24 hours, treated with PKIS drugs at 0.5 µM for 72 hours and incubated with Alamar Blue for 6h after treatment. Each sample was measured in triplicate. Fluorescence signals were read by the Victor X5 plate reader and data analysis was performed with MS Excel.

Based on the criteria of selecting “hit” compounds with an absolute value of Z-score which is higher than 2.33, we identified 12 compounds (Figure 4.20 and Appendix B, Figure S4.9). Only two compounds, GW305178X (cp103) and GW801372X (cp64) had highest differences of POC between 4KO and WT cell lines which were 9.9% and 9.1% respectively. The POC of 4KO was smaller than of WT cells indicating that those compounds kill more HAP1 cells when DBF4 is absent. The other compounds either having a POC of 4KO higher than of WT, or only triggering about 2% difference of POC between two cell lines, were excluded from the target list (Appendix B, Figure S4.9).

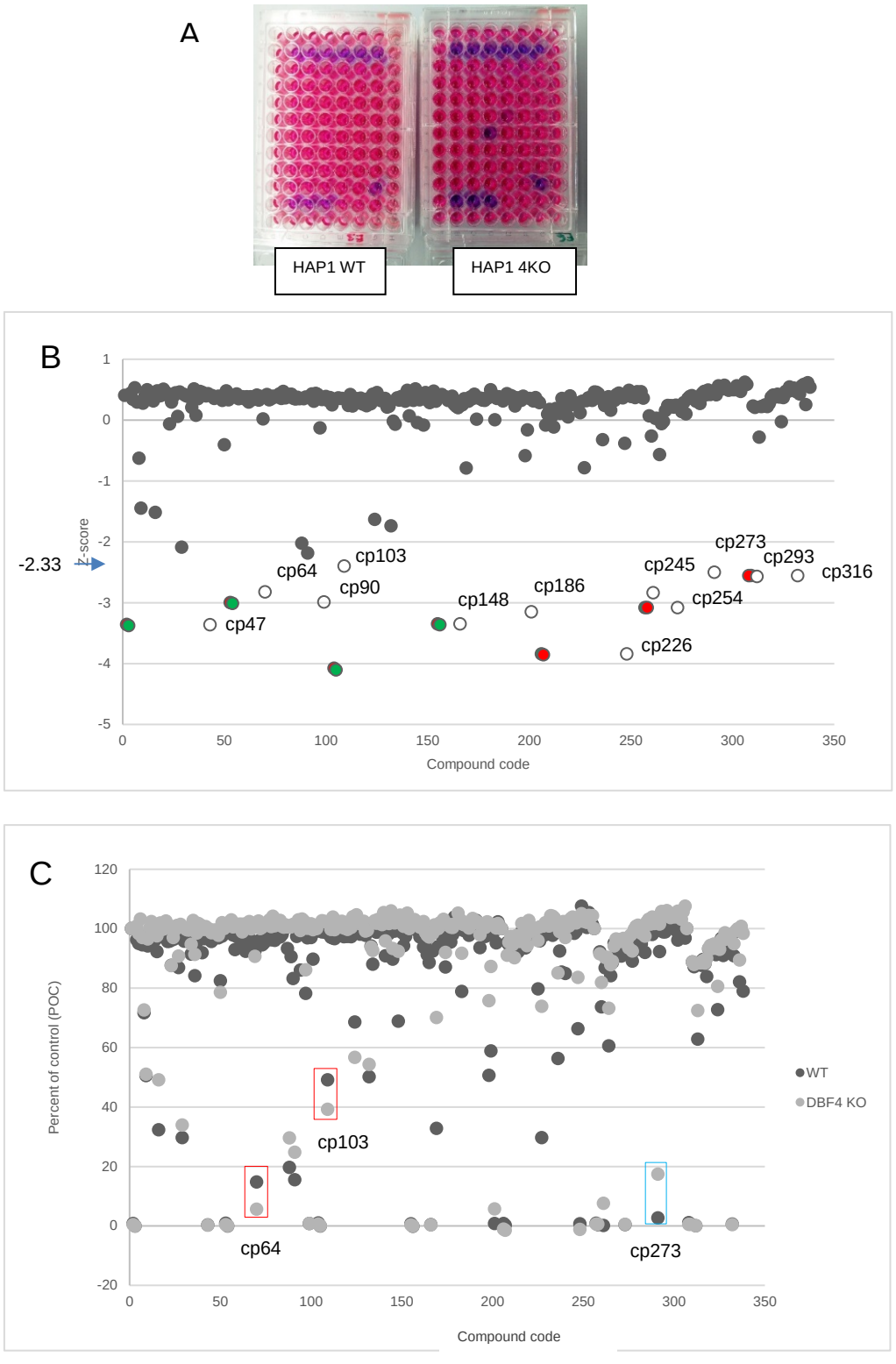


**Figure 4.20 Scatter graphs of PKIS screening with DBF4 wild-type (WT) and knock-out (KO) cells.**

(Legend is in the next page)

Cells were plated for 24 hours, treated with PKIS drugs at 0.5 µM for 72 hours and incubated with Alamar Blue for 6h after treatment. Each sample was performed in triplicate. (A): An example image of PKIS drug plate E; (B): Z-score graph of 4KO cells; (C): POC graph of WT and 4KO cells. : PHA-767491-treated cells; : HU-treated cells. Each sample was performed in triplicate. Experiment was performed once.

Interestingly, GW801372X (cp64), which was identified as a hit from the XL413 PKIS screen in MDA-MB-231 also turned up as a hit in this screen. This suggests that the inhibitory effects of the compound are not specific only for breast cancer. The other compound in the target list of HAP1 was GW305178X (cp103). This inhibitor targets many kinases which belongs to the CMGC, CAMK and STE families (Figure 4.21 and Appendix B, Figure S4.10). Relevant kinases might be MST1/2 and MELK (Appendix B, Figure S4.10).

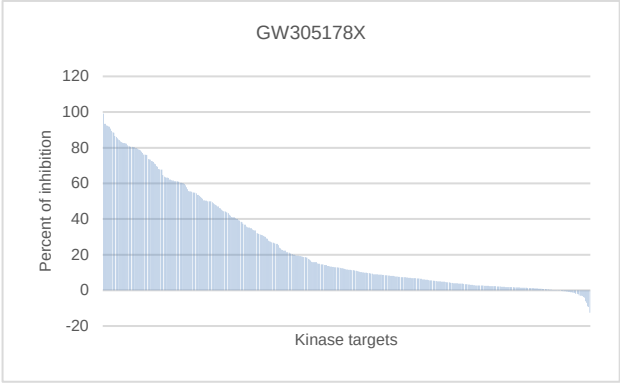


**Figure 4.21 Kinase inhibition profile of GW305178X (cp103).**
Data collected from the ChemBL database https://www.ebi.ac.uk/chembl/.

In summary, GW680191X, GW801372X and GW305178X were identified as hit compounds which greatly reduce cell viability of human cells while CDC7 kinase is inhibited by XL413 or DBF4 knock-out. GW680191X specifically targets HER1/4 and STK10, while GW801372X and GW305178X target multiple kinases, including AURKC, ARK5, GSK3β, DYRK1B, MELK and MST1/2 (discussed later). Further functional studies are required to confirm these results.

## 4.6 PLK1 inhibition restrains human DNA replication in a DBF4-dependent manner

In PKIS screening with a DBF4 knock-out cell line, we noticed that cells treated by some compounds belonging to the top 1% specific compounds have a higher POC than WT cells. For example, GW852849X (cp273)-treated cells have a POC of 4KO cells which is 14% higher than of WT cells (Section 4.5.3, Figure 4.20). One of the main targets of GW852849X is PLK1 (Appendix B, Figure S4.11). Therefore, we hypothesised that PLK1 inhibition affects cell viability of HAP1 cells in a DBF4-dependent manner.

### 4.6.1 Titration of PLK1 inhibitor BI6727

To test our hypothesis, we first titrated a selective PLK1 inhibitor BI6727, also known as volasertib, in HAP1 WT and 4KO cell lines. GW84362X which targets PLK1/PLK3 and other PLKs was also employed as a reference. Cells were plated in 96-well plates for 24 hours, and treated with DMSO or PLK inhibitors for 72 hours at the indicated concentrations. After being incubated with Alamar Blue for 6 hours, fluorescence emission intensities were read by CytoFluor and data analysis was performed with Excel/Minitab 17.

BI6727 decreased cell viability of HAP1 WT within a dose range of 0.01 to 1 µM and significantly decreased at 0.02 µM. Treated HAP1 WT cells at that dose showed a reduction in cell viability of more than 70% compared to only 20% in HAP1 4KO (Figure 4.22A, 0.02). GW84362X had a similar effect on both cell lines and at 0.1 µM, GW84362X-treated cells of HAP1 WT had a significantly lower fluorescence emission intensity than of HAP1 4KO (Figure 4.22B). This suggests that the inhibition of PLK1 either by BI6727 or GW84362X has a stronger inhibitory effect on cell viability for WT than 4KO cell lines.

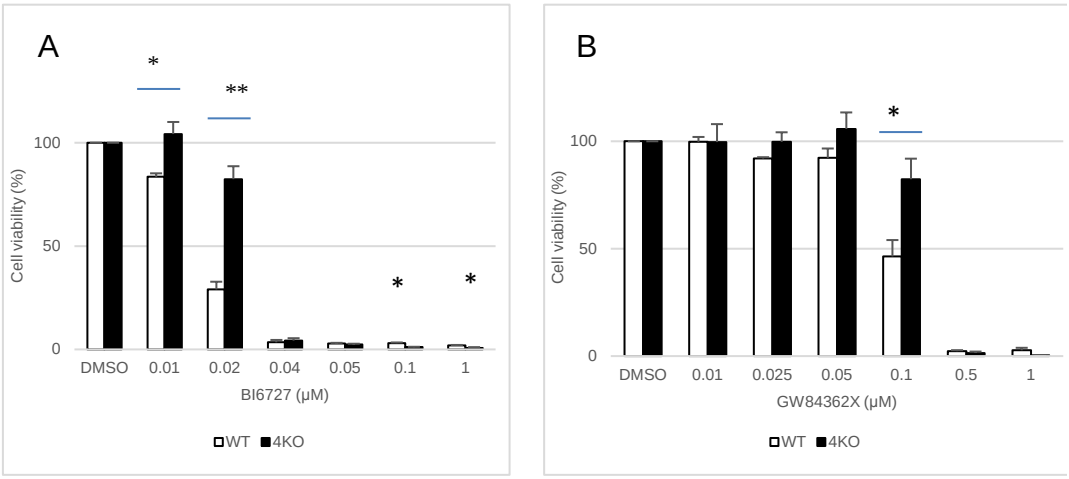


**Figure 4.22 Dose responses of HAP1 WT and DBF4 KO cells to PLK1 inhibitors BI6727 and GW84362X.**

Cells were plated in 96-well plates for 24 hours, treated with DMSO or inhibitors for 72 hours and incubated with Alamar Blue for 6 hours prior to fluorescence signals measured by CytoFluor. (A): BI6727; (B): GW84362X. * or **: $p<0.05$ (Two-sample Student t-test). Error bars represent the Mean ± SD. Each sample was performed in triplicate. Experiment was performed once.

### 4.6.2 DBF4 knock-out attenuates inhibitory effects of PLK1 inhibitor on DNA replication

PLK1 is a critical kinase involved in many steps in mitosis of mammalian cells, including mitotic entry – exit, spindle assembly and the G2/M checkpoint [222,223]. Its role in DNA replication was identified in previous studies [224,225] . However, no study has mentioned the effects of PLK1 inhibition on DNA replication in the absence of DBF4.

By PKIS screening, we found that a compound mainly targeting PLK1 prevents the proliferation of a DBF4-wild type cell line more than of a DBF4-knock out cell line. One hypothesis is that in the absence of DBF4, DNA replication of the HAP1 cell line is delayed and this absence also prevents apoptotic cell death triggered by PLK1 inhibition. To test this hypothesis, WT and 4KO cells were plated for 24 hours and treated with BI6727 at 20 nM for 24 and 48 hours. At each time point, treated cells were labelled with EdU for 30 minutes prior to harvest, fixed and subjected to EdU/DAPI staining for flow cytometry. Data analysis was performed with FlowJo.

In HAP1 WT cells 24 hours post-treatment, the percentage of S-phase population of BI6727-treated cells decreased to 0.4-fold of untreated cells (Figure 4.23, WT-DMSO vs WT-BI). Meanwhile, in HAP1 4KO cells, this population of 4KO was only reduced to 0.6-fold of untreated cells (Figure 4.23, 4KO-DMSO vs 4KO-BI). A similar phenomenon was observed 48 hours post-treatment in both cell lines (Figure 4.23, 48 h). This indicates that the reduction of EdU incorporation in HAP1 cells caused by BI6727 is lesser when cells lack DBF4.

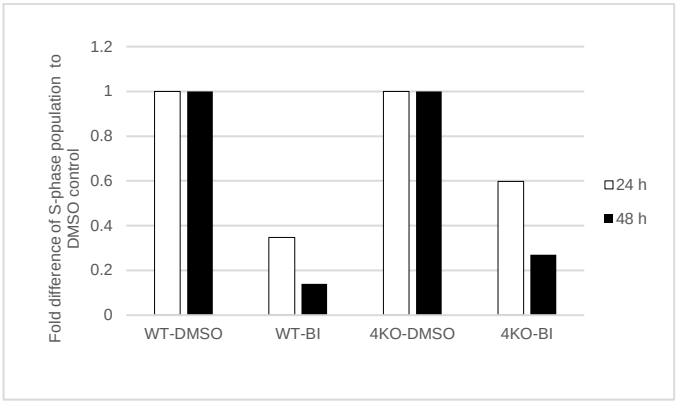


**Figure 4.23 Effects of BI6727 on EdU incorporation in HAP1 WT and 4KO cells.**
Cells were plated for 24 hours, treated with BI6727 at 20 nM for 24 and 48 hours. At each time point, treated cells were labelled with EdU for 30 minutes prior to harvest, fixed and subjected to EdU/DAPI staining for flow cytometry. Data analysis was performed with FlowJo. Experiment was performed once.

An explanation could be that DBF4 absence triggers a delay at S-phase, so cells enter apoptosis more slowly. To confirm this, cells were labelled using EdU and a pulse-chase method which allows tracking of DNA replication progression through the dynamics of a EdU-positive population in the cell cycle. Cells were plated for 24 hours, then labelled with EdU for 30 minutes. After the washing of the EdU-containing medium, cells were treated with BI6727 at 20 nM for 24, 48 and 72 hours. At each time point, cells were harvested, fixed and subjected to EdU/DAPI staining for flow cytometry. Data analysis was performed with FlowJo.

Twenty-four hours post-treatment, the EdU-positive population of WT cells moved to the subS area and a massive increase of subG1 population of WT cells from 4.05% at 0h to 40% 48 hours post-treatment (Figure 4.24 WT, subS/subG1, 0h vs 48h). The EdU-positive population of 4KO cells also moved to the subS area upon 48 hours

treatment and remained there 72 hours post-treatment (Figure 4.24 4KO, subS 48h and 72h). The increase of subG1 population in 4KO was less than in WT cells at any time point (Figure 4.24 4KO vs WT, subG1) This suggests that in the absence of DBF4, cells may delay the cell cycle progression and apoptosis.

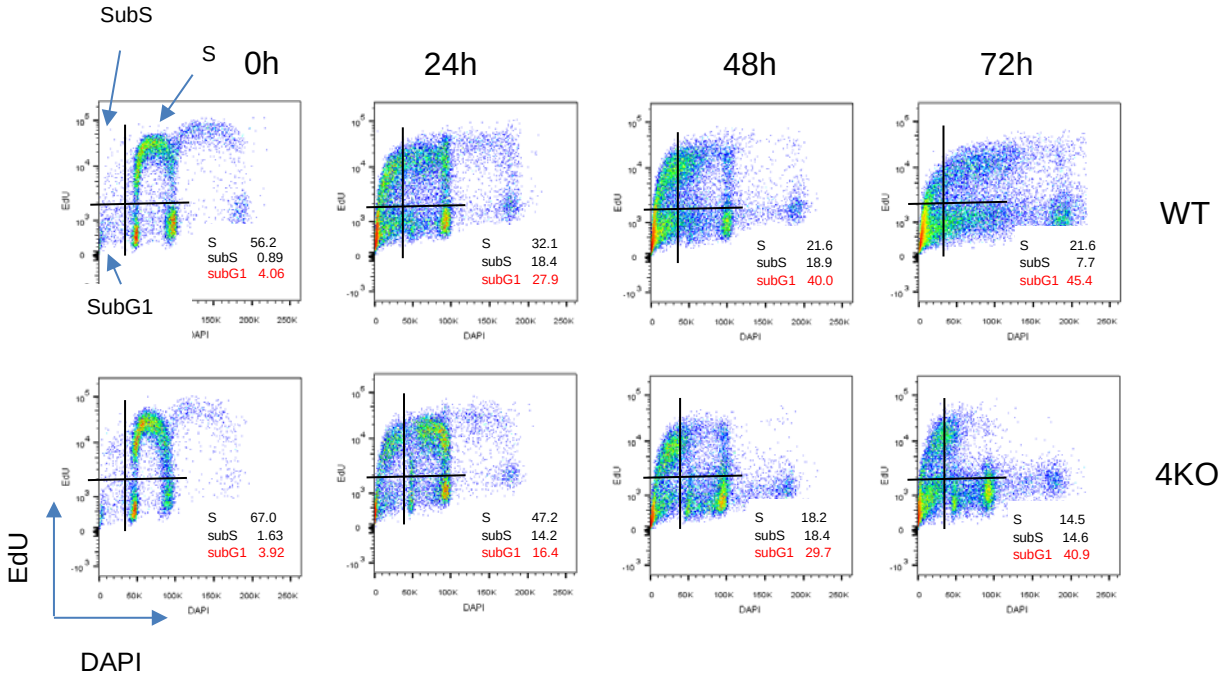


**Figure 4.24 Delay of cell cycle progression in BI6727-treated 4KO cells**

Cells were plated for 24 hours, EdU pulse chase for 30 minutes then treated with BI6727 at 20 nM for 24, 48 and 72 hours. At each time point, cells were harvested, fixed and subjected to EdU/DAPI staining for flow cytometry. Data analysis was performed with FlowJo. Experiment was performed once.

The accumulation of cells at subG1 was observed in 4KO cells when treated with BI6727 compared to WT cells (Section 4.6.2, Figure 4.24 4KO). We hypothesised that DBF4 knock-out affects the progression of apoptosis. To test this hypothesis, the patterns of poly (ADP-ribose) polymerase (PARP) and Caspase 3 cleavage were examined by immunoblotting. WT and 4KO cells were treated with BI6727 at 20 nM for 24, 48 and 72 hours. At each time point, cells were harvested and subjected to protein extraction using CSK lysis buffer. Soluble fraction was used for immunoblotting.

We observed that PARP was cleaved mostly 24 hours post-treatment in BI6727-treated WT cells but only partly in treated 4KO cells (Figure 4.25, cleaved PARP, lane 2 and 4). Similarly, after 48 hours of BI6727 treatment, uncleaved PARP disappeared in WT but still existed in 4KO cells (Figure 4.25, cleaved PARP, lane 6 and 8). A delay of Caspase 3 cleavage was also observed (Figure 4.25, cleaved Caspase 3, lane 2, 4, 6 and 8). This suggests that the absence of DBF4 or to some extent, the attenuation of CDC7 kinase may affect the apoptotic progression when PLK1 is inhibited.

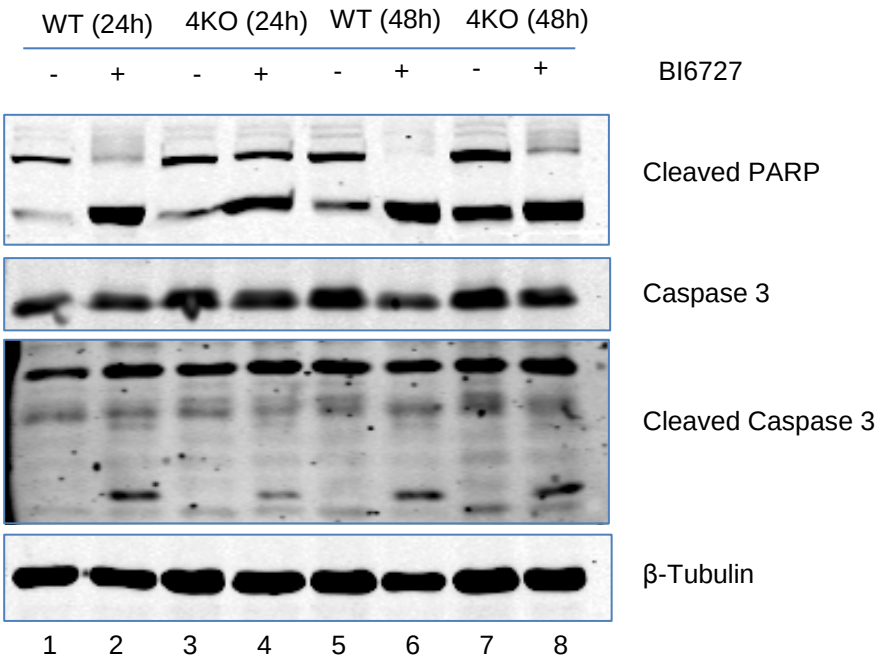


**Figure 4.25 PARP and Caspase 3 cleavage in BI6727-treated 4KO cells**

Cells were plated and treated with DMSO or BI6727 at 20 nM for 24 and 48 hours. Harvested cells were pelleted at each time point and subjected to protein extraction using CSK lysis buffer. Soluble fraction was used for immunoblotting. Experiment was performed once.

## 4.7 Conclusion

The combination of CDK1 and CDC7 inhibition, either by pharmacological compounds or by RNA interference (RNAi) strongly attenuates but does not abolish DNA replication in MCF10A cells. However, this combined inhibition does not affect DNA replication in MDA-MB-231 cells. DNA synthesis still occurs even when CDK1, CDK2 and CDC7 are co-inhibited, suggesting that another kinase may be involved in controlling DNA replication of human cells.

By screening the PKIS library, GW680191X, GW801372X and GW305178X were identified as potential hit compounds, which greatly restrain cell proliferation of human cells in the presence of XL413 or in a DBF4 knock-out cell line. Noticeably, a compound targeting PLK1 kills less DBF4 knock-out cells than wild-type cells. By biochemical tests, it was found that DBF4 knock-out weakens the inhibitory effects of PLK1 inhibitor BI6727 on DNA replication by affecting the apoptotic progression of HAP1 cells. Further studies are required to explain this phenomenon.

# Chapter 5: Effects of overexpressing DBF4 and its domains on human cells and identification of DBF4 interactors

## 5.1. Introduction

Dumbbell forming 4 (DBF4) is a key regulatory subunit of CDC7 [13]. In mammalian cells, DBF4 and CDC7 interact with different subunits of the MCM complex to promote DNA replication [226]. In addition, the DBF4 motif N is required for the interaction with Rad53/CHK2 human homolog [227], and a direct interaction between DBF4 and the PBD box of Cdc5/PLK1 human homolog may inhibit this mitotic kinase [153,154]. In the previous chapter, we observed the effects of DBF4 knock-out in human cell line HAP1 and found that the absence of DBF4 either enhances the sensitivity or the resistance of cells to different ATP-competitive inhibitors (chapter 4, section 4.5.3). However, the mechanism of these drug resistances was still unclear. Therefore, we generated TREx-293 cell lines in which DBF4 and its motifs were overexpressed in an inducible manner to detect novel DBF4-interactors that may reveal some unknown functions of DBF4 in human cells.

## 5.2. Generation of TREx-293 cell lines overexpressing DBF4 full-length and its domains

Flp-In T-REx (Invitrogen) is a system which allows integration of a gene of interest (GOI) into the genome of host cell at a specific locus. This system allows conditional expression of a gene when doxycycline or tetracycline is present (T-REx system). The Flp-In 293 cell line, which is commercially generated, contains a single Flp Recombination Target (FRT) site in the genome by transfecting a human embryonic kidney 293 (HEK-293) cell line as host cell with a Flp-In target site vector pFRT/*lac*Zeo. Zeocin-resistant clones carrying a single site of Flp-In confirmed by southern blot were selected. The Flp-In T-REx 293 cell line also carries pcDNA6/TR, a vector expressing *TetR* gene, resulting in stable expression of the Tetracycline repressor protein (Figure 5.1).


**Figure 5.1 Generation of Flp-In T-REx 293 cell line.**

Details were described in the text. Figure adapted from the Flp-In T-REx core kit manual (Thermo Fisher Scientific).

To generate stable cell lines, the Flp-In expression vector pAb1 containing genes encoding full length DBF4 or its domains (referred as DBF4s) (Table 5.1) with Strep- and Flag-tags fused at C-terminus domain was integrated into the genome of Flp-In T-REx 293 cells at the FRT site through homologous recombination. Plasmid pOG44, an expression vector encoding Flp recombinase, was co-transfected with pAb1-DBF4s to facilitate this homologous recombination (Figure 5.2).

**Table 5.1 Description of DBF4 domains.**

| DBF4 domains | Position (aa) | Expected size (kDa) | Description |
|---|---|---|---|
| **FL** | 1-674 | 74.1 | Full-length (wild-type) |
| **N** | 1-209 | 23 | N region |
| **N+MC** | 1-350 | 38.5 | N and MC region |
| **Tail** | 351-674 | 35.6 | Tail region |
| **DN** | 210-674 | 51.2 | MC and Tail region |
| **DMC** | 1-209 and 351-674 | 58.6 | N and Tail region |

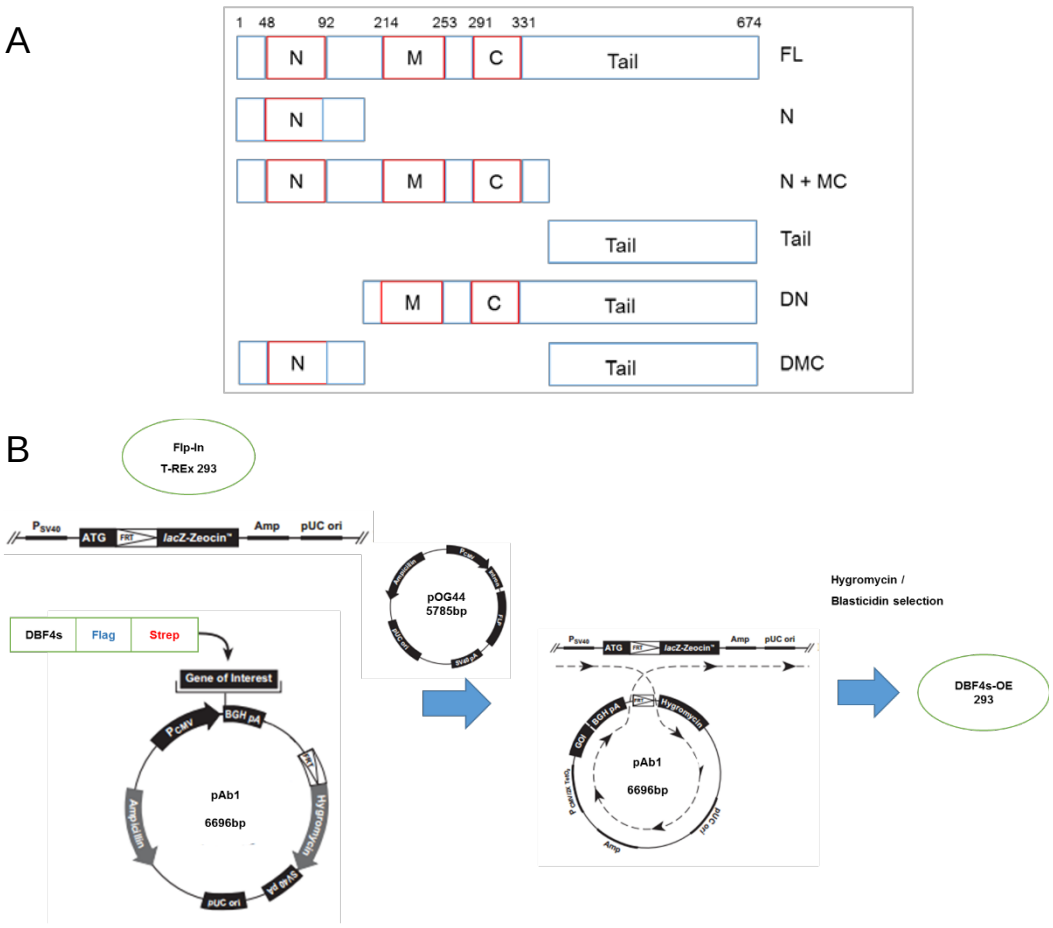


**Figure 5.2 Generation of DBF4-overexpressing 293 stable cell lines using Flp-In T-REx 293 system.**

Details were described in the text. (A) Scheme of DBF4 and its domains; (B) Diagram of generating DBF4s-OE 293 cell lines; DBF4s-OE 293: DBF4s-overexpressing 293 stable cell lines. Figure adapted from the Flp-In T-REx core kit manual (Thermo Fisher Scientific).

The expression of integrated DBF4 and its domains are controlled by Tetracycline repressor (TetR) system. TetR, a protein expressed by pcDNA6/TR, can bind to two Tet operators 2 ($TetO_2$) sequences located in the promoter pCMV which is upstream of the genes encoding DBF4 or its domains (DBF4s) and represses their transcription. In the presence of an inducer such as doxycycline, which can bind to TetR with a high affinity and induce conformational change of this protein [228,229], TetR is released from $TetO_2$ sequences and the transcription of DBF4 or its domains begins. To enable selection, a hygromycin-resistant gene was included within the expression vector pAb1. Upon successful transfection, cells become hygromycin-resistant, while untransfected cells are eliminated by selection medium (Figure 5.3).

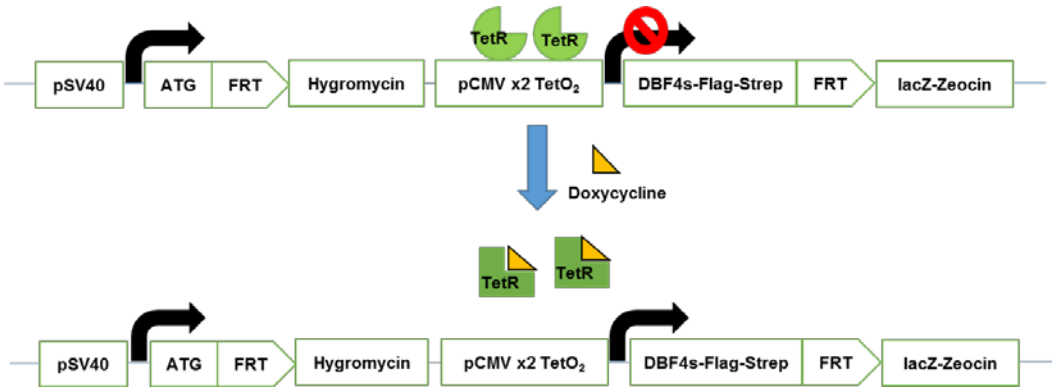


**Figure 5.3 Regulation of gene expression by the TetR system.**

Details were described in the text. Figure adapted from [230] and the Flp-In T-REx core kit manual (Thermo Fisher Scientific).

Flp-In T-REx 293, referred to here as the TREx-293 cell line, was transfected with each expression vector pAB1-EV, -FL, -N, -N+MC, -DN, -Tail and –DMC, and the plasmid pOG44 at ratio of 9:1 (w/w) using Fugene HD (Promega). Forty-eight hours post-transfection, cells were reseeded on TC dishes and incubated in selection medium containing hygromycin and blasticidin for at least 24 hours. Only hygromycin- and blasticidin-resistant cells were subjected to colony isolation for monoclonal selection. Seven monoclonal cell lines named as EV 1.1, FL 1.1, N 1.1, N+MC 1.1, Tail 4.1, DN 2.1, DMC 1.1 were isolated with the support of Dr Michael Rainey and Gemma O'Brien.

## 5.3. Characterisation of DBF4s-overexpressing TREx-293 cell lines

In order to confirm whether stably-expressing cell lines expressed the DBF4 domains under the regulation of TetR system, all the monoclonal cell lines were plated for 24 hours and treated with doxycycline for 24 hours. Harvested cells were pelleted and subjected to soluble protein extraction by CSK lysis buffer and immunoblotting. Data were collected and analysed by LiCOR/Image Studio software.

Western blot analysis of DBF4 domain expression in TREx-293 showed that each construct expressed as a strep-tagged protein. No strep-tagged protein was detected in the negative control EV cell line either with or without doxycycline treatment (Figure 5.4, lane 1 and 2). In contrast, each expression construct showed the specific induction of a band with the appropriate molecular weight after doxycycline treatment (Figure 5.4, lane 3 to 14) suggesting DBF4 domains were overexpressed under the regulation of TetR system.

It is noticeable that the endogenous protein level of DBF4 of this cell line is quite low. We did not observe any band of DBF4 and its domains in Dox(-) cells (Figure 5.4B, lane 1, 3, 5, 7, 9, 11 and 13). When being treated with Doxycycline, the protein level increased approximately 6 times in comparison with Dox-untreated cells, based on fluorescent intensities measured by LiCOR/Image Studio software.

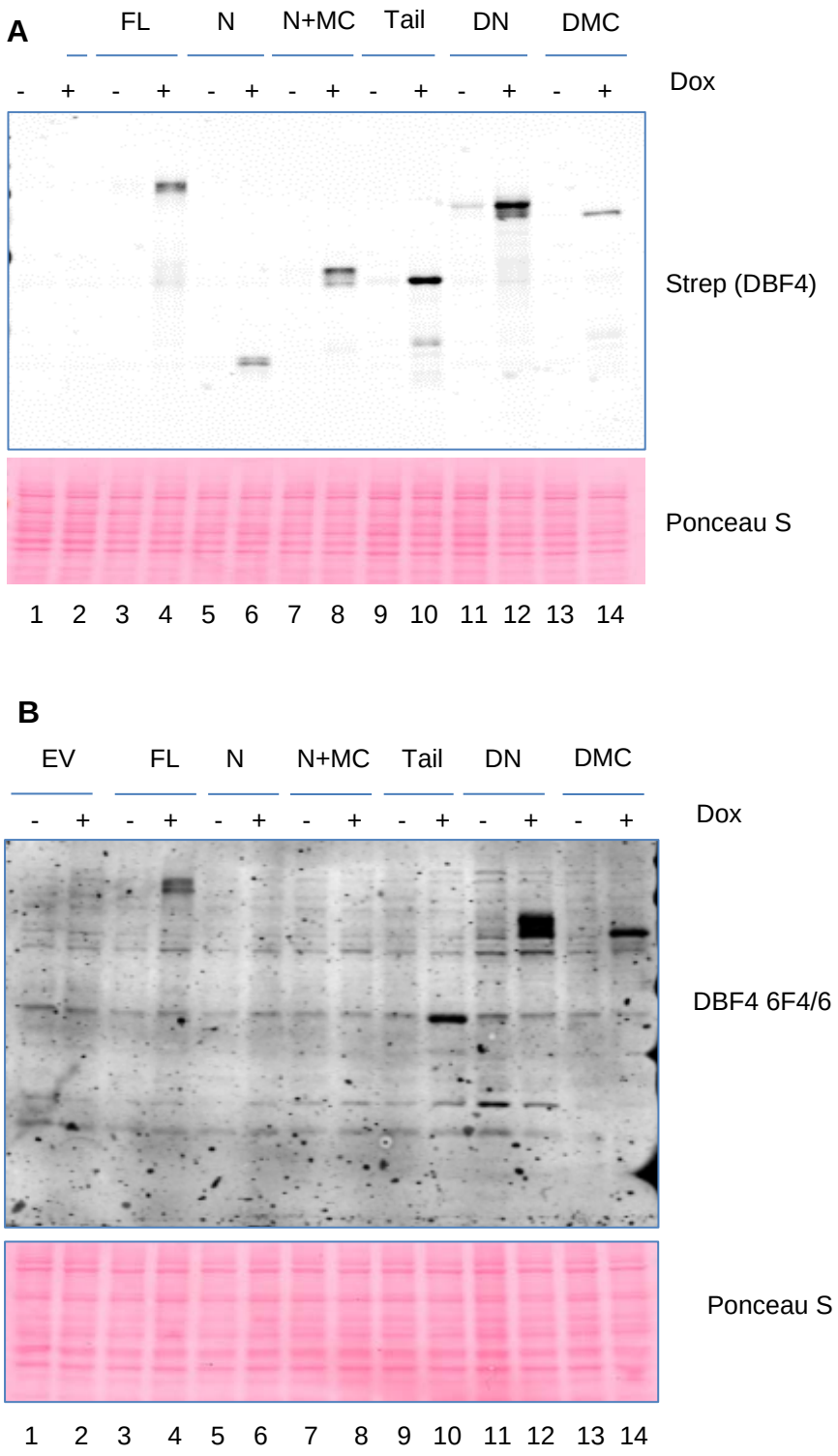


**Figure 5.4 Induction of overexpressed DBF4 and its domains upon doxycycline treatment.**

(Legend is in the next page).

FL, N, N+MC, DN, Tail and DMC-overexpressed cells were plated and treated with doxycycline for 24 hours. Harvested cells were pelleted and soluble extracted protein was subjected to immunoblotting. Data were collected and analysed by LiCOR/Image Studio software. (A): Detection of DBF4 overexpression by Strep Ab; (B) by DBF4 6F4/6 MAb. Experiments were performed once.

### 5.3.1. Overexpression of full-length DBF4 does not affect cell cycle progression

In HeLa cells, overexpressing DBF4 and CDC7 does not affect cell cycle progression [231]. On the other hand, the upregulation of DBF4 at a moderate level has been reported to arrest cells at G2/M and high level at G1-phase [232]. To clarify this issue, DBF4 FL, N, N+MC, DN, Tail and DMC monoclonal cells were plated for 24 hours and treated with doxycycline for 24 hours. Untreated cells were used as negative control. After treatment, cells were labelled with EdU for 30 minutes prior to harvest, fixed and subjected to EdU/DAPI staining for flow cytometry.

There was no difference in cell cycle profile when cells overexpressing DBF4 full-length were treated with doxycycline (Figure 5.5A). Similar results were observed in N, N+MC, Tail and DMC cell lines (Appendix C, Figure S5.1). However, a decrease of cells at S- and G2/M-phases were observed in the DN cell line (Figure 5.5B).

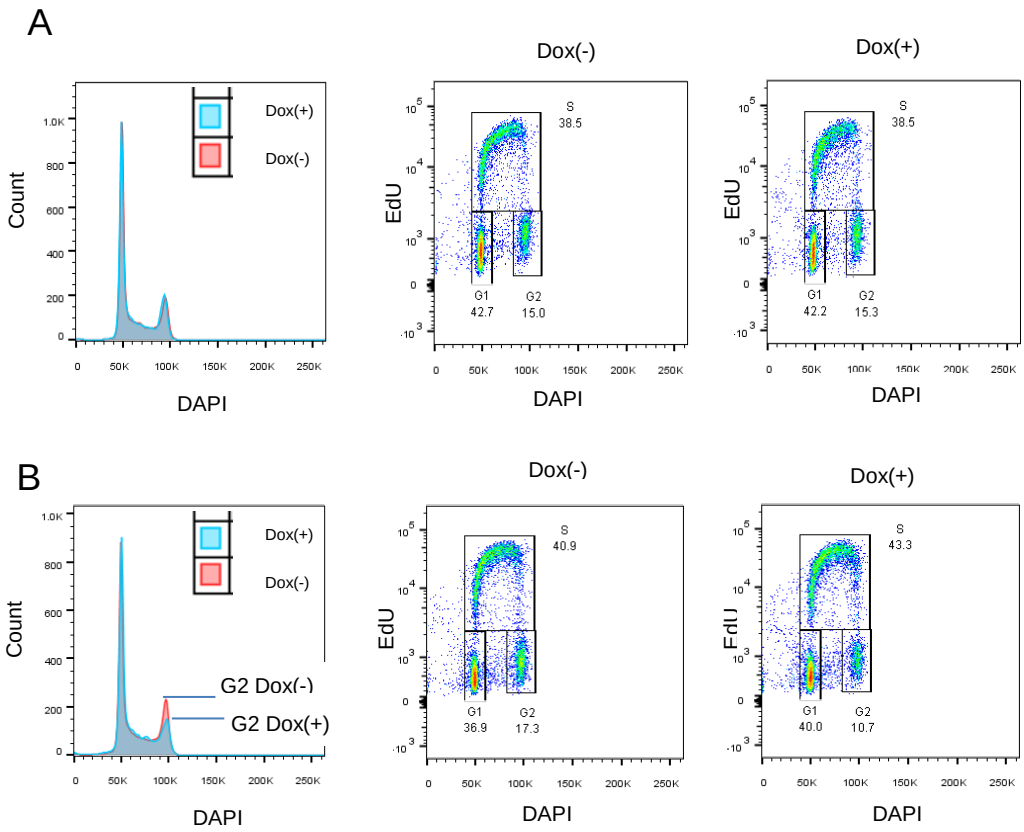


**Figure 5.5 Effects of overexpressing DBF4 and its domains on cell cycle progression.** Cells were plated for 24 hours, treated with doxycycline for 24 hours, labelled with EdU for 30 minutes prior to harvest, fixed and subjected to EdU/DAPI staining for flow cytometry. Experiments were performed once.

Overlay histogram of DNA content and data analysis of EdU/DAPI fluorescence signals of (A) DBF4-overexpressed cells; (B) DN domain-overexpressed cells.

### 5.3.2. Induction of full-length DBF4 and its domains does not affect cell proliferation

Twenty-four hours post-treatment of doxycycline DBF4-OE 293 cells expressed DBF4 domains with expected size and without any effect on cell cycle progression. To confirm that the overexpression of DBF4 FL and other fragments does not affect cell proliferation of 293 cells, FL, N, N+MC, DN, Tail and DMC monoclonal cells were plated in 96-well plates in triplicate, then incubated with doxycycline for 24, 48 and 72 hours. At each time point, cells were incubated with Alamar Blue for 6 hours and fluorescence signals were measured by CytoFluor. There was not any remarkable difference in growth curve of each clone in the presence of doxycycline (Appendix C, Figure S5.2).

### 5.3.3. Effects of the overexpression of DBF4 full-length and its domains on CDC7

In *Saccharomyces cerevisiae*, DBF4 protein levels fluctuate during cell cycle, with a low level at G1 and high level at S until end of M-phase. Meanwhile, CDC7 is abundant but Cdc7 kinase activity also fluctuates along with the level of DBF4, suggesting that DBF4 plays a role in regulating Cdc7 kinase activity [178,233]. To understand the effects of overexpressing each region of DBF4 on the kinase activity and modification of CDC7 in human cells, we examined the phosphorylation of MCM2 and CDC7 in doxycycline-treated cells.

DBF4 FL, N, N+MC, DN, Tail and DMC monoclonal cells were plated and treated with doxycycline for 24 hours, then pelleted and stored at -80$^{o}$C until being subjected to protein extraction. Soluble fraction was used for immunoblotting.

In the negative control EV cells, doxycycline treatment did not affect MCM2 phosphorylation (Figure 5.6, MCM2 and pMCM2, lane 1 and 2), CDC7 phosphorylation (Figure 5.6, CDC7 and pCDC7, lane 1 and 2) or the CDC7 kinase activity assessed by the level of phosphorylated MCM2 S40/41 (Figure 5.6, pMCM2 S40/41, lane 1 and 2). Cells overexpressing domains containing N motif like DBF4 FL or N+MC had a similar level of pMCM2 S40/41 in comparison with cells overexpressing domains lacking N motif like DN. This indicates that N motif does not play any role in CDC7 kinase activity (Figure 5.6, pMCM2 S40/41, lane 4, 8 and 12).

Noticeably, the level of phosphorylated MCM2 and phosphorylated CDC7 in those cell lines increase, suggesting a role of DBF4 FL, N+MC and DN domains in regulating MCM2 and CDC7 phosphorylation (Figure 5.6, pMCM2 lane 4, 8 and 12). Those fragments have a common DBF4 fragment MC region suggesting motif M and C plays a role in the phosphorylation of MCM2 and CDC7. This was confirmed in cells overexpressing domain lacking MC region DMC. Those cells had a very faint band of pMCM2 S40/41, no phospho-MCM2, and no phospho-CDC7 band in comparison with untreated cells (Figure 5.6, lane 14 vs 13).

Therefore, we concluded that the MC region of DBF4 plays a critical role in the phosphorylation of MCM2 as well as in regulating CDC7 kinase activity in our T-REx cell lines. This data is consistent with published works [127,234].

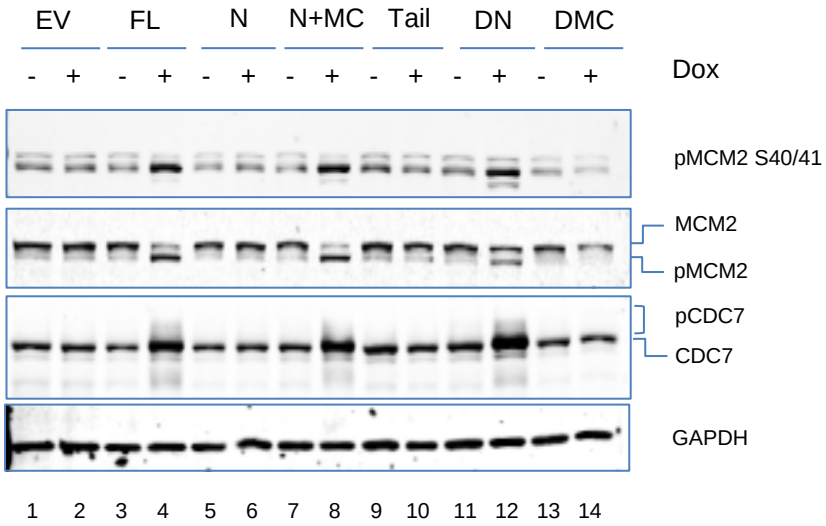


**Figure 5.6 Effects of overexpressing DBF4 and its domains on the phosphorylation of MCM2 and CDC7.**

DBF4 FL, N, N+MC, Tail, DN and DMC cell lines were plated and treated with doxycycline for 24 hours. After treatment, cell pellets were harvested and subjected to protein extraction by CSK lysis buffer. Soluble fraction was used for immunoblotting. Data were collected by LiCOR and analysed with Image Studio software. Experiments were performed once.

### 5.3.4. Effects of CDC7 kinase inhibitors on DBF4 phosphorylation and stability

The absence of M-C motif from DBF4 causes the reduction of CDC7 kinase activity. This data agrees with a study of Hughes *et al.* [127] which proved that M-C motif of DBF4, especially motif C is essential to activate CDC7 kinase activity. This study also found that XL413 and PHA-767491 bind to the nucleotide-binding pocket of CDC7, causing the inhibition of CDC7 kinase. This raises the question of whether the binding of XL413 or PHA-767491 to CDC7 may also modify its phosphorylated form, affecting the interaction between CDC7 and DBF4.

To address this question, strep-tag fused DBF4 was purified from DBF4-overexpressed TREx-293 cell line by affinity purification using strep-tactin resin (IBA), then binding of CDC7 to purified DBF4 was examined in the presence of

XL413. Strep-tag is an 8-amino-acid peptide Trp-Ser-His-Pro-Gln-Phe-Glu-Lys (WSHPQFEK) which can be fused at C-terminus of recombinant proteins and can bind to the biotin binding pocket of streptavidin [235]. In this experiment, we employed strep-tactin, an engineered streptavidin which has a binding affinity higher than streptavidin to strep-tag and is highly recommended for protein purification [235–237].

EV and FL monoclonal cells were plated for 24 hours, incubated with doxycycline for 24 hours, then treated with XL413, PHA-767491, or DMSO for another 24 hours. Treated cells were harvested and subjected to protein batch purification by affinity pull-down (AP) assay with strep-tactin sepharose resin.

It was confirmed that by using AP, CDC7 was co-purified with its main interactor DBF4 in untreated FL cells (Figure 5.7A, lane 10). An electrophoretic mobility shift of Strep-tagged protein was observed in XL413-treated FL cells, suggesting that inhibition of CDC7 kinase by XL413 altered the phosphorylation of overexpressed full-length DBF4 (Figure 5.7A, lane 3 and 11). This data agrees with a study of Wu *et al.* [238] and suggests that DBF4 is phosphorylated by CDC7 in human cells.

Interestingly, CDC7 was still co-purified with dephosphorylated DBF4 in XL413-treated FL cells but not in EV cells. This suggests that an interaction between DBF4 and CDC7 may occur in a DBF4 phosphorylation-independent manner (Figure 5.7A, lane 3 and 11). No strep-tagged DBF4 was detected in PHA-767491-treated FL cells from either in the input fraction or from boiled beads (Figure 5.7A, lane 4 and 12). This may be explained by the effects of PHA-767491 on the transcription of DBF4 as mentioned in the study of Rainey *et al.* [239].

Noticeably, signal intensities estimated using densitometry revealed a decrease of strep-tagged DBF4 intensity in XL413-treated FL cells in comparison with EV cells (Figure 5.7B, XL vs DMSO FL), even though Ponceau S staining indicates that gel loading was equal. One possible explanation for this finding is that XL413 affects the stability of DBF4 by increasing the degradation through the proteasome pathway, leading to the decrease of synthesised DBF4 protein.

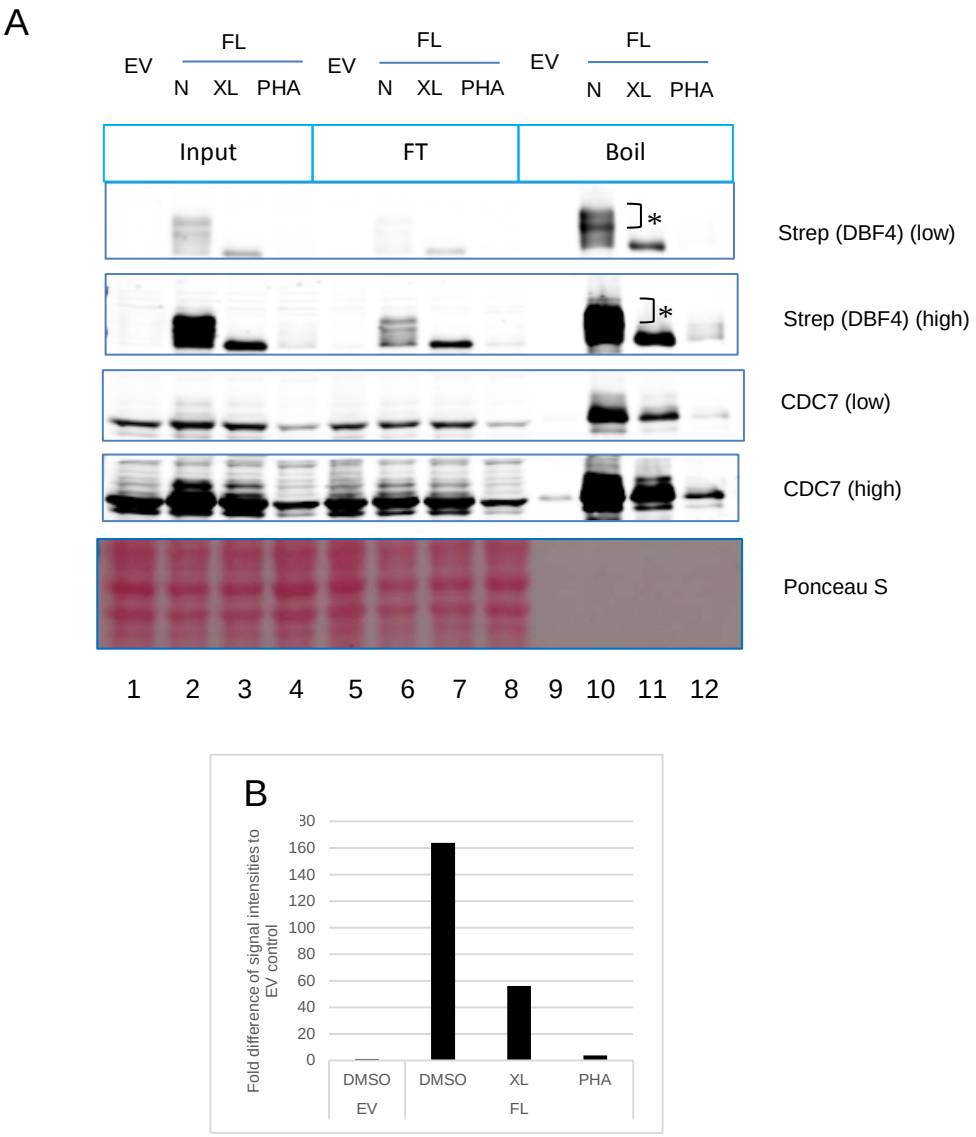


**Figure 5.7 Effects of XL413 and PHA-767491 on overexpressed DBF4.**

Cells were plated, treated with drugs for 24 hours, harvested and subjected to AP and immunoblotting. EV: empty vector; FL: DBF4 full-length; N: vehicle control DMSO; XL:XL413; PHA: PHA-767491 . (A) Immunoblotting of AP; (B) Data analysis of signal intensities measured by LiCOR/Image Studio. (*) Phosphorylated strep-tagged DBF4. Experiments were performed once

To investigate the effects of XL413 on DBF4 stability, we first tested whether XL413 affects the degradation rate of DBF4. Cells were first treated with cycloheximide to prevent protein synthesis and observed the change of protein levels in the presence of XL413. FL cells were plated and incubated with doxycycline for 24 hours. After induction, cells were treated with cycloheximide and XL413 or DMSO for 1 to 3

hours. Treated cells were harvested at every hour, pelleted and subjected to protein extraction by CSK lysis buffer. The soluble fraction was used for immunoblotting.

One hour post-treatment with cycloheximide, the total protein level of strep-tagged DBF4 decreased either in XL413-treated or untreated cells (Figure 5.8B) suggesting that the degradation of synthesised full-length DBF4 occurs after 1 hour of blocking the protein synthesis. However, in CHX-treated cells, the main DBF4 bands disappeared before the phosphorylated band at 2 hours of treatment (Figure 5.8A, Strep (DBF4), lane 2, 3 and 4). Meanwhile, in the presence of XL413, the degradation of phosphorylated DBF4 occurred first and the main band endured for longer (Figure 5.8A, Strep (DBF4), lane 6, 7 and 8). This data suggests that the degradation of DBF4 induced by doxycycline treatment depends on XL413 treatment or to some extent on CDC7 kinase activity.

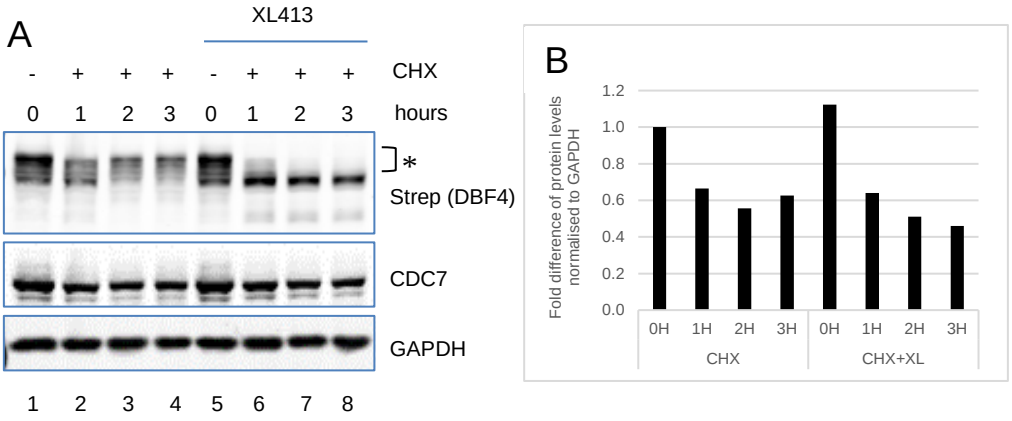


**Figure 5.8 Degradation of overexpressed DBF4 in the presence of XL413 and CHX.** Cells were treated with CHX and XL413 or DMSO for 1, 2 or 3 hours. At each time point, cells were harvested and subjected to protein extraction by CSK lysis buffer. Soluble fraction was used for immunoblotting. Signals were quantified by Image Studio. (A) Immunoblotting image (B) Data analysis of protein levels normalised to GAPDH. (*) Phosphorylated strep-tagged DBF4. Experiment was performed once.

To confirm if this degradation was triggered in a proteasome pathway, cells were treated with a protease inhibitor MG132 for 1, 2 or 3 hours together with XL413 or DMSO and subjected to protein extraction by CSK lysis buffer. Soluble fraction was used for immunoblotting.

It was observed that MG132-treated cells had a decrease of the main band of strep-tagged DBF4 after 3 hours of treatment (Figure 5.9A, Strep (DBF4), lane 4). In the presence of XL413, the phosphorylated band disappeared but the main band remains over time (Figure 5.9A, Strep (DBF4), lane 6, 7 and 8). By measuring the protein levels, we found that a decrease of strep-tagged protein level occurred after 1 hour of MG132 treatment and this decrease was greater in the presence of XL413 (Figure 5.9B), suggesting that the degradation of strep-tagged DBF4 may not be triggered by proteasome pathway and XL413 accelerated the degradation of doxycycline-induced DBF4 in human cells.

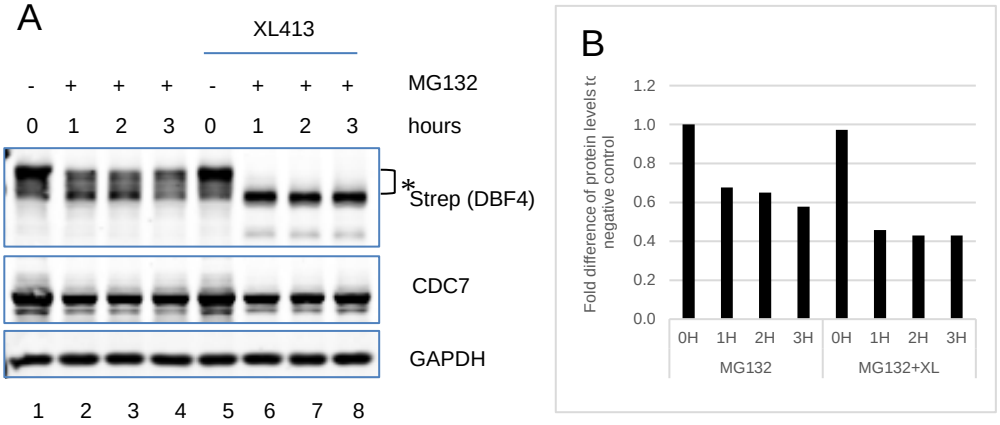


**Figure 5.9 Degradation of overexpressed DBF4 in the presence of XL413 and MG132**
Cells were treated with MG132 and XL413 or DMSO for 1, 2 or 3 hours. At each time point, cells were harvested and subjected to protein extraction by CSK lysis buffer. Soluble fraction was used for immunoblotting. Signals were quantified by Image Studio. (A) Immunoblotting image (B) Data analysis of protein levels normalised to GAPDH. (*) Phosphorylated strep-tagged DBF4. Experiment was performed once.

## 5.4 Detection of human DBF4 interactors using stable expression TREx-293 cell lines

Our DBF4-overexpressing stable cell lines were confirmed as a suitable tool to stably induce strep/FLAG-tagged DBF4 without affecting the growth rate or the cell cycle progression of TREx-293 cells. Similar to strep-tag, FLAG-tag is a small peptide of 8 amino acids AspTyrLysAspAspAspAspLys (DYKDDDDK) which can be fused to C-terminus of recombinant protein such as DBF4 and is detectable by anti-FLAG antibody [240].

Toward the goal of detecting novel DBF4 interactors, FLAG-tagged DBF4 was first purified by FLAG immunoprecipitation, then DBF4 interactors were detected by Mass spectrometry (Gemma O'Brien). The interaction between strep-tagged DBF4 and identified interactors was confirmed using affinity purification with strep-tactin resin. EV, FL and DMC cell lines were treated with doxycycline for 24 hours, harvested, and subjected to AP using strep-tactin sepharose resin and immunoblotting.

Strep-tagged proteins were detected in FL and DMC cells at the expected size of DBF4 FL and DMC (Figure 5.10, Strep (DBF4), lane 8 and 9). CDC7 was co-purified with strep-tagged DBF4 FL but not with DMC. This confirms the role of MC domains in promoting the interaction between DBF4 and CDC7. NAP1L1 and APE1 were detected in FL but not in EV cells suggesting that they are DBF4 interactors (Figure 5.10, NAP1L1 and APE1, lane 7 and 8). These proteins were also found in DMC cells, meaning that they interact with DBF4 in a CDC7-independent manner (Figure 5.10, NAP1L1 and APE1, lane 9).

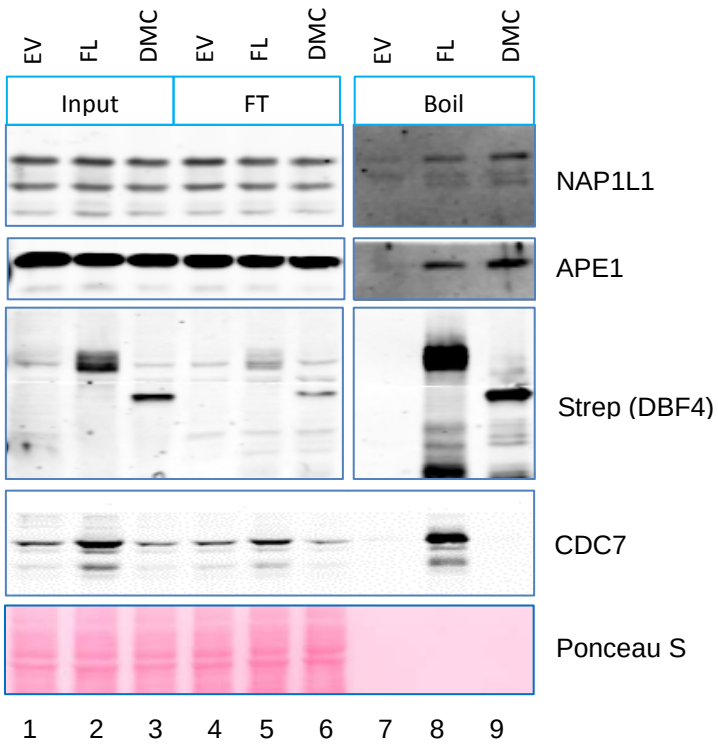


**Figure 5.10 Potential DBF4 interactors confirmed by Strep-tag AP assay.**
Cells were treated with doxycycline for 24 hours, harvested and subjected to affinity pull-down (AP) assay and immunoblotting. Blots were scanned using a LiCOR imager and analysed with Image Studio software. Experiments were performed once.

## 5.5 Conclusion

DBF4 is a regulatory subunit of CDC7 which has a role in regulating DNA replication and cell cycle progression through CDC7 kinase activity. By using Flp-In T-REx 293 system, we were successful in generating human cell lines that stably express DBF4 full-length, N, N+MC, Tail, DN and DMC and in that DBF4 full-length and its fragments can be conditionally overexpressed by doxycycline treatment.

DBF4 overexpression does not affect the rate of cell proliferation or the cell cycle of TREx-293 cells. CDC7 kinase inhibition by XL413 affects the phosphorylation and stability of DBF4 in an unknown pathway. Two DBF4 interactors NAP1L1 and APE1 were found using strep-tagged DBF4. Further experiments are required to characterise the role of these interactions in human cells.

# Chapter 6: Discussion

## 6.1. XL413 and PHA-767491 have distinct effects on two breast-derived human cell lines

Depletion of CDC7 abolishes DNA replication and induces p53-independent apoptosis in many cancer cell lines but not in normal fibroblast cells. However, it is unclear whether those effects are due to the lack of CDC7 kinase activity or its scaffolding role or both. Therefore, in this first result chapter, we aimed to characterise the biological effects of two ATP-competitive inhibitors of CDC7 on human cells, XL413 and PHA-767491.

In both MCF10A and MDA-MB-231 cell lines, pMCM2 S40/41, a biomarker of CDC7 kinase activity [86], is efficiently inhibited at 10 µM of each compound. Interestingly, the phosphorylation of MCM4, a target of CDC7 and other CDKs, still occurs in XL413-treated cells, but not in PHA-767491-treated cells (Chapter 3, Figure 3.1A and C, MCM4, lane 2-11). These effects were concomitant with the occurrence of DNA synthesis. Cells still incorporate EdU in the presence of XL413, but not of PHA-767491 (Chapter 3, Figure 3.2, XL413 2.5-50 and PHA-767491).

Noticeably, in a study of Alver *et al.*, authors found that the decrease of phosphorylated MCM4 was found in PHA-767491-treated cells, and DNA replication was concomitantly blocked in these cells. Hence, MCM4 phosphorylation was proposed to be a better marker that is correlated with DNA replication than MCM2 phosphorylation at S40 or S53 [139]. However, it should be noticed that the phosphorylation of MCM4 is mediated not only by CDC7 but also by other CDKs, such as CDK1 and CDK2 [129,241,242]. Those kinases are potential targets of PHA-767491 [127]. In addition, our findings show that PHA-767491 does reduce the protein level of CDC7 at indicated doses and in a p53-independent manner (Chapter 3, Figure 3.1A-D, CDC7, lane 7-11). This phenomenon is likely due to the down-regulation of CDC7 transcriptional level [239]. Those effects were not observed in XL413-treated cells, suggesting PHA-767491 may targets multiple kinases that are critical in regulating CDC7 stability and the co-inhibition of multiple kinases may

enhance the cytotoxicity and the effects on DNA synthesis of PHA-767491-treated cells.

In assessing the cellular responses of MCF10A and MDA-MB-231 to XL413, our data showed that XL413 has distinct effects on cell proliferation and viability. During a long-term treatment of 48 and 72 hours, XL413 prevents cell proliferation and induces apoptosis in MDA-MB-231 but not in MCF10A cells (Chapter 3, Figure 3.5 and Appendix A, Figure S3.1). An elevated level of γH2AX in XL413-treated MDA-MB-231 cells suggests that a spontaneous DNA damage may occur in this cell line (Chapter 3, Figure 3.13, γH2AX, lane 8). In addition, in a proposal model of Tudzarova *et al.*[177], authors indicated that CDC7 and p53 cooperate in maintaining cell viability through three origin activation checkpoint axes. Because cancer cells normally harbour defective p53 then they are sensitive to CDC7 inhibitors. Therefore, a possibility is that MDA-MB-231 cells were killed by XL413 due to the lack of wild-type p53.

A delay of S-phase progression occurring in MCF10A and MDA-MB-231 cells when they were treated with XL413 but no replication fork stalling or decrease of origin firing were observed (Chapter 3, Figure 3.10). This suggests that the attenuation of CDC7 kinase activity by XL413 may not affect the replication fork progression of human cells or cells are able to recover all stalled forks. We hypothesised that XL413 may not fully inhibit CDC7 kinase activity of MCF10A cells, even the biomarker pMCM2 S40/41 was undetectable. This could explain by the high affinity of CDC7 for ATP with a low $K_m$ value [189] and the abundant amount of ATP in cellular environment [243] leading to the difficulty of maintaining a continuous inhibition of CDC7 kinase activity in humans. The residual activity of CDC7 kinase may phosphorylate unfired replicative origins, such as dormant origins, to recover the replication fork progression [73,244,245]. Because the number of fired dormant origins in XL413-treated cells was equal to the number of fired replicative origins in mock-treated cells, hence in this study, we did not observe any change of replication fork patterns. Further experiments using an alternative method such as DNA combing may resolve this discrepancy.

However, we also do not exclude a hypothesis which is MCF10A cells may have alternative ways to overcome the effects of CDC7 inhibition on DNA replication and viability. Previous studies showed that the requirement of CDC7 could be bypassed by the existence of P83L mutation in Bob1/MCM5 human homolog, by the deletion of MCM4 N-terminal serine/threonine-rich domain, or by the phosphomimetic MCM4 or MCM6 at CDC7 target sites in *S.cerevisiae* [128,166,246]. The bypass of Hsk1/CDC7 human homolog was also found in *S.pombe* [247].

Finally, XL413 does not prevent cells from entering or exiting mitosis, but decreases the percentage of mitotic cells (Figure 3.11). This indicates that CDC7 kinase activity may have an unknown role in regulating G2/M transition, in addition to the role of preventing mitotic exit through interaction with Cdc5/PLK1 [154].

By this study, we also emphasise the role of CDC7 inhibition in breast cancer treatment, i.e. TNBC. The selective effects of XL413 on MCF10A cells used as "normal" model and MDA-MB-231 cells used as "cancer" model of human breast cells indicates that CDC7 inhibition may allow patients to avoid severe off-target effects that are commonly found with chemotherapy, or to some extent, CDC7 is a potential candidate of target therapy.

## 6.2. Co-inhibition of CDC7 with CDK1, CDK2 or CDK9 affects cell cycle progression of both cell lines but does not block DNA replication

In contrast to XL413, another CDC7 inhibitor PHA-767491 blocks DNA replication, prevents cell proliferation and mitotic entry and exit. This compound not only targets CDC7, but also other kinases including CDK9 (confirmed target), CDK1 and CDK2 (potential targets). To confirm that the different effects of two CDC7 inhibitors resulted from the effects of co-inhibition of CDC7 with other kinases, we observed the effects of depletion of CDK1, CDK2, CDK9 with or without XL413 on human cells.

In this study, we found that CDK1, but not CDK2, plays a critical role in promoting DNA synthesis of MCF10A cells. In unperturbed condition, CDK2-CycA is the principal regulator of this S-phase progression [16]. However, in mammalian cells, the proliferation still occurs in the absence of CDK2 due to compensation by CDK1, but not *vice versa* [248]. This observation was confirmed by our data in which the

decrease in CDK2 levels does not greatly affect the cell cycle progression or DNA replication, but the knock-down of CDK1 does (Chapter 4, Figure 4.1B).

The co-inhibition of CDK1 and CDC7 induces an accumulation of cells at late S- and G2/M-phase even there was no change in S-phase population (Chapter 4, Figure 4.1B). This indicates that CDK1 plays a main role in regulating S-phase progression and CDC7 kinase activity is required to fire origin in early S-phase. Noticeably, by co-inhibition of CDK1 and CDC7, we found that lacking CDC7 kinase activity increases the G2/M population, suggesting CDC7 has a role in regulating G2/M in human cells (Chapter 4, Figure 4.1B). However, it is unclear if that population is G2- or M- or both, then we cannot conclude if CDC7 promotes the mitotic entry or exit or both.

By immunoblotting, we confirmed that down-regulation of CDK9 does not affect the protein level of CDC7, suggesting CDK9 inhibition by PHA-767491 does not contribute to the decrease of protein level of CDC7 (Chapter 4, Figure 4.1A, CDK9, lane 5 and 11). We also noticed a role of CDK9 in regulating G1/S-phase transition. The depletion of this kinase triggers an accumulation of cells at G1-phase and a decrease of S-phase population (Chapter 4, Figure 4.1B). Interestingly, the co-inhibition of CDC7 with CDK9 results an accumulation of late S- and G2/M-phase, suggesting CDC7 kinase inhibition by XL413 attenuates the inhibitory effects CDK9 ablation on MCF10A cell line (Chapter 4, Figure 4.1B). To some extent, it indicates that CDC7 and CDK9 may cooperate in regulating S-phase progression.

To confirm if the same phenomenon occurs in other cell lines, we investigated the effects of CDK1, CDK2 and CDK9 depletion on cell cycle progression of MDA-MB-231. The down-regulation of each kinase does not affect the percentage of S-phase population suggesting the low levels of these CDKs are sufficient for cells maintaining DNA replication (Chapter 4, Figure 4.2B). In the presence of XL413, CDK-depleted cells accumulated at late S-phase, indicating CDC7 kinase activity may play a more critical role in regulating DNA replication.

A hypothesis is that CDK1 and CDK2 may compensate their role, therefore lacking one of them does not affect the DNA replication progression of this cancer cell line. By co-depleting both CDK1 and CDK2, we found that cells still incorporate EdU

(Chapter 4, Figure 4.3B). The inhibition of CDC7 kinase activity in cells lacking CDK1 and CDK2 additionally induces an increase of S-phase population, suggesting CDC7 promotes the DNA replication in a CDKs-independent manner (Chapter 4, Figure 4.3B). Further studies may confirm this phenomenon.

### 6.3. Critical factors to improve the robustness of Alamar Blue assay

In order to find out a newly potential kinase that cooperates with CDC7 in promoting DNA replication, we performed high-throughput screenings (HTS) with a compound library, PKIS, generated by GSK. PKIS is a library of more than 300 compounds that target to 90% of human kinome and was characterised *in vitro* with recombinant proteins and *in vivo* with NCI-60 human tumour cell line panel [220]. In addition, this library also has a kinase activity map constructed by Nanosyn and DSF screenings in which the percentage of inhibition of kinase at two different doses of compounds was determined. This is helpful for deciding the initial concentration of inhibitor treatment in primary screenings. Another important reason is that because the usage of compounds is likely simpler and less costly than using siGENOME library in achieve our purpose of inhibiting kinases in combination with CDC7 inhibition.

To obtain a screening with reliable results, we first tested the robustness of screening methods using Z-prime factor. This statistical tool assesses the robustness of assay through the variability of values between positive and negative control. A robust assay would have Z-factor value within the range of 0.5-1 and several factors were considered including cell density, number of repeats, time of inhibitor treatment and time of Alamar Blue incubation.

The cell density was optimised so that at the time point of incubation with Alamar Blue, cell density was not too high leading to the growth arrest due to contact inhibition, but also not too low leading to the decrease of signal sensitivity, hence an inadequate cell density could lead to bias data.

In addition, the time of inhibitor treatment was also considered as a factor of a robust screening. If it is too short, the compound may not inhibit kinases efficiently. If it is too long, cells may be killed all by PKIS compounds without CDC7 inhibition, then we would not be able to detect “hit” compounds. Therefore, we decided to test 24,

48 and 72 hours of inhibitor treatment with an expectation that after a specific time of periods, the difference of emission intensity of fluorescence signals between positive and negative control is remarkable.

Alamar Blue incubation time was also considered as a factor for optimisation. This compound was known as a non-toxic, strongly fluorescent when metabolised and stable. Incubation time of Alamar Blue was chosen between 4-6-8 hours due to the fact that less than 4 hours, cells might not be able to fully convert Alamar Blue to their products and the decrease of signals might be due to this fact rather than due to inhibitory effects of compound. Alamar Blue can be incubated for longer than 8 hours, but bacterial contamination may occur leading to a biased increase of signals.

After optimisation, we concluded that at cell density of $4x10^3$ cells/well for MCF10A and $8x10^3$ cells/well for MDA-MB-231 cell line, 48 hours of inhibitor treatment, and 6 hours of Alamar Blue incubation, the assay has the highest value of Z-factor, or to some extent, the assay is robust for a high-throughput screening with PKIS library and those two human breast cell lines (Chapter 4, Figure 4.14 and 4.15).

In the assay using HAP1 cell lines, an important requirement is the usage of cells with a low passage to avoid the transition from haploid to diploid cells. Using the same optimisation criteria, we found that $2.0x10^3$ cells/well for cell density of plating, 72 hours of inhibitor treatment and 6 hours of Alamar Blue incubation are the conditions by which the assay has the highest value of Z-factor (Appendix B, Figure S4.7 and S4.8).

Finally, data analysis is another important factor to be considered. We decided to use two methods for data analysis including assessment through Z-factor and through percentage of control. Z-factor is a statistical tool that was developed to assess the data of different batches of samples. In this screening, we have 7 plates of drugs and each plate needs to be duplicated to avoid bias data due to technical errors.

## 6.4. Identified kinase inhibitors that are potentiated by CDC7 inhibition in human cells and their targets

In the first PKIS screening, we chose MCF10A and MDA-MB-231, the human breast cells being characterised through our first studies (Chapter 3). In this screening,

MCF10A is considered as a control cell line and the differences of cell response to inhibitor treatment between two cell lines could be a hint for detecting potential kinase inhibitors that specifically kill breast cancer cells like MDA-MB-231 but do not kill non-malignant cells like MCF10A. Our screening data analysis showed that there were several compounds that inhibits cell proliferation more efficiently in the presence of XL413, including GW680191X and GW801372X (Chapter 4, Figure 4.16 and 4.17). However, this screening has a limitation which is the combination of two drugs in the screening could make some bias data, not only because of the technical errors but because of off-target effects induced by drug-drug interaction [221].

To confirm the results, instead of repeating experiments as in the primary screening, we performed another HTS with two other cell lines, HAP1 wild-type (WT) and HAP1 DBF4 knock-out (4KO). Before screening, we characterised the phenotype of those two cell lines. We found that the lack of CDC7 regulatory subunit DBF4 leads to the reduction of CDC7 kinase activity confirmed by the reduction of pMCM2 S40/41 and total phosphorylated MCM2 (Chapter 4, Figure 4.19B). We did not observe any decrease of phosphorylated MCM4 in DBF4 KO cell line (Chapter 4, Figure 4.19B), suggesting the lack of DBF4 does not affect the phosphorylation of this helicase subunit. In this secondary screening, hit compounds that can kill more cells while DBF4 is absent are GW801372X and GW305178X. GW801372X is the common inhibitor found by two screenings, suggesting it is a highly potential inhibitor candidate.

Below are relevant targeted kinases of hit compounds selected from our PKIS screenings, either using XL413 treatment with breast-derived human cells or using DBF4 knock-out HAP1 cell line.

**Human epidermal growth factor receptor 1 or 4 (HER1 or HER4)**

GW680191X mainly targets two members of epidermal growth factor receptor family including ErbB1/HER1 human homolog and ErbB4/HER4 human homolog (ChemBL). Inhibition of HER1 causes G1-phase arrest in Epidermal growth factor (EGF)-sensitive cell line as MCF10A [249].

**Serine/Threonine-protein kinase 10 (STK10)**

GW680191X also targets to lymphocyte-oriented kinase Lok/STK10 human homolog (ChemBL) that can phosphorylate PLK1 *in vitro* [250].

**Dual specificity tyrosine-phosphorylation-regulated kinase 1B (DYRK1B)**

DYRK1B is one of targets of GW801372X (ChemBL) and belongs to CMGC branch. Inhibition of this kinase triggers the overexpression of cyclin D1 and cells either shorten G1 and accelerate cell proliferation or co-stabilise cyclin D1 with CDK-inhibitor p21 and become quiescent [251].

**NUAK family SNF1-like kinase 1 (NUAK1 or ARK5)**

ARK5 is one of targets of GW801372X (ChemBL) and belongs to CAMK group. This kinase phosphorylates p53 *in vitro* and *in vivo* in the presence of liver kinase B 1 (LKB1) and regulates cell cycle by arresting cells at G0/G1-phase when it is overexpressed [252]. Inhibition of this serine threonine kinase restrains cancer growth and triggers pro-apoptotic responses leading to cell death in a Myc-dependent manner [253].

**Glycogen synthase kinase-3 beta (GSK3β)**

GSK3β is one of targets of GW801372X (ChemBL) and belongs to CMGC group. Inhibition of this kinase promotes apoptosis but also induces pro-survival autophagy signals in human pancreatic cancer cells [254,255].

**Aurora kinase C (AURKC)**

AURKC is one of targets of GW801372X (ChemBL) and belongs to S-T-PK group. Overexpression of AURKC can rescue multinucleation phenotype of Aurora kinase-depleted cells suggested a complement role between two kinases [256]. Inhibition of Aurora kinases by a small molecule inhibitor causes cell death in multiple cell lines, including MDA-MB-231 [257].

**Maternal embryonic leucine zipper kinase (MELK)**

MELK targeted by GW305178X belongs to CAMK branch. MELK is overexpressed in many breast cancer cell lines [258]. Depletion of this kinase can suppress cell growth and triggers apoptotic cascade through phosphorylating Bcl-$G_L$ [259].

**Mammalian Sterile20-like kinase 1 and 2 (MST1/2 or STK4/3)**

MST1/2 targeted by GW305178X belongs to STE group. MST1/2 is involved in Hippo pathways. Double knock-out of MST1/2 causes an early embryonic lethality while the single mutant *Mst1*$^{-/-}$ or *Mst2*$^{-/-}$ does affect its viability and fertility of mice, suggesting these kinases play critical roles in cell proliferation [260].

## 6.5. In the absence of CDC7 regulatory subunit DBF4, cells are less sensitive to PLK1 inhibitors

In PKIS screening, we noticed that cells treated by some compounds have a lower percent-of-control when DBF4 is wild-type. This means that treated cells survive better when DBF4 is absent. One of main target of those compounds is polo-like kinase 1 (PLK1) suggesting an unknown role of CDC7-DBF4 in maintaining cell viability and proliferation when PLK1 is inhibited.

PLK1 is one of critical kinases involved in mitosis through regulating mitotic entry and exit, centriole cycle or spindle assembly, as well as in DNA damage through inactivation of G2/M-phase checkpoint and DNA repair through phosphorylation of RAD51, a DNA repair protein [261]. The role of Cdc5/PLK1 in DNA replication was also reported through the interactions with pre-RC proteins including DBF4, MCMs, HBO1 in unperturbed condition and through phosphorylation of ORC2 to maintain the pre-RC complex under DNA replication stress condition [225,262]

To confirm this unexpected result, we conducted another study in which the effects of PLK1 inhibition in HAP1 DBF4 knock-out cells were investigated using an well-known PLK1 inhibitor BI6727 [263,264]. We found that DBF4-knock out cells delays the apoptotic progression (Chapter 4, Figure 4.24) in the comparison with DBF4-wild type cells, either by delaying PARP cleavage or Caspase 3 activation or both (Chapter 4, Figure 4.25). This indicates that the inhibitory effects of PLK1 is attenuated by the absence of DBF4 suggesting an unknown role of DBF4 or CDC7 kinase activity in regulating apoptosis.

A previous study showed that when leukaemia cells are treated with CDC7 inhibitor PHA-767491, cells are resistant because the upregulation of anti-apoptotic protein such as Bcl-2. Therefore, further studies on the activation of apoptotic markers, including pro-apoptotic and anti-apoptotic, as well as apoptotic regulators may

explain this phenomenon. In addition, the usage of a kinase-dead CDC7 or CDC7 inhibitor XL413 on cells treated with PLK1 inhibitor might be useful to confirm if those effects are induced by the absence of DBF4 protein or due to the reduction of CDC7 kinase activity.

### 6.6. The degradation of DBF4 occurs in a XL413-dependent manner, but not in a proteasomal pathway

In yeast, the N domain of DBF4 plays a role in the interaction between DBF4 with Rad53/CHK2, ORC and PLK1. Meanwhile, the MC domain is critical for binding and activating CDC7 [265]. To discover new roles of DBF4 in humans, we aimed to identify DBF4 interactors using TREx-293 system, a genetically modified human cell line that allows to integrate and conditionally express different domains of DBF4 using Tet inducer system.

DBF4 domains are expressed with expected sizes in the presence of Doxycycline, a derivate chemical inducer of tetracycline, without affecting cell viability, cell growth rate as well as cell cycle progression (Chapter 5, Figure 5.5 and Appendix C, Figure S5.1 and S5.2). In addition, the overexpression of fragments harbouring MC domain induces the phosphorylation of MCM2, i.e phospho-MCM2 at S40/41, and of CDC7 (Chapter 5, Figure 5.6, lane 4, 8 and 12). This confirms that the overexpressed MC domain is biologically functional. Finally, by using affinity pull-down (AP) assay, we found that without MC domain, the binding of CDC7 to DBF4 was abolished, confirming the role of this domain in tethering DBF4 to CDC7 (Chapter 5, Figure 5.10, CDC7, lane 9).

In this project, we found that XL413 decreases the mobility shift of DBF4 protein, suggesting DBF4 phosphorylation is attenuated by the CDC7 inhibitor (Chapter 5, Figure 5.7A, lane 11). This is consistent with the observation in a study of Wu *et al.* [238]. However, we also noticed a decrease of strep-tagged DBF4 intensity in XL413-treated FL cells in comparison with EV cells (Chapter 5, Figure 5.7B). This indicates that XL413 may also affect the degradation rate of this protein.

To test this hypothesis, cells were treated with cycloheximide to prevent protein synthesis allowing the determination of degradation time. We found that 1 hour is a maximal time for maintaining stability and the degradation of over-expressed DBF4

occurs in a XL413-dependent manner, or to some extent, it depends on CDC7 kinase activity (Chapter 5, Figure 5.8).

Noticeably, the treatment with the protease inhibitor MG132 does not rescue the decrease of DBF4 protein level, suggesting the degradation of strep-tagged DBF4 may not be triggered by the proteasome pathway (Chapter 5, Figure 5.9). This was suggested in a study of Nougarede *et al.* [180] and still remains as an unanswered question.

## 6.7. NAP1L1 and APE1 were identified as novel DBF4 interactors in human cells

By using DBF4-overexpressed cell line, our laboratory identified more than 90 proteins that are potential DBF4 interactors (data from Gemma O'Brien). However, those interactors were only detected using FLAG-tag while our overexpressed domains contain both FLAG- and Strep-tags. In order to confirm the interaction between DBF4 and selected interactors, we used Strep-tag affinity pull-down assay as an alternative and independent method. This assay is based on the strong binding between Strep-tag fused in overexpressed proteins and Strep-tactin resin.

We found that only 2 out of 8 tested interactors were confirmed, suggesting there are some differences between two experiments (Chapter 5, Figure 5.10). Interestingly, one of those proteins is nucleosome assembly protein 1-like 1 (NAP1L1), a kinase that is mainly involved in chromatin modeling by dissociating histones H2A-H2B from folded nucleosomes and transporting histone variant containing H2A dimers to assembled nucleosomes [266]. Another protein is apurinic/apyrimidinic endonuclease 1 (APE1), a multifunctional protein that is involved in DNA repair through base excision repair pathway and transcriptional regulation through interactions with transcriptional factors [267]. Further functional studies are required to clarify those new roles.

## 6.8. Conclusion

In short, this project expands some knowledge about the effects of CDC7 inhibition in breast-derived human cells that is critical to understand the biological function of CDC7. In addition, it is the first time the screening of PKIS compounds was performed in the combination with CDC7 inhibitor or DBF4 knock-out cell line.

Potential kinases that cooperate CDC7 in promoting cell proliferation were revealed. A newly unknown role of DBF4 in sensitising cells to PLK1 inhibition was found but further studies are required to reveal the mechanism. Finally, by identifying NAP1L1 and APE1 as novel DBF4 interactors, new roles of DBF4 in human cells are potentially revealed in future.

# References

1. O'Farrell, P. Quiescence : early evolutionary origins and universality do not imply uniformity. *Phil. Trans. R. Soc. B* **2011**, 3498–3507.

2. O'Farrell, P. How metazoans reach their full size: the natural history of bigness. In *Cell Growth: Control of Cell Size*; Hall, M.; Raff, M.; Thomas, G., Eds.; CSHL Press, 2004; pp. 1–22.

3. Munoz-Espin, D.; Serrano, M. Cellular senescence: from physiology to pathology. *Nat. Rev. Mol. Cell Biol.* **2014**, *15*, 482–496.

4. Cooper, G. The Eukaryotic Cell Cycle. In *The Cell: A Molecular Approach. 2nd edition*; Sunderland (MA): Sinauer Associates, 2000.

5. Goranov, A. I.; Cook, M.; Ricicova, M.; Goranov, A. I.; Cook, M.; Ricicova, M.; Ben-ari, G.; Gonzalez, C.; Hansen, C.; Tyers, M.; Amon, A. The rate of cell growth is governed by cell cycle stage The rate of cell growth is governed by cell cycle stage. *Genes Dev.* **2009**, *23*, 1408–1422.

6. Foster, D. A.; Yellen, P.; Xu, L.; Saqcena, M. Regulation of G1 Cell Cycle Progression: Distinguishing the Restriction Point from a Nutrient-Sensing Cell Growth Checkpoint(s). *Genes Cancer* **2010**, *1*, 1124–31.

7. Hartwell, L. H. Saccharomyces cerevisiae cell cycle. *Bacteriol. Rev.* **1974**, *38*, 164–198.

8. Pardee, a B. A restriction point for control of normal animal cell proliferation. *Proc. Natl. Acad. Sci. U. S. A.* **1974**, *71*, 1286–90.

9. Spencer, S.; Cappell, S.; Tsai, F.; Overton, K.; Wang, C.; Meyer, T. The Proliferation-Quiescence Decision Is Controlled by a Bifurcation in CDK2 Activity at Mitotic Exit. *Cell* **2013**, *155*, 369–83.

10. Lodish, H.; Berk, A.; Zipursky, S.; et al. Cell-cycle control in mammalian cells. In *Molecular Cell Biology 4th edition*; New York: W.H. Freeman, 2000; p. section 13.6.

11. Alberts, B.; Johnson, A.; Lewis, J.; Morgan, D.; Raff, M.; Roberts, K.; Walter, P. The Cell cycle. In *Molecular Biology of the Cell. 6th edition*; Garland Science, 2015.

12. Mendenhall, M. D.; Hodge, a E. Regulation of Cdc28 cyclin-dependent protein kinase activity during the cell cycle of the yeast Saccharomyces cerevisiae. *Microbiol. Mol. Biol. Rev.* **1998**, *62*, 1191–1243.

13. Jackson, a L.; Pahl, P. M.; Harrison, K.; Rosamond, J.; Sclafani, R. a Cell cycle regulation of the yeast Cdc7 protein kinase by association with the Dbf4 protein. *Mol. Cell. Biol.* **1993**, *13*, 2899–2908.

14. Dirick, L.; Goetsch, L.; Ammerer, G.; Byers, B. Regulation of Meiotic S Phase

by Ime2 and a Clb5 , 6-Associated Kinase in Saccharomyces cerevisiae. *Science (80-. ).* **1998**, *281*, 1854–1858.

15. Vermeulen, K.; Van Bockstaele, D. R.; Berneman, Z. N. Z. N.; Vermeulen, K.; Van Bockstaele, D. R.; Berneman, Z. N. Z. N.; Vermeulen,K.,Van Bockstaele,D.R.,Berneman, Z. N.; Vermeulen, K.; Van Bockstaele, D. R.; Berneman, Z. N. Z. N. The cell cycle:a review of regulation,deregulation and therapeutic targets in cancer. *Cell Prolif.* **2003**, *36*, 131–149.

16. Suryadinata, R.; Sadowski, M.; Sarcevic, B. Control of cell cycle progression by phosphorylation of cyclin-dependent kinase (CDK) substrates. *Biosci. Rep.* **2010**, *30*, 243–55.

17. King, R.; Deshaies, R.; Peters, J.; Kirschner, M. How proteolysis drives the cell cycle. *Science (80-. ).* **1996**, *274*, 1652–1679.

18. Harbour, J. W.; Dean, D. C. The Rb/E2F pathway: Expanding roles and emerging paradigms. *Genes Dev.* **2000**, *14*, 2393–2409.

19. Giacinti, C.; Giordano, A. RB and cell cycle progression. *Oncogene* **2006**, *25*, 5220–5227.

20. Schulze, a; Zerfass, K.; Spitkovsky, D.; Middendorp, S.; Bergès, J.; Helin, K.; Jansen-Dürr, P.; Henglein, B. Cell cycle regulation of the cyclin A gene promoter is mediated by a variant E2F site. *Proc. Natl. Acad. Sci. U. S. A.* **1995**, *92*, 11264–11268.

21. Blagosklonny, M.; Pardee, A. The Restriction Point of the Cell Cycle. In *Madame Curie Bioscience Database (Internet)*; Landes Biociences, Austin (TX); pp. 2000–2013.

22. Bouldin, C. M.; Kimelman, D. Cdc25 and the importance of G2 control: Insights from developmental biology. *Cell Cycle* **2014**, *13*, 2165–2171.

23. Lindqvist, A.; Rodríguez-Bravo, V.; Medema, R. H. The decision to enter mitosis: feedback and redundancy in the mitotic entry network. *J. Cell Biol.* **2009**, *185*, 193–202.

24. Arias, E. E.; Walter, J. C. Strength in numbers: preventingrereplication via multiple mechanisms in eukaryotic cells. *Genes Dev.* **2007**, *21*, 497–518.

25. Marston, A. L.; Amon, A. Meiosis: cell-cycle controls shuffle and deal. *Nat. Rev. Mol. Cell Biol.* **2004**, *5*, 983–997.

26. Bolte, M.; Steigemann, P.; Braus, G. H.; Irniger, S. Inhibition of APC-mediated proteolysis by the meiosis-specific protein kinase Ime2. *Proc. Natl. Acad. Sci. U. S. A.* **2002**, *99*, 4385–4390.

27. Cha, R. S.; Weiner, B. M.; Keeney, S.; Dekker, J.; Kleckner, N. Progression of meiotic DNA replication is modulated by interchromosomal interaction proteins, negatively by Spo11p and positively by Rec8p. *Genes Dev.* **2000**, *14*, 493–503.

28. Davis, L.; Barbera, M.; McDonnell, A.; McIntyre, K.; Sternglanz, R.; Jin, Q.

W.; Loidl, J.; Engebrecht, J. A. The Saccharomyces cerevisiae MUM2 gene interacts with the DNA replication machinery and is required for meiotic levels of double strand breaks. *Genetics* **2001**, *157*, 1179–1189.

29. Keeney, S.; Giroux, C. N.; Kleckner, N. Meiosis-specific DNA double-strand breaks are catalyzed by Spo11, a member of a widely conserved protein family. *Cell* **1997**, *88*, 375–384.

30. Murakami, H.; Keeney, S. Regulating the formation of DNA double-strand breaks in meiosis. *Genes Dev.* **2008**, *22*, 286–292.

31. Roeder, G. S.; Bailis, J. M. The pachytene checkpoint. *Trends Genet.* **2000**, *16*, 395–403.

32. Hochegger, H.; Klotzbücher, A.; Kirk, J.; Howell, M.; le Guellec, K.; Fletcher, K.; Duncan, T.; Sohail, M.; Hunt, T. New B-type cyclin synthesis is required between meiosis I and II during Xenopus oocyte maturation. *Development* **2001**, *128*, 3795–3807.

33. Furuno, N.; Nishizawa, M. Suppression of DNA replication. *EMBO J.* **1994**, *13*, 2399–2410.

34. Buonomo, S. B. C.; Rabitsch, K. P.; Fuchs, J.; Gruber, S.; Sullivan, M.; Uhlmann, F.; Petronczki, M.; Tóth, A.; Nasmyth, K. Division of the nucleolus and its release of CDC14 during anaphase of meiosis I depends on separase, SPO12, and SLK19. *Dev. Cell* **2003**, *4*, 727–739.

35. Rock, J. M.; Amon, A. The FEAR network. *Curr. Biol.* **2009**, *19*, 1–10.

36. Theis, J. F.; Newlon, C. S. The ARS309 chromosomal replicator of Saccharomyces cerevisiae depends on an exceptional ARS consensus sequence. *Proc. Natl. Acad. Sci.* **1997**, *94*, 10786–10791.

37. Marahrens, Y.; Stillman, B. A yeast chromosomal origin of DNA replication defined by multiple functional elements. *Science* **1992**, *255*, 817–823.

38. Bell, S. P. The origin recognition complex: From simple origins to complex functions. *Genes Dev.* **2002**, *16*, 659–672.

39. Rhode, P. R.; Elsasser, S.; Campbell, J. L. Role of multifunctional autonomously replicating sequence binding factor 1 in the initiation of DNA replication and transcriptional control in *Saccharomyces cerevisiae*. *Mol. Cell. Biol.* **1992**, *12*, 1064–1077.

40. Leonard, A. C.; Mechali, M.; Méchali, M. DNA replication origins. *Cold Spring Harb. Perspect. Biol.* **2013**, *5*, a010116.

41. Xu, J.; Yanagisawa, Y.; Tsankov, A. M.; Hart, C.; Aoki, K.; Kommajosyula, N.; Steinmann, K. E.; Bochicchio, J.; Russ, C.; Regev, A.; Rando, O. J.; Nusbaum, C.; Niki, H.; Milos, P.; Weng, Z.; Rhind, N. Genome-wide identification and characterization of replication origins by deep sequencing. *Genome Biol.* **2012**, *13*, R27.

42. Okuno, Y.; Satoh, H.; Sekiguchi, M.; Masukata, H. Clustered adenine/thymine stretches are essential for function of a fission yeast replication origin. *Mol. Cell. Biol.* **1999**, *19*, 6699–6709.

43. Evertts, A. G.; Coller, H. a Back to the origin: reconsidering replication, transcription, epigenetics, and cell cycle control. *Genes Cancer* **2012**, *3*, 678–96.

44. Sasaki, T.; Sawado, T.; Yamaguchi, M.; Shinomiya, T. Specification of regions of DNA replication initiation during embryogenesis in the 65-kilobase DNApolalpha-dE2F locus of Drosophila melanogaster. *Mol. Cell. Biol.* **1999**, *19*, 547–555.

45. Hyrien, O.; Maric, C.; Mechali, M. Transition in specification of embryonic metazoan DNA replication origins. *Science (80-. ).* **1995**, *270*, 994–7.

46. Remus, D.; Beall, E. L.; Botchan, M. R. DNA topology, not DNA sequence, is a critical determinant for Drosophila ORC-DNA binding. *EMBO J.* **2004**, *23*, 897–907.

47. MacAlpine, D. M.; Rodriguez, H. K.; Bell, S. P. Coordination of replication and transcription along a Drosophila chromosome. *Genes Dev.* **2004**, *18*, 3094–105.

48. Cayrou, C.; Coulombe, P.; Vigneron, A.; Stanojcic, S.; Ganier, O.; Peiffer, I.; Rivals, E.; Puy, A.; Laurent-Chabalier, S.; Desprat, R.; Méchali, M. Genome-scale analysis of metazoan replication origins reveals their organization in specific but flexible sites defined by conserved features. *Genome Res.* **2011**, *21*, 1438–1449.

49. Jackson, D. A.; Pombo, A. Replicon Clusters Are Stable Units of Chromosome Structure Evidence That Nuclear Organization Contributes to the Efficient Activation and Propagation of S Phase in Human Cells. *J Cell Biol* **1998**, *140*, 1285–1295.

50. DePamphilis, M. L. Replication origins in metazoan chromosomes: fact or fiction? *Bioessays* **1999**, *21*, 5–16.

51. Cayrou, C.; Coulombe, P.; Puy, A.; Kaplan, N.; Segal, E. New insights into replication origin characteristics in metazoans © 2012 Landes Bioscience . Do not distribute . **2012**, *11*, 658–667.

52. Forrester, W. C.; Epner, E.; Catherine Driscoll, M.; Enver, T.; Brice, M.; Papayannopoulou, T.; Groudine, M. A deletion of the human β-globin locus activation region causes a major alteration in chromatin structure and replication across the entire β-globin locus. *Genes Dev.* **1990**, *4*, 1637–1649.

53. Levens, D. L. Reconstructing MYC. *Genes Dev.* **2003**, *17*, 1071–1077.

54. Swarnalatha, M.; Singh, A. K.; Kumar, V. The epigenetic control of E-box and Myc-dependent chromatin modifications regulate the licensing of lamin B2 origin during cell cycle. *Nucleic Acids Res.* **2012**, *40*, 9021–9035.

55. Robinson, K.; Asawachaicharn, N.; Galloway, D. A.; Grandori, C. c-Myc accelerates S-phase and requires WRN to avoid replication stress. *PLoS One* **2009**,

*4*, e5951.

56. Eaton, M. L.; Galani, K.; Kang, S.; Bell, S. P.; Macalpine, D. M. Conserved nucleosome positioning defines replication origins service. *Genes Dev.* **2010**, *24*, 748–753.

57. Berbenetz, N. M.; Nislow, C.; Brown, G. W. Diversity of Eukaryotic DNA replication origins revealed by Genome-wide analysis of chromatin structure. *PLoS Genet.* **2010**, *6*, e1001092.

58. Renard-Guillet, C.; Kanoh, Y.; Shirahige, K.; Masai, H. Temporal and spatial regulation of eukaryotic DNA replication: From regulated initiation to genome-scale timing program. *Semin. Cell Dev. Biol.* **2014**, *30*, 110–120.

59. Yin, S.; Deng, W.; Hu, L.; Kong, X. The impact of nucleosome positioning on the organization of replication origins in eukaryotes. *Biochem. Biophys. Res. Commun.* **2009**, *385*, 363–368.

60. Lubelsky, Y.; Sasaki, T.; Kuipers, M. A.; Lucas, I.; Le Beau, M. M.; Carignon, S.; Debatisse, M.; Prinz, J. A.; Dennis, J. H.; Gilbert, D. M. Pre-replication complex proteins assemble at regions of low nucleosome occupancy within the Chinese hamster dihydrofolate reductase initiation zone. *Nucleic Acids Res.* **2011**, *39*, 3141–3155.

61. Hiratani, I.; Ryba, T.; Itoh, M.; Yokochi, T.; Schwaiger, M.; Chang, C. W.; Lyou, Y.; Townes, T. M.; Schübeler, D.; Gilbert, D. M. Global reorganization of replication domains during embryonic stem cell differentiation. *PLoS Biol.* **2008**, *6*, 2220–2236.

62. Yaffe, E.; Farkash-Amar, S.; Polten, A.; Yakhini, Z.; Tanay, A.; Simon, I. Comparative analysis of DNA replication timing reveals conserved large-scale chromosomal architecture. *PLoS Genet.* **2010**, *6*, 1–12.

63. Alabert, C.; Groth, A. Chromatin replication and epigenome maintenance. *Nat. Rev MCB* **2012**, *13*, 153–167.

64. Raghuraman, M. K.; Brewer, B. J.; Fangman, W. L. Cell cycle-dependent establishment of a late replication program. *Science* **1997**, *276*, 806–809.

65. Dimitrova, D. S.; Gilbert, D. M. The spatial position and replication timing of chromosomal domains are both established in early G1 phase. *Mol. Cell* **1999**, *4*, 983–993.

66. McNairn, A. J.; Gilbert, D. M. Epigenomic replication: Linking epigenetics to DNA replication. *BioEssays* **2003**, *25*, 647–656.

67. Rhind, N.; Gilbert, D. M. DNA replication timing. *Cold Spring Harb. Perspect. Biol.* **2013**, *5*, 1–26.

68. Kim, S.; Dubey, D. D.; Huberman, J. A. Early-replicating heterochromatin. **2003**, 330–335.

69. Hayashi, M. T.; Takahashi, T. S.; Nakagawa, T.; Nakayama, J.; Masukata, H.

The heterochromatin protein Swi6/HP1 activates replication origins at the pericentromeric region and silent mating-type locus. *Nat. Cell Biol.* **2009**, *11*, 357–362.

70. Wu, P. J.; Nurse, P. Establishing the program of origin firing during S phase in fission yeast. *Cell* **2009**, *136*, 852–864.

71. Fragkos, M.; Ganier, O.; Coulombe, P.; Méchali, M. DNA replication origin activation in space and time. *Nat. Rev. Mol. Cell Biol.* **2015**, *16*, 360–374.

72. Anglana, M.; Apiou, F.; Bensimon, A.; Debatisse, M. Dynamics of DNA replication in mammalian somatic cells: Nucleotide pool modulates origin choice and interorigin spacing. *Cell* **2003**, *114*, 385–394.

73. Blow, J. J.; Ge, X. Q.; Jackson, D. a How dormant origins promote complete genome replication. *Trends Biochem. Sci.* **2011**, *36*, 405–414.

74. Aparicio, O. M.; Stout, A. M.; Bell, S. P. Differential assembly of Cdc45p and DNA polymerases at early and late origins of DNA replication. *Proc. Natl. Acad. Sci. U. S. A.* **1999**, *96*, 9130–9135.

75. Bell, S. P.; Stillman, B. ATP-dependent recognition of eukaryotic origins of DNA replication by a multiprotein complex. *Nature* **1992**, *357*, 128–34.

76. Chuang, R.-Y.; Kelly, T. J. The fission yeast homologue of Orc4p binds to replication origin DNA via multiple AT-hooks. *Biochemistry* **1999**, *96*, 2656–2661.

77. Kara, N.; Hossain, M.; Prasanth, S. G.; Stillman, B. Orc1 Binding to Mitotic Chromosomes Precedes Spatial Patterning during $G_1$ Phase and Assembly of the Origin Recognition Complex in Human Cells. *J. Biol. Chem.* **2015**, *290*, 12355–12369.

78. DePamphilis, M. L. The “ORC cycle”: A novel pathway for regulating eukaryotic DNA replication. *Gene* **2003**, *310*, 1–15.

79. Méndez, J.; Stillman, B. Chromatin association of human origin recognition complex, cdc6, and minichromosome maintenance proteins during the cell cycle: assembly of prereplication complexes in late mitosis. *Mol. Cell. Biol.* **2000**, *20*, 8602–12.

80. Hua, X. H.; Newport, J. Identification of a preinitiation step in DNA replication that is independent of origin recognition complex and cdc6, but dependent on cdk2. *J. Cell Biol.* **1998**, *140*, 271–281.

81. Symeonidou, I. E.; Kotsantis, P.; Roukos, V.; Rapsomaniki, M. A.; Grecco, H. E.; Bastiaens, P.; Taraviras, S.; Lygerou, Z. Multi-step loading of human minichromosome maintenance proteins in live human cells. *J. Biol. Chem.* **2013**, *288*, 35852–35867.

82. Zhai, Y.; Cheng, E.; Wu, H.; Li, N.; Yuk, P.; Yung, K.; Gao, N.; Tye, B. Open-ringed structure of the Cdt1 – Mcm2 – 7 complex as a precursor of the MCM double hexamer. **2017**, *24*.

83. Sun, J.; Fernandez-cid, A.; Riera, A.; Tognetti, S.; Yuan, Z.; Stillman, B.; Speck, C.; Li, H. Structural and mechanistic insights into Mcm2 – 7 double-hexamer assembly and function. *Genes Dev.* **2014**, *28*, 2291–2303.

84. Montagnoli, A.; Moll, J.; Colotta, F. Targeting cell division cycle 7 kinase: a new approach for cancer therapy. *Clin. Cancer Res.* **2010**, *16*, 4503–8.

85. Thu, Y. M.; Bielinsky, A.-K. Enigmatic roles of Mcm10 in DNA replication. *Trends Biochem. Sci.* **2013**, *38*, 184–94.

86. Montagnoli, A.; Valsasina, B.; Brotherton, D.; Troiani, S.; Rainoldi, S.; Tenca, P.; Molinari, A.; Santocanale, C. Identification of Mcm2 phosphorylation sites by S-phase-regulating kinases. *J. Biol. Chem.* **2006**, *281*, 10281–10290.

87. Poh, W. T.; Chadha, G. S.; Gillespie, P. J.; Kaldis, P.; Blow, J. J. Xenopus Cdc7 executes its essential function early in S phase and is counteracted by checkpoint-regulated protein phosphatase 1. *Open Biol.* **2014**, *4*, 130138.

88. Heller, R. C.; Kang, S.; Lam, W. M.; Chen, S.; Chan, C. S.; Bell, S. P. Eukaryotic origin-dependent DNA replication in vitro reveals sequential action of DDK and S-CDK kinases. *Cell* **2011**, *146*, 80–91.

89. Yeeles, J. T. P.; Deegan, T. D.; Janska, A.; Early, A.; Diffley, J. F. X. Regulated eukaryotic DNA replication origin firing with purified proteins. *Nature* **2015**, *519*, 431–435.

90. Sansam, C. G.; Goins, D.; Siefert, J. C.; Clowdus, E. a; Sansam, C. L. Cyclin-dependent kinase regulates the length of S phase through TICRR / TRESLIN phosphorylation. *Genes Dev.* **2015**, *29*, 555–566.

91. Matsuno, K.; Kumano, M.; Kubota, Y.; Hashimoto, Y.; Takisawa, H. The N-terminal noncatalytic region of Xenopus RecQ4 is required for chromatin binding of DNA polymerase alpha in the initiation of DNA replication. *Mol. Cell. Biol.* **2006**, *26*, 4843–4852.

92. Kumagai, A.; Shevchenko, A.; Shevchenko, A.; Dunphy, W. G. Direct regulation of Treslin by cyclin-dependent kinase is essential for the onset of DNA replication. *J. Cell Biol.* **2011**, *193*, 995–1007.

93. Boos, D.; Yekezare, M.; Diffley, J. Identification of a heteromeric complex that promotes DNA replication origin firing in human cells. *Sc* **2013**, *340*, 981–4.

94. Brady, M.; Vlatković, N.; Boyd, M. Regulation of p53 and MDM2 activity by MTBP. *Mol. Cell. Biol.* **2005**, *25*, 545–553.

95. Pellegrini, L.; Costa, A. New Insights into the Mechanism of DNA Duplication by the Eukaryotic Replisome. *Trends Biochem. Sci.* **2016**, *41*, 859–871.

96. Yuzhakov, A.; Kelman, Z.; Hurwitz, J.; O'Donnell, M. Multiple competition reactions for RPA order the assembly of the DNA polymerase ?? holoenzyme. *EMBO J.* **1999**, *18*, 6189–6199.

97. Burgers, P. M. J. Polymerase dynamics at the eukaryotic DNA replication fork.

*J. Biol. Chem.* **2009**, *284*, 4041–4045.

98. Walsh, E.; Eckert, K. A. Chapter 2 Eukaryotic Replicative DNA Polymerases. In *Eukaryotic Replicative DNA polymerases*; K., M.; M., T., Eds.; Springer Berlin Heidelberg, 2014; Vol. 30, pp. 17–41.

99. Yao, N.; O'Donnell, M. The RFC Clamp Loader: Structure and Function. *Subcell. Biochem.* **2012**, *62*, 259–79.

100. Moldovan, G. L.; Pfander, B.; Jentsch, S. PCNA, the Maestro of the Replication Fork. *Cell* **2007**, *129*, 665–679.

101. Garg, P.; Burgers, P. M. J. DNA polymerases that propagate the eukaryotic DNA replication fork. *Crit. Rev. Biochem. Mol. Biol.* **2005**, *40*, 115–128.

102. Kang, S.; Kang, M.-S.; Ryu, E.; Myung, K. Eukaryotic DNA replication: Orchestrated action of multi-subunit protein complexes. *Mutat. Res. Mol. Mech. Mutagen.* **2017**, 0–1.

103. Jiang, Z.; Xu, M.; Lai, Y.; Laverde, E.; Terzidis, M.; Masi, A.; Chatgilialoglu, C.; Liu, Y. Bypass of a 5′,8-cyclopurine-2′-deoxynucleoside by DNA polymerase β during DNA replication and base excision repair leads to nucleotide misinsertions and DNA strand breaks. *DNA Repair (Amst).* **2015**, *33*, 24–34.

104. Graziewicz, M. A.; Longley, M. J.; Copeland, W. C. DNA polymerase γ in mitochondrial DNA replication and repair. *Chem. Rev.* **2006**, *106*, 383–405.

105. Choi, J.; Lim, S.; Kim, E.; Jo, A.; Guengerich, F. Translesion Synthesis Across Abasic Lesions by Human B- family and Y-family DNA Polymerases α, δ, η, ι, κ, and REV1. *J Mol Biol.* **2010**, *404*, 34–44.

106. Hirota, K.; Tsuda, M.; Mohiuddin; Tsurimoto, T.; Cohen, I. S.; Livneh, Z.; Kobayashi, K.; Narita, T.; Nishihara, K.; Murai, J.; Iwai, S.; Guilbaud, G.; Sale, J. E.; Takeda, S. In vivo evidence for translesion synthesis by the replicative DNA polymerase δ. *Nucleic Acids Res.* **2016**, *44*, 7242–7250.

107. Seki, M.; Masutani, C.; Yang, L. W.; Schuffert, A.; Iwai, S.; Bahar, I.; Wood, R. D. High-efficiency bypass of DNA damage by human DNA polymerase Q. *EMBO J.* **2004**, *23*, 4484–4494.

108. Tissier, A.; Frank, E. G.; McDonald, J. P.; Iwai, S.; Hanaoka, F.; Woodgate, R. Misinsertion and bypass of thymine-thymine dimers by human DNA polymerase iota. *EMBO J.* **2000**, *19*, 5259–66.

109. Ogi, T.; Lehmann, A. R. The Y-family DNA polymerase κ (pol κ) functions in mammalian nucleotide-excision repair. *Nat. Cell Biol.* **2006**, *8*, 640–642.

110. Avkin, S.; Goldsmith, M.; Velasco-Miguel, S.; Geacintov, N.; Friedberg, E. C.; Livneh, Z. Quantitative analysis of translesion DNA synthesis across a benzo[a]pyrene-guanine adduct in mammalian cells: The role of DNA polymerase. *J. Biol. Chem.* **2004**, *279*, 53298–53305.

111. Villani, G.; Hubscher, U.; Gironis, N.; Parkkinen, S.; Pospiech, H.; Shevelev,

I.; Di Cicco, G.; Markkanen, E.; Syväoja, J. E.; Le Gac, N. T. In vitro gap-directed translesion DNA synthesis of an abasic site involving human DNA polymerases ε, λ, and β. *J. Biol. Chem.* **2011**, *286*, 32094–32104.

112. Takata, K. I.; Shimizu, T.; Iwai, S.; Wood, R. D. Human DNA polymerase N (POLN) is a low fidelity enzyme capable of error-free bypass of 5S-thymine glycol. *J. Biol. Chem.* **2006**, *281*, 23445–23455.

113. Motea, E.; Berdis, A. Terminal Deoxynucleotidyl Transferase: The Story of a Misguided DNA Polymerase. *Biochim. Biophys. Acta* **2010**, *1804*, 1151–66.

114. Biertümpfel, C.; Zhao, Y.; Kondo, Y.; Ramón-Maiques, S.; Gregory, M.; Lee, J. Y.; Masutani, C.; Lehmann, A. R.; Hanaoka, F.; Yang, W. Structure and mechanism of human DNA polymerase eta. *Nature* **2010**, *465*, 1044–1048.

115. Johnson, R. E. Fidelity of Human DNA Polymerase eta. *J. Biol. Chem.* **2000**, *275*, 7447–7450.

116. de Padula, M.; Slezak, G.; van Der Kemp, P. A.; Boiteux, S. The post-replication repair RAD18 and RAD6 genes are involved in the prevention of spontaneous mutations caused by 7,8-dihydro-8-oxoguanine in Saccharomyces cerevisiae. *Nucleic Acids Res.* **2004**, *32*, 5003–5010.

117. Haracska, L.; Prakash, S.; Prakash, L. Yeast Rev1 protein is a G template-specific DNA polymerase. *J. Biol. Chem.* **2002**, *277*, 15546–15551.

118. Nair, D. T. Rev1 Employs a Novel Mechanism of DNA Synthesis Using a Protein Template. *Science (80-. ).* **2005**, *309*, 2219–2222.

119. Nair, D. T.; Johnson, R. E.; Prakash, L.; Prakash, S.; Aggarwal, A. K. Protein-Template-Directed Synthesis across an Acrolein-Derived DNA Adduct by Yeast Rev1 DNA Polymerase. *Structure* **2008**, *16*, 239–245.

120. Prakash, S.; Johnson, R. E.; Prakash, L. Eukaryotic translesion synthesis DNA polymerases: specificity of structure and function. *Annu. Rev. Biochem.* **2005**, *74*, 317–53.

121. Sale, J. E. Translesion DNA Synthesis and Mutagenesis in Eukaryotes. *Cold Spring Harb. Lab. Press* **2013**, *5*, 1–22.

122. Johnson, R. E.; Washington, M. T.; Haracska, L.; Prakash, S.; Prakash, L. Eukaryotic polymerases iota and zeta act sequentially to bypass DNA lesions. *Nature* **2000**, *406*, 1015–1019.

123. Maric, M.; Maculins, T.; De Piccoli, G.; Labib, K. Cdc48 and a ubiquitin ligase drive disassembly of the CMG helicase at the end of DNA replication. *Science (80-. ).* **2014**, *346*, 1253596–1253596.

124. Dewar, J. M.; Budzowska, M.; Walter, J. C. The mechanism of DNA replication termination in vertebrates. *Nature* **2015**, *525*, 345–50.

125. Jiang, W.; Hunter, T. Identification and characterization of a human protein kinase related to budding yeast Cdc7p. *Biochemistry* **1997**, *94*, 14320–14325.

126. Byung, J. K.; Kim, S. Y.; Lee, H. Identification and characterization of human Cdc7 nuclear retention and export sequences in the context of chromatin binding. *J. Biol. Chem.* **2007**, *282*, 30029–30038.

127. Hughes, S.; Elustondo, F.; Fonzo, A. Di; Leroux, F. G.; Wong, A. C.; Snijders, A. P.; Matthews, S. J.; Cherepanov, P.; Di Fonzo, A.; Leroux, F. G.; Wong, A. C.; Snijders, A. P.; Matthews, S. J.; Cherepanov, P. Crystal structure of human CDC7 kinase in complex with its activator DBF4. *Nat. Struct. Mol. Biol.* **2012**, *19*, 1101–1107.

128. Sheu, Y.; Stillman, B. The Dbf4-Cdc7 kinase promotes S phase by alleviating an inhibitory activity in Mcm4. *Nature* **2010**, *463*, 113–7.

129. Sheu, Y.-J.; Kinney, J. B.; Lengronne, A.; Pasero, P.; Stillman, B. Domain within the helicase subunit Mcm4 integrates multiple kinase signals to control DNA replication initiation and fork progression. *Proc. Natl. Acad. Sci. U. S. A.* **2014**, *111*, E1899-908.

130. Masai, H.; Taniyama, C.; Ogino, K.; Matsui, E.; Kakusho, N.; Matsumoto, S.; Kim, J.-M. M.; Ishii, A.; Tanaka, T.; Kobayashi, T.; Tamai, K.; Ohtani, K.; Arai, K.-I. I. Phosphorylation of MCM4 by Cdc7 kinase facilitates its interaction with Cdc45 on the chromatin. *J. Biol. Chem.* **2006**, *281*, 39249–61.

131. Brown, G. W.; Kelly, T. J. Purification of Hsk1, a minichromosome maintenance protein kinase from fission yeast. *J. Biol. Chem.* **1998**, *273*, 22083–22090.

132. Lee, J.-K.; Seo, Y.-S.; Hurwitz, J. The Cdc23 (Mcm10) protein is required for the phosphorylation of minichromosome maintenance complex by the Dfp1-Hsk1 kinase. *Proc. Natl. Acad. Sci. U. S. A.* **2003**, *100*, 2334–9.

133. Masai, H.; Matsui, E.; You, Z.; Ishimi, Y.; Tamai, K.; Arai, K. I. Human Cdc7-related kinase complex. In vitro phosphorylation of MCM by concerted actions of Cdks and Cdc7 and that of a criticial threonine residue of Cdc7 bY Cdks. *J. Biol. Chem.* **2000**, *275*, 29042–52.

134. Bruck, I.; Kaplan, D. Dbf4-Cdc7 phosphorylation of Mcm2 is required for cell growth. *J. Biol. Chem.* **2009**, *284*, 28823–28831.

135. Cortez, D.; Glick, G.; Elledge, S. J. Minichromosome maintenance proteins are direct targets of the ATM and ATR checkpoint kinases. **2004**, *101*.

136. Larasati; Duncker, B. Mechanisms Governing DDK Regulation of the Initiation of DNA Replication. *Genes (Basel).* **2016**, *8*, 3.

137. Hiraga, S. I.; Alvino, G. M.; Chang, F.; Lian, H. Y.; Sridhar, A.; Kubota, T.; Brewer, B. J.; Weinreich, M.; Raghuraman, M. K.; Donaldson, A. D. Rif1 controls DNA replication by directing Protein Phosphatase 1 to reverse Cdc7- mediated phosphorylation of the MCM complex. *Genes Dev.* **2014**, *28*, 372–383.

138. Hiraga, S.; Ly, T.; Garzón, J.; Hořejší, Z.; Ohkubo, Y.; Endo, A.; Obuse, C.; Boulton, S. J.; Lamond, A. I.; Anne, D. Human RIF1 and Protein Phosphatase 1

stimulate DNA replication origin licensing but suppress origin activation. *EMBO Rep.* **2017**, *18*, 403–419.

139. Alver, R. C.; Chadha, G. S.; Gillespie, P. J.; Blow, J. J. Reversal of DDK-Mediated MCM Phosphorylation by Rif1-PP1 Regulates Replication Initiation and Replisome Stability Independently of ATR/Chk1. *Cell Rep.* **2017**, *18*, 2508–2520.

140. Boddy, M. N.; Russell, P. DNA replication checkpoint control. *Curr. Biol.* **2001**, *11*, R953-6.

141. Matsumoto, S.; Shimmoto, M.; Kakusho, N.; Yokoyama, M.; Kanoh, Y.; Hayano, M.; Russell, P.; Masai, H. Hsk1 kinase and Cdc45 regulate replication stress-induced checkpoint responses in fission yeast. *Cell Cycle* **2010**, *9*, 4627–4637.

142. Ogi, H.; Wang, C. Z.; Nakai, W.; Kawasaki, Y.; Masumoto, H. The role of the Saccharomyces cerevisiae Cdc7-Dbf4 complex in the replication checkpoint. *Gene* **2008**, *414*, 32–40.

143. Kim, J. M.; Kakusho, N.; Yamada, M.; Kanoh, Y.; Takemoto, N.; Masai, H. Cdc7 kinase mediates Claspin phosphorylation in DNA replication checkpoint. *Oncogene* **2008**, *27*, 3475–82.

144. Rainey, M. D.; Harhen, B.; Wang, G.-N.; Murphy, P. V; Santocanale, C. Cdc7-dependent and -independent phosphorylation of Claspin in the induction of the DNA replication checkpoint. *Cell Cycle* **2013**, *12*, 1560–8.

145. Montagnoli, A.; Tenca, P.; Sola, F.; Carpani, D.; Brotherton, D.; Albanese, C.; Santocanale, C. <Cdc7 Inhibition Reveals a p53-Dependent Replication Checkpoint That Is Defective in Cancer Cells.pdf>. *Cancer Res* **2004**, *64*, 7110–7116.

146. Gold, D. A.; Dunphy, W. G. Drf1-dependent kinase interacts with claspin through a conserved protein motif. *J. Biol. Chem.* **2010**, *285*, 12638–12646.

147. Wan, L.; Zhang, C.; Shokat, K. M.; Hollingsworth, N. M. Chemical inactivation of Cdc7 kinase in budding yeast results in a reversible arrest that allows efficient cell synchronization prior to meiotic recombination. *Genetics* **2006**, *174*, 1767–1774.

148. Valentin, G.; Schwob, E.; Della Seta, F. Dual role of the Cdc7-regulatory protein Dbf4 during yeast meiosis. *J. Biol. Chem.* **2006**, *281*, 2828–2834.

149. Matos, J.; Lipp, J. J.; Bogdanova, A.; Guillot, S.; Okaz, E.; Junqueira, M.; Shevchenko, A.; Zachariae, W. Dbf4-Dependent Cdc7 Kinase Links DNA Replication to the Segregation of Homologous Chromosomes??in Meiosis I. *Cell* **2008**, *135*, 662–678.

150. Ogino, K.; Hirota, K.; Matsumoto, S.; Takeda, T.; Ohta, K.; Arai, K.; Masai, H. Hsk1 kinase is required for induction of meiotic dsDNA breaks without involving checkpoint kinases in fission yeast. *Proc. Natl. Acad. Sci. U. S. A.* **2006**, *103*, 8131–8136.

151. Katis, V. L.; Lipp, J. J.; Imre, R.; Bogdanova, A.; Okaz, E.; Habermann, B.; Mechtler, K.; Nasmyth, K.; Zachariae, W. Rec8 phosphorylation by casein kinase 1 and Cdc7-Dbf4 kinase regulates cohesin cleavage by separase during meiosis. *Dev. Cell* **2010**, *18*, 397–409.

152. Lo, H.-C.; Kunz, R. C.; Chen, X.; Marullo, a.; Gygi, S. P.; Hollingsworth, N. M. Cdc7-Dbf4 Is a Gene-Specific Regulator of Meiotic Transcription in Yeast. *Mol. Cell. Biol.* **2012**, *32*, 541–557.

153. Miller, C. T.; Gabrielse, C.; Chen, Y. C.; Weinreich, M. Cdc7p-Dbf4p regulates mitotic exit by inhibiting polo kinase. *PLoS Genet.* **2009**, *5*.

154. Chen, Y. C.; Weinreich, M. Dbf4 regulates the Cdc5 polo-like kinase through a distinct non-canonical binding interaction. *J. Biol. Chem.* **2010**, *285*, 41244–41254.

155. Suzuki, T.; Tsuzuku, J.; Hayashi, A.; Shiomi, Y.; Iwanari, H.; Hamakubo, T.; Mochizuki, Y.; Hamakubo, T.; Kodama, T.; Nishitani, H.; Masai, H.; Yamamoto, T. Inhibition of DNA damage-induced apoptosis through Cdc7-mediated stabilization of Tob. *J. Biol. Chem.* **2012**, *287*, 40256–65.

156. Winkler, G. S. The mammalian anti-proliferative BTG/Tob protein family. *J. Cell. Physiol.* **2010**, *222*, 66–72.

157. Vaziri, C.; Masai, H. Integrating DNA replication with trans-lesion synthesis via Cdc7. *Cell Cycle* **2010**, *9*, 4818–4823.

158. Montagnoli, A.; Bosotti, R.; Villa, F.; Rialland, M.; Brotherton, D.; Mercurio, C.; Berthelsen, J.; Santocanale, C. Drf1, a novel regulatory subunit for human Cdc7 kinase. *EMBO J.* **2002**, *21*, 3171–3181.

159. Duncker, B. P.; Shimada, K.; Tsai-Pflugfelder, M.; Pasero, P.; Gasser, S. M. An N-terminal domain of Dbf4p mediates interaction with both origin recognition complex (ORC) and Rad53p and can deregulate late origin firing. *Proc. Natl. Acad. Sci. U. S. A.* **2002**, *99*, 16087–16092.

160. Yoshizawa-Sugata, N.; Ishii, A.; Taniyama, C.; Matsui, E.; Arai, K. I.; Masai, H. A second human Dbf4/ASK-related protein, Drf1/ASKL1, is required for efficient progression of S and M phases. *J. Biol. Chem.* **2005**, *280*, 13062–13070.

161. Takahashi, T. S.; Walter, J. C. Cdc7 – Drf1 is a developmentally regulated protein kinase required for the initiation of vertebrate DNA replication. *Genes Dev.* **2005**, *19*, 2295–2300.

162. Toh, G. T.; Masai, H. Cdc7l1. **2012**, *1*.

163. Yoon, H. J.; Loo, S.; Campbell, J. L. Regulation of Saccharomyces cerevisiae CDC7 function during the cell cycle. *Mol. Biol. Cell* **1993**, *4*, 195–208.

164. Georges, S. A.; Biery, M. C.; Kim, S. Y.; Schelter, J. M.; Guo, J.; Chang, A. N.; Jackson, A. L.; Carleton, M. O.; Linsley, P. S.; Cleary, M. A.; Chau, B. N. Coordinated regulation of cell cycle transcripts by p53-inducible microRNAs, miR-

192 and miR-215. *Cancer Res.* **2008**, *68*, 10105–10112.

165. Tudzarova, S.; Mulholland, P.; Dey, A.; Stoeber, K.; Okorokov, A. L.; Williams, G. H. p53 controls CDC7 levels to reinforce G1 cell cycle arrest upon genotoxic stress. *Cell Cycle* **2016**, *15*, 2958–2972.

166. Hardy, C. F. J.; Dryga, O.; Seematter, S.; Pahl, P. M. B.; Sclafani, R. A. mcm5$\overline{c}$dc46-bob1 bypasses the requirement for the S phase activator Cdc7p. *Genetics* **1997**, *94*, 3151–3155.

167. Hoang, M. L.; Leon, R. P.; Pessoa-Brandao, L.; Hunt, S.; Raghuraman, M. K.; Fangman, W. L.; Brewer, B. J.; Sclafani, R. A. Structural Changes in Mcm5 Protein Bypass Cdc7-Dbf4 Function and Reduce Replication Origin Efficiency in Saccharomyces cerevisiae. *Mol. Cell. Biol.* **2007**, *27*, 7594–7602.

168. Masai, H.; Miyake, T.; Arai, K. hsk1+, a Schizosaccharomyces pombe gene related to Saccharomyces cerevisiae CDC7, is required for chromosomal replication. *EMBO J.* **1995**, *14*, 3094–3104.

169. Takeda, T.; Ogino, K.; Tatebayashi, K.; Ikeda, H.; Arai Ki; Masai, H. Regulation of initiation of S phase, replication checkpoint signaling, and maintenance of mitotic chromosome structures during S phase by Hsk1 kinase in the fission yeast. *Mol. Biol. Cell* **2001**, *12*, 1257–1274.

170. Walter, J. C. Evidence for sequential action of cdc7 and cdk2 protein kinases during initiation of DNA replication in Xenopus egg extracts. *J. Biol. Chem.* **2000**, *275*, 39773–39778.

171. Takahashi, T. S.; Basu, A.; Bermudez, V.; Hurwitz, J.; Walter, J. C. Cdc7-Drf1 kinase links chromosome cohesion to the initiation of DNA replication in Xenopus egg extracts. *Genes Dev.* **2008**, *22*, 1894–1905.

172. Kim, J. M.; Nakao, K.; Nakamura, K.; Saito, I.; Katsuki, M.; Arai, K. Inactivation of Cdc7 kinase in mouse ES cells results in S-phase arrest and p53-dependent cell death. **2002**, *21*.

173. Kim, J. Functions of mammalian Cdc7 kinase in initiation/monitoring of DNA replication and development. *Mutat. Res. Mol. Mech. Mutagen.* **2003**, *532*, 29–40.

174. Swords, R.; Mahalingam, D.; O'Dwyer, M.; Santocanale, C.; Kelly, K.; Carew, J.; Giles, F. Cdc7 kinase - a new target for drug development. *Eur J Cancer* **2010**, *46*, 33–40.

175. Jiang, W.; McDonald, D.; Hope, T. J.; Hunter, T. Mammalian Cdc7-Dbf4 protein kinase complex is essential for initiation of DNA replication. *EMBO J.* **1999**, *18*, 5703–13.

176. Im, J.-S.; Lee, J.-K. ATR-dependent Activation of p38 MAP Kinase Is Responsible for Apoptotic Cell Death in Cells Depleted of Cdc7. *J. Biol. Chem.* **2008**, *283*, 25171–25177.

177. Tudzarova, S.; Trotter, M. W. B.; Wollenschlaeger, A.; Mulvey, C.; Godovac-

Zimmermann, J.; Williams, G. H.; Stoeber, K. Molecular architecture of the DNA replication origin activation checkpoint. *EMBO J.* **2010**, *29*, 3381–3394.

178. Weinreich, M.; Stillman, B. Cdc7p-Dbf4p kinase binds to chromatin during S phase and is regulated by both the APC and the RAD53 checkpoint pathway. *EMBO J.* **1999**, *18*, 5334–5346.

179. Yamada, M.; Watanabe, K.; Mistrik, M.; Vesela, E.; Protivankova, I.; Mailand, N.; Lee, M. H.; Masai, H.; Lukas, J.; Bartek, J. ATR-Chk1-APC/CCdh1-dependent stabilization of Cdc7-ASK (Dbf4) kinase is required for DNA lesion bypass under replication stress. *Genes Dev.* **2013**, *27*, 2459–2472.

180. Nougarède, R.; Della Seta, F.; Zarzov, P.; Schwob, E. Hierarchy of S-phase-promoting factors: yeast Dbf4-Cdc7 kinase requires prior S-phase cyclin-dependent kinase activation. *Mol. Cell. Biol.* **2000**, *20*, 3795–3806.

181. Francis, L. I.; Randell, J. C. W.; Takara, T. J.; Uchima, L.; Bell, S. P. Incorporation into the prereplicative complex activates the Mcm2 – 7 helicase for Cdc7 – Dbf4 phosphorylation. *Genes Dev.* **2009**, *23*, 643–654.

182. Varrin, A. E.; Prasad, A. a; Scholz, R.-P.; Ramer, M. D.; Duncker, B. P. A mutation in Dbf4 motif M impairs interactions with DNA replication factors and confers increased resistance to genotoxic agents. *Mol. Cell. Biol.* **2005**, *25*, 7494–504.

183. Dowell, S. J.; Romanowski, P.; Diffley, J. F. X.; Dowell, S. J.; Romanowski, P.; Diffley, J. F. X. Interaction of Dbf4 , the Cdc7 Protein Kinase Regulatory Subunit , with Yeast Replication Origins in Vivo Published by : American Association for the Advancement of Science Stable URL : http://www.jstor.org/stable/2884886 JSTOR is a not-for-profit service. *Science (80-. ).* **1994**, *265*, 1243–1246.

184. Kihara, M.; Nakai, W.; Asano, S.; Suzuki, A.; Kitada, K.; Kawasaki, Y.; Johnston, L. H.; Sugino, A. Characterization of the yeast Cdc7p/Dbf4p complex purified from insect cells. *J. Biol. Chem.* **2000**, *275*, 35051–35062.

185. Jones, D. R.; Prasad, A. A.; Chan, P. K.; Duncker, B. P. The Dbf4 motif C zinc finger promotes DNA replication and mediates resistance to genotoxic stress. *Cell Cycle* **2010**, *9*, 2018–2026.

186. Day, T. A.; Palle, K.; Barkley, L. R.; Kakusho, N.; Zou, Y.; Tateishi, S.; Verreault, A.; Masai, H.; Vaziri, C. Phosphorylated Rad18 directs DNA polymerase eta to sites of stalled replication. *J. Cell Biol.* **2010**, *191*, 953–966.

187. Kumagai, H.; Sato, N.; Yamada, M.; Mahony, D.; Seghezzi, W.; Lees, E.; Arai, K.; Masai, H. A novel growth- and cell cycle-regulated protein, ASK, activates human Cdc7-related kinase and is essential for G1/S transition in mammalian cells. *Mol. Cell. Biol.* **1999**, *19*, 5083–95.

188. Matsumoto, S.; Masai, H. Regulation of chromosome dynamics by Hsk1/Cdc7 kinase. *Biochem Soc Trans* **2013**, *41*, 1712–1719.

189. Montagnoli, A.; Valsasina, B.; Croci, V.; Menichincheri, M.; Rainoldi, S.; Marchesi, V.; Tibolla, M.; Tenca, P.; Brotherton, D.; Albanese, C.; Patton, V.; Alzani, R.; Ciavolella, A.; Sola, F.; Molinari, A.; Volpi, D.; Avanzi, N.; Fiorentini, F.; Cattoni, M.; Healy, S.; Ballinari, D.; Pesenti, E.; Isacchi, A.; Moll, J.; Bensimon, A.; Vanotti, E.; Santocanale, C. A Cdc7 kinase inhibitor restricts initiation of DNA replication and has antitumor activity. *Nat. Chem. Biol.* **2008**, *4*, 357–65.

190. Natoni, A.; Murillo, L. S.; Kliszczak, A. E.; Catherwood, M. a; Montagnoli, A.; Samali, A.; O'Dwyer, M.; Santocanale, C. Mechanisms of action of a dual Cdc7/Cdk9 kinase inhibitor against quiescent and proliferating CLL cells. *Mol. Cancer Ther.* **2011**, *10*, 1624–34.

191. Natoni, A.; Coyne, M. R. E. E.; Jacobsen, A.; Rainey, M. D.; O'Brien, G.; Healy, S.; Montagnoli, A.; Moll, J.; O'Dwyer, M.; Santocanale, C. Characterization of a Dual CDC7/CDK9 Inhibitor in Multiple Myeloma Cellular Models. *Cancers (Basel).* **2013**, *5*, 901–18.

192. Erbayraktar, Z.; Alural, B.; Erbayraktar, R. S.; Erkan, E. P. Cell division cycle 7-kinase inhibitor PHA-767491 hydrochloride suppresses glioblastoma growth and invasiveness. *Cancer Cell Int.* **2016**, *16*, 88.

193. Huggett, M. T.; Tudzarova, S.; Proctor, I.; Loddo, M.; Keane, M. G.; Stoeber, K.; Williams, G. H.; Pereira, S. P. Cdc7 is a potent anti-cancer target in pancreatic cancer due to abrogation of the DNA origin activation checkpoint. *Oncotarget* **2016**, *7*, 18495–507.

194. Koltun, E. S.; Tsuhako, A. L.; Brown, D. S.; Aay, N.; Arcalas, A.; Chan, V.; Du, H.; Engst, S.; Ferguson, K.; Franzini, M.; Galan, A.; Holst, C. R.; Huang, P.; Kane, B.; Kim, M. H.; Li, J.; Markby, D.; Mohan, M.; Noson, K.; Plonowski, A.; Richards, S. J.; Robertson, S.; Shaw, K.; Stott, G.; Stout, T. J.; Young, J.; Yu, P.; Zaharia, C. a; Zhang, W.; Zhou, P.; Nuss, J. M.; Xu, W.; Kearney, P. C. Discovery of XL413, a potent and selective CDC7 inhibitor. *Bioorg. Med. Chem. Lett.* **2012**, *22*, 3727–31.

195. Sasi, N. K.; Tiwari, K.; Soon, F.-F.; Bonte, D.; Wang, T.; Melcher, K.; Xu, H. E.; Weinreich, M. The Potent Cdc7-Dbf4 (DDK) Kinase Inhibitor XL413 Has Limited Activity in Many Cancer Cell Lines and Discovery of Potential New DDK Inhibitor Scaffolds. *PLoS One* **2014**, *9*, e113300.

196. Chacón, R. D.; Costanzo, M. V Triple-negative breast cancer. *Breast Cancer Res.* **2010**, *12 Suppl 2*, S3.

197. Wahba, H. A.; El-Hadaad, H. A. Current approaches in treatment of triple-negative breast cancer. *Cancer Biol. Med.* **2015**, *12*, 106–16.

198. Morikawa, A.; Seidman, A. D. Treating Triple-Negative Breast Cancer : Where Are We ? *Arch. Pathol.* **2015**, *13*, 8–18.

199. Rodriguez-Acebes, S.; Proctor, I.; Loddo, M.; Wollenschlaeger, A.; Rashid, M.; Falzon, M.; Prevost, a T.; Sainsbury, R.; Stoeber, K.; Williams, G. H.

Targeting DNA replication before it starts: Cdc7 as a therapeutic target in p53-mutant breast cancers. *Am. J. Pathol.* **2010**, *177*, 2034–45.

200. Franken, N. a P.; Rodermond, H. M.; Stap, J.; Haveman, J.; van Bree, C. Clonogenic assay of cells in vitro. *Nat. Protoc.* **2006**, *1*, 2315–9.

201. L'Italien, L.; Tanudji, M.; Russell, L.; Schebye, X. M. Unmasking the redundancy between Cdk1 and Cdk2 at G2 phase in human cancer cell lines. *Cell Cycle* **2006**, *5*, 984–993.

202. Garriga, J.; Graña, X. CDK9 inhibition strategy defines distinct sets of target genes. *BMC Res. Notes* **2014**, *7*, 301.

203. Ji-Hu Zhang, Thomas D. Y. Chung, and K. R. O. A Simple Statistical Parameter for Use in Evaluation and Validation of High Throughput Screening Assays. *J Biomol Screen* **1999**, *4*, 67–73.

204. Malo, N.; Hanley, J. A.; Cerquozzi, S.; Pelletier, J.; Nadon, R. Statistical practice in high-throughput screening data analysis. *Nat Biotechnol* **2006**, *24*, 167–175.

205. Erickson, J. Standard Normal Probabilities. *African J. Bus. Manag.* **1867**, *33*, 465–468.

206. Im, J. S.; Lee, J. K. ATR-dependent activation of p38 MAP kinase is responsible for apoptotic cell death in cells depleted of Cdc7. *J. Biol. Chem.* **2008**, *283*, 25171–25177.

207. Tenca, P.; Brotherton, D.; Montagnoli, A.; Rainoldi, S.; Albanese, C.; Santocanale, C. Cdc7 is an active kinase in human cancer cells undergoing replication stress. *J. Biol. Chem.* **2007**, *282*, 208–15.

208. Salic, A.; Mitchison, T. J. A chemical method for fast and sensitive detection of DNA synthesis in vivo. *Proc. Natl. Acad. Sci. U. S. A.* **2008**, *105*, 2415–2420.

209. Sawa, M.; Masai, H. Drug design with Cdc7 kinase : a potential novel cancer therapy target and checkpoint regulation. *Drug Des. Devel. Ther.* **2008**, *2*, 255–264.

210. Vermes, I.; Haanen, C.; Steffens-Nakken, H.; Reutelingsperger, C. A novel assay for apoptosis. Flow cytometric detection of phosphatidylserine expression on early apoptotic cells using fluorescein labelled Annexin V. *J. Immunol. Methods* **1995**, *184*, 39–51.

211. Munshi, A.; Hobbs, M.; Meyn, R. E. Clonogenic cell survival assay. *Methods Mol. Med.* **2005**, *110*, 21–8.

212. Bousset, K.; Diffley, J. F. X. The Cdc7 protein kinase is required for origin firing during S phase. *Genes Dev.* **1998**, *12*, 480–490.

213. Krystof, V.; Baumli, S.; Furst, R. Perspective of Cyclin-dependent kinase 9 (CDK9) as a Drug Target. *Curr. Pharm. Des.* **2012**, *18*, 2883–2890.

214. Cai, D.; Latham, V. M.; Zhang, X.; Shapiro, G. I. Combined depletion of cell

cycle and transcriptional cyclin-dependent kinase activities induces apoptosis in cancer cells. *Cancer Res.* **2006**, *66*, 9270–9280.

215. Aleem, E.; Kiyokawa, H.; Kaldis, P. Cdc2-cyclin E complexes regulate the G1/S phase transition. *Nat. Cell Biol.* **2005**, *7*, 831–6.

216. Borel, F.; Lacroix, F. B.; Margolis, R. L. Prolonged arrest of mammalian cells at the G1 / S boundary results in permanent S phase stasis. **2002**.

217. Zhang, Z.-H.; Chung, T. D. Y.; Oldenburg, K. R. A Simple Statistical Parameter for Use in Evaluation and Validation of High Throughput Screening Assays. *J Biomol Screen* **1999**, *4*, 67–73.

218. Elkins, J. M.; Fedele, V.; Szklarz, M.; Abdul Azeez, K. R.; Salah, E.; Mikolajczyk, J.; Romanov, S.; Sepetov, N.; Huang, X.-P.; Roth, B. L.; Al Haj Zen, A.; Fourches, D.; Muratov, E.; Tropsha, A.; Morris, J.; Teicher, B. A.; Kunkel, M.; Polley, E.; Lackey, K. E.; Atkinson, F. L.; Overington, J. P.; Bamborough, P.; Müller, S.; Price, D. J.; Willson, T. M.; Drewry, D. H.; Knapp, S.; Zuercher, W. J. Supplementary Comprehensive characterization of the Published Kinase Inhibitor Set. *Nat. Biotechnol.* **2015**.

219. Drewry, D. H.; Willson, T. M.; Zuercher, W. J. Seeding collaborations to advance kinase science with the GSK Published Kinase Inhibitor Set (PKIS). *Curr. Top. Med. Chem.* **2014**, *14*, 340–342.

220. Elkins, J. M.; Fedele, V.; Szklarz, M.; Abdul Azeez, K. R.; Salah, E.; Mikolajczyk, J.; Romanov, S.; Sepetov, N.; Huang, X. P.; Roth, B. L.; Al Haj Zen, A.; Fourches, D.; Muratov, E.; Tropsha, A.; Morris, J.; Teicher, B. A.; Kunkel, M.; Polley, E.; Lackey, K. E.; Atkinson, F. L.; Overington, J. P.; Bamborough, P.; Muller, S.; Price, D. J.; Willson, T. M.; Drewry, D. H.; Knapp, S.; Zuercher, W. J. Comprehensive characterization of the Published Kinase Inhibitor Set. *Nat. Biotechnol.* **2016**, *34*, 95–103.

221. Kerns, E. H.; Di, L. Chapter 17 Toxicity. In *Drug-like Properties: Concepts, Structure Design and Methods from ADME to Toxicity Optimization*; Academic Press - Elsevier, 2008; pp. 215–223.

222. van Vugt, M. A.; Medema, R. H. Getting in and out of mitosis with Polo-like kinase-1. *Oncogene* **2005**, *24*, 2844–2859.

223. O'Connor, A.; Maffini, S.; Rainey, M. D.; Kaczmarczyk, A.; Gaboriau, D.; Musacchio, A.; Santocanale, C. Requirement for PLK1 kinase activity in the maintenance of a robust spindle assembly checkpoint. *Biol. Open* **2015**, *5*, 11–9.

224. Song, B.; Liu, X. S.; Davis, K.; Liu, X. Plk1 phosphorylation of Orc2 promotes DNA replication under conditions of stress. *Mol Cell Biol* **2011**, *31*, 4844–4856.

225. Song, B.; Liu, X. S.; Liu, X. Polo-like kinase 1 (Plk1): an Unexpected Player in DNA Replication. *Cell Div* **2012**, *7*, 3.

226. Ramer, M. D.; Suman, E. S.; Richter, H.; Stanger, K.; Spranger, M.;

Bieberstein, N.; Duncker, B. P. Dbf4 and Cdc7 proteins promote DNA replication through interactions with distinct Mcm2-7 protein subunits. *J. Biol. Chem.* **2013**, *288*, 14926–35.

227. Matthews, L. A.; Jones, D. R.; Prasad, A. A.; Duncker, B. P.; Guarne, A. Saccharomyces cerevisiae Dbf4 has unique fold necessary for interaction with Rad53 kinase. *J. Biol. Chem.* **2012**, *287*, 2378–2387.

228. Degenkolb, J.; Takahashi, M.; Ellestad, G. a; Hillenl, W. Structural requirements of tetracycline-Tet repressor interaction : determination of equilibrium binding constants for tetracycline Structural Requirements of Tetracycline-Tet Repressor Interaction : Determination of Equilibrium Binding Constants for Tetr. *Antimicrob. Agents Chemother.* **1991**, *35*, 1591.

229. Gossen, M.; Freundlieb, S.; Bender, G.; Moller, G.; Hillen, W.; Bujardt, H. Transcriptional Activation by Tetracyclines in Mammalian Cells Author ( s ): Manfred Gossen , Sabine Freundlieb , Gabriele Bender , Gerhard Müller , Wolfgang Hillen and Hermann Bujard Published by : American Association for the Advancement of Science Stab. *Science (80-. ).* **2016**, *268*, 1766–1769.

230. Berens, C.; Hillen, W. Gene regulation by tetracyclines: Constraints of resistance regulation in bacteria shape TetR for application in eukaryotes. *Eur. J. Biochem.* **2003**, *270*, 3109–3121.

231. Sato, N.; Sato, M.; Nakayama, M.; Saitoh, R.; Arai, K.; Masai, H. Cell cycle regulation of chromatin binding and nuclear localization of human Cdc7-ASK kinase complex. *Genes Cells* **2003**, *8*, 451–63.

232. Guo, B.; Romero, J.; Kim, B.-J.; Lee, H. High levels of Cdc7 and Dbf4 proteins can arrest cell-cycle progression. *Eur. J. Cell Biol.* **2005**, *84*, 927–38.

233. Oshiro, G.; Owens, J. C.; Shellman, Y.; Sclafani, R. a; Li, J. J. Cell cycle control of Cdc7p kinase activity through regulation of Dbf4p stability. *Mol. Cell. Biol.* **1999**, *19*, 4888–96.

234. Kitamura, R.; Fukatsu, R.; Kakusho, N.; Cho, Y.-S.; Taniyama, C.; Yamazaki, S.; Toh, G.; Yanagi, K.; Arai, N.; Chang, H.-J.; Masai, H. Molecular mechanism of activation of human Cdc7 kinase: bipartite interaction with Dbf4/activator of S phase kinase (ASK) activation subunit stimulates ATP binding and substrate recognition. *J. Biol. Chem.* **2011**, *286*, 23031–43.

235. Skerra, A.; Schmidt, T. G. M. Use of the Strep-Tag and streptavidin for detection and purification of recombinant proteins. *Methods Enzymol.* **2000**, *326*, 271–304.

236. Lichty, J. J.; Malecki, J. L.; Agnew, H. D.; Michelson-Horowitz, D. J.; Tan, S. Comparison of affinity tags for protein purification. *Protein Expr. Purif.* **2005**, *41*, 98–105.

237. Schmidt, T. G. M.; Skerra, A. The Strep-tag system for one-step purification and high-affinity detection or capturing of proteins. *Nat. Protoc.* **2007**, *2*, 1528–1535.

238. Wu, K. Z. L. L.; Wang, G. N.; Fitzgerald, J.; Quachthithu, H.; Rainey, M. D.; Cattaneo, A.; Bachi, A.; Santocanale, C. DDK dependent regulation of TOP2A at centromeres revealed by a chemical genetics approach. *Nucleic Acids Res.* **2016**, *44*, 8786–8798.

239. Rainey, M.; Quachthithu, H.; Gaboriau, D.; Santocanale, C. DNA Replication Dynamics and Cellular Responses To ATP Competitive Cdc7 Kinase Inhibitors. *ACS Chem. Biol.* **2017**, *12*, 18930–1902.

240. Einhauer, A.; Jungbauer, A. The FLAG peptide, a versatile fusion tag for the purification of recombinant proteins. *J. Biochem. Biophys. Methods* **2001**, *49*, 455–465.

241. Ishimi, Y.; Komamura-Kohno, Y.; Karasawa-Shimizu, K.; Yamada, K. Levels of MCM4 phosphorylation and DNA synthesis in DNA replication block checkpoint control. *J. Struct. Biol.* **2004**, *146*, 234–241.

242. Komamura-Kohno, Y.; Karasawa-Shimizu, K.; Saitoh, T.; Sato, M.; Hanaoka, F.; Tanaka, S.; Ishimi, Y. Site-specific phosphorylation of MCM4 during the cell cycle in mammalian cells. *FEBS J.* **2006**, *273*, 1224–39.

243. Gribble, F. M.; Loussouarn, G.; Tucker, S. J.; Zhao, C.; Nichols, C. G.; Ashcroft, F. M. A novel method for measurement of submembrane ATP concentration. *J. Biol. Chem.* **2000**, *275*, 30046–30049.

244. Chen, Y.; Jones, M. J. K.; Yin, Y.; Crist, S. B.; Colnaghi, L.; Iii, R. J. S.; Rothenberg, E.; Jallepalli, P. V; Huang, T. T. ATR-mediated phosphorylation of FANCI regulates dormant origin firing in response to replication stress. *Mol Cell* **2015**, *58*, 323–338.

245. Yekezare, M.; Gómez-González, B.; Diffley, J. F. X. Controlling DNA replication origins in response to DNA damage - inhibit globally, activate locally. *J. Cell Sci.* **2013**, *126*, 1297–306.

246. Randell, J. C. W.; Fan, A.; Chan, C.; Francis, L. I.; Heller, R. C.; Galani, K.; Bell, S. P. Mec1 is one of multiple kinases that prime the Mcm2-7 helicase for phosphorylation by Cdc7. *Mol. Cell* **2010**, *40*, 353–63.

247. Matsumoto, S.; Hayano, M.; Kanoh, Y.; Masai, H. Multiple pathways can bypass the essential role of fission yeast Hsk1 kinase in DNA replication initiation. *J. Cell Biol.* **2011**, *195*, 387–401.

248. Hochegger, H.; Takeda, S.; Hunt, T. Cyclin-dependent kinases and cell-cycle transitions: does one fit all? *Nat. Rev. Mol. Cell Biol.* **2008**, *9*, 910–916.

249. Bishop, P. C.; Myers, T.; Robey, R.; Fry, D. W.; Liu, E. T.; Blagosklonny, M. V; Bates, S. E. Diferential sensitivity of cancer cells to inhibitors of the epidermal growth factor receptor family. *Oncogene* **2002**, *21*, 119–127.

250. Walter, S. A.; Cutler, R. E.; Martinez, R.; Gishizky, M.; Hill, R. J. Stk10, a new member of the polo-like kinase kinase family highly expressed in hematopoietic tissue. *J. Biol. Chem.* **2003**, *278*, 18221–18228.

251. Chen, J.; Lin, J.; Tsai, F.; Meyer, T. Dosage of Dyrk1a shifts cells within a p21-cyclin D1 signaling map to control the decision to enter the cell cycle. *Mol Cell* **2013**, *52*, 87–100.

252. Hou, X.; Liu, J.; Liu, W.; Liu, C.; Liu, Z.; Sun, Z. A new role of NUAK1 : directly phosphorylating p53 and regulating cell proliferation. *Oncogene* **2011**, *30*, 2933–2942.

253. Liu, L.; Ulbrich, J.; Müller, J.; Wüstefeld, T.; Aeberhard, L.; Kress, T. R.; Muthalagu, N.; Rycak, L.; Rudalska, R.; Moll, R.; Kempa, S.; Zender, L.; Eilers, M.; Murphy, D. J. Deregulated MYC expression induces dependence upon AMPK-related kinase 5. *Nature* **2012**, *483*, 608–612.

254. Yoshino, Y.; Ishioka, C. Inhibition of glycogen synthase kinase-3 beta induces apoptosis and mitotic catastrophe by disrupting centrosome regulation in cancer cells. *Nat. Publ. Gr.* **2015**, 1–14.

255. Marchand, B.; Arsenault, D.; Raymond-Fleury, A.; Boisvert, F.-M.; and Boucher, M.-J. Glycogen Synthase Kinase-3 (GSK3) Inhibition Induces Prosurvival Autophagic Signals in Human Pancreatic Cancer Cells. *J Biol Chem* **2015**, *290*, 5592–605.

256. Sasai, K.; Katayama, H.; Stenoien, D. L.; Fujii, S.; Honda, R.; Kimura, M.; Okano, Y.; Tatsuka, M.; Suzuki, F.; Nigg, E. A.; Earnshaw, W. C.; Brinkley, W. R. Aurora-C Kinase Is a Novel Chromosomal Passenger Protein That Can Complement Aurora-B Kinase Function in Mitotic Cells. *Cell Motil. Cytoskeleton* **2004**, *59*, 249–263.

257. Payton, M.; Bush, T. L.; Chung, G.; Ziegler, B.; Eden, P.; McElroy, P.; Ross, S.; Cee, V. J.; Deak, H. L.; Hodous, B. L.; Nguyen, H. N.; Olivieri, P. R.; Romero, K.; Schenkel, L. B.; Bak, A.; Stanton, M.; Dussault, I.; Patel, V. F.; Geuns-Meyer, S.; Radinsky, R.; Kendall, R. L. Preclinical evaluation of AMG 900, a novel potent and highly selective pan-aurora kinase inhibitor with activity in taxane-resistant tumor cell lines. *Cancer Res.* **2010**, *70*, 9846–9854.

258. Saito-Hisaminato, A.; Katagiri, T.; Kakiuchi, S.; Nakamura, T.; Tsunoda, T.; Nakamura, Y. Genome-wide profiling of gene expression in 29 normal human tissues with a cDNA microarray. *DNA Res.* **2002**, *9*, 35–45.

259. Lin, M.-L.; Park, J.-H.; Nishidate, T.; Nakamura, Y.; Katagiri, T. Involvement of maternal embryonic leucine zipper kinase (MELK) in mammary carcinogenesis through interaction with Bcl-G, a pro-apoptotic member of the Bcl-2 family. *Breast Cancer Res.* **2007**, *9*, R17.

260. Oh, S.; Lee, D.; Kim, T.; Kim, T.-S.; Oh, H. J.; Hwang, C. Y.; Kong, Y.-Y.; Kwon, K.-S.; Lim, D.-S. Crucial role for Mst1 and Mst2 kinases in early embryonic development of the mouse. *Mol. Cell. Biol.* **2009**, *29*, 6309–20.

261. Zitouni, S.; Nabais, C.; Jana, S. C.; Guerrero, A.; Bettencourt-Dias, M. Polo-like kinases: structural variations lead to multiple functions. *Nat Rev Mol Cell Biol* **2014**, *15*, 433–452.

262. Wu, Z.-Q.; Liu, X. Role for Plk1 phosphorylation of Hbo1 in regulation of replication licensing. *Proc. Natl. Acad. Sci. U. S. A.* **2008**, *105*, 1919–24.

263. Rudolph, D.; Steegmaier, M.; Hoffmann, M.; Grauert, M.; Baum, A.; Quant, J.; Haslinger, C.; Garin-Chesa, P.; Adolf, G. R. BI 6727, a polo-like kinase inhibitor with improved pharmacokinetic profile and broad antitumor activity. *Clin. Cancer Res.* **2009**, *15*, 3094–3102.

264. Talati, C.; Griffiths, E. A.; Wetzler, M.; Wang, E. S. Polo-like kinase inhibitors in hematologic malignancies. *Crit. Rev. Oncol. Hematol.* **2016**, *98*, 200–210.

265. Matthews, L. a; Guarné, A.; Dbf, K. Dbf4: the whole is greater than the sum of its parts. *Cell Cycle* **2013**, *12*, 1180–8.

266. Park, Y. J.; Chodaparambil, J. V.; Bao, Y.; McBryant, S. J.; Luger, K. Nucleosome assembly protein 1 exchanges histone H2A-H2B dimers and assists nucleosome sliding. *J. Biol. Chem.* **2005**, *280*, 1817–1825.

267. Tell, G.; Quadrifoglio, F.; Tiribelli, C.; Kelley, M. R. The Many Functions of APE1/Ref-1: Not Only a DNA Repair Enzyme. *Antioxid. Redox Signal.* **2009**, *11*, 601–619.

# Appendix A

Supplementary figures of chapter 3. Experiment details were described.

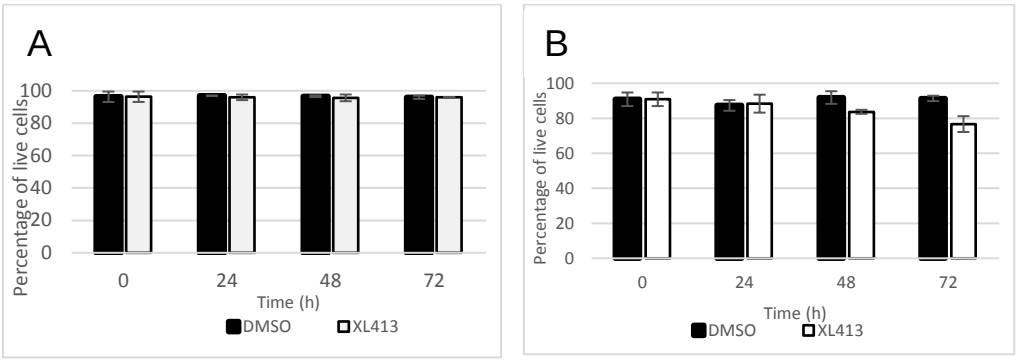


**Figure S3.1 Cell viability of MCF10A and MDA-MB-231 cells during the long-term treatment.**

Cells were seeded for 24 hours, then treated with inhibitor (XL413) or vehicle (DMSO) for 24, 48 and 72 hours. At each time point, cells were harvested and counted. Cell viability were also determined by Trypan Blue staining. Each treatment was performed in triplicate. (A) MCF10A; (B) MDA-MB-231. Each sample was performed in triplicate.

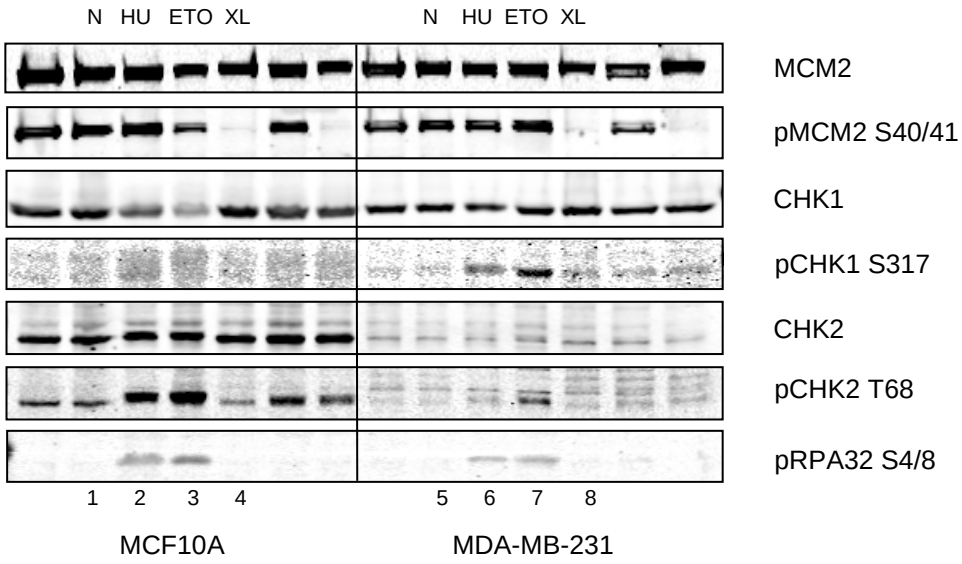


**Figure S3.2 XL413 does not activate DNA damage checkpoint in MCF10A and MDA-MB-231 cells.**

Cells were treated with XL413 (XL), Etoposide (Eto), HU or DMSO (N) for 24 hours, then harvested and pelleted. Total protein lysate was extracted by TCA extraction and subjected to immunoblotting.

# Appendix B

Supplementary figures of chapter 4. Experiment details were described in the figure legends or in chapter 4.

A

| Z' factor (PHA) | | | | |
|---|---|---|---|---|
| | | 1x10^3 cells | 2x10^3 cells | 4x10^3 cells |
| 48h treatment | 4H read | 0.212639895 | 0.665020899 | 0.716442637 |
| | 6H read | 0.164937602 | 0.682946451 | 0.741298171 |
| | 12H read | 0.182465146 | 0.672551883 | 0.843226473 |
| | | | | |
| | 4H read | 0.009275925 | 0.652252823 | 0.73626064 |
| | 6H read | -0.055639893 | 0.663830108 | 0.771428025 |
| | 12H read | -0.024722777 | 0.670859472 | 0.910897935 |
| | | | | |
| Z' factor (HU) | | | | |
| | | | | |
| 48h treatment | 4H read | -0.1881525 | 0.537298771 | 0.628797707 |
| | 6H read | -0.193164683 | 0.556089054 | 0.664946417 |
| | 12H read | -0.095223372 | 0.563797247 | 0.775927146 |
| | | | | |
| | 4H read | -0.511865935 | 0.525998616 | 0.646589146 |
| | 6H read | -0.563357386 | 0.541088325 | 0.692343855 |
| | 12H read | -0.419882089 | 0.563103248 | 0.843155151 |

B

| Z' factor (PHA) | | | | |
|---|---|---|---|---|
| | | 1x10^3 cells | 2x10^3 cells | 4x10^3 cells |
| 72h treatment | 4H read | 0.400577275 | 0.130103665 | 0.506884589 |
| | 6H read | 0.356228985 | 0.074446675 | 0.402157739 |
| | 12H read | 0.361311765 | 0.090094019 | 0.495574915 |
| | | | | |
| | 4H read | 0.453036613 | 0.168207819 | 0.411282696 |
| | 6H read | 0.375568999 | 0.124192426 | 0.536115401 |
| | 12H read | 0.384084646 | 0.148755864 | 0.68076453 |
| | | | | |
| Z' factor (HU) | | | | |
| | | 1x10^3 cells | 2x10^3 cells | 4x10^3 cells |
| 72h treatment | 4H read | 0.175564826 | -0.128561104 | 0.431406827 |
| | 6H read | 0.163759292 | -0.17721192 | 0.294566033 |
| | 12H read | 0.182517718 | -0.13635304 | 0.401961228 |
| | | | | |
| | 4H read | 0.194149764 | -0.063474832 | 0.304663033 |
| | 6H read | 0.122481277 | -0.095896812 | 0.465839778 |
| | 12H read | 0.157674139 | -0.049915546 | 0.620814278 |

**Figure S4.1 Z-factor of positive controls PHA-767491 (PHA) and HU in MCF10A cells.** Cells were plated at different densities and treated with drugs for different periods of time. AlamarBlue was added and measured after indicated time points. Each sample was plated in duplicate. Z-factor was calculated by MS Excel, according to Zhang *et al.* [203].

(A) 48h inhibitor treatment

(B) 72h inhibitor treatment

A

| Z' factor (PHA) | | | | |
|---|---|---|---|---|
| | | 2x10^3 cells | 4x10^3 cells | 8x10^3 cells |
| 48h treatment | 4H read | -0.152619562 | 0.576350784 | 0.651240995 |
| | 6H read | -0.198792008 | 0.617306159 | 0.772489409 |
| | 12H read | -0.132632901 | 0.671603093 | 0.816028269 |
| | | | | |
| | 4H read | -0.135727336 | 0.598469183 | 0.652928107 |
| | 6H read | -0.134814276 | 0.670579816 | 0.770143579 |
| | 12H read | -0.088161862 | 0.724097314 | 0.825510574 |
| | | | | |
| Z' factor (HU) | | | | |
| | | 2x10^3 cells | 4x10^3 cells | 8x10^3 cells |
| 48h treatment | 4H read | -3.183560541 | -0.812252543 | -0.230792824 |
| | 6H read | -3.224409141 | -0.628697926 | 0.227620756 |
| | 12H read | -2.813108431 | -0.33150107 | 0.418359508 |
| | | | | |
| | 4H read | -2.891345276 | -0.867843838 | -0.16768705 |
| | 6H read | -2.987337939 | -0.566290176 | 0.303213765 |
| | 12H read | -2.582300445 | -0.259662567 | 0.453762575 |

B

| Z' factor (PHA) | | | | |
|---|---|---|---|---|
| | | 2x10^3 cells | 4x10^3 cells | 8x10^3 cells |
| 72h treatment | 4H read | -0.467390847 | 0.572443374 | 0.571734193 |
| | 6H read | -0.512896262 | 0.562075435 | 0.592769105 |
| | 12H read | -0.437636888 | 0.609599956 | 0.648446867 |
| | | | | |
| | 4H read | -0.494587758 | 0.488823545 | 0.626069167 |
| | 6H read | -0.53276495 | 0.529982732 | 0.662219276 |
| | 12H read | -0.450597128 | 0.582270882 | 0.72269373 |
| | | | | |
| Z' factor (HU) | | | | |
| | | 2x10^3 cells | 4x10^3 cells | 8x10^3 cells |
| 72h treatment | 4H read | -2.093024854 | 0.036552448 | 0.075765153 |
| | 6H read | -2.189510133 | -0.02865186 | 0.12987666 |
| | 12H read | -1.987357999 | 0.093224841 | 0.223167527 |
| | | | | |
| | 4H read | -2.269634171 | -0.050434185 | 0.209550822 |
| | 6H read | -2.284012785 | -0.025206327 | 0.321938271 |
| | 12H read | -2.006173162 | 0.084900989 | 0.412121983 |

**Figure S4.2: Z-factor of positive controls PHA and HU in MDA-MB-231 cells.**
Cells were plated at different densities and treated with drugs for different periods of time. Alamar Blue was added and measured after indicated time points. Each sample was plated in duplicate. Z-factor was calculated by MS Excel, according to Zhang *et al.* [203].

(A) 48h inhibitor treatment
(B) 72h inhibitor treatment

| **10A** | Plate code | Substance_LOT_ID | \|Z-score (XL413)\| | POC (XL)- POC(DMSO) |
|---|---|---|---|---|
| 1 | Cp64 | GW801372X | 2.953557516 | 2.400502674 |
| 2 | Cp120 | GSK1751853A | 2.367635305 | 1.600966527 |
| 3 | Cp226 | GW778894X | 3.290801398 | 1.135507116 |
| 4 | Cp180 | SB-732881 | 2.874006395 | 1.038153602 |
| 5 | Cp47 | GW779439X | 3.028687857 | 0.177711505 |
| 6 | Cp154 | GSK1173862A | 2.764358729 | -0.852755121 |
| 7 | Cp293 | GW780056X | 2.980552034 | -1.572830908 |
| 8 | Cp254 | GW806290X | 3.383845193 | -2.043221832 |
| 9 | Cp85 | GSK1392956A | 2.367618528 | -2.815777452 |
| 10 | Cp83 | GSK1220512A | 2.838289767 | -3.176629759 |
| 11 | Cp20 | GSK2220400A | 2.615438486 | -3.87672628 |
| 12 | Cp118 | GSK1326255A | 2.987459772 | -3.992396157 |
| 13 | Cp18 | GW680191X | 2.447109569 | -9.530723906 |

**Figure S4.3 List of PKIS compounds that have Z-score higher than 2.33 in the screening with MCF10A cell line.**

Experiment details were described in section 4.4.3.

| **231** | Plate code | Substance_LOT_ID | \|Z-score (XL413)\| | POC (XL)-POC(DMSO) |
|---|---|---|---|---|
| 1 | Cp148 | GSK571989A | 3.278688778 | 6.83970615 |
| 2 | Cp293 | GW780056X | 3.325272846 | 3.572683355 |
| 3 | Cp226 | GW778894X | 4.631060826 | 0.807748076 |
| 4 | Cp254 | GW806290X | 4.59605098 | -2.137085723 |
| 5 | Cp47 | GW779439X | 4.628468606 | -3.0965536 |
| 6 | Cp64 | GW801372X | 3.38437316 | -7.507910005 |

**Figure S4.4: List of PKIS compounds that have Z-score higher than 2.33 in the screening with MDA-MB-231 cell line.**

Experiment details were described in section 4.4.3.

| **Cp18** | % Inhibition | Protein accession | Name |
|---|---|---|---|
| 1 | 97.65 | P00533 | Epidermal growth factor receptor erbB1 |
| 2 | 97.56 | P00533 | Epidermal growth factor receptor erbB1 |
| 3 | 96.79 | P00533 | Epidermal growth factor receptor erbB1 |
| 4 | 91.7 | P00533 | Epidermal growth factor receptor erbB1 |
| 5 | 85.43 | P00533 | Epidermal growth factor receptor erbB1 |
| 6 | 75.88 | P00533 | Epidermal growth factor receptor erbB1 |
| 7 | 75.42 | O94804 | Serine/threonine-protein kinase STK10 |
| 8 | 63.8 | Q15303 | Receptor protein-tyrosine kinase erbB-4 |
| 9 | 46.69 | Q9BUB5 | MAP kinase-interacting serine/threonine-protein kinase MNK1 |
| 10 | 39.51 | P11309 | Serine/threonine-protein kinase PIM1 |

**Figure S4.5: List of main kinases targeted by GW680191X (cp18).**

Experiment details were described in section 4.4.3.

| **Cp64** | % Inhibition | Protein accession | Name |
|---|---|---|---|
| 1 | 109.74 | P24941 | Cyclin-dependent kinase 2 |
| 2 | 99.86 | P49760 | Dual specificity protein kinase CLK2 |
| 3 | 99.2 | P49760 | Dual specificity protein kinase CLK2 |
| 4 | 98.13 | P10721 | Stem cell growth factor receptor |
| 5 | 97.26 | P10721 | Stem cell growth factor receptor |
| 6 | 96.2 | P10721 | Stem cell growth factor receptor |
| 7 | 95.87 | Q14289 | Protein tyrosine kinase 2 beta |
| 8 | 94.42 | Q9UQB9 | Serine/threonine-protein kinase Aurora-C |
| 9 | 94.25 | O14965 | Serine/threonine-protein kinase Aurora-A |
| 10 | 94.17 | P07333 | Macrophage colony stimulating factor receptor |

**Figure S4.6: List of main kinases targeted by GW801372X (cp64).**

Experiment details were described in section 4.4.3.

A

| Z' factor (HU) | | | | |
|---|---|---|---|---|
| | | 0.5x10^3 cells | 1x10^3 cells | 2x10^3 cells |
| 48h treatment | 4H read | 0.216825496 | 0.427593636 | 0.781220073 |
| | 6H read | 0.232096553 | 0.435025597 | 0.81066806 |
| | | | | |
| | | | | |
| Z' factor (PHA) | | | | |
| | | 0.5x10^3 cells | 1x10^3 cells | 2x10^3 cells |
| 48h treatment | 4H read | 0.188744353 | 0.436132913 | 0.804473682 |
| | 6H read | 0.224606391 | 0.452147247 | 0.842141314 |

B

| Z' factor (HU) | | | | |
|---|---|---|---|---|
| | | 0.5x10^3 cells | 1x10^3 cells | 2x10^3 cells |
| 72h treatment | 4H read | 0.476348668 | 0.649534383 | 0.882557656 |
| | 6H read | 0.527667735 | 0.677775665 | 0.914803181 |
| | | | | |
| | | | | |
| Z' factor (PHA) | | | | |
| | | 0.5x10^3 cells | 1x10^3 cells | 2x10^3 cells |
| 72h treatment | 4H read | 0.476489356 | 0.646662761 | 0.890069012 |
| | 6H read | 0.525219083 | 0.678213723 | 0.925471109 |

**Figure S4.7: Z-factor of positive controls PHA and HU in HAP1 WT cell line.**

Cells were plated at different densities and treated with drugs for different periods of time. AlamarBlue was added and measured after indicated time points. Z-factor was calculated according to Zhang *et al.* [203].

(A) 48h inhibitor treatment
(B) 72h inhibitor treatment

A

| Z' factor (HU) | | | | |
|---|---|---|---|---|
| | | 0.5x10^3 cells | 1x10^3 cells | 2x10^3 cells |
| 48h treatment | 4H read | 0.432983091 | 0.843133349 | 0.861787446 |
| | 6H read | 0.455519362 | 0.881766895 | 0.944247606 |
| | | | | |
| | | | | |
| Z' factor (PHA) | | | | |
| | | 0.5x10^3 cells | 1x10^3 cells | 2x10^3 cells |
| 48h treatment | 4H read | 0.431937949 | 0.834399533 | 0.853916252 |
| | 6H read | 0.448594103 | 0.874110488 | 0.936772593 |

B

| Z' factor (HU) | | | | |
|---|---|---|---|---|
| | | 0.5x10^3 cells | 1x10^3 cells | 2x10^3 cells |
| 72h treatment | 4H read | 0.673820706 | 0.881160061 | 0.948112429 |
| | 6H read | 0.71378507 | 0.920287497 | 0.966140166 |
| | | | | |
| | | | | |
| Z' factor (PHA) | | | | |
| | | 0.5x10^3 cells | 1x10^3 cells | 2x10^3 cells |
| 72h treatment | 4H read | 0.670998253 | 0.878169151 | 0.938660172 |
| | 6H read | 0.711960791 | 0.917222189 | 0.955462369 |

**Figure S4.8: Z-factor of positive controls PHA and HU in HAP1 4KO cell line.**

Cells were plated at different densities and treated with drugs for different periods of time. Alamar Blue was added and measured after indicated time points. Z-factor was calculated according to Zhang *et al.* [203].

(A) 48h inhibitor treatment
(B) 72h inhibitor treatment.

| HAP1 | Plate code | Substance_LOT_ID | \|Z-score (4KO)\| | POC(4KO)-POC(WT) |
|---|---|---|---|---|
| 1 | Cp273 | GW852849X | 2.500223667 | 14.71360473 |
| 2 | Cp245 | GSK317315A | 2.838544079 | 7.439553085 |
| 3 | Cp186 | GW843682X | 3.151173952 | 4.993617253 |
| 4 | Cp254 | GW806290X | 3.083963187 | 0.078397099 |
| 5 | Cp90 | SB-814597 | 2.988230376 | -0.016194887 |
| 6 | Cp293 | GW780056X | 2.569250097 | -0.022288774 |
| 7 | Cp47 | GW779439X | 3.364695298 | -0.057064349 |
| 8 | Cp148 | GSK571989A | 3.350575468 | -0.09327717 |
| 9 | Cp316 | GSK579289A | 2.55683591 | -0.137995007 |
| 10 | Cp226 | GW778894X | 3.844471235 | -1.836846909 |
| 11 | Cp64 | GW801372X | 2.82581668 | -9.174032997 |
| 12 | Cp103 | GW305178X | 2.398233892 | -9.938118912 |

**Figure S4.9 List of compounds have Z-score absolute value higher than 2.33 in HAP1 screening.**

Experiment details were described in section 4.5.3.

| Cp103 | % Inhibition | Protein accession | Name |
|---|---|---|---|
| 1 | 99.21 | Q00526 | Cyclin-dependent kinase 3 |
| 2 | 93.42 | Q14680 | Maternal embryonic leucine zipper kinase MELK |
| 3 | 93.38 | P24941 | Cyclin-dependent kinase 2 |
| 4 | 92.4 | P16234 | Platelet-derived growth factor receptor alpha |
| 5 | 92.31 | P16234 | Platelet-derived growth factor receptor alpha |
| 6 | 91.94 | Q9UQB9 | Serine/threonine-protein kinase Aurora-C |
| 7 | 91.78 | O14965 | Serine/threonine-protein kinase Aurora-A |
| 8 | 90.67 | P10721 | Stem cell growth factor receptor |
| 9 | 89.48 | Q13043 | Serine/threonine-protein kinase MST1 |
| 10 | 88.64 | P35968 | Vascular endothelial growth factor receptor 2 |
| 11 | 88.28 | Q13188 | Serine/threonine-protein kinase MST2 |
| 12 | 86.59 | P24941 | Cyclin-dependent kinase 2 |
| 13 | 85.96 | P35916 | Vascular endothelial growth factor receptor 3 |
| 14 | 85.37 | O60285 | NUAK family SNF1-like kinase 1 |
| 15 | 84.59 | Q13043 | Serine/threonine-protein kinase MST1 |
| 16 | 84.26 | P24941 | Cyclin-dependent kinase 2 |
| 17 | 83.42 | Q00535 | Cyclin-dependent kinase 5 |
| 18 | 83.06 | P24941 | Cyclin-dependent kinase 2 |
| 19 | 82.78 | P09619 | Platelet-derived growth factor receptor beta |
| 20 | 82.69 | P07949 | Tyrosine-protein kinase receptor RET |

**Figure S4.10: List of main kinases targeted by GW305178X (cp103).**

Experiment details were described in section 4.5.3.

| Cp273 | % inhibition | Protein accession | Name |
|---|---|---|---|
| 1 | 99 | O94804 | Serine/threonine-protein kinase 10 |
| 2 | 96.3 | P53350 | Serine/threonine-protein kinase PLK1 |
| 3 | 93.76 | P53350 | Serine/threonine-protein kinase PLK1 |
| 4 | 90.47 | P16234 | Platelet-derived growth factor receptor alpha |
| 5 | 86.49 | P09619 | Platelet-derived growth factor receptor beta |
| 6 | 83.35 | P16234 | Platelet-derived growth factor receptor alpha |
| 7 | 83 | Q12866 | Proto-oncogene tyrosine-protein kinase MER |
| 8 | 82.19 | P16234 | Platelet-derived growth factor receptor alpha |
| 9 | 69.73 | P16234 | Platelet-derived growth factor receptor alpha |
| 10 | 67.28 | O94804 | Serine/threonine-protein kinase 10 |

**Figure S4.11: List of main kinases targeted by GW852849X (cp273).**

Experiment details were described in section 4.5.3.

# Appendix C

Supplementary figures of chapter 5. Experiment details were described in the figure legends or in chapter 5.

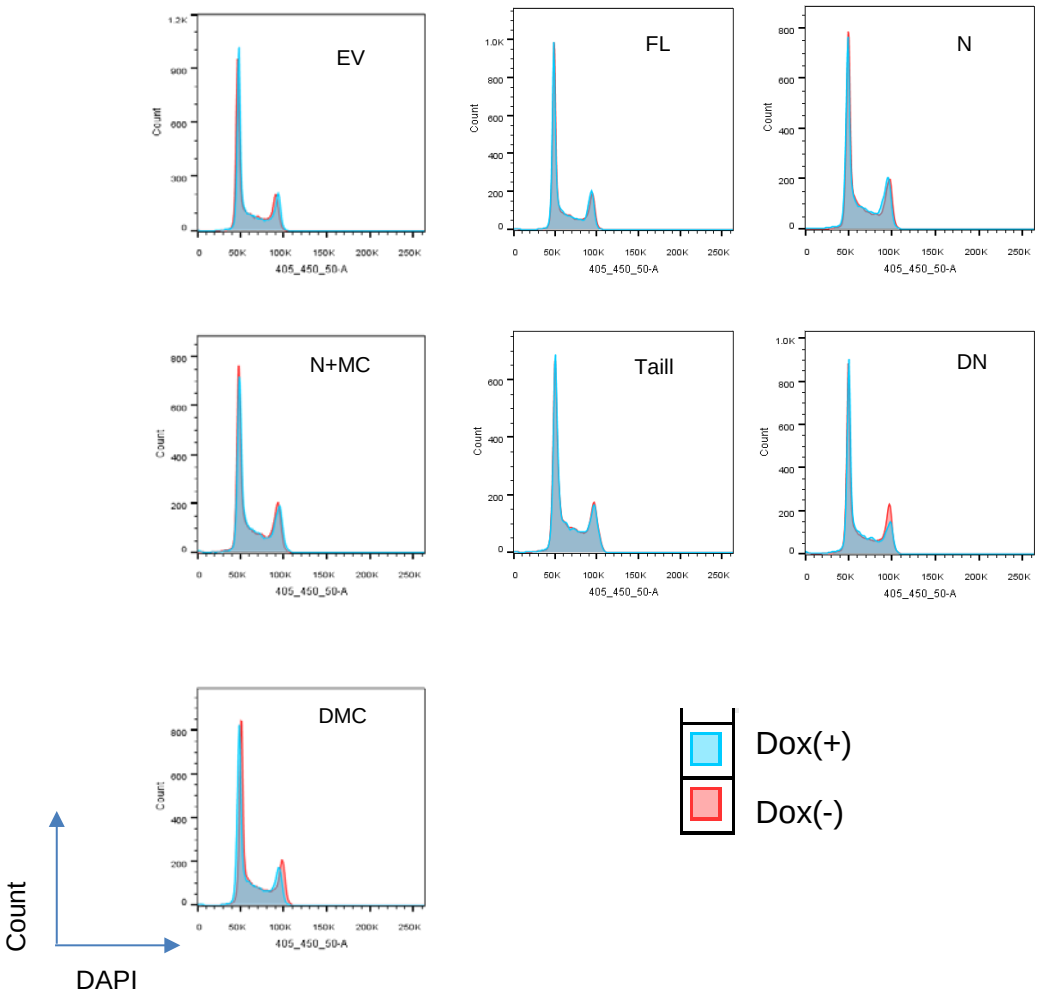


**Figure S5.1: Overlapped histogram of DBF4s-overexpressed TREx-293 cells after being treated with or without Doxycycline**

Cells were treated Doxycycline for 24 hrs, harvested and subjected to EdU/DAPI staining for flow cytometry.

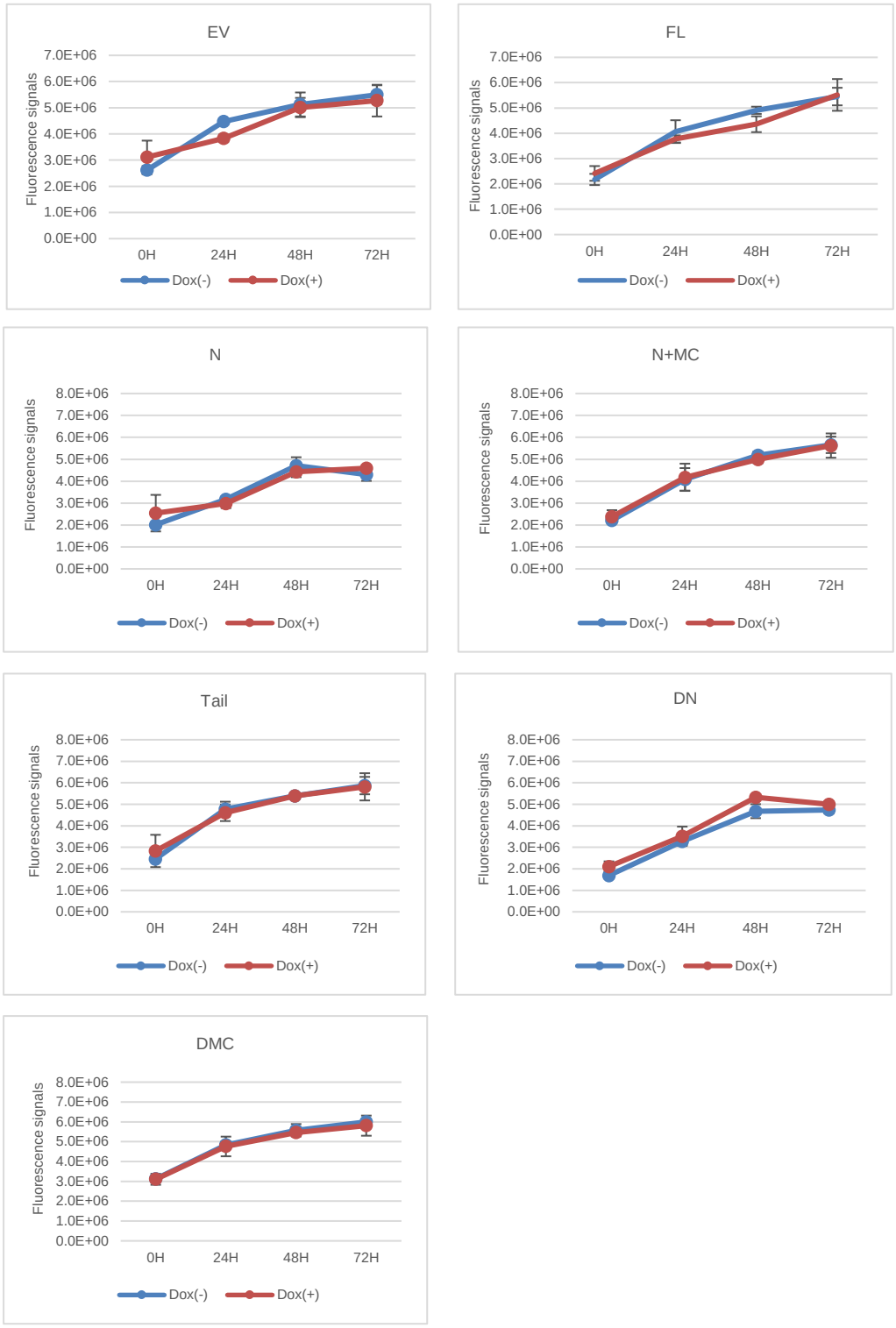


**Figure S5.2: Growth curve of DBF4s-overexpressed TREx-293 cells after being treated with or without Doxycycline**

Experiment details were described in section 5.3.2. Error bars represent the Mean ± SD.

# Published papers

1. M. Rainey, **H. Quachthithu,** D. Gaboriau, and C. Santocanale, “DNA Replication Dynamics and Cellular Responses To ATP Competitive Cdc7 Kinase Inhibitors,” *ACS Chem. Biol.*, 2017.

2. K. Z. L. Wu, G. N. Wang, J. Fitzgerald, **H. Quachthithu**, M. D. Rainey, A. Cattaneo, A. Bachi, and C. Santocanale, “DDK dependent regulation of TOP2A at centromeres revealed by a chemical genetics approach,” *Nucleic Acids Res.*, vol. 44, no. 18, pp. 8786–8798, 2016.

ACS chemical biology

Articles

pubs.acs.org/acschemicalbiology

# DNA Replication Dynamics and Cellular Responses to ATP Competitive CDC7 Kinase Inhibitors

Michael D. Rainey, Huong Quachthithu, David Gaboriau,‡ and Corrado Santocanale*

Centre for Chromosome Biology, School of Natural Sciences, National University of Ireland Galway H91 TK33, Ireland

Supporting Information

**ABSTRACT:** The CDC7 kinase, by phosphorylating the MCM DNA helicase, is a key switch for DNA replication initiation. ATP competitive CDC7 inhibitors are being developed as potential anticancer agents; however how human cells respond to the selective pharmacological inhibition of this kinase is controversial and not understood. Here we have characterized the mode of action of the two widely used CDC7 inhibitors, PHA-767491 and XL-413, which have become important tool compounds to explore the kinase's cellular functions. We have used a chemical genetics approach to further characterize pharmacological CDC7 inhibition and CRISPR/CAS9 technology to assess the requirement for kinase activity for cell proliferation. We show that, in human breast cells, CDC7 is essential and that CDC7 kinase activity is formally required for proliferation. However, full and sustained inhibition of the kinase, which is required to block the cell-cycle progression with ATP competitor compounds, is problematic to achieve. We establish that MCM2 phosphorylation is highly sensitive to CDC7 inhibition and, as a biomarker, it lacks in dynamic range since it is easily lost at concentrations of inhibitors that only mildly affect DNA synthesis. Furthermore, we find that the cellular effects of selective CDC7 inhibitors can be altered by the concomitant inhibition of cell-cycle and transcriptional CDKs. This work shows that DNA replication and cell proliferation can occur with reduced CDC7 activity for at least 5 days and that the bulk of DNA synthesis is not tightly coupled to MCM2 phosphorylation and provides guidance for the development of next generation CDC7 inhibitors.

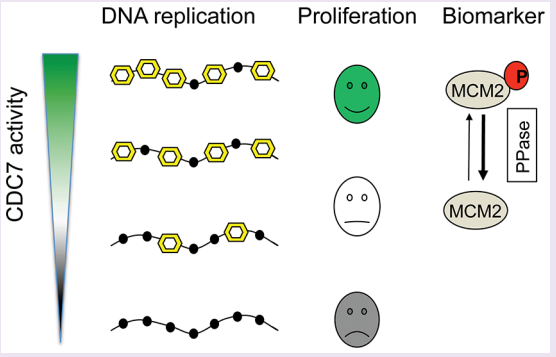


CDC7 serine/threonine kinase is considered a key molecular switch for the initiation of DNA replication in eukaryotic cells.[1] The MCM2−7 DNA helicase is its best-characterized substrate. It is generally accepted that CDC7-dependent phosphorylation is required for MCM helicase activation, promoting the recruitment of other proteins, such as CDC45, that are required to assemble and activate the initiation complex.[1] MCM phosphorylation by CDC7 occurs mainly on three subunits of the MCM complex, MCM2−4−6.[2] In particular CDC7 phosphorylation of MCM2 at Ser40 only occurs when Ser41 is also phosphorylated by a yet unidentified kinase, which acts as a priming event.[3] While MCM2 Ser41 phosphorylation is constitutive, phosphorylation on Ser40 fluctuates during the cell-cycle strictly correlating with CDC7 activity,[3] and it is considered a robust and reliable indicator or biomarker of cellular CDC7 activity.[3−5] CDC7 dependent phosphorylation of the MCM complex is counteracted by the protein phosphatase 1.[6−8] In S-phase, human CDC7 has other important functions, such as in the DNA replication stress response by phosphorylating the checkpoint mediator Claspin[9,10] and in the regulation of translesion DNA synthesis.[11]

The rationale for targeting CDC7 in cancers originates from multiple experiments assessing cellular phenotypes upon siRNA-mediated CDC7 depletion, which occurs over 48−72 h. We and others have shown that CDC7 depletion causes several cancer cell lines to arrest DNA synthesis and enter apoptosis, while primary fibroblasts only stop the cell-cycle. When CDC7 is depleted, p53 as well the transcription factor FOXO3A, the cyclin dependent kinase inhibitor $p15^{INK4}$, and the Wnt/b-catenin signaling antagonist DDK3 are important both for restraining DNA synthesis and preserving cell viability in primary and nontransformed cells, altogether defining the origin firing checkpoint pathway.[12,13] These studies highlighted the relevance of tumor suppressor proteins in the response to CDC7 inhibition, contributing to the vision of a CDC7 inhibitor-based therapy for the most aggressive p53 deficient cancers.

Despite this, it is not yet known what to expect from the inhibition of CDC7's enzymatic activity by small molecules, either at the cellular level or, even more so, in different tumor contexts, as the mechanism and kinetics of inhibition by small molecules are very different compared to protein depletion.[14]

Among the first described ATP competitive CDC7 inhibitors, PHA-767491 and XL-413 have become widely used tool compounds to probe the function of CDC7 in different cellular processes and conditions.[15−17] Intriguingly,

Received: February 9, 2017
Accepted: May 30, 2017
Published: May 31, 2017





DOI: 10.1021/acschembio.7b00117
ACS Chem. Biol. 2017, 12, 1893−1902

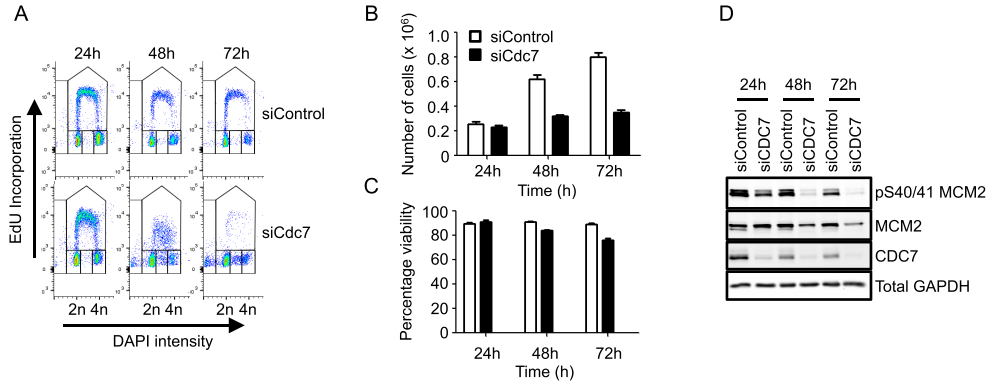


**Figure 1.** DNA replication and proliferation are impaired upon siRNA-mediated CDC7 depletion. MCF10A cells were subject to siRNA-mediated CDC7 knockdown for the indicated times and pulse-labeled with EdU prior to harvest. DNA content and EdU incorporation was assessed by flow cytometry (A), while cell proliferation (B) and viability (C) were monitored, in triplicate, using trypan blue exclusion cell counting. Soluble cell lysates were analyzed by SDS-PAGE and Western blotting (D).

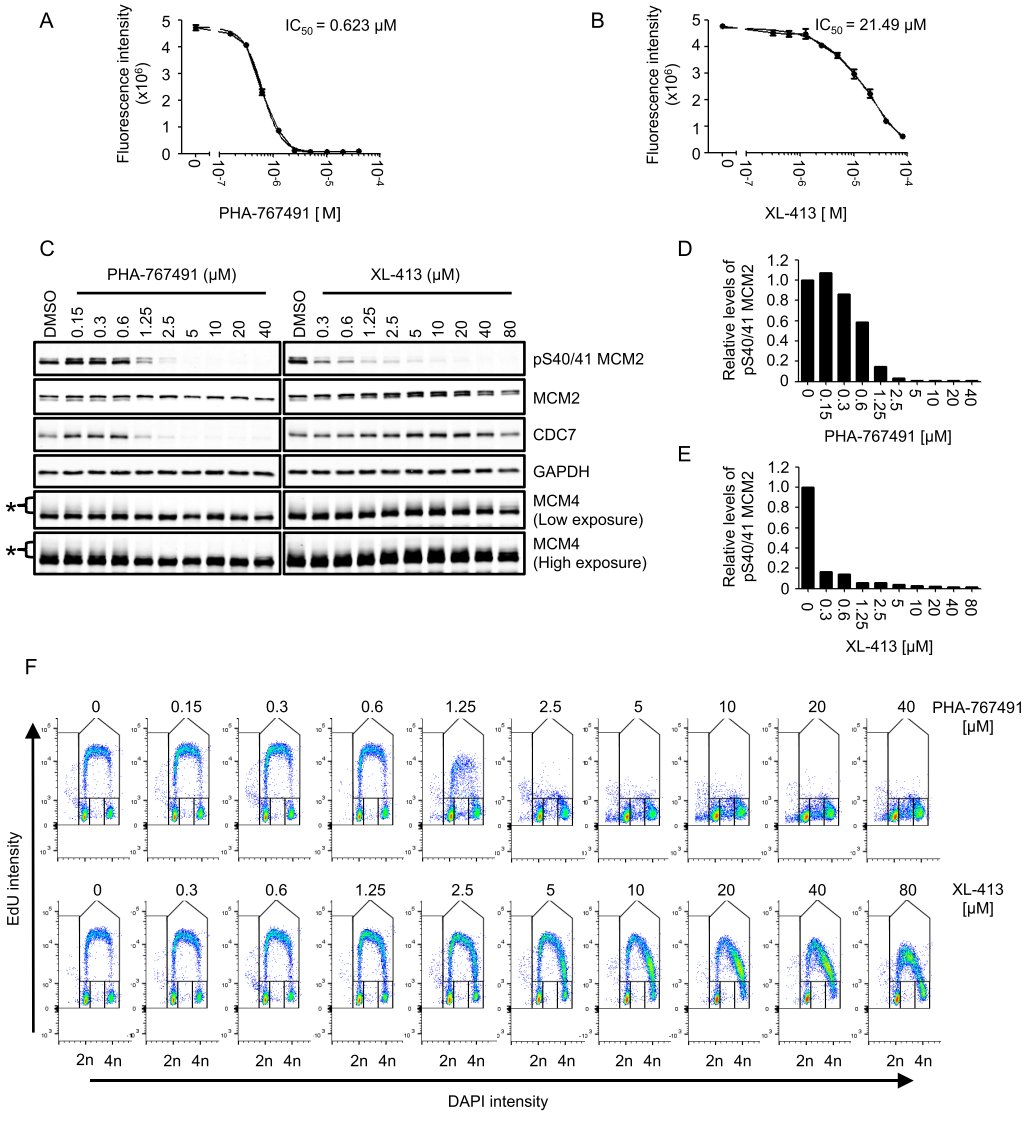


**Figure 2.** CDC7 inhibitors PHA-767491 and XL-413 exert dissimilar cellular responses. MCF10A cells were treated with DMSO or with the indicated doses of the CDC7 inhibitors PHA-767491 and XL-413. The resazurin reduction assay was performed 72 h following treatment to determine $IC_{50}$ values for cell growth (A and B). After 24 h of treatment, soluble protein extracts (C) were analyzed by SDS-PAGE and Western blotting and pS40/41 MCM2 levels were quantified (D and E). The MCM4 mobility shift attributed to phosphorylation is indicated (*). Cells were labeled with EdU for 30 min and analyzed by flow cytometry (F).



DOI: 10.1021/acschembio.7b00117
ACS Chem. Biol. 2017, 12, 1893−1902

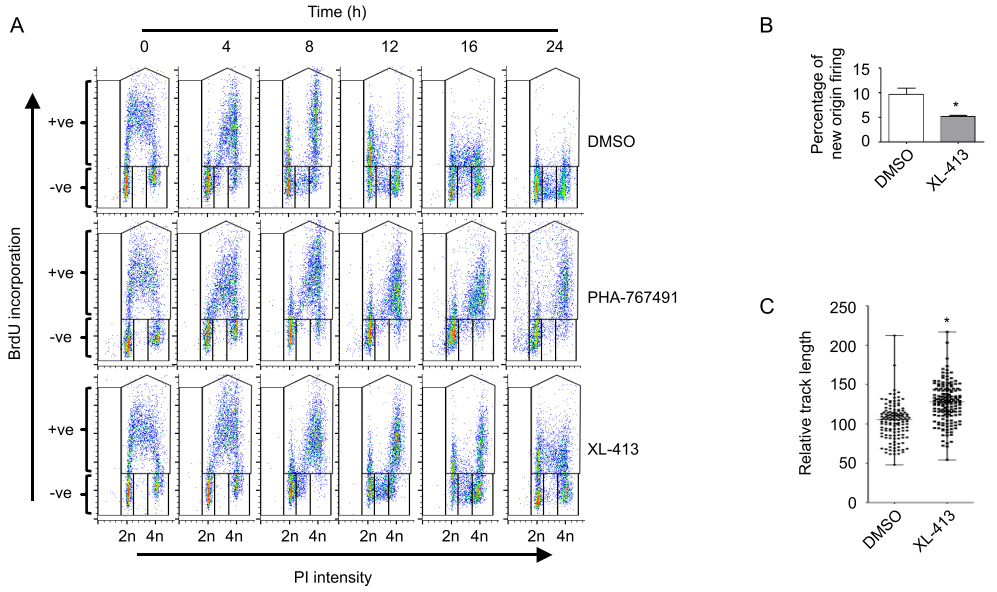


**Figure 3.** XL-413 slows S-phase progression but does not prevent entry into S or passage through mitosis. MCF10A cells were pulse-labeled with BrdU prior to treatment with DMSO or the CDC7 inhibitors XL-413 and PHA-767491. Samples were incubated for the indicated times before flow cytometric analysis and gating of BrdU-labeled (+ve) and BrdU-unlabeled (−ve) cell populations (A). Single-molecule analysis of DNA replication was performed by sequential labeling of nascent DNA with IdU/CldU-pulses either in the presence or absence of XL-413 during the labeling period. DNA fiber spreads were scored for ongoing, terminated/stalled forks, and new origin firing (B) and relative DNA track length (C). Three independent experiments were analyzed (*$p < 0.05$).

they have dramatically different effects on cells although they both inhibit CDC7 *in vitro* at similar nanomolar potency. Specifically PHA-767491 stops replication causing cell death in a wide range of cancer cell types,[18] while the activity of XL-413 is limited to few colorectal cancer derived cell lines.[4,19]

Notably, both compounds suffer from compound-specific off-target effects, with PHA-767491 also evidently inhibiting CDK9, presumably affecting the transcription of several genes, as well as other cell-cycle CDKs.[18,20,21] XL-413, which has much better specificity profile, still cross reacts with PIM1 and CK2 kinases.[20]

## RESULTS AND DISCUSSION

### Phenotypes Caused by CDC7 Depletion or Inhibition.

In order to understand the differences in the cellular responses after CDC7 inhibition or depletion, we focused our analysis on the epithelial MCF10A breast derived cells, which are immortalized cells with a near diploid karyotype and well-characterized cell cycle and checkpoint regulation and behave in a similar manner to human mammary epithelial primary cells (HMEpC) following CDC7 depletion.[22−24]

As expected, when CDC7 protein was depleted by siRNA, after 72 h post-transfection, MCF10A cells stopped DNA synthesis, arresting the cell cycle in either G1 or G2 with a strong block to proliferation and minimal loss of viability (Figure 1A,B,C). CDC7 depletion correlated with loss of phosphorylation of the MCM2 protein at the CDC7-dependent phosphorylation site Ser40/41 (Figure 1D), all in accordance with observations previously reported in primary dermal fibroblasts and MCF10A cells.[12,13,24] The same MCF10A cells were challenged with increasing concentration of CDC7 inhibitors, either PHA-767491 or XL-413, which have been shown to inhibit CDC7 with a similar potency in *in vitro* kinase assay,[19] and in a three day-long proliferation assay, we calculated an $IC_{50}$ of 0.62 $\mu$M for PHA-767491 and 21.49 $\mu$M for XL-413 (Figure 2A,B). Consistently in real-time monitoring, we observed that only concentrations above 25 $\mu$M of XL-413 caused a decrease in the proliferation rate (Supplementary Figure S1). Similar findings were observed using a fully transformed, p53 deficient breast cancer cell line, MDA-MB-231 (Supplementary Figure S2). After 24 h of treatment, MCM2 phosphorylation was strongly reduced at 0.3 $\mu$M XL-413 and at 1.25 $\mu$M of PHA-767491 and virtually abolished at 10 $\mu$M of both compounds (Figure 2C−E). In PHA-767491 treated cells this correlated with a profound blockade in DNA replication, with cells arresting in either G1 or G2 phases of the cell cycle. In contrast, XL-413 treated cells continued to synthesize DNA and, in a dose dependent manner, accumulated in mid to late S-phase consistent with a decrease in the rate of progressing through S-phase (Figure 2F). Interestingly, we observed that while the mobility shift of the MCM4 protein, known to be due to phosphorylation and shown to be at least partially CDC7 dependent in different systems,[2,8,25,26] was clearly abolished by low levels of PHA-767491, this was only possibly partially attenuated by XL-413 at all concentrations tested (Figure 2C). Most strikingly we noticed that the levels of CDC7 itself were strongly reduced by PHA-767491 but unaffected by XL-413 (Figure 2C−E).

Thus, although the two compounds are similarly potent in *in vitro* kinase reactions and in modulating MCM2 phosphorylation in cells, their potency in stopping proliferation is markedly different.

To further characterize the effects of the compounds on cell-cycle progression and DNA synthesis, S-phase MCF10A cells were pulse-labeled for 30 min with the thymidine analogue BrdU, followed by wash off and addition of fresh media containing either PHA-767491 or XL-413. In this and all of the following experiments, both compounds were used at 10 $\mu$M as this concentration severely compromises MCM2 phosphorylation. The progression of both BrdU-unlabeled (BrdU −ve) and BrdU-labeled (BrdU +ve) cells was then followed over 24


DOI: 10.1021/acschembio.7b00117
ACS Chem. Biol. 2017, 12, 1893−1902

h. Using this approach, we could determine that with PHA-767491 treatment the cells that were in S-phase (BrdU +ve) arrested in G2, while unlabeled G1 cells were completely prevented from entering S-phase. In contrast, XL-413 did not prevent passage of labeled cells through G2 and mitosis nor the entry into S-phase of unlabeled G1 cells. Importantly both compounds similarly delayed S-phase progression of the labeled cells compared to mock treated cells (Figure 3A). Analysis of DNA replication dynamics by the fiber labeling technique indicated that origin firing was decreased in cells treated with 10 $\mu$M XL-413, while the average speed of replication forks was increased (Figure 3B,C), a finding that is consistent with the compensatory mechanisms that occur when rate of origin firing is decreased and as previously determined with PHA-767491.[18,27]

Interestingly when the cells were cotreated with both PHA-767419 and XL-413, we found that the phenotype imposed by PHA-767491 was dominant over the one observed with XL-413 strongly suggesting that PHA-767491 has further activities important for preventing cell-cycle progression that are absent in XL-413 (Figure 4). Additionally, this observation excludes

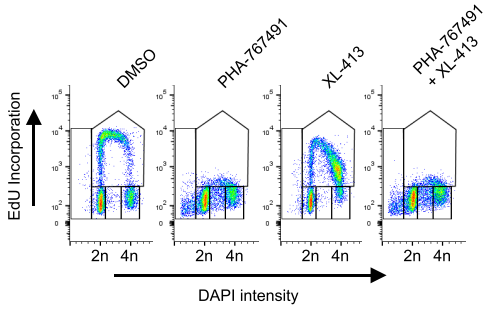


**Figure 4.** XL-413 does not override the cell cycle arrest imposed by PHA-767491. MCF10A cells were treated with DMSO or the CDC7 inhibitors XL-413 and PHA-767491 alone or in combination over a 16 h period. Cells were pulse labeled with EdU prior to harvest and flow cytometric analysis.

the possibility that off target effects of XL-413 could be causing bypass of the origin firing checkpoint, a response mechanism that limits entry into S-phase in response to CDC7 inhibition.[13]

Thus, we conclude that both compounds can inhibit cellular CDC7, that they similarly affect progression of the cells through S-phase, but that they cause profoundly different cellular responses mainly in the G1 and G2 phases of the cell cycle, with PHA-767491 more closely recapitulating the phenotypes observed by depletion of CDC7 by siRNA than XL-413.

At the molecular level, similarly to siRNA depletion, the treatment of cells with PHA-767491 results in a dramatic drop in CDC7 protein levels, and this observation may suggest that the absence of CDC7 protein could exacerbate the effects of kinase inhibition, possibly suggesting a scaffolding activity for the protein; however how PHA-767491 but not XL-413 causes the disappearance of CDC7 protein is not known. We first tested the hypothesis that PHA-767491 binding to CDC7 could alter its conformation leading to its degradation, but we observed that, in the presence of the protein synthesis inhibitor cycloheximide, CDC7 protein degradation rate was identical in mock or PHA-767491 treated cells (Figure 5A,B) and that in response to PHA-767491 alone, both soluble and chromatin bound forms of CDC7 are degraded alike (Figure 5C–E). We then measured mRNA levels by qPCR in untreated or XL-413 and PHA-767491 treated cells and found that not only CDC7, but also the mRNA levels of both CDC7 regulatory subunits DBF4 and DRF1 were profoundly decreased by PHA-767491 but not by XL-413 (Figure 5F,G). This is consistent with the idea that PHA-767491 affects transcription, most likely by targeting other cellular kinases and that the concomitant inhibition of multiple kinases could enhance the antiproliferative activity of a selective CDC7 inhibitor.

**Co-inhibition of CDC7 and CDKs.** In an attempt to determine the relevant kinases that modulate cellular responses to CDC7, we focused our attention on CDK1, CDK2, and CDK9 as major cell cycle and transcriptional kinases as well as potential (CDK1 and CDK2) or verified (CDK9) targets of PHA-767491.[18,20] MCF10A cells were transfected with siRNA against CDK1, CDK2, and CDK9, and after 24 h, XL-413 was added to the medium. After a further 24 h, cells were labeled with EdU, collected, and analyzed by flow-cytometry and Western blotting. Under these experimental conditions, none of the siRNA caused significant cell death; furthermore depletion of CDK2 and CDK9 did not obviously affect the distribution of cells in the cell-cycle, while CDK1 depletion led to an increase in cells with G2/M DNA content, which is likely due to prevented mitotic entry in a large fraction of the population. Notably we observed that the depletion of either one of these three kinases further increased the number of cells accumulating in late S-phase compared to XL-413 treatment alone, indicating cooperativity with CDC7 in promoting passage through S-phase (Figures 6A–C).

To further support this idea, subefficacious doses of a pan-CDK inhibitor, roscovitine, and of RO-3306, which preferentially targets CDK1, were identified with high content imaging (Supplementary Figure S3A,B). Both roscovitine and RO-3306 at 3 $\mu$M mildly reduced EdU incorporation but, when used in combination with XL-413, further attenuated DNA synthesis and caused cells to accumulate in late-S phase (Supplementary Figure S3C–E). Pulse–chase experiments further indicated that the partial inhibition of CDKs in combination with XL-413 resulted in a strong delay in S-phase entry and progression, while the treatments with roscovitine and RO-3306 alone had only marginal effects on the progression of cells through S-phase (Figures 6D,E and Supplementary Figure S3F).

These findings are consistent with the known roles of CDK1 and CDK2 in promoting and supporting DNA synthesis in a partially redundant manner[28−31] and possibly with the role of CDK9 in dealing with replication stress.[32] Intriguingly we found that levels of CDC7 protein are unchanged in CDK9 depleted cells, suggesting that the down-regulation of CDC7 observed in PHA-767491 treated cells is not solely caused by CDK9 inhibition.

Altogether these experiments indicate that off-target activities of compounds can significantly affect cellular responses to CDC7 inhibitors.

**Requirement for CDC7 Kinase Activity.** In order to better understand the phenotypes associated with specific inhibition of CDC7, we exploited a chemical genetic approach, known as "analogue sensitive kinase", where the gatekeeper residue of the kinase is mutated thus enlarging the ATP binding pocket allowing entry of bulky pyrazolopyrimidine compounds (PP1s). Binding of these compounds inhibit the engineered kinase with great specificity as they are too bulky to enter the ATP pocket of most other cellular kinases.[33−36] Analogue sensitive MCF10A (AS-CDC7) cells were generated by first


DOI: 10.1021/acschembio.7b00117
ACS Chem. Biol. 2017, 12, 1893−1902

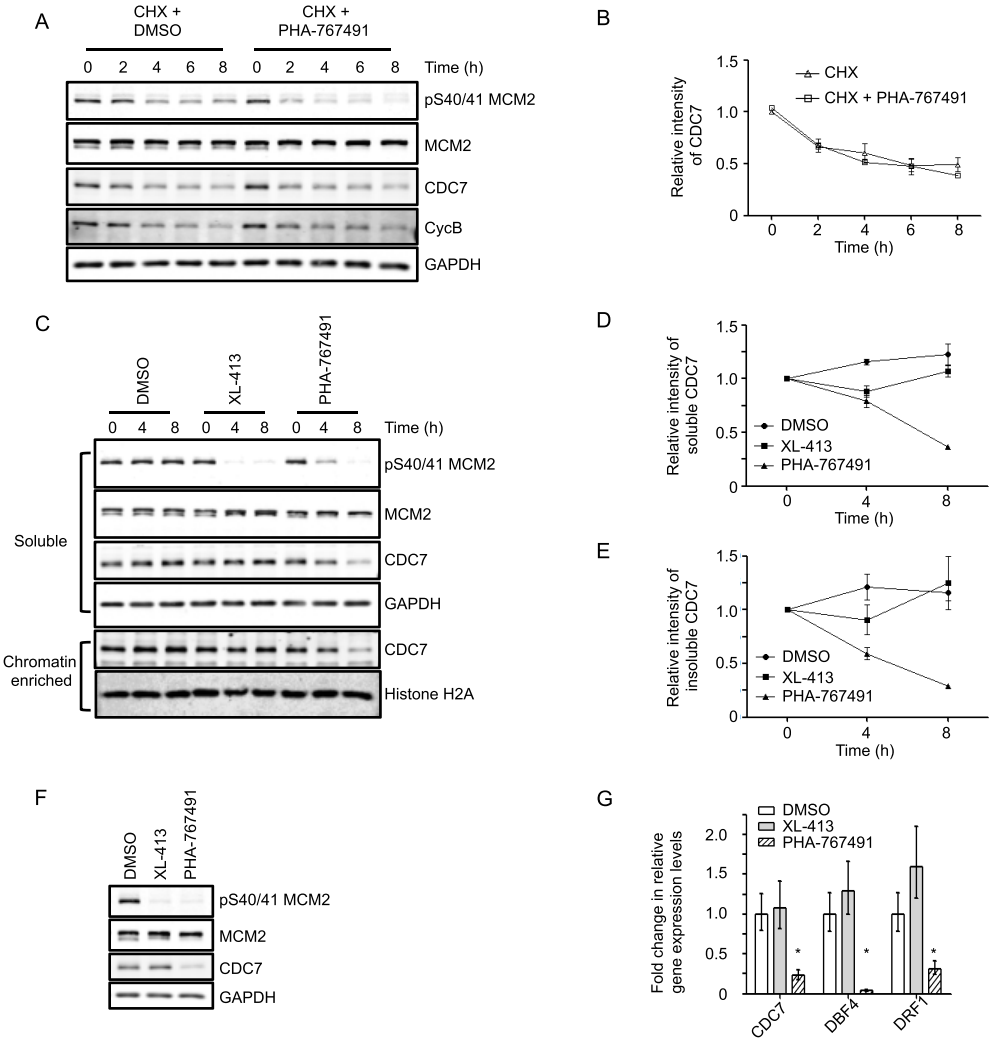


**Figure 5.** PHA-767491 down regulates gene expression of CDC7, DBF4, and DRF1. MCF10A cells were treated with DMSO or PHA-767491 (10 $\mu$M) in the presence of the protein synthesis inhibitor cycloheximide (20 $\mu$g/mL) or with DMSO, PHA-767491 (10 $\mu$M), or XL-413 (10 $\mu$M) alone for the indicated times. Soluble protein extracts (A and C) or chromatin enriched fractions (C) were analyzed by SDS-PAGE and Western blotting and relative CDC7 protein levels determined (B, D, and E). In panels F and G, cells were treated for 8 h with the indicated CDC7 inhibitors prior to harvest. Soluble protein extracts were analyzed by Western blotting (F), or total RNA was extracted and CDC7, DBF4, and DRF1 mRNA levels were determined by quantitative PCR (G). Three independent experiments were analyzed (*$p < 0.05$).

expressing a CRISPR resistant CDC7 transgene encoding for a M118A−M134A protein,[37] which were further infected with lentivirus expressing Cas9. Isolated clones were then transfected with small guide RNAs (sgRNAs) that targeted exon 4 of the endogenous CDC7 gene (Figure 7A). Clones were selected and the presence of biallelic null mutations were confirmed by PCR sequencing (Supporting Information and Supplementary figure S4, Tables 1.1 and 1.2).

AS-CDC7 cells grew at a normal rate and did not show obvious alterations in DNA replication dynamics or in progression through the cell-cycle (Figure 7B). When these cells were challenged for 24 h with the bulky inhibitor 3MB-PP1, we observed that MCM2 phosphorylation was suppressed at concentrations starting from 5 $\mu$M without loss of CDC7 protein (Figure 7C). Higher doses of 3MB-PP1 up to 25 $\mu$M also caused an accumulation of cells in mid to late S-phase but further dose escalation was prevented by toxicity of 3MB-PP1, and related compounds, seen also with the parental WT cell line (data not shown). These phenotypes are very similar to the ones observed with up to 10 $\mu$M XL-413, and these findings together can be rationalized either by the fact that CDC7 kinase activity is not strictly required for the bulk of DNA synthesis or by incomplete or lack of continuous inhibition of cellular CDC7.

To distinguish between these two possibilities, we devised a genetic assay to probe for the requirement of CDC7 kinase activity to form viable clones. We first established stable cell lines carrying CRISPR resistant transgenes coding for either WT or kinase dead K90A CDC7 that were further infected with lentivirus expressing Cas9 (MCF10A$^{\text{parental-WT-CDC7}}$ and MCF10A$^{\text{parental-KD-CDC7}}$). Clones expressing similar levels of either WT or KD CDC7 and Cas9 were selected and then transfected with the sgRNA targeting endogenous CDC7 (Figure 7A); as a control MCF10A cells only expressing Cas9 (MCF10A$^{\text{EditR}}$) were used. After stringent selection, surviving single cells were plated and allowed to form colonies that were further amplified and genotyped (Supplementary Tables 2.1, 2.2, and 2.3). Using this procedure and starting with MCF10A$^{\text{parental-WT-CDC7}}$ cells, we were able to identify clones with biallelic null mutations in the endogenous CDC7 gene at


DOI: 10.1021/acschembio.7b00117
ACS Chem. Biol. 2017, 12, 1893−1902

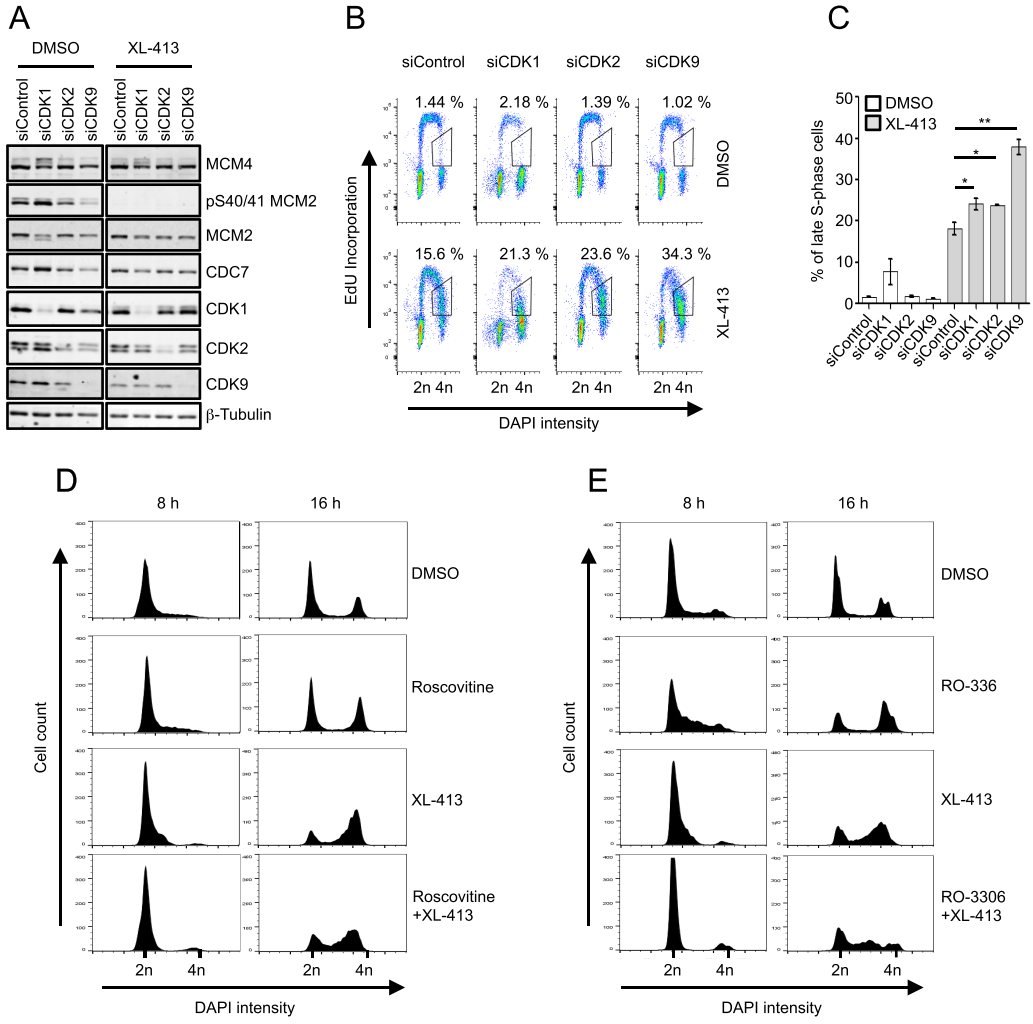


**Figure 6.** CDK inhibition cooperates with CDC7 inhibition in delaying S-phase progression. MCF10A cells were transfected with the indicated siRNAs and after 24 h were treated with DMSO or XL-413 for a further 24 h, then pulse-labeled with EdU and harvested. Soluble proteins were analyzed by Western blotting, and DNA synthesis and DNA content were analyzed by flow cytometry. Representative images from one experiment are shown (A and B). Percentage of late S-phase cells (EdU positive with near 4*N* DNA content) was calculated in three independent experiments (*$p < 0.05$; **$p < 0.005$) (C). MCF10A cells were pulse labeled with EdU before treatment with DMSO or XL-413 (10 $\mu$M) alone or in combination with subefficacious doses of (D) roscovitine (3 $\mu$M) or (E) RO-3306 (3 $\mu$M). Cells were then incubated for the indicated periods before flow cytometric analysis. The position of the EdU-negative cells (Supplementary Figure S3F) in the cell cycle after either 8 or 16 h is shown.

very high frequency, with 11 of 13 clones analyzed showing genetic rearrangements at the CDC7 loci, 9 of which were biallelic null mutations (Table 1 and Supplementary Table 2.1). In contrast when we started from the MCF10A$^{EditR}$ cell line we could not identify any clones with biallelic null mutations, although 6 of these clearly had undergone cutting and error prone DNA repair in the CDC7 gene (Table 1 and Supplementary Table 2.2). A lower rate of rearrangements is consistent with the idea that clones with biallelic null-mutation are selected against and only clones that have repaired by error-free homology directed DNA repair survive. Similarly using the MCF10A$^{parental\text{-}KD\text{-}CDC7}$ cell lines, after sequencing of 23 independent clones and the identification of at least 6 clones with rearrangements in the CDC7 gene, we failed to identify a single clone with null mutations in both copies of endogenous CDC7 (Table 1 and Supplementary Table 2.3). Together these results strongly indicate that CDC7 kinase activity is essential for cell proliferation and colony formation, although we cannot exclude that kinase independent functions may exist.

**CDC7 Biomarkers.** While a large number of preclinical drug discovery programs have been initiated to identify novel CDC7 inhibitors, to date there is little understanding of how these novel classes of agents perform in a cellular context and how to improve their characteristics. Our work clarifies several aspects of the mechanism of action of current CDC7 ATP competitive inhibitors in a cellular context. The use of highly selective inhibitors such as XL-413 up to 10 $\mu$M or 3MB-PP1 in the AS-CDC7 cells may suggest that the observable phenotype with pure CDC7 inhibitors would be a slow progression through S-phase without major effect on cell proliferation, and this is consistent with the fact that the modulation of the only available biomarker, MCM2 phosphorylation, is fully achieved. However, here we provide the formal demonstration that CDC7 activity is indeed required for proliferation in human cells.

In order to explain this apparent discrepancy, two key aspects of CDC7 biochemistry and biology should be considered: the first one is that CDC7 has a very high affinity for ATP with a calculated $K_m$ of 0.7 $\mu$M,[18] making it difficult to achieve


DOI: 10.1021/acschembio.7b00117
ACS Chem. Biol. 2017, 12, 1893−1902

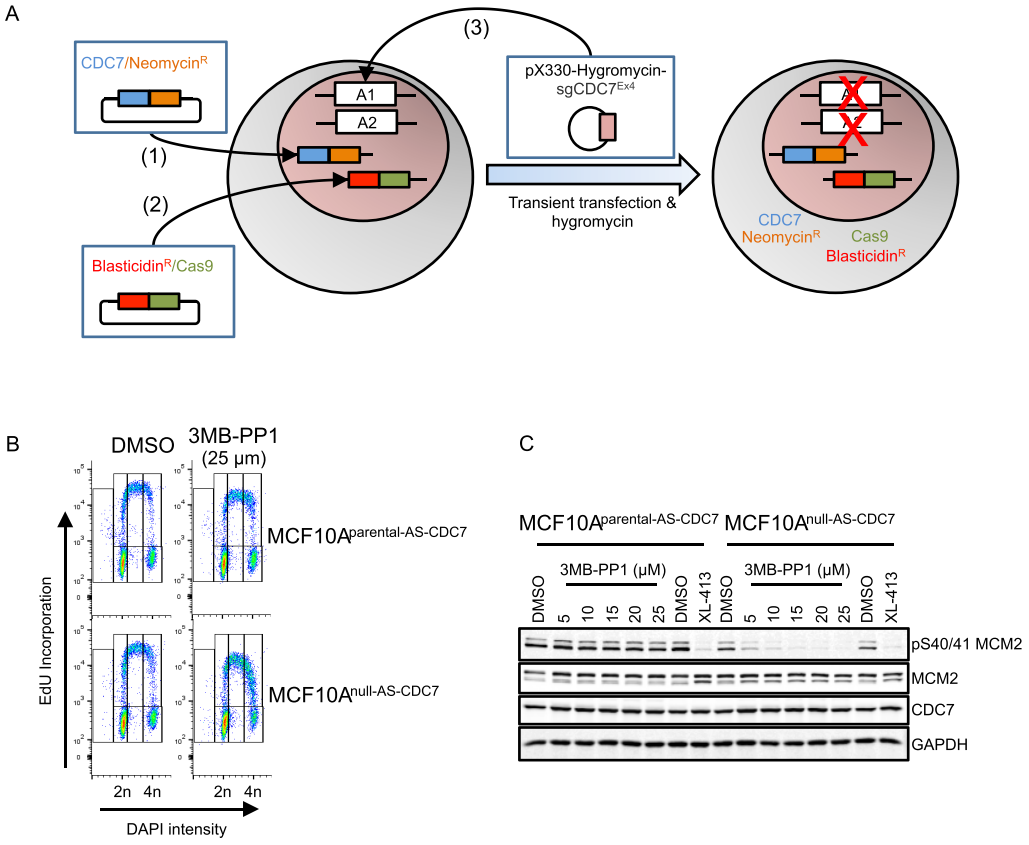


**Figure 7.** DNA replication delay and MCM2 dephosphorylation in an analogue-sensitive CDC7 kinase cell line upon 3MB-PP1 treatment. Strategy adopted for CRISPR/Cas9-mediated gene ablation and assessment of transgene-mediated rescue (A). Briefly, cells were transduced with CRISPR-resistant CDC7 variant transgenes and selected (1). CDC7 transgene expressing cells were subsequently transduced and selected for Cas9 expression (2). Finally, CRISPR-sgRNAs directed to exon 4 of genomic CDC7 (pX330−hygromycin−sgCDC7$^{Ex4}$) were transiently expressed and selected in these cells, followed by single cell cloning, expansion, isolation of genomic DNA, and sequencing to establish genotype. MCF10A$^{parental\text{-}AS\text{-}CDC7}$ and MCF10A$^{null\text{-}AS\text{-}CDC7}$ cells were treated with DMSO or the indicated doses of the bulky-PP1 inhibitor, 3MB-PP1, over a 24 h period. For flow cytometric analysis (B), cells were pulse labeled with EdU prior to harvest. Soluble protein lysates were also analyzed by SDS-PAGE and Western blotting (C).

**Table 1. Both CDC7 Protein and Its Kinase Activity Are Essential for Cell Proliferation**[a]

| | number of isolated clones with a particular genotype | | | | | | | |
|---|---|---|---|---|---|---|---|---|
| | homozygous | | | heterozygous | | | gene editing summary | |
| target cell line | wt/wt | null/null | Δif/Δif | wt/null | null/Δif | total number of clones | loci altered (%) | loci ablated (%) |
| MCF10a$^{EditR}$ | 8 | 0 | 0 | 6 | 0 | 14 | 43 [6/14] | 0 |
| MCF10a$^{parental\text{-}WT\text{-}CDC7}$ | 2 | 9 | 1 | 0 | 1 | 13 | 85 [11/13] | 69 [9/13] |
| MCF10a$^{parental\text{-}KD\text{-}CDC7}$ | 17 | 0 | 0 | 6 | 0 | 23 | 26 [6/23] | 0 |

[a]CRISPR/Cas9-mediated CDC7 gene ablation and assessment of transgene-mediated rescue (see text for details). The table summarizes the total number of clones recovered, their genotypes, and the percentages of gene editing events detected (Loci altered) and resulting biallelic null mutations (Loci ablated) in CDC7. WT = wild type; Δif = in frame deletion.

continuous and sustained inhibition in cellular environment where ATP concentration is in the millimolar range.[38,39] The second is related to the large abundance and redundancy of replication origins in the human genome[40] and that the full replication of the DNA can be achieved by activation of only a minority of DNA replication origins and under conditions where levels of MCM proteins are decreased.[40,41] Thus only strong and sustained CDC7 inhibition is expected to cause cell-cycle arrest.

MCM2 phosphorylation at Ser40 is an excellent pharmacodynamics marker for CDC7 inhibition and has been used widely for the development of CDC7 inhibitors. As a biomarker, its exquisite responsiveness to CDC7 inhibition is very likely related to the presence of very active counteracting protein phosphatases that target this specific phosphosite, and PP1 has been reported in yeast, *Xenopus*, and very recently human to be involved together with RIF1.[6−8,42,43] Thus only a partial downregulation of CDC7 may be sufficient to shift the balance from the phosphorylated to the unphosphorylated form; also it should be noted that the biological relevance of phosphorylation of MCM2 at this site is still unclear and unlikely to be required to promote DNA synthesis. Indeed it mainly occurs on soluble MCM2 protein that is not engaged on chromatin, and we previously suggested that it might contribute to preventing re-replication within the same cell cycle.[3] In contrast, MCM4 phosphorylation, generally detected as altered


DOI: 10.1021/acschembio.7b00117
ACS Chem. Biol. 2017, 12, 1893−1902

mobility shift in SDS-PAGE, in our experiments appears to be more resilient to CDC7 inhibition. This is either because CDC7 phosphorylation only marginally contributes to the overall changes in electrophoretic mobility of the protein or because its dephosphorylation is much less efficient than MCM2. Development of new immunological reagents detecting MCM4-phosphorylation at specific sites will be required to address this point.

The use of unusually high doses of XL-413 can stop cell proliferation although entry and progression through a slow S-phase is not impeded; this is possibly related to the fact that at these concentrations the CDC7 activity drops below the critical levels; however we cannot completely rule out that off-target effects may contribute to this phenotype. Indeed we show that concomitant inhibition of several kinases in the presence of a lower amount of XL-413 further affects S-phase progression. Thus while such cross-reactivities can be accepted and are possibly very beneficial in terms of anticancer activity, they should be taken under careful consideration when using CDC7 inhibitors as tool compounds to probe for the biological functions of CDC7.

Looking into the future of selective CDC7 inhibitors, we propose that the identification of more potent compounds with low dissociation rates or possibly nonreversible inhibitors could be the way to achieve the critical levels of kinase inhibition required to fully block DNA replication and cell proliferation in most cell types. This should also be accompanied by the development of less sensitive biomarkers with a greater dynamic range that could be better predictors of the efficacy of the compounds.

## METHODS

**Cell Culture and Chemicals.** MCF10A, MDA-MB-231, and HEK293T cells (ATCC) were maintained (37 °C, 5% $CO_2$) in a humidified atmosphere in complete media (Supporting Information). Cell proliferation and viability were determined using Trypan blue exclusion, cell counting (Countess, Invitrogen), resazurin reduction, or xCELLigence assays (Supporting Information). DNA and siRNA transfections and CRISPR/Cas9-mediated generation of MCF10A derived cell lines are described in Supporting Information. Cell culture reagents and chemicals were obtained from Sigma-Aldrich unless otherwise stated: PHA-767491 (Tocris), XL-413 (synthesized in house[10]), 3MB-PP1 (Cambridge biosciences), Hygromycin B and RO-3306 (Merck-Millipore), and EdU and 6-carboxy fluorescine TEG-azide (Berry and Associates).

**Protein Manipulations.** Cells were lysed in CSK buffer,[3] obtaining soluble extracts, while pellets were resuspended in Laemmli buffer (chromatin enriched fraction). Primary antibodies included pS40/41MCM2,[5] MCM2 (AbD-Serotec), CDC7 (MBL-international), histone-H2A (Merck-Millipore), GAPDH, CDK1, CDK2, CDK9, cyclin B1, and MCM4 (Santa-Cruz biotech.), and $\beta$-tubulin (Abcam). IRDye secondary antibodies (Li-COR) were used with the Odyssey infrared imaging system for detection.

**Cell Cycle and DNA Synthesis Analysis.** To label nascent DNA, cells were incubated with EdU (10 $\mu$M) or BrdU (25 $\mu$M) for 30 min prior to harvest or prior to further treatments. Cells were fixed (70% EtOH/PBS) and stained for BrdU/PI analysis,[12] or for EdU/DAPI analysis, incorporated-EdU was labeled with CLICK chemistry (10 $\mu$M 6-carboxyfluorescine-TEG-azide, 10 mM sodium-L-ascorbate, 2 mM copper(II) sulfate) for 30 min. Cells were washed (1% BSA, 5% Tween-20 in PBS), and DNA was stained with DAPI (1 $\mu$g/mL, 1% BSA/PBS). Data was acquired on a BD FACS Canto II and analyzed using FlowJo software.

**DNA Fiber Spreads.** Cells were labeled with 20 $\mu$M IdU for 30 min, media exchanged, and then labeled with 200 $\mu$M CldU for 30 min. DNA fibers were prepared and analyzed as previously described.[44,45] Images were captured with an IX71-Olympus microscope and 60 X oil-immersion objective. Measurements were performed with ImageJ software.

**Quantitative PCR.** Total RNA was isolated using Nucleospin RNA II kit (Macherey-Nagel). RNA (0.5 $\mu$g) was subject to SuperScript first-strand cDNA synthesis (Invitrogen) according to manufacturer's instructions. TaqMan assays (Thermo Fisher) for CDC7 (Hs00177487_m1), DBF4 (Hs00272696_m1), DRF1 (Hs01069195_m1), and 18s RNA (Hs99999901_s1) were used with FastStart Universal Probe Master Mix (Roche). Quantitative PCR was performed using the FastPlate protocol on a StepOne Plus quantitative PCR machine and analyzed with StepOne Plus v2.3 software.

## ASSOCIATED CONTENT

### Supporting Information

The Supporting Information is available free of charge on the ACS Publications website at DOI: 10.1021/acschembio.7b00117.

Supplementary methods, effects of CDC7 inhibitors on cell growth, MCM phosphorylation, DNA synthesis, cell cycle progression with CDK inhibitors, strategy to generate CDC7 KO, rescue of CDC7 ablation, and sequence data from CRISPR/Cas9 targeting experiments (PDF)

## AUTHOR INFORMATION


### Corresponding Author

*Tel +353-91-495174. E-mail: corrado.santocanale@nuigalway.ie.

### ORCID

Corrado Santocanale: 0000-0003-1337-5656

### Present Address

‡D.G.: FILM (Facility for Imaging by Light Microscopy), National Heart and Lung Institute, Imperial College London, London SW7 2AZ, United Kingdom.


### Author Contributions

M.D.R. designed and performed most of the experiments, H.Q. performed dose response and siRNA depletion experiments (Figure 6A,B and S2), D.G. analyzed Operetta high content images (Supplementary Figure S3A–E), and C.S. directed the research. C.S. and M.D.R. wrote the manuscript.


### Funding

This work was supported by Breast Cancer Now [2015MayPR506] and H.Q. by a Molecular Medicine Ireland fellowship.


### Notes

The authors declare no competing financial interest.

## ACKNOWLEDGMENTS

We thank A. O'Connor, R. O'Dea, E. McGarry, K. Wu, J. McAuliffe, and all the members of the Santocanale laboratory for support and discussion and S. Healy for reading and editing the manuscript. We also thank the NCBES Flow Cytometry and screening core facilities at NUIG, which are funded by NUIG and the Irish Government's Program PRTLI4-5.

## REFERENCES

(1) Sclafani, R. A., and Holzen, T. M. (2007) Cell cycle regulation of DNA replication. *Annu. Rev. Genet. 41*, 237–280.

(2) Masai, H., Taniyama, C., Ogino, K., Matsui, E., Kakusho, N., Matsumoto, S., Kim, J. M., Ishii, A., Tanaka, T., Kobayashi, T., Tamai,



DOI: 10.1021/acschembio.7b00117
*ACS Chem. Biol.* 2017, 12, 1893–1902

K., Ohtani, K., and Arai, K.-I. (2006) Phosphorylation of MCM4 by Cdc7 kinase facilitates its interaction with Cdc45 on the chromatin. *J. Biol. Chem. 281*, 39249−39261.
(3) Montagnoli, A., Valsasina, B., Brotherton, D., Troiani, S., Rainoldi, S., Tenca, P., Molinari, A., and Santocanale, C. (2006) Identification of Mcm2 phosphorylation sites by S-phase-regulating kinases. *J. Biol. Chem. 281*, 10281−10290.
(4) Koltun, E. S., Tsuhako, A. L., Brown, D. S., Aay, N., Arcalas, A., Chan, V., Du, H., Engst, S., Ferguson, K., Franzini, M., Galan, A., Holst, C. R., Huang, P., Kane, B., Kim, M. H., Li, J., Markby, D., Mohan, M., Noson, K., Plonowski, A., Richards, S. J., Robertson, S., Shaw, K., Stott, G., Stout, T. J., Young, J., Yu, P., Zaharia, C. A., Zhang, W., Zhou, P., Nuss, J. M., Xu, W., and Kearney, P. C. (2012) Discovery of XL-413, a potent and selective CDC7 inhibitor. *Bioorg. Med. Chem. Lett. 22*, 3727−3731.
(5) FitzGerald, J., Murillo, L. S., O'Brien, G., O'Connell, E., O'Connor, A., Wu, K., Wang, G.-N., Rainey, M. D., Natoni, A., Healy, S., O'Dwyer, M., and Santocanale, C. (2014) A High Through-Put Screen for Small Molecules Modulating MCM2 Phosphorylation Identifies Ryuvidine as an Inducer of the DNA Damage Response. *PLoS One 9*, e98891.
(6) Hiraga, S.-I., Alvino, G. M., Chang, F., Lian, H.-Y., Sridhar, A., Kubota, T., Brewer, B. J., Weinreich, M., Raghuraman, M. K., and Donaldson, A. D. (2014) Rif1 controls DNA replication by directing Protein Phosphatase 1 to reverse Cdc7-mediated phosphorylation of the MCM complex. *Genes Dev. 28*, 372−383.
(7) Dave, A., Cooley, C., Garg, M., and Bianchi, A. (2014) Protein Phosphatase 1 Recruitment by Rif1 Regulates DNA Replication Origin Firing by Counteracting DDK Activity. *Cell Rep. 7*, 53−61.
(8) Poh, W. T., Chadha, G. S., Gillespie, P. J., Kaldis, P., and Blow, J. J. (2014) Xenopus Cdc7 executes its essential function early in S phase and is counteracted by checkpoint-regulated protein phosphatase 1. *Open Biol. 4*, 130138−130138.
(9) Kim, J. M., Kakusho, N., Yamada, M., Kanoh, Y., Takemoto, N., and Masai, H. (2008) Cdc7 kinase mediates Claspin phosphorylation in DNA replication checkpoint. *Oncogene 27*, 3475−3482.
(10) Rainey, M. D., Harhen, B., Wang, G.-N., Murphy, P. V., and Santocanale, C. (2013) Cdc7-dependent and -independent phosphorylation of Claspin in the induction of the DNA replication checkpoint. *Cell Cycle 12*, 1560−1568.
(11) Yamada, M., Masai, H., and Bartek, J. (2014) Regulation and roles of Cdc7 kinase under replication stress. *Cell Cycle 13*, 1859−1866.
(12) Montagnoli, A., Tenca, P., Sola, F., Carpani, D., Brotherton, D., Albanese, C., and Santocanale, C. (2004) Cdc7 inhibition reveals a p53-dependent replication checkpoint that is defective in cancer cells. *Cancer Res. 64*, 7110−7116.
(13) Tudzarova, S., Trotter, M. W. B., Wollenschlaeger, A., Mulvey, C., Godovac-Zimmermann, J., Williams, G. H., and Stoeber, K. (2010) Molecular architecture of the DNA replication origin activation checkpoint. *EMBO J. 29*, 3381−3394.
(14) Weiss, W. A., Taylor, S. S., and Shokat, K. M. (2007) Recognizing and exploiting differences between RNAi and small-molecule inhibitors. *Nat. Chem. Biol. 3*, 739−744.
(15) Yamada, M., Watanabe, K., Mistrik, M., Vesela, E., Protivankova, I., Mailand, N., Lee, M., Masai, H., Lukas, J., and Bartek, J. (2013) ATR-Chk1-APC/CCdh1-dependent stabilization of Cdc7-ASK (Dbf4) kinase is required for DNA lesion bypass under replication stress. *Genes Dev. 27*, 2459−2472.
(16) Suzuki, T., Tsuzuku, J., Hayashi, A., Shiomi, Y., Iwanari, H., Mochizuki, Y., Hamakubo, T., Kodama, T., Nishitani, H., Masai, H., and Yamamoto, T. (2012) Inhibition of DNA damage-induced apoptosis through Cdc7-mediated stabilization of Tob. *J. Biol. Chem. 287*, 40256−40265.
(17) Liachko, N. F., McMillan, P. J., Guthrie, C. R., Bird, T. D., Leverenz, J. B., and Kraemer, B. C. (2013) CDC7 Inhibition Blocks Pathological TDP-43 Phosphorylation and Neurodegeneration. *Ann. Neurol. 74*, 39−52.
(18) Montagnoli, A., Valsasina, B., Croci, V., Menichincheri, M., Rainoldi, S., Marchesi, V., Tibolla, M., Tenca, P., Brotherton, D., Albanese, C., Patton, V., Alzani, R., Ciavolella, A., Sola, F., Molinari, A., Volpi, D., Avanzi, N., Fiorentini, F., Cattoni, M., Healy, S., Ballinari, D., Pesenti, E., Isacchi, A., Moll, J., Bensimon, A., Vanotti, E., and Santocanale, C. (2008) A Cdc7 kinase inhibitor restricts initiation of DNA replication and has antitumor activity. *Nat. Chem. Biol. 4*, 357−365.
(19) Sasi, N. K., Tiwari, K., Soon, F.-F., Bonte, D., Wang, T., Melcher, K., Xu, H. E., and Weinreich, M. (2014) The Potent Cdc7-Dbf4 (DDK) Kinase Inhibitor XL-413 Has Limited Activity in Many Cancer Cell Lines and Discovery of Potential New DDK Inhibitor Scaffolds. *PLoS One 9*, e113300.
(20) Hughes, S., Elustondo, F., Di Fonzo, A., Leroux, F. G., Wong, A. C., Snijders, A. P., Matthews, S. J., and Cherepanov, P. (2012) Crystal structure of human CDC7 kinase in complex with its activator DBF4. *Nat. Struct. Mol. Biol. 19*, 1101−1107.
(21) Natoni, A., Murillo, L. S., Kliszczak, A. E., Catherwood, M. A., Montagnoli, A., Samali, A., O'Dwyer, M., and Santocanale, C. (2011) Mechanisms of action of a dual Cdc7/Cdk9 kinase inhibitor against quiescent and proliferating CLL cells. *Mol. Cancer Ther. 10*, 1624−1634.
(22) Soule, H. D., Maloney, T. M., Wolman, S. R., Peterson, W. D., Brenz, R., McGrath, C. M., Russo, J., Pauley, R. J., Jones, R. F., and Brooks, S. C. (1990) Isolation and characterization of a spontaneously immortalized human breast epithelial cell line, MCF-10. *Cancer Res. 50*, 6075−6086.
(23) Marella, N. V., Malyavantham, K. S., Wang, J., Matsui, S. I., Liang, P., and Berezney, R. (2009) Cytogenetic and cDNA Microarray Expression Analysis of MCF10 Human Breast Cancer Progression Cell Lines. *Cancer Res. 69*, 5946−5953.
(24) Rodriguez-Acebes, S., Proctor, I., Loddo, M., Wollenschlaeger, A., Rashid, M., Falzon, M., Prevost, A. T., Sainsbury, R., Stoeber, K., and Williams, G. H. (2010) Targeting DNA replication before it starts: Cdc7 as a therapeutic target in p53-mutant breast cancers. *Am. J. Pathol. 177*, 2034−2045.
(25) Sheu, Y.-J., and Stillman, B. (2006) Cdc7-Dbf4 phosphorylates MCM proteins via a docking site-mediated mechanism to promote S phase progression. *Mol. Cell 24*, 101−113.
(26) Randell, J. C. W., Fan, A., Chan, C., Francis, L. I., Heller, R. C., Galani, K., and Bell, S. P. (2010) Mec1 is one of multiple kinases that prime the Mcm2−7 helicase for phosphorylation by Cdc7. *Mol. Cell 40*, 353−363.
(27) Conti, C., Saccà, B., Herrick, J., Lalou, C., Pommier, Y., and Bensimon, A. (2007) Replication fork velocities at adjacent replication origins are coordinately modified during DNA replication in human cells. *Mol. Biol. Cell 18*, 3059−3067.
(28) Labib, K. (2010) How do Cdc7 and cyclin-dependent kinases trigger the initiation of chromosome replication in eukaryotic cells? *Genes Dev. 24*, 1208−1219.
(29) Hochegger, H., Takeda, S., and Hunt, T. (2008) Cyclin-dependent kinases and cell-cycle transitions: does one fit all? *Nat. Rev. Mol. Cell Biol. 9*, 910−916.
(30) Ortega, S., Prieto, I., Odajima, J., Martin, A., Dubus, P., Sotillo, R., Barbero, J. L., Malumbres, M., and Barbacid, M. (2003) Cyclin-dependent kinase 2 is essential for meiosis but not for mitotic cell division in mice. *Nat. Genet. 35*, 25−31.
(31) Hochegger, H., Dejsuphong, D., Sonoda, E., Saberi, A., Rajendra, E., Kirk, J., Hunt, T., and Takeda, S. (2007) An essential role for Cdk1 in S phase control is revealed via chemical genetics in vertebrate cells. *J. Cell Biol. 178*, 257−268.
(32) Yu, D. S., Zhao, R., Hsu, E. L., Cayer, J., Ye, F., Guo, Y., Shyr, Y., and Cortez, D. (2010) Cyclin-dependent kinase 9-cyclin K functions in the replication stress response. *EMBO Rep. 11*, 876−882.
(33) Alaimo, P. J., Shogren-Knaak, M. A., and Shokat, K. M. (2001) Chemical genetic approaches for the elucidation of signaling pathways. *Curr. Opin. Chem. Biol. 5*, 360−367.
(34) Bishop, A. C., Ubersax, J. A., Petsch, D. T., Matheos, D. P., Gray, N. S., Blethrow, J., Shimizu, E., Tsien, J. Z., Schultz, P. G., Rose, M. D.,


DOI: 10.1021/acschembio.7b00117
*ACS Chem. Biol.* 2017, 12, 1893−1902

Wood, J. L., Morgan, D. O., and Shokat, K. M. (2000) A chemical switch for inhibitor-sensitive alleles of any protein kinase. *Nature 407*, 395−401.
(35) Zhang, C., Lopez, M. S., Dar, A. C., Ladow, E., Finkbeiner, S., Yun, C.-H., Eck, M. J., and Shokat, K. M. (2013) Structure-guided inhibitor design expands the scope of analog-sensitive kinase technology. *ACS Chem. Biol. 8*, 1931−1938.
(36) Lopez, M. S., Choy, J. W., Peters, U., Sos, M. L., Morgan, D. O., and Shokat, K. M. (2013) Staurosporine-derived inhibitors broaden the scope of analog-sensitive kinase technology. *J. Am. Chem. Soc. 135*, 18153−18159.
(37) Wu, K. Z. L., Wang, G.-N., FitzGerald, J., Quachthithu, H., Rainey, M. D., Cattaneo, A., Bachi, A., and Santocanale, C. (2016) DDK dependent regulation of TOP2A at centromeres revealed by a chemical genetics approach. *Nucleic Acids Res. 44*, 8786−8798.
(38) Yung-Chi, C., and Prusoff, W. H. (1973) Relationship between the inhibition constant (K1) and the concentration of inhibitor which causes 50% inhibition (I50) of an enzymatic reaction. *Biochem. Pharmacol. 22*, 3099−3108.
(39) Gribble, F. M., Loussouarn, G., Tucker, S. J., Zhao, C., Nichols, C. G., and Ashcroft, F. M. (2000) A novel method for measurement of submembrane ATP concentration. *J. Biol. Chem. 275*, 30046−30049.
(40) Alver, R. C., Chadha, G. S., and Blow, J. J. (2014) The contribution of dormant origins to genome stability: From cell biology to human genetics. *DNA Repair 19*, 182−189.
(41) Ge, X. Q., Jackson, D. A., and Blow, J. J. (2007) Dormant origins licensed by excess Mcm2−7 are required for human cells to survive replicative stress. *Genes Dev. 21*, 3331−3341.
(42) Hiraga, S.-I., Ly, T., Garzón, J., Hořejší, Z., Ohkubo, Y.-N., Endo, A., Obuse, C., Boulton, S. J., Lamond, A. I., and Donaldson, A. D. (2017) Human RIF1 and protein phosphatase 1 stimulate DNA replication origin licensing but suppress origin activation. *EMBO Rep. 18*, 403−419.
(43) Alver, R. C., Chadha, G. S., Gillespie, P. J., and Blow, J. J. (2017) Reversal of DDK-Mediated MCM Phosphorylation by Rif1-PP1 Regulates Replication Initiation and Replisome Stability Independently of ATR/Chk1. *Cell Rep. 18*, 2508−2520.
(44) Merrick, C. J., Jackson, D., and Diffley, J. (2004) Visualization of altered replication dynamics after DNA damage in human cells. *J. Biol. Chem. 279*, 20067−20075.
(45) McGarry, E., Gaboriau, D., Rainey, M. D., Restuccia, U., Bachi, A., and Santocanale, C. (2016) The Deubiquitinase USP9X Maintains DNA Replication Fork Stability and DNA Damage Checkpoint Responses by Regulating CLASPIN during S-Phase. *Cancer Res. 76*, 2384−2393.


DOI: 10.1021/acschembio.7b00117
*ACS Chem. Biol.* 2017, 12, 1893−1902

*8786–8798* *Nucleic Acids Research, 2016, Vol. 44, No. 18* *Published online 12 July 2016*
*doi: 10.1093/nar/gkw626*

# DDK dependent regulation of TOP2A at centromeres revealed by a chemical genetics approach

**Kevin Z. L. Wu[1], Guan-Nan Wang[1], Jennifer Fitzgerald[1], Huong Quachthithu[1], Michael D. Rainey[1], Angela Cattaneo[2], Angela Bachi[2] and Corrado Santocanale[1,*]**

[1]Centre for Chromosome Biology, School of Natural Sciences, National University of Ireland Galway, Ireland and [2]IFOM-FIRC Institute of Molecular Oncology, Milan 20139, Italy

Received December 18, 2015; Revised June 30, 2016; Accepted July 02, 2016

## ABSTRACT

**In eukaryotic cells the CDC7/DBF4 kinase, also known as DBF4-dependent kinase (DDK), is required for the firing of DNA replication origins. CDC7 is also involved in replication stress responses and its depletion sensitises cells to drugs that affect fork progression, including Topoisomerase 2 poisons. Although CDC7 is an important regulator of cell division, relatively few substrates and bona-fide CDC7 phosphorylation sites have been identified to date in human cells. In this study, we have generated an active recombinant CDC7/DBF4 kinase that can utilize bulky ATP analogues. By performing *in vitro* kinase assays using benzyl-thio-ATP, we have identified TOP2A as a primary CDC7 substrate in nuclear extracts, and serine 1213 and serine 1525 as *in vitro* phosphorylation sites. We show that CDC7/DBF4 and TOP2A interact in cells, that this interaction mainly occurs early in S-phase, and that it is compromised after treatment with CDC7 inhibitors. We further provide evidence that human DBF4 localises at centromeres, to which TOP2A is progressively recruited during S-phase. Importantly, we found that CDC7/DBF4 down-regulation, as well S1213A/S1525A TOP2A mutations can advance the timing of centromeric TOP2A recruitment in S-phase. Our results indicate that TOP2A is a novel DDK target and have important implications for centromere biology.**

## INTRODUCTION

In order to divide, cells must completely and accurately replicate their DNA once every cell cycle. Incomplete or over-replication can lead to cell death or genomic instability, which is a major contributing factor in the development of cancer (1,2). As such, DNA replication is a tightly regulated and monitored process (reviewed in (3,4)). The DBF4-dependent kinase (DDK), which is a complex formed by the CDC7 catalytic subunit bound to either DBF4 or DBF4B (5,6) is involved in multiple aspects of the regulation of DNA replication. It is required for the firing of replication origins by phosphorylating multiple subunits of the MCM2-7 helicase complex (7–9). In addition, CDC7 kinase has important roles in the replication stress response and chromatin function. For instance, in human cells CDC7 phosphorylation of the mediator protein CLASPIN is important for full activation of CHK1 by ATR and for maintaining cell viability in the presence of drugs that affect replication fork progression (10–12,13). Also, CDC7 phosphorylation of RAD18 is required for the efficient recruitment of the translesion synthesis (TLS) polymerase Polη to stalled forks (14,15). In human cells, CDC7 kinase has also been shown to affect the function of the p150 Chromatin Assembly Factor 1 (CAF1) subunit (16), while in yeast it participates in the control of core histone levels (17), contributes to centromeric heterochromatin function (18), and directly phosphorylates Histone H3 at Ser45 during replication (19). Importantly, several laboratories have elucidated the role of CDC7 kinase in controlling the formation of DNA double strand breaks during meiotic DNA replication to promote meiotic recombination (20–25).

In recent years, a chemical genetics approach has been developed that provides a novel tool for inhibiting a specific kinase. The target kinase is mutated at a specific residue in the ATP binding pocket, termed a 'gatekeeper' residue, and this mutation enlarges the binding site sufficiently to allow entry and binding of novel small-molecule inhibitors, namely bulky pyrazolo pyrimidine compounds (PP1s) and novel staurosporine derivatives. Binding of these compounds can inhibit the engineered kinase but they are too bulky to enter the ATP pocket of other cellular kinases and are therefore unable to inhibit them (26,27). This approach has been

*To whom correspondence should be addressed. Tel: +353 91 495174; Email: corrado.santocanale@nuigalway.ie
Present addresses:
Kevin Z. L. Wu, MRC ProteinPhosphorylation and Ubiquitylation Unit, University of Dundee, Dundee, UK.
Jennifer Fitzgerald, Eli Lilly S.A. Irish Branch, Kinsale, Ireland.

widely used in a variety of organisms from budding yeast to cultured human cells and transgenic mice with the specific goal of studying the function of a given kinase (28,29). However, the identification of direct substrates and phosphorylation sites is still a challenging task. A recent important advance in this kinase chemical genetics approach was the finding that the engineered kinase can now accept and utilize an unnatural and bulky ATP analogue ($N^6$-(benzyl)ATP). These analogues are very poor substrates for wild-type kinases, thus only the analogue-sensitive kinase (AS-kinase) can use the bulky ATP analogue. Further modification of this analogue into $N^6$-(benzyl)ATP-γ-S (benzyl-thio-ATP) allows the transfer of a thio-phosphate reactive group as a distinctive molecular tag by the AS-kinase onto the substrate protein. Therefore, after an *in vitro* kinase reaction and further derivatization of these reactive groups with p-nitrobenzylmesylate (PNBM), labeled proteins that are direct substrates of the AS-kinase can be detected by western blotting (30). Furthermore, peptides containing this unique thio-phosphate modification can be specifically captured from digests of labeled protein mixtures; mass spectrometry is then used to reveal the identity of the corresponding protein species and the location of the phosphorylation site(s) (28,31–33).

In order to obtain further insights into possible substrates and roles of human DDK in the mitotic cell cycle, we have used the above-described approach and identified Topoisomerase 2 alpha (TOP2A) as a prime *in vitro* substrate of the kinase. Topoisomerase 2 (TOP2) enzymes resolve DNA catenates that form during DNA replication by catalysing the transient breakage and religation of duplex DNA, while allowing the passage of a second duplex through the gap (34,35). Of the two isoforms present in humans, only the alpha isoform, TOP2A, is essential for proliferation of cultured cells (36). Although reportedly dispensable for DNA replication, TOP2A is essential for proper chromosome condensation and sister chromatid separation, as TOP2A-deficient cells exhibit an increased number of amorphous and severely entangled chromosomes (36,37). TOP2A also plays an important role in resolving ultrafine anaphase DNA bridges arising from centromeric loci (38,39).

We have previously reported that treatment with etoposide, a TOP2 poison that prevents the religation step of the TOP2 catalytic cycle, thus stabilizing an intermediate TOP2-DNA covalent complex (40,41), induced more extensive cell death when cells were also depleted of CDC7 (10). The increased sensitivity to etoposide may be due to the roles of CDC7 in the general response to replication stress, or could perhaps reflect a functional interaction between CDC7 kinase and TOP2. In this study, we explored the latter hypothesis and we found that CDC7/DBF4 physically and functionally interacts with TOP2A in human cells.

## MATERIALS AND METHODS

### Cell culture and chemicals

Flp-In T-REx 293 cells (Invitrogen) and U2OS (obtained from the Centre for Chromosome Biology, NUI Galway, and validated by STR analysis), were grown in Dulbecco's modified Eagle's medium containing 10% fetal bovine serum and maintained at 37°C with 5% $CO_2$ in a humidified atmosphere. Nocodazole (Sigma) was used at 1 μM, mimosine (Sigma) at 1 mM, PHA-767491 (Tocris) and XL413 (synthesized in house (11)) at 10 μM, DMSO was used as control. Plasmids and siRNA transfections were performed using jetPEI and jetPRIME (Polyplus Transfection) respectively according to manufacturer's instructions. siRNAs for CDC7 and DBF4 were obtained from Dharmacon. Control non-targeting siRNA AGUACUGCUUACGAUACGG from Ambion.

### DNA plasmids

EGFP-DBF4 expression construct was obtained by cloning DBF4 coding sequence into vector pIC111 (42). N-terminal tagged (S-Tag-2xFLAG) TOP2A was obtained from Luo (43), and the coding sequence was PCR amplified and cloned into vector pcDNA3.1. The plasmid was subject to site-directed mutagenesis (Agilent, Quickchange II XL) to obtain constructs expressing S-Tag-2xFLAG-TOP2A WT, S1213A/S1525A and S1213D/S1525D mutants. All constructs were verified by sequencing.

### Recombinant protein expression and purification

All recombinant proteins were expressed in *Escherichia coli* and purified using GSTrap FF or HisTrap FF columns (GE Healthcare) according to manufacturer's instructions. GST-tagged recombinant human CDC7–DBF4$_{[197–333]}$ complex and MCM2$_{[Nterm]}$ were eluted using PreScission protease to remove the GST-tag. The M118A, M134A and M118/M134A CDC7 was obtain by site directed mutagenesis of pGEX-CDC7/DBF4MC previously described (11).

### Preparation of nuclear extract

Cells were resuspended in hypotonic buffer (10 mM HEPES pH 7.5, 1.5 mM $MgCl_2$, 10 mM KCl, 0.5 mM TCEP and protease inhibitors) and allowed to swell on ice for 20 min. An equal volume of lysis buffer (10 mM HEPES pH 7.5, 1.5 mM $MgCl_2$, 10 mM KCl, 0.5 mM TCEP, 1.0% NP40 and protease inhibitors) was added to the cells and mixed by brief vortex. Nuclei were pelleted by centrifugation (450 × *g*, 5 min, 4°C) and lysed (50 mM HEPES pH 7.5, 150 mM NaCl, 1.5 mM $MgCl_2$, 0.5 mM TCEP, 0.05% (v/v) Tween-20, protease inhibitors, and 0.25 U/μl Benzonase (Sigma) to digest chromatin).

### *In vitro* thio-phosphorylation

Twenty microgram of nuclear extract was incubated with 200 ng of AS-CDC7/DBF4MC in the presence of ATP or 50 μM $N^6$-(benzyl)ATP-γ-S, 1 mM GTP in kinase buffer (50 mM HEPES pH 7.5, 10 mM $MgCl_2$, 0.5 mM TCEP and protease inhibitor) for 30 min at 30°C in a final volume of 20 μl. The reaction was terminated by adding EDTA to 20 mM. The mixture was alkylated with 2.5 mM *p*-nitrobenzylmesylate (PNBM) for 1.5 h at room temperature, heated in Laemmli buffer, and analyzed by western blot with anti-thiophosphate ester antibody (30).

### Covalent capture of thio-phosphorylated AS-CDC7 substrates

Eight milligrams of nuclear extract prepared from XL413-treated cells was incubated with purified recombinant AS-CDC7/DBF4MC to 1% by mass of total protein, 50 μM $N^6$-(benzyl)ATP-γ-S, and 1.5 mM GTP in kinase buffer for 30 min at 30°C. The reactions were stopped by the addition of 20 mM EDTA. The proteins were precipitated with methanol/chloroform and digested with trypsin. The desalted peptides were added to iodoacetylagarose beads (SulfoLink gel, Pierce) in buffer (25 mM HEPES pH 7.0, BSA 25 μg/ml, TCEP 2 mM, 50% acetonitrile). The beads were incubated overnight in the dark with rotation, washed once with water, followed by 5 M NaCl, 50% acetonitrile, and 5% formic acid in water. The beads were then incubated in 1 ml 10 mM DTT prior to elution with 200 μl of freshly prepared 2 mg/ml Oxone. The phosphopeptides were desalted and enriched by Pierce™ Magnetic Titanium Dioxide Phosphopeptide Enrichment Kit (ThermoFisher Scientific). The recovered peptides were analyzed by LC–MS/MS.

### Liquid chromatography–tandem MS (LC–MS/MS) analysis

Five microliters of desalted solution was injected in a capillary chromatographic system (Agilent 1100 Series, Agilent Technologies, Waldbronn, Germany). Peptide separations occurred on a RP homemade 15 cm reverse-phase spraying fused silica capillary column (75 μm i.d. × 15 cm), packed with 3 μm ReproSil C18 AQ (Dr. Maisch GmbH, Germany). A gradient of eluents A (5% acetonitrile, 0.1% formic acid) and B (acetonitrile, 0.1% formic acid) was used to achieve separation, from 8% B to 80% B in 48 min, at 0.3 μl/min flow rate. The LC system was connected to a Fourier transformed-LTQ Ultra mass spectrometer (FT-LTQ Ultra, Thermo Electron, San Jose, CA, USA) equipped with a nanoelectrospray ion source (Proxeon Biosystems, Odense, Denmark). Survey MS scans were acquired in the FT from $m/z$ 350–1650 with 100 000 resolution. The six most intense doubly and triply charged ions were automatically selected for fragmentation. Target ions already selected for the MS/MS were dynamically excluded for 30s; the data-dependent neutral loss algorithm was enabled for each MS/MS spectra to trigger a $MS^3$ scan (44). DATABASE SEARCHING–Raw MS files were converted using Raw2msm software (.msm files); MS2 and MS3 peak lists were analyzed using (Matrix Science, London, UK; version 2.3.02). Mascot was set up to search the UniProt_CP_Human_20150401 database (unknown version, 90 411 entries) with trypsin as digestion enzyme. Mascot was searched with a fragment ion mass tolerance of 0.50 Da and a parent ion tolerance of 10 PPM. Deamidation of asparagine and glutamine, oxidation and dioxidation of methionine, acetylation of the N-terminus, carbamidomethyl of cysteine, phosphorylation of serine, threonine and tyrosine were specified in Mascot as variable modifications. Criteria for protein identification—Scaffold (version Scaffold_4.4.3, Proteome Software Inc., Portland, OR, USA) was used to validate MS/MS based peptide and protein identifications. Peptide identifications were accepted if they could be established at >95.0% probability by the Peptide Prophet algorithm (45) with Scaffold delta-mass correction. Protein identifications were accepted if they could be established at greater than 99,0% probability and contained at least two identified peptides. Protein probabilities were assigned by the Protein Prophet algorithm (46). Proteins that contained similar peptides and could not be differentiated based on MS/MS analysis alone were grouped to satisfy the principles of parsimony.

### Immunoprecipitations

Nuclei were isolated as described, and chromatin-bound proteins were released by Benzonase treatment in IP buffer (50 mM Tris pH 7.6, 150 mM NaCl, 2 mM $MgCl_2$, 1 mM EDTA, 1% Triton X-100). IgG or anti-TOP2A antibody were prebound to protein A resin (GeneSpin) and equal amounts of precleared nuclear extract were immunoprecipitated for 2 h with rotation at 4°C. Following washes with IP buffer, proteins were recovered in 1× Laemmli buffer and analysed by SDS-PAGE and western blotting.

### Antibodies and western blotting

Primary antibodies included: anti-CDC7 (MBL International), anti-TOP2A (Millipore), anti-NWSHPQFEK/Strep-tag (GenScript), anti-centromere antibodies (ACA) (Antibodies Incorporated), anti-MCM2 (AbD Serotec), anti-pSer40/41 MCM2 described in (7), β-actin (Sigma), anti-RPB1 (Santa-Cruz Biotechnology), anti-β-tubulin (Santa-Cruz Biotechnology), and anti-thiophosphate ester (Abcam). Equal amounts of cell extract were resolved on 7.5% or 10% gels for standard SDS-PAGE, or 5% gels with 5 μM Phos-tag acrylamide (Wako Pure Chemical Industries) and 10 μM $MnCl_2$ for phosphorylation-dependent mobility shift detection, and subject to western blot analysis. IRDye® secondary antibodies for protein detection using the Odyssey infrared imaging system were used (Li-COR Biosciences). For dephosphorylation assays, 20 μg of extracts were incubated with 20 U of Lambda Phosphatase (Sigma) for 30 min before SDS-PAGE.

### Immunofluorescence microscopy

Cells were grown on glass coverslips and treated as described in the text. Soluble proteins were pre-extracted on ice for 5 min with ice-cold HPEM buffer (30 mM HEPES, 65 mM PIPES, 100 mM NaCl, 10 mM EGTA, 2 mM $MgCl_2$, 0.5% Triton X-100) and fixed with 4% PFA for 10 min at room temperature. Coverslips were incubated in blocking buffer (3% bovine serum albumin in PBS) for 30 min, followed by primary antibodies diluted in blocking buffer for 1 h. For EdU labeling, coverslips were then incubated in Click reaction solution (10 μM azide-fluor 545, 10 mM sodium-L-ascorbate, 2 mM $CuSO_4$) for 30 min and washed. Finally, coverslips were incubated with the appropriate Alexa Fluor secondary antibodies (ThermoFisher Scientific), and DNA was counterstained with 4′,6-diamidino-2-phenylindole (DAPI). Images were captured using a DeltaVision Core system (Applied Precision) controlling an interline charge-coupled device camera (Coolsnap HQ2; Roper Technologies) mounted on an inverted microscope (IX-71; Olympus). Images were collected

at 2× binning using a 60× or 100× oil objective. Z-series were collected using 0.2 μm intervals. Images were deconvolved using SoftWoRx (Applied Precision).

### Flow cytometry

For the analysis of DNA content, cells were fixed with 70% ethanol/PBS, centrifuged, resuspended in PBS containing RNase A (2 μg/ml) and propidium iodide (5 μg/ml), and incubated for 30 min. Samples were analyzed using a BD FACS CantoA (BD Biosciences).

### Chromatin immunoprecipitation (ChIP)

Cells were washed once with cold PBS, counted, and resuspended in PBS at room-temperature. Cross-linking was performed with 1.5 mM ethylene glycol bis (succinimidyl succinate) (EGS) from Thermo Fisher Scientific and 1% PFA for a total of 35 and 10 min, respectively. Fixation was quenched with 50 mM glycine. Nuclei were isolated by sequential incubation in Buffer A (100 mM Tris pH 8, 10 mM DTT), Buffer B (10 mM HEPES pH 7.5, 0.25% Triton X-100) and buffer C (10 mM HEPES pH 7.5, 200 mM NaCl). Chromatin was digested with MNase in digestion buffer (50 mM Tris pH 8, 5 mM $CaCl_2$), to mostly mono and dinucleosomes with some trinucleosomes, and briefly sonicated to lyse nuclear membranes. Insoluble material was removed by centrifugation (16 000 × *g*, 10 min). Supernatant was diluted with ChIP IP buffer (20 mM Tris pH 8, 150 mM NaCl, 2.5 mM $MgCl_2$, 0.5% Triton X-100, 0.1% Nonidet P-40) and incubated for 16 h with primary antibodies. Antibody complexes were recovered with Protein A/G beads (Thermo Fisher Scientific), and washed extensively with IP buffer, LiCl wash buffer (10 mM Tris pH 8, 1 mM EDTA, 250 mM $LiCl_2$, 1% Nonidet P-40, 1% sodium deoxycholate) and TE buffer. Samples were eluted with elution buffer (0.1 M $NaHCO_3$, 1% SDS) for 45 min at 65°C with constant agitation. Cross-links were reversed by incubation at 65°C for 18 h. Recovered DNA was analysed on a StepOnePlus Real-Time PCR System (Applied Biosystems). Primers were selected to amplify a 201 bp centromeric sequence specific to chromosome 1 (Fwd: GG CCTATGGCAGCAGAGGATATAACTGCC, Rev: GT GAGTTTTCTCCCGTATCCAACGAAATCC) (47), and a 165 bp non-centromeric sequence at the GAPDH promoter (sequences provided by Thermo Fisher Scientific; Fwd: TACTAGCGGTTTTACGGGCG, Rev: TCGAAC AGGAGGAGCAGAGAGCGA).

### Statistics

Graphs and statistical analyses were performed using GraphPad Prism software.

## RESULTS

### Generation of an engineered CDC7 kinase and identification of TOP2A as an *in vitro* substrate

Based on sequence alignments and structural information, M118 and M134 appear to constrict the CDC7 ATP-binding pocket and could be considered the putative gate-keeper residues of the kinase (48,49). By site directed mutagenesis, we changed the codons for M118 and M134 either individually or in combination, in order to generate three different potential analogue sensitive (AS) alleles of CDC7, namely M118A, M134A and the double M118A/M134A. The wild type (WT) and the three potential AS-CDC7 proteins were then expressed in *E. coli* as GST-fusions together with a polypeptide corresponding to amino acids 197 to 334 of the DBF4 protein, which is sufficient to bind to and activate the kinase (11). Proteins were purified on GST affinity beads, GST-tags were cleaved, and their capability to transfer thio-phosphate groups from $N^6$-(benzyl)ATP-γ-S to the MCM2 protein was tested in *in vitro* kinase reactions. We found that all the three putative AS-CDC7 proteins, but not WT CDC7 could thio-phosphorylate MCM2 and observed that M118A/M134A double mutant was the most efficient in catalyzing the reaction (Figure 1A). Thus, for all the subsequent experiments, we used the M118A/M134A double mutant as the AS-CDC7 protein kinase.

In order to maximise the chances of identifying relevant cellular CDC7 substrates, we prepared large quantities of benzonase-treated nuclear extracts from HEK293 cells that had been challenged with the CDC7 inhibitor XL413 (50),

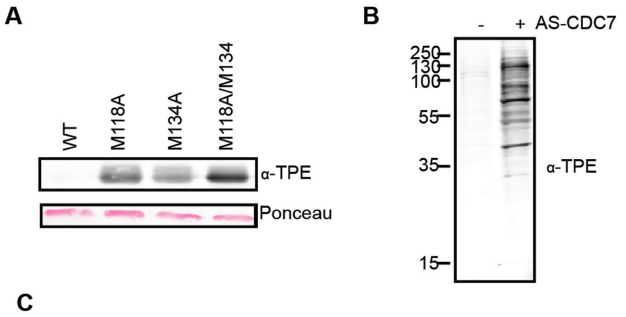


C

| Identified protein | Gene Name | Protein accession numbers | Peptides | Phospho-site |
|---|---|---|---|---|
| Cell division cycle 7-related protein kinase | CDC7 | O00311 | EGSVGLSVQR | S277 |
| | | | NFNIHSSISHESPAVK | S296 |
| | | | NFNIHSSISHESPAVKLMK | S297 |
| | | | FVQSEAQQER | S216 |
| | | | SHIITGNIPLSGPVPK | S239 |
| | | | TVDVLSRK | S318 |
| | | | EGSVGLSVQRSVFGER | S285 |
| DBF4 homolog A | DBF4 | Q9UBU7 | IQTDGDKYGGTSIQLQLK | T273 |
| | | | IQTDGDKYGGTSIQLQLKEK | T281 |
| | | | YEDLETHLLSEQHR | S312 |
| DNA topoisomerase 2 | TOP2A | P11388 | KPIKYLEESDEDDLF | S1525 |
| | | | TQMAEVLPSPR | S1213 |
| Microfibrillar-associated protein | MFAP1 | P55081 | IVEPEVVGESDSEVEGDAWR | S116 |
| Nucleophosmin | NPM1 | P06748 | LLSISGKR | S137 |
| | | | SIRDTPAKNAQK | T199 |
| Nucleolin | NCL | P19338 | ALVATPGKK | T76 |
| | | | VAVATPAKK | T121 |

**Figure 1.** Covalent capture of thio-phosphorylated peptides by AS-CDC7. (**A**) *In vitro* kinase assay with recombinant WT or M118A, M134A and M118A/M1134A CDC7/DBF4, recombinant MCM2 and $N^6$-(benzyl)ATP-γ-S. Thio-phosphorylated MCM2 and CDC7 proteins are detected by western blotting. Ponceau-stained membrane shows equal amount of MCM2 substrate in reactions. (**B**) Western blot detection of thio-phosphorylated proteins after kinase reaction with nuclear extracts and $N^6$-(benzyl)ATP in the presence or absence of AS-CDC7. (**C**) List of proteins and peptides identified after covalent capture of thio-phosphorylated peptides. The sites of modification are indicated in red.

thus leading to the *in vivo* dephosphorylation of relevant substrates by counteracting protein phosphatases and to the solubilization of chromatin-bound proteins. After *in vitro* kinase reactions with AS-CDC7 and $N^6$-(benzyl)ATP-γ-S, we could detect several specific thio-phosphorylated bands by western blotting, with the most intense one migrating similarly to the recombinant AS-CDC7 kinase (Figure 1B and data not shown).

Proteins were then digested, thio-phosphorylated peptides captured on iodoacetylagarose beads, eluted as phosphopeptides by oxidation with Oxone, and identified by mass spectrometry. With this methodology, we identified several peptides derived from CDC7 and DBF4 proteins, indicating that the kinase undergoes extensive autophosphorylation. We also identified several phosphorylated peptides from cellular proteins, and most notably peptides derived from TOP2A phosphorylated at serine 1213 and serine 1525 (Figure 1C and Supplementary Figure S1).

These observations, together with the previous findings that CDC7 and TOP2 inhibitors synergise in causing cell death of cancer cells (10), lead us to postulate that the two proteins could functionally interact in cells.

### CDC7/DBF4 and TOP2A interact *in vivo*

To begin assessing if active DDK physically interacts with TOP2 in cell extracts, we devised new tools to purify DBF4 and its associated proteins. Specifically, we used the Flp-In T-REx 293 system to generate a stable cell line with a single-site integration of DBF4 fused to tandem FLAG and Strep tags on the carboxyl-terminus (T-REx–DBF4). In this cell line, tagged DBF4 expression is normally repressed by upstream TetO2 sequences bound by the Tet repressor, but its expression is induced by the addition of doxycycline. A control cell line with integration of the empty vector (EV) was generated in parallel. We found that expression of tagged DBF4 did not obviously affect viability or cell cycle progression (Supplementary Figure S2A and S2B). Having assessed that TOP2A can only be solubilized by chromatin digestion when nuclear extracts are prepared at 150 mM NaCl, and knowing that CDC7 kinase under the same condition is also partially chromatin associated (Figure 2A and (10)) we then performed immunoprecipitations (IP) from benzonase-treated extracts prepared from both T-REx–DBF4 and T-REx–EV cells with anti-FLAG antibodies. After western blotting we observed that tagged DBF4 not only interacts with endogenous CDC7, but also co-immunoprecipitates with TOP2A (Figure 2B).

Three short conserved motifs, named motifs N, M and C can be recognized in the DBF4 protein (6,51,52). The N terminal motif contains a BRCA1 C-terminal (BRCT) domain predicted to be involved in protein-protein interactions, while motifs M and C bind directly to the CDC7 subunit and activate the kinase (5,49). Human DBF4 additionally contains a large tail region, representing almost half of the protein, which contains no recognisable motifs. To map the DBF4 domains required for its interaction with TOP2A, we cloned several fragments of DBF4 open reading frames containing deletions of their N (residues 1–209), MC (210–350), or Tail (351–674) domains (Figure 2C). Flp-In T-REx cell lines were then generated as before, and the expression of the tagged DBF4 fragments were confirmed by western blotting although to different levels with the C-terminal tail expressing the least (Figure 2D). We then immunoprecipitated endogenous TOP2A from extracts prepared from these cell lines, and the co-purification of each of the DBF4 fragments was determined by west-

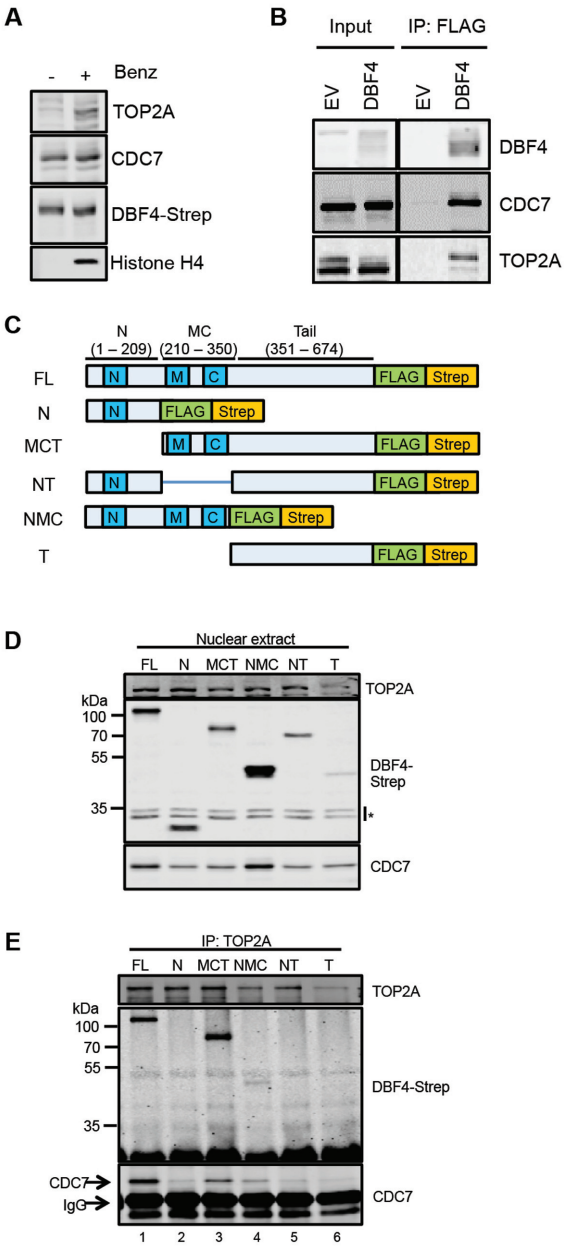


**Figure 2.** CDC7/DBF4 interacts with TOP2A. (**A**) Proteins extracted from nuclei with or without Benzonase were analysed by western blotting with the indicated antibodies. (**B**) Immunoprecipitations (IP) with anti-FLAG antibodies were performed from T-REx-EV and T-REx-DBF4 cells. (**C**) Schematic of DBF4 deletion mutant alleles used to generate Flp-In T-REx 293 conditionally expressing cell lines. (**D**) Detection of DBF4 fragments by western blotting in nuclear extracts prepared from Flp-In T-REx 293 cells upon addition of doxycycline. Asterisks indicate cross-reactive bands. (**E**) Endogenous TOP2A was immunoprecipitated from nuclear extracts and immunoprecpitated material was analysed by western blotting.

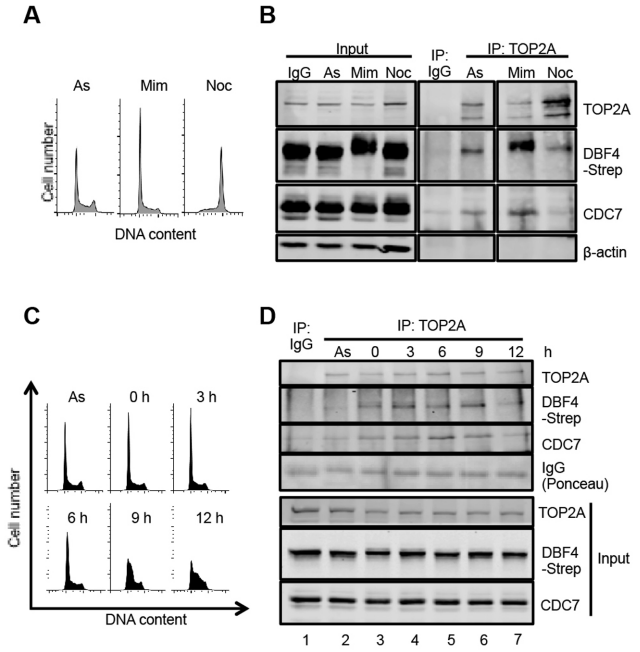


**Figure 3.** CDC7/DBF4 interacts with TOP2A predominantly in early S-phase. (**A**) T-REx-DBF4 cells were treated with mimosine or nocodazole for 19 h and DNA content analysed by Flow Cytometry. (**B**) Extracts were prepared from asynchronously growing, mimosine and nocodazole treated cells as in panel A and TOP2A was immunopreciptiated with specific antibodies. As control, unrelated mouse IgG was used. Immunoprecipitated proteins were then analysed by western blotting. (**C**) DNA content of cells treated with mimosine for 15 h and released into fresh media. Samples were collected at the indicated time-points. (**D**) TOP2A immunoprecipitates from extracts of cells released from mimosine block as in panel C.

ern blotting. As expected, full-length DBF4 (FL) was co-immunoprecipitated with TOP2A (Figure 2E, lane 1). Of the fragments, only the DBF4 MCT (210–674) and NMC (1–350) were co-immunoprecipitated with TOP2A (Figure 2E, lanes 3 and 4), indicating that the N domain is dispensable and that the MC domains are required. While we could not detect a direct binding between TOP2A and the C-terminal tail of DBF4 in these experiments, we observed that the binding of the MCT fragment was more pronounced compared to the NMC, strongly suggesting that the tail contributes to this protein-protein interaction. This could be achieved either by stabilizing the overall structure of the CDC7 complex or by providing a second independent binding site.

## CDC7/DBF4-TOP2A interaction occurs early in S-phase

In order to determine when, during the cell cycle, CDC7/DBF4 interacts with TOP2A, we immunoprecipitated TOP2A from T-REx-DBF4 cells that had been treated with mimosine or nocodazole. Mimosine blocks S-phase entry through activation of ATM checkpoint signaling and inhibition of the chromatin binding of key replication proteins (53,54), while nocodazole, a microtubule depolymerizing agent, prevents mitotic progression through activation of the spindle assembly checkpoint (Figure 3A) (55). We found that the amount of endogenous CDC7 and tagged DBF4 co-immunoprecipitated was higher in cells arrested with mimosine, and reduced in nocodazole-treated cells (Figure 3B). We noted that DBF4 migrates slower in SDS-PAGE when cells were treated with mimosine, possibly due to phosphorylation by either ATM or ATR (56).

To examine if the interaction between TOP2A and CDC7/DBF4 is modulated during progression through S-phase, T-REx-DBF4 cells were released from mimosine arrest and samples collected at 3-h intervals. DNA content analysis and EdU incorporation assay indicated that T-REx cells progressed slowly into S-phase (Figure 3C) in a manner that was independent from DBF4 overexpression (Supplementary Figure S3). After IP-Western, we found that the interaction of TOP2A with CDC7 and tagged DBF4 was significantly higher in mimosine-trapped cells compared to a control-treated asynchronous population (Figure 3D, lanes 2 and 3), that it peaked between 3 and 9 h after release, when most cells were in early to mid S-phase (Figure 3C and D lanes 4–6) and decreased significantly by 12 h when most cells were in mid and late S-phase (Figure 3C and D, lane 7).

## CDC7 inhibition reduces TOP2A phosphorylation levels and TOP2A-DDK protein-protein interaction *in vivo*

Since TOP2A interacts with DDK during S-phase and it is a good *in vitro* substrate of the kinase, we asked if TOP2A is phosphorylated in a CDC7-dependent manner in a cellular context. For this purpose, T-REx-EV cells were treated for 3 h with XL413, a specific CDC7 inhibitor (49,50), or mock treated. Under these conditions, phosphorylation of MCM2 at Ser40/41, a reliable marker of cellular CDC7 activity (7), is strongly reduced (Figure 4A). When TOP2A was analyzed by western blot on standard SDS-PAGE we did not observe differences in the mobility of the protein in the two samples. Thus, to facilitate separation of differentially phosphorylated TOP2A species, Phos-tag acrylamide, which slows the migration of phosphorylated proteins relative to their unphosphorylated or less-phosphorylated forms (57), was added to the SDS-PAGE gels. In mock-treated cells, the TOP2A band becomes less distinct in the presence of the Phos-tag reagent, with slight smearing observed beneath the main band. Upon treatment with the CDC7 inhibitor, a second, faster migrating form was detected (Figure 4A), suggesting that at least some TOP2A phosphorylation could be attributed to CDC7 kinase.

During the course of these experiments, we observed that the electrophoretic mobility of DFB4-Strep protein was greatly altered by the CDC7 inhibitor (Figure 4B), indicating that DBF4 itself is phosphorylated by CDC7, consistent with the identification of thio-phosphorylated DBF4 peptides in our initial experiments (Figure 1C) as well as with increased mobility after phosphatase treatment of the extract (Figure 4C). Significantly, treatment with XL413 also caused an evident and sudden drop in DBF4 levels that were only marginally rescued by the co-treatment with the proteasome inhibitor MG132; yet, XL413 did not affect CDC7 levels (Figure 4B and D).

We then investigated if the TOP2A-DDK interaction was also affected by the compound. To this end, cells were treated with either DMSO or XL413 for 3 h, and TOP2A

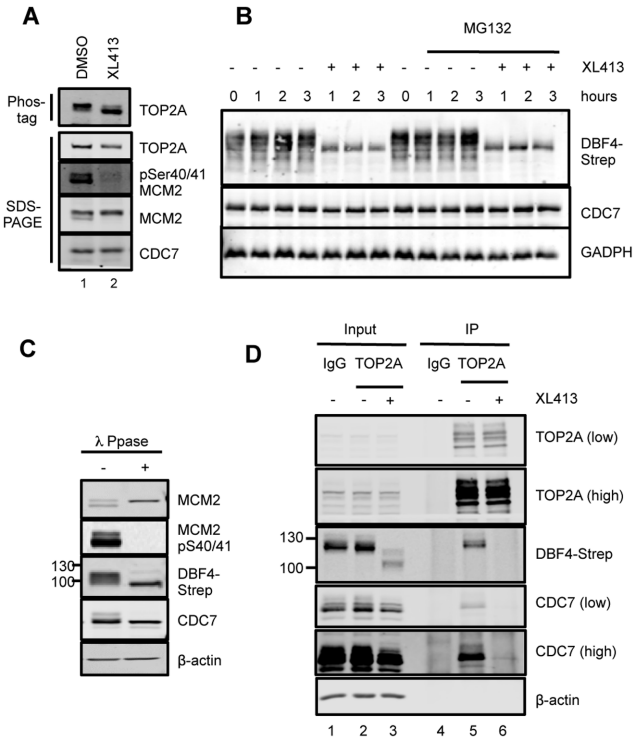


**Figure 4.** CDC7 inhibitors affect the phosphorylation levels of cellular TOP2A and its interaction with the kinase. (**A**) T-REx-EV cells were treated with 10 μM XL413 or DMSO for 3 h, and cell extracts were separated on a 5% SDS-PAGE supplemented with 5 μM Phos-tag acrylamide or on a standard 6% SDS-PAGE. (**B**) T-REx-DBF4 cells were treated with DMSO or XL413 for the indicated times in the presence of absence of proteasome inhibitor MG132. (**C**) Extracts prepared from T-REx-DBF4 cells were incubated in phosphatase reaction buffer in the presence or absence of λ-phosphatase. (**D**) T-REx-DBF4 cells were treated with mimosine for 12 h, then with 10 μM XL413 or DMSO for a further 3 h and immunoprecipitations were performed with anti-TOP2A antibody or control IgG. Immunoprecipiations were perfomed from 1.5 mg of extract and 20 μg of the input material (1.33%) was loaded on the gel. In all cases proteins were analyzed by western blotting; where indicated, low or high intensity scans of the same blot are shown.

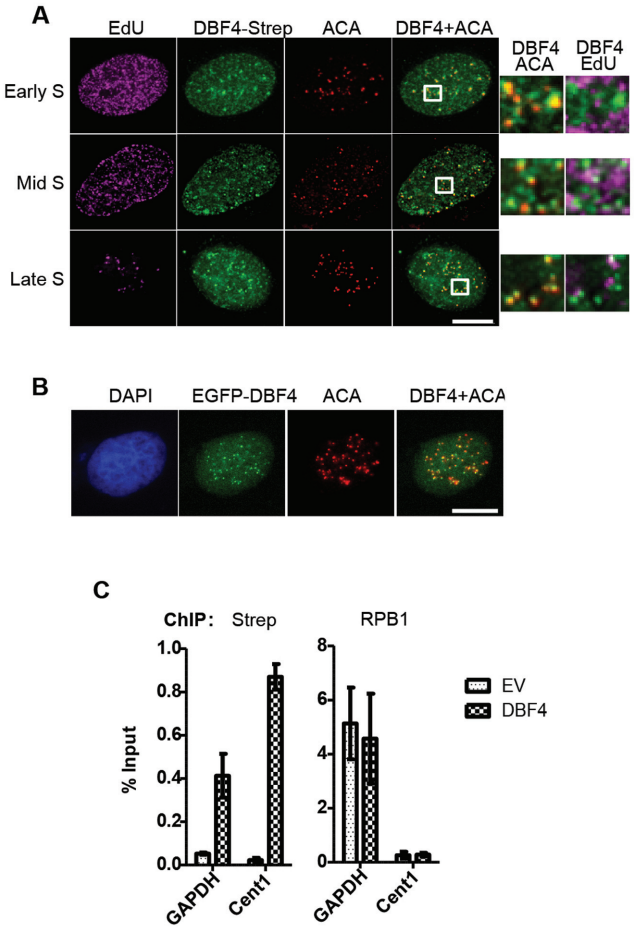


**Figure 5.** DBF4 is localized at centromeres throughout S-phase. (**A**) U2OS cells transiently expressing DBF4-FLAG-Strep were treated with 10 μM EdU for 15 min prior to pre-extraction and fixation. EdU-containing DNA is shown in magenta, DBF4 in green, and centromeres (ACA) in red. Early, mid or late S-phase cells were determined according to the pattern of EdU incorporation. Areas indicated in boxes are magnified next to the respective images. Scale bar = 10 μm. (**B**) U2OS cells were transfected with plasmid expressing EGFP-DBF4 fusion protein and analysed by fluorescence microscopy. EGFP signal is in green and ACA centromeric staining in red. (**C**) Chromatin immunoprecipitations (ChIP) were performed with anti-Strep and anti-RNA pol II (RPB1) antibodies from extracts of T-REx-EV and T-REx-DBF4 cells. The amounts of the non-centromeric GAPDH promoter and Chromosome 1 centromeric (Cent1) DNA recovered were determined by qPCR relative to the input samples. Bars represent the Mean ± S.D. of three technical replicates. Results are representative of three independent experiments.

immunoprecipitation experiments were performed. Both CDC7 and DBF4 were detected in the immunoprecipitated material from the control-treated sample, but not in the XL413-treated sample (Figure 4D, lanes 5 and 6). Altogether these data show that inhibition of CDC7 kinase activity has multiple consequences on the phosphorylation, the levels, and the capability of CDC7/DBF4 to interact with and phosphorylate relevant substrates, including TOP2A.

### DBF4 localises to centromeres throughout S-phase

Both CDC7 and DBF4 are known to be mostly nuclear proteins (5,6,58), but their sub-nuclear localization has not been well characterized, particularly in human cells due to the lack of sensitive and specific immunological reagents. We therefore examined the localization of tagged DBF4 by immunofluorescence microscopy with an anti-Strep antibody. Firstly, we confirmed that full-length tagged DBF4 is mostly confined to the nucleus, where it is largely diffused. However, extraction of soluble proteins before fixation revealed the presence of multiple DBF4 foci. By performing co-localization experiments, we observed that DBF4 foci did not obviously overlap with sites of active DNA replication, but co-staining with anti-centromere antibodies (ACA) showed that DBF4 foci could always be detected at centromeres (Figure 5A). DBF4 was present at centromeres at all stages of S-phase, and, interestingly, this was not affected by CDC7 kinase inhibition by XL413 (Supplementary Figure S4). Using the same DBF4 deletion mutants previously described, we investigated the domains required for its chromatin and centromeric localization. Expression plasmids for the DBF4 fragments were transfected into U2OS cells, and their localization detected by IF as before.

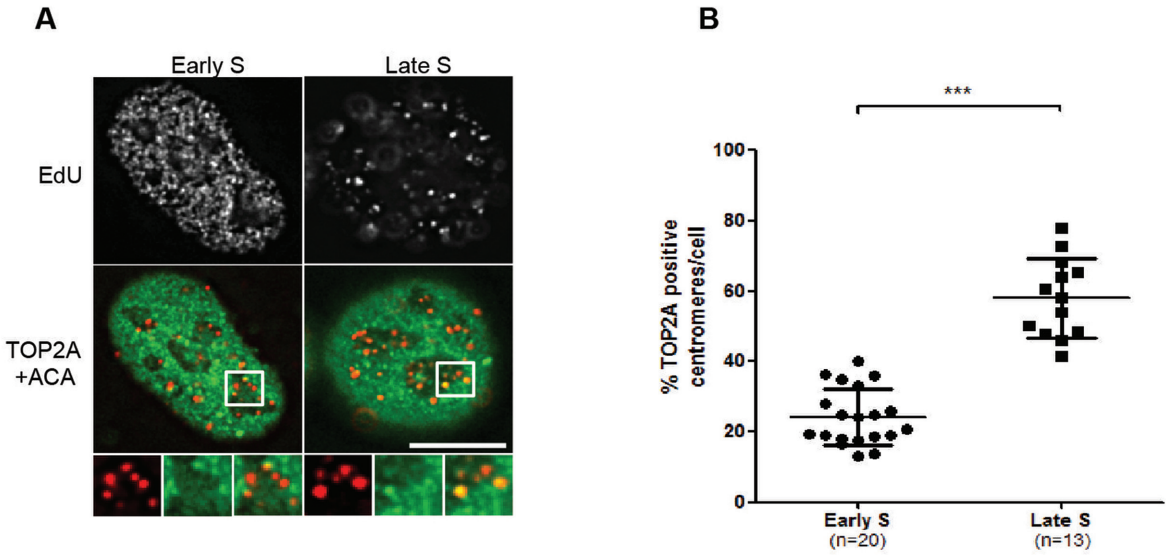


**Figure 6.** TOP2A is recruited to, and is active at centromeres in mid to late S-phase. (**A**) U2OS cells were treated with 10 μM EdU and 50 μg/ml ICRF-187 for 15 min prior to pre-extraction, fixation and immunofluorecence microscopy analysis. On top the pattern of EdU incorporation is shown in grey while on the bottom TOP2A is shown in green and centromeres (ACA) in red. Areas indicated in boxes are magnified below the respective images. Scale bar = 10 μm. (**B**) Cells in early and late S-phase were randomly selected and the proportion of centromeres co-incident with TOP2A foci were manually quantified. Each point on the graph represents data from 1 cell. Bars represent the mean ± S.D. ****$P < 0.0001$, Student's *t*-test.

We found that while the N-terminal domain alone was sufficient for chromatin binding, all three NMC domains are required for centromeric recruitment (Supplementary Figure S5).

To confirm DBF4 localization at centromeres, we first expressed a EGFP-DBF4 fusion protein in U2OS cells; again, we observed that this protein was largely diffused in the nucleus but also accumulated in foci that, to great extent, overlapped with ACA foci (Figure 5B). Secondly, we used chromatin immunoprecipitation (ChIP) technique. qPCR primers were selected to amplify a centromere-specific target sequence on Chromosome 1 (Cent1) (47) and a non-centromeric sequence corresponding to the GAPDH promoter close to the transcription start site. We performed ChIP using a long spacer cross-linker and anti-Strep and anti-RNA polymerase II (RPB1) antibodies. As the baseline control for background antibody binding, ChIP from T-REx-EV cells was performed alongside T-REx-DBF4 cells. By qPCR analysis, the abundance of each target locus recovered was calculated relative to the 2% input sample (Figure 5C). As the positive control for the ChIP protocol, occupancy of RNA polymerase II at the GAPDH promoter was used. ChIP with the anti-Strep antibody showed increased occupancy of tagged DBF4 at centromeric compared to a non-centromeric locus, again supporting the idea that DBF4 accumulates at centromeres.

### TOP2A recruitment at centromeres occurs throughout S-phase

We then investigated if CDC7/DBF4 affects either the activity or subcellular localization of TOP2A. To detect catalytically active TOP2A, we used the Differential Retention of Topoisomerase (DRT) assay (37). Briefly, asynchronously growing U2OS cells were treated with the TOP2A catalytic inhibitor ICRF-187/dexrazoxane, which prevents the release of catalytically-committed TOP2A from DNA (34,35). Soluble proteins, including TOP2A molecules not involved in strand passage activity during the time of treatment, are then salt-and detergent-extracted prior to formaldehyde fixing and immunofluorescence microscopy; for reference, centromeres were detected using anti-centromere antibodies. As previously reported, TOP2A was detected along the chromosome axes and concentrated at centromeres of mitotic chromosomes (Supplementary Figure S6 and (37,59)). Interestingly, we also observed centromeric localization in a number of interphase cells. In contrast to mitotic cells, however, not all interphase centromeres co-localized with TOP2A, and the proportion of TOP2A positive centromeres differed between cells. To further stratify the interphase cells within the cell cycle, a brief treatment with EdU was introduced, and cells were determined to be in early, mid, or late S-phase according to the pattern of EdU incorporation observed (60). The proportion of TOP2A positive centromeres per cell appeared to correlate with S-phase progression, low in early S-phase and increasing in late S-phase (Figure 6A). To quantify this result, the total number of discernible centromeres in a single optical section of a randomly selected cell was counted, and the percentage of centromeres that were also co-stained with TOP2A was determined (Figure 6B). A significantly higher proportion of TOP2A positive centromeres was found in late S-phase cells compared to early S-phase. Thus, we conclude that TOP2A recruitment to centromeres is a gradual process that occurs throughout S-phase.

### CDC7/DBF4 limits TOP2A recruitment in early S-phase

Since both CDC7/DBF4 and TOP2A are localized at centromeres in S-phase, we postulated that CDC7/DBF4

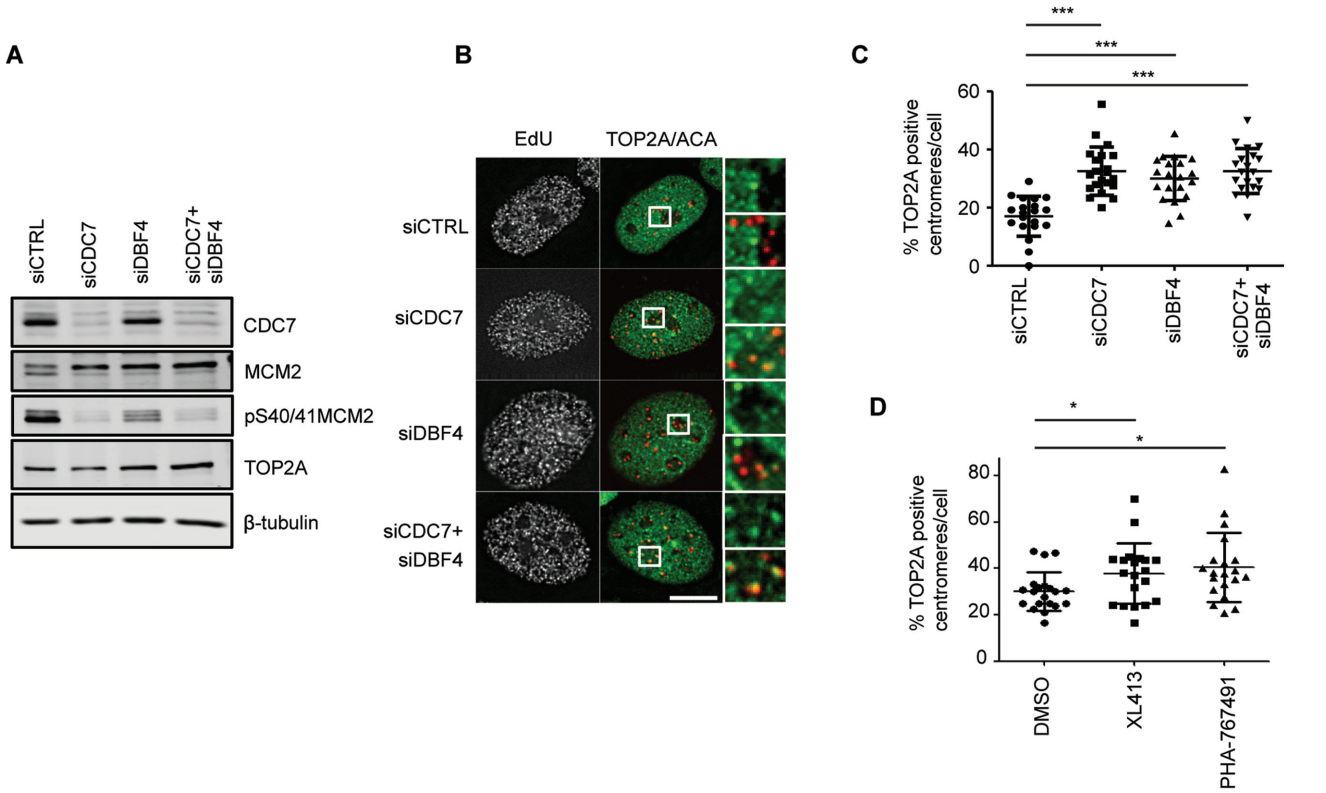


**Figure 7.** CDC7/DBF4 inhibition increases the recruitment of TOP2A to centromeres. U2OS cells were transfected with siRNA against CDC7 and/or DBF4 for 48 h. Cell extracts were then prepared and analysed by western blotting (**A**) or cells were treated with 10 μM EdU and 50 μg/ml ICRF-187 for 15 min prior to pre-extraction, fixation and immunofluorecence microscopy analysis (**B**). Representative images of early S-phase cells are shown. (**C**) Quantification was performed as in Figure 6. ***$P < 0.001$, Student's *t*-test. Scale bar = 10 μm. (**D**) U2OS cells were challenged with 10 μM XL413, 10 μM PHA767491 or with DMSO as control. 15 min before harvesting cells were also treated with 10 μM EdU and 50 μg/ml ICRF-187 and analysed as above. *$P < 0.05$, Student's *t*-test.

might regulate the centromeric recruitment or activity of TOP2A at these locations. Using the DRT assay we therefore examined the localization of TOP2A after 48 h of transfection with siRNA targeting CDC7 and/or DBF4. While endogenous CDC7 can be easily detected by western blotting, the detection of endogenous DBF4 in these cells was problematic, therefore in these experiments, the biological readout of the efficiency of siRNA-mediated depletion of DDK subunits was also determined indirectly through a reduction in MCM2 phosphorylation, either as a mobility shift or at a specific CDC7–dependent phosphorylation site Ser40/41 (Figure 7A). After 48 h of transfection of siRNAs a large proportion of the cells were still actively proliferating despite low DDK activity, and importantly, in those cells that were actively undergoing DNA synthesis, we observed an increased proportion of centromeres marked with active TOP2A. This was particularly striking in cells with an early S-phase replication pattern (Figure 7B), where the number of TOP2A positive centromeres is typically low in unperturbed conditions (Figure 6). Quantification of randomly selected early S-phase cells confirmed a large increase in TOP2A positive centromeres caused by CDC7 kinase depletion (Figure 7C). Notably, combined depletion of CDC7 and DBF4 did not result in an additive effect on TOP2A centromeric recruitment. Similarly to siRNA depletion of the protein, a 3-h treatment with CDC7 inhibitors, XL413 or PHA767491, also caused increased localization of active TOP2A at centromeres in early S-phase cells (Figure 7D). These data are consistent with either TOP2A activity at centromeres being directly regulated through TOP2A phosphorylation by CDC7/DBF4, or indirectly through a different mechanism.

In order to discriminate between these alternative models, we expressed either FLAG- tagged TOP2A WT, a phosphorylation-deficient TOP2A protein carrying alanine substitutions in the two serines that were identified as CDC7 phospho-sites *in vitro*, namely S1213A/S1525A, or the corresponding potential phospho-mimetic protein S1213D/S1525D. All these proteins were catalytically active in the cells as they could be trapped on chromatin with ICRF187 although we noticed their expression level was reproducibly different, with S1213A/S1525A protein accumulating to higher levels (Figure 8A). This may be due to protein or mRNA stabilization caused by the single S1525A substitution, as an independent report showed that a S1525A TOP2A was consistently expressed at a higher level than the WT protein (43). When we analysed centromeric occupancy in early S-phase cells, we found that the ectopically expressed FLAG-tagged TOP2A WT, just like endogenous TOP2A or the S1213D/S1525D TOP2A, was detected at low frequency at centromeres, while, in contrast, the phospho-deficient S1213A/S1525A protein dis-

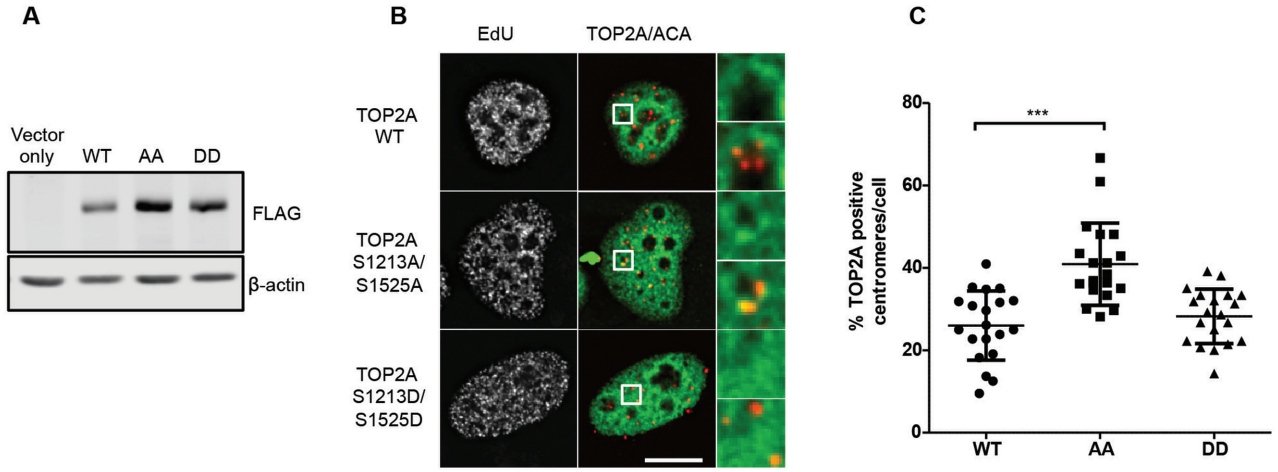


**Figure 8.** Phosphorylation at Ser1213 and S1525 controls the timing of TOP2A recruitment at centromeres. U2OS cells were tranfected with constructs expressing either WT, S1213A/S1525A or S1213D/S1525D FLAG-tagged TOP2A. After 48 h, cell extracts were prepared and analysed by western blotting (**A**) or cells were treated with 10 μM EdU and 50 μg/ml ICRF-187 for 15 min prior to pre-extraction, fixation and immunofluorecence microscopy analysis (**B**). Representative images of early S-phase cells are shown. (**C**) Quantification was performed as in Figures 6 and 7. ***$P < 0.001$, Student's *t*-test. Scale bar = 10 μm.

played increased occupancy, to a level similar to what was observed with endogenous TOP2A when CDC7 kinase was depleted (Figure 8B and C). Since the amount of TOP2A active at centromeres is a very small fraction of the total TOP2A pool in each cell analysed, it is unlikely that centromeric recruitment is driven solely by mass action equilibrium suggesting instead that phosphorylation at these sites regulates TOP2A centromeric function.

## DISCUSSION

In this work, we have used a chemical genetics approach to identify potential substrates of CDC7 kinase from nuclear extracts. During this process we have validated the idea that two methionines, M118 and M134, can act as gatekeeper residues, and their substitution with a smaller amino acid such as alanine, either in combination or on their own, allows the bulky ATP analogue $N^6$-(benzyl)ATP to bind and to be used as a cofactor instead of ATP for both auto- and trans-phosphorylation of proteins. Our attempts to label and capture CDC7 substrates from nuclear extracts have led to the identification of TOP2A as a main substrate and to the identification of S1213 and S1525 as CDC7 *in vitro* phospho-sites. However, the list of potential substrates is not exhaustive, as we did not retrieve known CDC7 substrates, such as the MCM complex or CLASPIN. This could be due to a combination of technical reasons, including the use of an engineered kinase that lacks portions of DBF4 sequence that could be relevant to promote substrate recognition. We also mapped seven sites of autophosphorylation on the CDC7 catalytic subunit, and three on DBF4. All the mapped CDC7 sites reside in the large insert domain, for which structural information is lacking. This insert domain interrupts the contiguity of the canonical kinase domain structure, a feature which is peculiar to CDC7 and has been shown to mediate protein-protein interactions (61). Interestingly, several of these sites were also previously identified in large phosphoproteomics studies and have been annotated in the PhosphositePlus database (62), suggesting that CDC7 auto-phosphorylation can occur *in vivo*.

We have demonstrated that DBF4 can be detected at centromeres. To our knowledge, this is the first evidence that DBF4 is recruited to centromeres in human cells. We found that dual crosslinking with formaldehyde and ethylene glycol bis (succinimidyl succinate) (EGS) was necessary to immunoprecipitate DBF4-associated chromatin. EGS is a protein-protein cross-linking agent with a long spacer arm that, in combination with formaldehyde, stabilises proteins that are not directly bound to DNA (63). This suggests that CDC7/DBF4 is instead recruited through other protein factor(s). We have also found that the N-terminal 1–209 residues of DBF4 are sufficient for chromatin binding. This region remains poorly characterized, but it contains a BRCT domain proposed to be involved in protein–protein interactions. Interestingly, the equivalent domain of DBF4 in budding yeast, *Saccharomyces cerevisiae,* has been shown to be required for interaction with several replication and checkpoint proteins, including ORC, RAD53 and RIF1 (64–66). The mechanism regulating CDC7/DBF4 centromeric recruitment, however, is likely to be distinct, as the DBF4 M and C domains, in an addition to the N domain, are also required for this.

It was recently reported that in *S. cerevisiae*, CDC7/DBF4 is recruited to kinetochores where it promotes the replication of centromeric regions early in S-phase through the recruitment of the essential replication proteins SLD3 and SLD7 (Treslin/TICRR and MTBP in humans) to pericentromeric origins (67). Differently from budding yeast, however, human centromeric DNA is replicated asynchronously between mid to late S-phase (68,69) while here DBF4 was detected at all centromeres from early S-phase, inconsistent with normal centromeric replication timing. As our experiments rely on the overexpression of DBF4, future studies would be necessary to verify if the overexpression of DBF4 is sufficient to alter

centromeric DNA replication timing. In the same study, the authors also reported that centromeric ScCDC7/DBF4 independently recruits the SCC2–SCC4 cohesin loading complex for the establishment of robust pericentromeric sister chromatid cohesion (67). *X. laevis* CDC7/DBF4B, which is the predominant CDC7 kinase complex in egg extracts, also physically interacts with SCC2-SCC4 and is required for its chromatin binding (70). Thus, it is plausible that human CDC7/DBF4 may also be involved in the establishment of pericentromeric sister chromatid cohesion, and it would be interesting to verify if the homologous complex in humans, NIPBL-MAU2, is also regulated by CDC7 kinase in a similar manner.

CDC7/DBF4 interacts with and phosphorylates TOP2A *in vitro*. The interaction likely occurs on chromatin, requires a region of DBF4 that is sufficient for CDC7 activation, is further stabilized by the C-terminal tail of DBF4 and, interestingly, it is abolished by a very specific CDC7 ATP-competitive inhibitor XL413. At present, it is not fully clear if this interaction is solely mediated by CDC7 or if it is phosphorylation-dependent, as CDC7 kinase inhibition has dramatic effects on both CDC7 and DBF4 phosphorylation levels as well as causing a rapid drop in DBF4 levels. TOP2A is a highly modified protein with many residues phosphorylated in its C-terminus (62) and several kinases have been implicated in its regulation during the cell cycle including CK2 and proline directed kinases (71) which have mainly been studied using *in vitro* assays. As the treatment with XL413 causes a reduction in the overall levels of TOP2A phosphorylation, we propose that CDC7 is also directly involved in the regulation *in vivo*. Future studies, involving the development and thorough validation of multiple anti-phosphopeptide antibodies will be important to determine the contribution of CDC7 and other kinases to TOP2A phosphorylation at different sites.

Our work has also revealed that active TOP2A can be detected at an increasing number of centromeres as cell progress through S-phase. We observed that TOP2A activity at centromeric regions does not always overlap with ongoing DNA synthesis at these sites, and that the timing of TOP2A centromeric recruitment is advanced by CDC7 depletion. Similarly, the timing of centromeric recruitment of a phosphorylation-deficient TOP2A at two key serines, putative CDC7 target sites S1213 and S1525, is advanced.

Based on these results, we propose that phosphorylation of TOP2A by CDC7/DBF4 in early S-phase prevents its localization and/or activity at centromeres, and inhibition of TOP2A function could be relevant to prevent premature separation of centromeric DNA.

CDC7 regulation of TOP2A at centromeres may have important significance with respect to centromeric replication and cohesion, and could also explain the increased sensitivity to TOP2 poisons in cells lacking CDC7 activity.

## SUPPLEMENTARY DATA

Supplementary Data are available at NAR Online.

## ACKNOWLEDGEMENTS

Ed Luk, Stony Brook University, for FLAG IP protocol, Adrian Bracken, Trinity College Dublin, for RPB1 antibody and advice on ChIP, Kuntian Luo for TOP2A plasmid, Enda O'Connell, NUIG, for advice on qPCR protocol and Peter Cherepanov for insight on CDC7 structural features before publication, Elaine Dunleavy for help with microscopy, Sandra Healy and Bob Lahue for critical reading of the manuscript, Gemma O'Brien and all the members of the Santocanale laboratory for support and discussion. We also thank the NCBES Flow Cytometry core facility at NUIG, a facility that is funded by NUIG and the Irish Government's Programme for Research in Third Level Institutions, Cycles 4 and 5, National Development Plan 2007–2013.

*Author's contribution*: K.W. designed and performed most of the experiments, G.N.W. and J.F. developed covalent capture methodology with AS-CDC7, H.Q. generated cell lines and performed experiments in Figure 4B and Supplementary Figure S2, M.D.R. generated TOP2A mutants, A.C. and A.B. performed mass spectrometry analysis and data analysis, C.S. directed research, K.W. and C.S. wrote the manuscript.

## FUNDING

Science Foundation Ireland (SFI) [08/IN.1/B2064 to C.S.]; Irish Research Council postdoctoral fellowship (to G.N.W.); Molecular Medicine Ireland fellowship (to H.Q.).
*Conflict of interest statement*. None declared.

## REFERENCES

1. Zeman,M.K. and Cimprich,K.A. (2014) Causes and consequences of replication stress. *Nat. Cell Biol.*, **16**, 2–9.
2. Hills,S.A. and Diffley,J.F.X. (2014) DNA replication and oncogene-induced replicative stress. *Curr. Biol.*, **24**, R435–R444.
3. Symeonidou,I.-E., Taraviras,S. and Lygerou,Z. (2012) Control over DNA replication in time and space. *FEBS Lett.*, **586**, 2803–2812.
4. Sclafani,R.A. and Holzen,T.M. (2007) Cell cycle regulation of DNA replication. *Annu. Rev. Genet.*, **41**, 237–280.
5. Jiang,W., McDonald,D., Hope,T.J. and Hunter,T. (1999) Mammalian Cdc7-Dbf4 protein kinase complex is essential for initiation of DNA replication. *EMBO J.*, **18**, 5703–5713.
6. Kumagai,H., Sato,N., Yamada,M., Mahony,D., Seghezzi,W., Lees,E., Arai,K. and Masai,H. (1999) A novel growth- and cell cycle-regulated protein, ASK, activates human Cdc7-related kinase and is essential for G1/S transition in mammalian cells. *Mol. Cell. Biol.*, **19**, 5083–5095.
7. Montagnoli,A., Valsasina,B., Brotherton,D., Troiani,S., Rainoldi,S., Tenca,P., Molinari,A. and Santocanale,C. (2006) Identification of Mcm2 phosphorylation sites by S-phase-regulating kinases. *J. Biol. Chem.*, **281**, 10281–10290.
8. Masai,H., Taniyama,C., Ogino,K., Matsui,E., Kakusho,N., Matsumoto,S., Kim,J.M., Ishii,A., Tanaka,T., Kobayashi,T. *et al.* (2006) Phosphorylation of MCM4 by Cdc7 kinase facilitates its interaction with Cdc45 on the chromatin. *J. Biol. Chem.*, **281**, 39249–39261.
9. Sheu,Y.-J. and Stillman,B. (2006) Cdc7-Dbf4 phosphorylates MCM proteins via a docking site-mediated mechanism to promote S phase progression. *Mol. Cell*, **24**, 101–113.
10. Tenca,P., Brotherton,D., Montagnoli,A., Rainoldi,S., Albanese,C. and Santocanale,C. (2007) Cdc7 is an active kinase in human cancer cells undergoing replication stress. *J. Biol. Chem.*, **282**, 208–215.
11. Rainey,M.D., Harhen,B., Wang,G.-N., Murphy,P.V. and Santocanale,C. (2013) Cdc7-dependent and -independent phosphorylation of Claspin in the induction of the DNA replication checkpoint. *Cell Cycle*, **12**.
12. Kim,J.M., Kakusho,N., Yamada,M., Kanoh,Y., Takemoto,N. and Masai,H. (2008) Cdc7 kinase mediates Claspin phosphorylation in DNA replication checkpoint. *Oncogene*, **27**, 3475–3482.

13. Suzuki,T., Tsuzuku,J., Hayashi,A., Shiomi,Y., Iwanari,H., Mochizuki,Y., Hamakubo,T., Kodama,T., Nishitani,H., Masai,H. *et al.* (2012) Inhibition of DNA damage-induced apoptosis through Cdc7-mediated stabilization of Tob. *J. Biol. Chem.*, **287**, 40256–40265.
14. Day,T.A., Palle,K., Barkley,L.R., Kakusho,N., Zou,Y., Tateishi,S., Verreault,A., Masai,H. and Vaziri,C. (2010) Phosphorylated Rad18 directs DNA polymerase η to sites of stalled replication. *J. Cell Biol.*, **191**, 953–966.
15. Yamada,M., Watanabe,K., Mistrik,M., Vesela,E., Protivankova,I., Mailand,N., Lee,M., Masai,H., Lukas,J. and Bartek,J. (2013) ATR-Chk1-APC/CCdh1-dependent stabilization of Cdc7-ASK (Dbf4) kinase is required for DNA lesion bypass under replication stress. *Genes Dev.*, **27**, 2459–2472.
16. Gérard,A., Koundrioukoff,S., Ramillon,V., Sergère,J.-C., Mailand,N., Quivy,J.-P. and Almouzni,G. (2006) The replication kinase Cdc7-Dbf4 promotes the interaction of the p150 subunit of chromatin assembly factor 1 with proliferating cell nuclear antigen. *EMBO Rep.*, **7**, 817–823.
17. Takayama,Y., Mamnun,Y.M., Trickey,M., Dhut,S., Masuda,F., Yamano,H., Toda,T. and Saitoh,S. (2010) Hsk1- and SCF(Pof3)-dependent proteolysis of S. pombe Ams2 ensures histone homeostasis and centromere function. *Dev. Cell*, **18**, 385–396.
18. Bailis,J.M., Bernard,P., Antonelli,R., Allshire,R.C. and Forsburg,S.L. (2003) Hsk1-Dfp1 is required for heterochromatin-mediated cohesion at centromeres. *Nat. Cell Biol.*, **5**, 1111–1116.
19. Baker,S.P., Phillips,J., Anderson,S., Qiu,Q., Shabanowitz,J., Smith,M.M., Yates,J.R., Hunt,D.F. and Grant,P.A. (2010) Histone H3 Thr 45 phosphorylation is a replication-associated post-translational modification in S. cerevisiae. *Nat. Cell Biol.*, **12**, 294–298.
20. Lo,H.-C., Kunz,R.C., Chen,X., Marullo,A., Gygi,S.P. and Hollingsworth,N.M. (2012) Cdc7-Dbf4 is a gene-specific regulator of meiotic transcription in yeast. *Mol. Cell. Biol.*, **32**, 541–557.
21. Matos,J., Lipp,J.J., Bogdanova,A., Guillot,S., Okaz,E., Junqueira,M., Shevchenko,A. and Zachariae,W. (2008) Dbf4-dependent CDC7 kinase links DNA replication to the segregation of homologous chromosomes in meiosis I. *Cell*, **135**, 662–678.
22. Valentin,G., Schwob,E. and Della Seta,F. (2006) Dual role of the Cdc7-regulatory protein Dbf4 during yeast meiosis. *J. Biol. Chem.*, **281**, 2828–2834.
23. Wan,L., Niu,H., Futcher,B., Zhang,C., Shokat,K.M., Boulton,S.J. and Hollingsworth,N.M. (2008) Cdc28-Clb5 (CDK-S) and Cdc7-Dbf4 (DDK) collaborate to initiate meiotic recombination in yeast. *Genes Dev.*, **22**, 386–397.
24. Sasanuma,H., Hirota,K., Fukuda,T., Kakusho,N., Kugou,K., Kawasaki,Y., Shibata,T., Masai,H. and Ohta,K. (2008) Cdc7-dependent phosphorylation of Mer2 facilitates initiation of yeast meiotic recombination. *Genes Dev.*, **22**, 398–410.
25. Murakami,H. and Keeney,S. (2014) Temporospatial coordination of meiotic DNA replication and recombination via DDK recruitment to replisomes. *Cell*, **158**, 861–873.
26. Bishop,A.C., Ubersax,J.A., Petsch,D.T., Matheos,D.P., Gray,N.S., Blethrow,J., Shimizu,E., Tsien,J.Z., Schultz,P.G., Rose,M.D. *et al.* (2000) A chemical switch for inhibitor-sensitive alleles of any protein kinase. *Nature*, **407**, 395–401.
27. Alaimo,P.J., Shogren-Knaak,M.A. and Shokat,K.M. (2001) Chemical genetic approaches for the elucidation of signaling pathways. *Curr. Opin. Chem. Biol.*, **5**, 360–367.
28. Koch,A. and Hauf,S. (2010) Strategies for the identification of kinase substrates using analog-sensitive kinases. *Eur. J. Cell Biol.*, **89**, 184–193.
29. Elphick,L.M., Lee,S.E., Gouverneur,V. and Mann,D.J. (2007) Using chemical genetics and ATP analogues to dissect protein kinase function. *ACS Chem. Biol.*, **2**, 299–314.
30. Allen,J.J., Li,M., Brinkworth,C.S., Paulson,J.L., Wang,D., Hübner,A., Chou,W.-H., Davis,R.J., Burlingame,A.L., Messing,R.O. *et al.* (2007) A semisynthetic epitope for kinase substrates. *Nat. Methods*, **4**, 511–516.
31. Allen,J.J., Lazerwith,S.E. and Shokat,K.M. (2005) Bio-orthogonal affinity purification of direct kinase substrates. *J. Am. Chem. Soc.*, **127**, 5288–5289.
32. Blethrow,J.D., Glavy,J.S., Morgan,D.O. and Shokat,K.M. (2008) Covalent capture of kinase-specific phosphopeptides reveals Cdk1-cyclin B substrates. *Proc. Natl. Acad. Sci. U.S.A.*, **105**, 1442–1447.
33. Carlson,S.M. and White,F.M. (2012) Labeling and identification of direct kinase substrates. *Sci. Signal.*, **5**, pl3.
34. Nitiss,J.L. (2009) DNA topoisomerase II and its growing repertoire of biological functions. *Nat. Rev. Cancer*, **9**, 327–337.
35. Pommier,Y., Leo,E., Zhang,H. and Marchand,C. (2010) DNA topoisomerases and their poisoning by anticancer and antibacterial drugs. *Chem. Biol.*, **17**, 421–433.
36. Gonzalez,R.E., Lim,C.-U., Cole,K., Bianchini,C.H., Schools,G.P., Davis,B.E., Wada,I., Roninson,I.B. and Broude,E.V. (2011) Effects of conditional depletion of topoisomerase II on cell cycle progression in mammalian cells. *Cell Cycle*, **10**, 3505–3514.
37. Agostinho,M., Rino,J., Braga,J., Ferreira,F., Steffensen,S. and Ferreira,J. (2004) Human topoisomerase II alpha: Targeting to subchromosomal sites of activity during interphase and mitosis. *Mol. Biol. Cell*, **15**, 2388–2400.
38. Rouzeau,S., Cordelières,F.P., Buhagiar-Labarchède,G., Hurbain,I., Onclercq-Delic,R., Gemble,S., Magnaghi-Jaulin,L., Jaulin,C. and Amor-Guéret,M. (2012) Bloom's syndrome and PICH helicases cooperate with topoisomerase IIα in centromere disjunction before anaphase. *PLoS ONE*, **7**, e33905.
39. Broderick,R., Nieminuszczy,J., Blackford,A.N., Winczura,A. and Niedzwiedz,W. (2015) TOPBP1 recruits TOP2A to ultra-fine anaphase bridges to aid in their resolution. *Nat. Commun.*, **6**, 6572.
40. Meresse,P., Dechaux,E., Monneret,C. and Bertounesque,E. (2004) Etoposide: discovery and medicinal chemistry. *Curr. Med. Chem.*, **11**, 2443–2466.
41. Pommier,Y. (2013) Drugging topoisomerases: lessons and challenges. *ACS Chem. Biol.*, **8**, 82–95.
42. Cheeseman,I.M. and Desai,A. (2005) A combined approach for the localization and tandem affinity purification of protein complexes from metazoans. *Sci. STKE*, pl1.
43. Luo,K., Yuan,J., Chen,J. and Lou,Z. (2009) Topoisomerase II alpha controls the decatenation checkpoint. *Nat. Cell Biol.*, **11**, U204–U196.
44. Gruhler,A., Olsen,J.V., Mohammed,S., Mortensen,P., Faergeman,N.J., Mann,M. and Jensen,O.N. (2005) Quantitative phosphoproteomics applied to the yeast pheromone signaling pathway. *Mol. Cell Proteomics*, **4**, 310–327.
45. Keller,A., Nesvizhskii,A.I., Kolker,E. and Aebersold,R. (2002) Empirical statistical model to estimate the accuracy of peptide identifications made by MS/MS and database search. *Anal. Chem.*, **74**, 5383–5392.
46. Nesvizhskii,A.I., Keller,A., Kolker,E. and Aebersold,R. (2003) A statistical model for identifying proteins by tandem mass spectrometry. *Anal. Chem.*, **75**, 4646–4658.
47. Dunham,I., Lengauer,C., Cremer,T. and Featherstone,T. (1992) Rapid generation of chromosome-specific alphoid DNA probes using the polymerase chain reaction. *Hum. Genet.*, **88**, 457–462.
48. Swords,R., Mahalingam,D., O'Dwyer,M., Santocanale,C., Kelly,K., Carew,J. and Giles,F. (2010) Cdc7 kinase - a new target for drug development. *Eur. J. Cancer*, **46**, 33–40.
49. Hughes,S., Elustondo,F., Di Fonzo,A., Leroux,F.G., Wong,A.C., Snijders,A.P., Matthews,S.J. and Cherepanov,P. (2012) Crystal structure of human CDC7 kinase in complex with its activator DBF4. *Nat. Struct. Mol. Biol.*, doi:10.1038/nsmb.2404.
50. Koltun,E.S., Tsuhako,A.L., Brown,D.S., Aay,N., Arcalas,A., Chan,V., Du,H., Engst,S., Ferguson,K., Franzini,M. *et al.* (2012) Discovery of XL413, a potent and selective CDC7 inhibitor. *Bioorg. Med. Chem. Lett.*, doi:10.1016/j.bmcl.2012.04.024.
51. Ogino,K., Takeda,T., Matsui,E., Iiyama,H., Taniyama,C., Arai,K. and Masai,H. (2001) Bipartite binding of a kinase activator activates Cdc7-related kinase essential for S phase. *J. Biol. Chem.*, **276**, 31376–31387.
52. Montagnoli,A., Bosotti,R., Villa,F., Rialland,M., Brotherton,D., Mercurio,C., Berthelsen,J. and Santocanale,C. (2002) Drf1, a novel regulatory subunit for human Cdc7 kinase. *EMBO J.*, **21**, 3171–3181.
53. Park,S.-Y., Im,J.-S., Park,S.-R., Kim,S.-E., Wang,H.-J. and Lee,J.-K. (2012) Mimosine arrests the cell cycle prior to the onset of DNA replication by preventing the binding of human Ctf4/And-1 to chromatin via Hif-1α activation in HeLa cells. *Cell Cycle*, **11**, 761–766.
54. Kubota,S., Fukumoto,Y., Ishibashi,K., Soeda,S., Kubota,S., Yuki,R., Nakayama,Y., Aoyama,K., Yamaguchi,N. and Yamaguchi,N. (2014)

Activation of the prereplication complex is blocked by mimosine through reactive oxygen species-activated ataxia telangiectasia mutated (ATM) protein without DNA damage. *J. Biol. Chem.*, **289**, 5730–5746.
55. Zieve,G.W., Turnbull,D., Mullins,J.M. and McIntosh,J.R. (1980) Production of large numbers of mitotic mammalian cells by use of the reversible microtubule inhibitor nocodazole. Nocodazole accumulated mitotic cells. *Exp. Cell Res.*, **126**, 397–405.
56. Lee,A.Y.-L., Chiba,T., Truong,L.N., Cheng,A.N., Do,J., Cho,M.J., Chen,L. and Wu,X. (2012) Dbf4 is direct downstream target of ataxia telangiectasia mutated (ATM) and ataxia telangiectasia and Rad3-related (ATR) protein to regulate intra-S-phase checkpoint. *J. Biol. Chem.*, **287**, 2531–2543.
57. Kosako,H. (2009) Phos-tag Western blotting for detecting stoichiometric protein phosphorylation in cells. *Protocol Exchange*, doi:10.1038/nprot.2009.170.
58. Jiang,W. and Hunter,T. (1997) Identification and characterization of a human protein kinase related to budding yeast Cdc7p. *Proc. Natl. Acad. Sci. U.S.A.*, **94**, 14320–14325.
59. Tavormina,P.A., Côme,M.-G., Hudson,J.R., Mo,Y.-Y., Beck,W.T. and Gorbsky,G.J. (2002) Rapid exchange of mammalian topoisomerase II alpha at kinetochores and chromosome arms in mitosis. *J. Cell Biol.*, **158**, 23–29.
60. Dimitrova,D.S. and Berezney,R. (2002) The spatio-temporal organization of DNA replication sites is identical in primary, immortalized and transformed mammalian cells. *J. Cell. Sci.*, **115**, 4037–4051.
61. Kim,B.J., Kim,S.-Y. and Lee,H. (2007) Identification and characterization of human Cdc7 nuclear retention and export sequences in the context of chromatin binding. *J. Biol. Chem.*, **282**, 30029–30038.
62. Hornbeck,P.V., Zhang,B., Murray,B., Kornhauser,J.M., Latham,V. and Skrzypek,E. (2015) PhosphoSitePlus, 2014: mutations, PTMs and recalibrations. *Nucleic Acids Res.*, **43**, D512–D520.
63. Zeng,P.-Y., Vakoc,C.R., Chen,Z.-C., Blobel,G.A. and Berger,S.L. (2006) In vivo dual cross-linking for identification of indirect DNA-associated proteins by chromatin immunoprecipitation. *BioTechniques*, **41**, 694–698.
64. Duncker,B.P., Shimada,K., Tsai-Pflugfelder,M., Pasero,P. and Gasser,S.M. (2002) An N-terminal domain of Dbf4p mediates interaction with both origin recognition complex (ORC) and Rad53p and can deregulate late origin firing. *Proc. Natl. Acad. Sci. U.S.A.*, **99**, 16087–16092.
65. Matthews,L.A., Jones,D.R., Prasad,A.A., Duncker,B.P. and Guarné,A. (2012) Saccharomyces cerevisiae Dbf4 has unique fold necessary for interaction with Rad53 kinase. *J. Biol. Chem.*, **287**, 2378–2387.
66. Hiraga,S.-I., Alvino,G.M., Chang,F., Lian,H.-Y., Sridhar,A., Kubota,T., Brewer,B.J., Weinreich,M., Raghuraman,M.K. and Donaldson,A.D. (2014) Rif1 controls DNA replication by directing Protein Phosphatase 1 to reverse Cdc7-mediated phosphorylation of the MCM complex. *Genes Dev.*, **28**, 372–383.
67. Natsume,T., Müller,C.A., Katou,Y., Retkute,R., Gierliński,M., Araki,H., Blow,J.J., Shirahige,K., Nieduszynski,C.A. and Tanaka,T.U. (2013) Kinetochores coordinate pericentromeric cohesion and early DNA replication by cdc7-dbf4 kinase recruitment. *Mol. Cell*, **50**, 661–674.
68. Ten Hagen,K.G., Gilbert,D.M., Willard,H.F. and Cohen,S.N. (1990) Replication timing of DNA sequences associated with human centromeres and telomeres. *Mol. Cell. Biol.*, **10**, 6348–6355.
69. Erliandri,I., Fu,H., Nakano,M., Kim,J.H., Miga,K.H., Liskovykh,M., Earnshaw,W.C., Masumoto,H., Kouprina,N., Aladjem,M.I. *et al.* (2014) Replication of alpha-satellite DNA arrays in endogenous human centromeric regions and in human artificial chromosome. *Nucleic Acids Res.*, **42**, 11502–11516.
70. Takahashi,T.S., Basu,A., Bermudez,V., Hurwitz,J. and Walter,J.C. (2008) Cdc7-Drf1 kinase links chromosome cohesion to the initiation of DNA replication in Xenopus egg extracts. *Genes Dev.*, **22**, 1894–1905.
71. Isaacs,R.J., Davies,S.L., Sandri,M.I., Redwood,C., Wells,N.J. and Hickson,I.D. (1998) Physiological regulation of eukaryotic topoisomerase II. *Biochim. Biophys. Acta*, **1400**, 121–137.